1999

Single cell gel electrophoresis-based investigations of UVR- and visible light-induced single strand breakage in cultured human cells

Kendall , Jeremy Fraser

http://hdl.handle.net/10026.1/2448

http://dx.doi.org/10.24382/3566
University of Plymouth

SINGLE CELL GEL ELECTROPHORESIS-BASED INVESTIGATIONS OF UVR-
AND VISIBLE LIGHT-INDUCED SINGLE STRAND BREAKAGE IN CULTURED
HUMAN CELLS

By

JEREMY FRASER KENDALL

A thesis submitted to the University of Plymouth

In partial fulfilment for the degree of

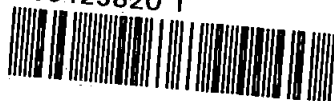**DOCTOR OF PHILOSOPHY**

Plymouth Postgraduate Medical School

In collaboration with

Cornwall Skin Cancer Research Group

August 1999

JEREMY FRASER KENDALL

SINGLE CELL GEL ELECTROPHORESIS-BASED INVESTIGATIONS OF UVR-
AND VISIBLE LIGHT-INDUCED SINGLE STRAND BREAKAGE IN CULTURED
HUMAN CELLS

Abstract

Single strand breaks induced by very low fluence UVR (20 μW cm^{-2}, 310 nm) and visible
light (70 μW cm^{-2}, 405 nm) and higher fluence unfiltered xenon arc lamp radiation
(3 mW cm^{-2}) were measured by single cell gel electrophoresis. The normal responses of 6
cell lines to the low fluence radiation show a peak in single strand breaks after
approximately 2 minutes, after which time the single strand breakage returns to
background levels despite continued irradiation. This was not observed with the higher
fluence irradiation. The repair of these single strand breaks was observed to be complete
within 4 minutes after both high and low fluence irradiation.

The dose responses were modulated by beta-carotene and o-phenanthroline; these
molecules appeared to have both photosensitising and photoprotective properties, in the
cells tested at least. Inorganic arsenic (V) was observed to inhibit single strand break
repair and the religation of repair-related excised lesions. Arsenic-induced crosslinking
and the excision of the crosslinked lesions were observed.

The Area Moment, a new parameter for the image analysis of these low dose phenomena
based on the measurement of the Comet Area and DNA migration, is proposed. The Area
Moment displayed a higher level of sensitivity to the dose responses. Lower variance in
Area Moment data enabled statistical significance ($p < 0.05$, t-test) to be attained where
existing parameters returned only borderline significance at best.

TABLE OF CONTENTS

4

5

7

9

12

TABLE OF ILLUSTRATIONS

14

15

16

17

18

19

of arsenic as a relevant environmental skin carcinogen provided the basis for Chapters 6 and 8 respectively.

AUTHOR'S DECLARATION

At no time during the registration for the degree of Master of Philosophy / Doctor of Philosophy has the author been registered for any other University award.

This study was financed with the aid of a studentship from Cornwall College in collaboration with the Cornwall Skin Cancer Research Group. The project was funded by a grant from the Duchy Health Charity Ltd.

The equipment for the laboratory was purchased during the period March 1997 to August 1997. This period included 3-days training in the comet assay technique at the University of Sussex under the direction of Prof. M. Green. The practical elements of the research were undertaken during the period August 1997 to January 1999 at Laboratory G14, Public Health Laboratories, Truro.

Training in cell culture techniques was provided by The European Collection of Animal Cell Cultures (ECACC) at Porton Down, Salisbury, UK. The course was a gift from Sigma UK.

The Dip.H.E. course 'Photochemistry' was completed during the initial period of research at Cornwall College. Selected modules from the statistics component of HND course 'Environmental Monitoring' were also undertaken at the College.

Research seminars at Cornwall College, Treliske Hospital and the departmental seminars at the University of Plymouth were attended whenever possible and presentations were made to staff, students and members of the public at these three locations.

Presentation of some of this work (the early studies with beta-carotene) was presented, in the form of a poster, at the British Association of Dermatologists Annual Meeting in July 1998.

Fraser Kendall

12.1.2000

ABBREVIATIONS USED IN THIS THESIS

$(^1O_2)$.	singlet oxygen
$(\bullet O_2^-)$	superoxide anion radical
$(\bullet OH)$	hydroxyl radical
(H_2O_2)	hydrogen peroxide
6-4	Pyrimidine (6-4) pyrimidone photoproduct
AP	Apurinic or Apyrimidinic
b-car	synthetic beta-carotene
BER	Base Excision Repair
CDK	Cyclin Dependent Kinase
CHO	Chinese Hamster Ovary
CPD	Cyclobutane Pyrimidine Dimer
DMEM	Dulbecco's Modified Eagles medium
DMR	DNA Mismatch Repair
DOK	Dysplastic Oral Keratinocyte
DSB	double strand breakage
E	(when used as a suffix) mixed epidermal cells
FCS	foetal calf serum
GSH	Reduced glutathione
GSSG	Glutathione dithyl Glutathione
HNPCC	Hereditary Non-Polyposis Colorectal Cancer
IMS	industrial methylated spirits (methanol)
L-Glu	L-Glutamine
MMB	Middle aged Males Blood
NADH	Reduced nicotinamide adenine dinucleotide
NADPH	Reduced nicotinamide adenine dinucleotide phosphate
NER	Nucleotide Excision Repair

ophen	o-phenanthroline (1,10 phenanthroline)
PARP	Poly(ADP-ribose) polymerase
PBS	Phosphate Buffered Saline made up with 'Elgastat' deionised water
PBS(t)	Phosphate Buffered Saline made up with tissue culture grade water
PUFA	Polyunsaturated fatty acid
RPMI	Roswell Park Memorial Institute
SCC	Squamous cell carcinoma
SOD	Superoxide dismutase
SSB	single strand breakage, includes plural form where necessary
UVA	radiation of wavelength 320 nm to 400 nm
UVB	radiation of wavelength 280 nm to 320 nm
UVR	ultra violet radiation, radiation of wavelength less than 400 nm
VIS	radiation of wavelength 400 nm to 700 nm
XP	Xeroderma Pigmentosum
YBF	Young Boy's Foreskin
YLB	Young Lady's Blood

CHAPTER 1

GENERAL INTRODUCTION

1.1 BACKGROUND

Malignant Cutaneous Melanoma is one of the most serious cancers affecting the human population. Melanoma incidence has risen continuously for the past two decades (Mackie *et al.* 1997). Cornwall has the highest level of melanoma incidence in Britain (D.Gould, personal communication). The Cornwall Skin Cancer Research group obtained funding from the Duchy Health Charity Ltd. in 1997 and Laboratory G14 (Public Health Laboratory Service, Truro) was leased and equipped to investigate this problem. A number of factors are potentially involved in the genesis of melanoma and of these factors, the lesions associated with oxidative stress induced by Ultra Violet Radiation (UVR) and the repair of these lesions were identified as being of particular interest. This thesis reports the results of pilot studies in these two areas. This introduction outlines the background processes of melanomagenesis and oxidative damage. The principles of the assay employed in the investigation, single cell gel electrophoresis (the 'comet assay'), and the formation and nature of the lesions it measures (Single Strand Breaks, SSB) are also introduced. The final section (Section 1.4) briefly outlines the contents of the remaining Chapters.

1.2 A SHORT REVIEW OF MELANOMAGENESIS

1.2.1 The three stage model of carcinogenesis

Cancer mortality is a sign of a successful society. In the western world, in countries that have succeeded in combating nutritional deficiency and infectious diseases, neoplastic disease comes second (only to cardiovascular disease) as a cause of death (Woolf, 1988).

The term neoplasia is defined by Willis (quoted by Woolf, 1988) as

"A neoplasm is an abnormal mass of tissue, the growth of which exceeds and is uncoordinated with that of the normal tissues, and which persists in the same excessive manner after cessation of the stimulus which has evoked the change."

There are thus three types of disturbance to consider in carcinogenesis (Woolf, 1988)

(i)   cell proliferation

(ii)   cell differentiation

(iii)   the relationship between cells and their surrounding stroma

These three types of disturbance are manifested in a multistage process of cancer

development (or carcinogenesis[#]) from a normal cell to a malignant tumour. It involves

both genetic and epigenetic changes (Fearon and Vogelstein, 1990).

Initially, a two-stage model of epidermal tumorigenesis was developed in the mouse during

the 1940s (Wigley and Balmain, 1991), but it later became clear that at least two stages

followed the initial stage, and thus a three-stage model of carcinogenesis was developed.

The three stages (Pitot and Dragan, 1991) are initiation of tumours by mutation(s),

promotion of tumours by mitogen activity, and progression of tumours to malignancy by

karyotype instability. During initiation, a cell undergoes a mutational event that is then

replicated and thus fixed in the daughter cell. This cellular change is permanent and

irreversible. The mutational process is stochastic; not all mutations are initiating. The

probability of an initiating mutation occurring is additive and does not display a threshold

effect. Promotion, however, is a reversible process and emphasises the non-reversible

---

[#] In the strictest of terms, carcinogenesis refers only to the development of carcinomas - malignant tumours

arising from epithelial tissues (Appel *et al.*, 1990) - but the term carcinogenesis will be used throughout this

thesis to indicate the development of malignant tumours of all kinds, including melanoma. The term

melanomagenesis will be used to specifically indicate factors that have been identified in the formation of

melanoma and is not to be confused with the term melanogenesis - the production of the photoprotective

pigment melanin. Attention is drawn to this as the two processes have overlapping causes i.e. UVR-induced

DNA damage (Eller *et al.*, 1996).

29

nature of initiation: regression of tumours after removal of a promoting agent is reversed on its reapplication. Promoting agents display both a threshold effect and a maximal response. The latter is directly related to the number of initiated cells available for promotion: the number of tumours promoted by an agent with promoting properties only can not exceed this number. Progression is an irreversible process characterised by progressive karyotype instability, ultimately resulting in the development of aneuploidy. This results in increased growth rates, invasiveness, metastatic capability and other biochemical changes. Some carcinogenic agents (e.g. Ultra Violet Radiation, UVR) can act in all three stages and produce malignant tumours by themselves (Robinson *et al.*, 1994) although the timing of exposure to these agents is important (Gensler *et al.*, 1992). These 'complete' carcinogens can bypass the promotion stages at sufficiently high doses, although this is usually accompanied by necrosis and compensatory hyperplasia in the surrounding tissue(s).

Passive carcinogenesis (the spontaneous occurrence of an initiating mutation, the loss of normal growth characteristics or the loss of karyotype stability) is a ubiquitous phenomenon in humans and in experimental animals. The likelihood of passive carcinogenesis increases with cell proliferation: a population of cells being driven to proliferate by a promoting agent can therefore serve as a pool of cells within which new initiating mutations or progression events can occur.

The process of cancer development is therefore a continuum. Genetic models have been formulated for a number of cancers, including melanoma (Walker *et al.*, 1995).

1.2.2   An overview of the pathogenesis of Malignant Cutaneous Melanoma

1.2.2.1   Epidemiology of malignant melanoma

Anecdotally, Cornwall has the highest incidence of malignant melanoma in Britain. Several factors may contribute to this - the high proportion of a population from Celtic stock, the presence of high levels of arsenic in the environment (Thornton and Farago,

1997), the existence of high levels of radon exposure (Henshaw *et al.*, 1990) and a lifestyle which is oriented to the outdoors - especially the sea and beach. This section presents an overview of melanomagenesis with an intention of beginning to address the combination of issues relevant to the regional population.

Malignant melanoma has continued to rise over the past 20 years in most parts of the world where data are available (MacKie *et al.*, 1997; Rees, 1996), although it appears that this might be stabilising (MacKie *et al.*, 1997; Melia, 1997; Giles *et al.*, 1996; Newton and Redburn, 1995). The genetics of melanoma are still being unravelled (Fountain *et al.*, 1990; Kamb, 1996; Newton, 1994). The complete aetiology of melanoma is not fully elucidated, but UVR is an overwhelmingly important factor (Gilchrest *et al.*, 1999; Lee, 1989; Pitcher and Longstreth, 1991).

UVR is a complete carcinogen (IARC, 1992; Cridland and Saunders, 1994). The spectrum of electromagnetic radiation between the wavelengths of 200 nm and 400 nm (i.e. the ultraviolet spectrum) is traditionally divided into 3 bands by photobiologists. These (artificial) divisions are based on their main cellular effects and consequently the limits of the bands vary to a small extent in the literature. Figure 1.1 is redrawn from Cadet (1994) and illustrates the main effects on DNA by UVR.

The UVR-exposure profile in melanomagenesis is, however, subject to an unknown number of modifying factors. Sunburn in childhood was considered by some to be a significant risk factor (Lee, 1989; Donawho and Wolf, 1996) although the evidence is 'shaky' (Finkel, 1998). The incidence of melanoma is higher in people with light coloured skin (Marks, 1995), people with red hair (Rees and Healy, 1997) and higher in males than females (Mackie *et al.*, 1997). There is an association of male (but not female) melanoma incidence with arsenic (Phillip *et al.*, 1984) a well documented skin carcinogen (Urbach, 1993). The use of sunscreens has also been associated with an increased risk of melanoma (Autier *et al.*, 1995).

31

There are at least two inherited form of melanoma susceptibility- mutations or deletions in the p16 tumour suppressor gene (Ranade *et al.*, 1995; de Gruis, 1995; Liu, L. *et al.*, 1995) and at least one HLA allelotype (HLA-DQB1*0301) is associated with an increased melanoma risk (Lee *et al.*, 1994).

Figure 1.1 The effects of UVR on cellular DNA (Cadet, 1994)

RADIATION (nm)	CHROMOPHORES	PHOTOREACTIONS	PHOTOPRODUCTS

240

UVC — DNA bases — Dimerisation / Adduct Formation — Pyr$\diamond$Pyr

Pyr(6-4)Pyo

280

UVB

320 — Photosensitisers — $^1P \longrightarrow {}^3P$

UVA

$^1P \to {}^3P$ electron transfer from bases, O$_2$, ^{1}O$_2$, O$_2^{-}$

DNA strand breaks
DNA-protein crosslinks
Oxidised bases

360 — Other Photosensitisers (no oxygen requirement) — Photoaddition — e.g. psoralen$\diamond$ thymine

VISIBLE

Pyr$\diamond$Pyr = Pyrimidine dimers; Pyr(6-4)Pyo=Pyrimidine (6-4) pyrimidone photoproduct;
^1P= ground state (singlet) photosensitiser; ^3P= excited state (triplet) photosensitiser;
O$_2$=ground state (triplet) oxygen; ^{1}O$_2$= excited state (singlet) oxygen

<u>1.2.2.2   Models of melanomagenesis</u>

Melanomas can be induced in several species of experimental animals by a number of means, although the majority of these models employ a chemical or chemical plus UVR induction strategy (Ingram, 1992). Three models exist for UVR-induced melanoma; these are the *Mondelphis domestica* opossum model (Ley *et al.*, 1989), the *Xiphophorus* fish hybrid model (Setlow *et al.*, 1989) and the transgenic mouse model (Mintz and Silvers, 1993; Klein-Szanto *et al.*, 1994).

There are at least two inherited form of melanoma susceptibility- mutations or deletions in the p16 tumour suppressor gene (Ranade *et al.*, 1995; de Gruis, 1995; Liu, L. *et al.*, 1995) and at least one HLA allotype (HLA-DQB1*0301) is associated with an increased melanoma risk (Lee *et al.*, 1994).

Figure 1.1 The effects of UVR on cellular DNA (Cadet, 1994)

RADIATION (nm)	CHROMOPHORES	PHOTOREACTIONS	PHOTOPRODUCTS
240 UVC	DNA bases	Dimerisation Adduct Formation	Pyr<>Pyr Pyr(6-4)Pyo
280 UVB		O_2 $^1O_2$ electron	DNA strand breaks
320	Photosensitisers	^{1}P ^{3}P transfer from bases	DNA-protein crosslinks
UVA		O_2 O_2^{-*}	Oxidised bases
360	Other Photosensitisers (no oxygen requirement)	Photoaddition	e.g. psoralen<> thymine
VISIBLE			

Pyr<>Pyr = Pyrimidine dimers; Pyr(6-4)Pyo=Pyrimidine (6-4) pyrimidone photoproduct; ^{1}P= ground state (singlet) photosensitiser; ^{3}P= excited state (triplet) photosensitiser; O_2=ground state (triplet) oxygen;$^1O_2$= excited state (singlet) oxygen

1.2.2.2 Models of melanomagenesis

Melanomas can be induced in several species of experimental animals by a number of means, although the majority of these models employ a chemical or chemical plus UVR induction strategy (Ingram, 1992). Three animal models exist for UVR-induced melanoma; these are the *Mondelphis domestica* opossum model (Ley *et al.*, 1989), the *Xiphophorus* fish hybrid model (Setlow *et al.*, 1989) and the transgenic mouse model (Mintz and Silvers, 1993; Klein-Szanto *et al.*, 1994).

The South American opossum, *Mondelphis domestica*, has been used to study UVR-induced skin tumours because it possesses a photoreactivation pathway i.e. it can monomerise cyclobutane pyrimidine dimers (CPD) when exposed to radiation of 300 - 500 nm (Ley *et al.*, 1989). Melanomas are induced in this model by chronic UVB exposure (25 mJ cm^{-2}, 3 times per week for 81 weeks (Ley, 1997)). Melanoma precursor lesions were induced by 2.5 mJ cm^{-2} UVA 3 times per week for 81 weeks (Ley, 1997).

Melanoma in *Xiphophorus* fish hybrids is caused by the activity of a dominant oncogene, Xmrc (Wittbrodt *et al.*, 1989; Adam *et al.*, 1993). Tumour formation in wild type fish is suppressed by the activity of a tumour suppressor locus, R (Adam *et al.*, 1993). Melanoma occurs spontaneously in both wild-type and the hybrid fish (Schartl *et al.*, 1995). Tumours are induced above control levels by UVB, UVA and visible light: UVB-induced tumour formation was maximal at 313 nm and visible light-induced tumour formation at 405 nm (Setlow *et al.*, 1993). When corrected for quantum efficiency, 302 nm was the most effective wavelength for melanoma induction (Setlow *et al.*, 1993)

Skin from highly susceptible transgenic mice, when grafted onto histocompatible mice develop melanomas that closely resemble the situation seen in humans (Mintz *et al.*, 1993; Klein-Szanto *et al.*, 1994). This model indicated that growth factors and cytokines involved in healing and wound repair were responsible for triggering the conversion of the genetically susceptible grafted melanocytes to melanoma (Mintz and Silvers, 1993). Genetically susceptible melanocytes (but not wild type melanocytes) in this model were converted to anchorage independence and malignancy by single UVB exposures of 0.7 and 1.75 mJ cm^{-2} respectively (Larue *et al.*, 1992). At least 2 genetic changes are implied by this and other (Larue *et al.*, 1993) studies.

The influence of UVB on melanocyte activity was studied *in vitro* using reconstructed human skin with a melanocyte component (Bessou *et al.*, 1995), this model could possibly serve for studies of melanomagenesis. An *in vitro* model of human melanomagenesis,

33

based on allelic losses was proposed by Walker *et al.* in 1995 and is reproduced in Figure

1.2.

Figure 1.2 An in vitro model based on allelic losses (Walker et al., 1995).

Normal melanocyte

Inherited mutator

phenotype

Inherited mutation of 1p

(MLM1) or 9p (MLM2) familial

melanoma genes

Dysplastic or common naevus   Loss of 9p and/or 10q

RER+

somatic

instability

Radial growth phase primary melanoma   loss of gene on 6q

Vertical growth phase primary melanoma

loss of genes on 1p, 11q, 17q

and other chromosomes

Metastatic melanoma
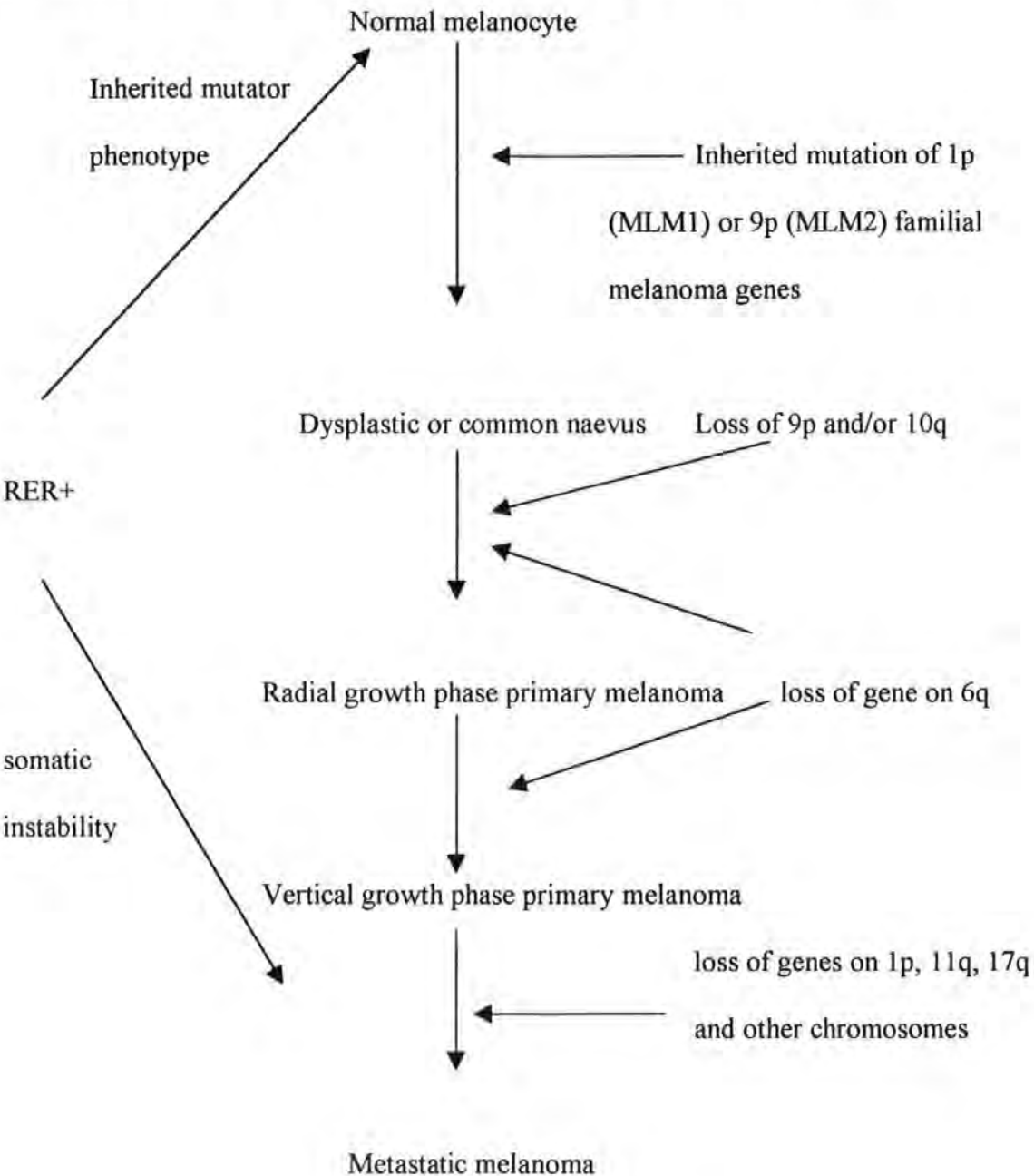
RER+ : Replication Error positive, a phenotype which, due to a number of different factors

causes an increased likelihood of unfaithful DNA replication (see below).

1.2.3 An overview of some cellular and molecular processes of melanomagenesis

1.2.3.1 Cell proliferation and differentiation

In normal development and growth, there is a precise mechanism that allows individual organs to reach a specific size and maintain this size during the normal turnover of tissue and in the case of injury. The more specialised (i.e. differentiated) an individual cell is, the less likely it is that this cell can divide - there exist, therefore, relatively undifferentiated cells ('stem' cells) whose purpose is to proliferate and generate replacement cells when necessary. Approximately half the progeny from these cells enter a differentiation pathway, while most of the remainder remain as stem cells (Woolf, 1988). The stimulatory and inhibitory factors responsible for controlling this process are therefore a major target of the carcinogenic process.

Proliferating cells follow a basic pattern that is similar in all somatic cells (Alberts *et al.*, 1989; Franks, 1991). This is the cell cycle and, for illustration, can be visualised as a clock face. The actual process of cell division, mitosis ('M' phase), will be visualised as taking place between 12 and 1 o' clock and is followed by a 'gap' period, 'G1'. The length of G1 varies between cell types and circumstance, but for illustration it will be (arbitrarily) described as taking place between 1 and 6 o' clock. The synthesis (of DNA especially) ('S' phase) takes place between 6 and 9 or 10 o'clock and is followed by a second gap phase, 'G2' leading to a new mitotic episode at 12 o' clock. There exists an alternative phase between G2 and G1, 'G0'. This is a resting quiescent phase. Cells deprived of growth factors will leave the cycle during G2 and enter G0 (Franks, 1991). At approximately 5 o'clock there is a major control point termed 'R' (restriction). Once a cell has passed R it is committed to complete the cycle and divide. It is therefore of prime importance that the DNA (subsequently to be replicated) is in a fully functional condition prior to passing the restriction point.

The regulation of the cell cycle is effected through phase-specific transcription of defined sets of genes (Muller, 1995). At the centre of the regulatory network are the cyclin dependent kinases (CDKs) that are responsible for activating (and deactivating) the molecules that control DNA replication and mitosis. The CDKs themselves are positively regulated by 'Cyclins' and negatively regulated by a family of proteins named after their molecular weights - e.g. p21, p16. The interaction of the CDKs and their regulators form the basis of cell cycle control and subversion of this regulatory machinery leads to a deregulation of growth control. (For introductory reviews see Kamb, 1995; Draetta, 1994; Elledge and Harper, 1994)

The genes that exert influence on the proliferation and differentiation processes fall into two broad categories: those that promote cell growth and those that restrain it. The former are the 'protooncogenes' and if overexpressed, uninhibited or mutated ('oncogenes'), can lead to excessive growth. The Tumour Suppressor Genes (TSGs) (sometimes confusingly referred to as 'antioncogenes', erroneously implying that they specifically work against the oncogene(s)) restrain growth. Loss of function through alleic loss, genetic mutation or viral inactivation can also lead to deregulation of growth. Thus one mutant allele of an oncogene or the loss of both functional copies of a TSG are sufficient to permit tumorigenesis. The number and types of oncogenes and TSG are many and varied (for general reviews see Marshall, 1991; Levine, 1993; Weinberg, 1989; Birchmeir and Behrens, 1994.)

Over 75% of melanoma cell lines contain inactivating mutations of the TSG p16 (Kamb, 1995) and in a recent study, this figure reached 92% (Castellano *et al.*, 1997).The p16 is a specific inhibitor of CDK4 and CDK6 and inhibits cell cycle progression through G1 (Serrano *et al.*, 1993; Wick *et al.*, 1995) by inhibiting the phosphorylation of another tumour suppressor gene, pRb. (The translation of pRb itself is inhibited by UVB in human melanocytes and causes reduced cell cycle regulation (Pedley *et al.*, 1996)). The gene encodes two unrelated proteins that are totally different in primary structure but strikingly

36

they both cause G1 arrest (p19 also causes G2 arrest) (Valle *et al.*, 1997). p16 is frequently non-functional in a large number of human cancers (Kamb, 1995). p16 is inactivated by different mechanisms, deletions, rearrangements or mutations in defined tumours (Larsen, 1996) including aberrant methylation of the upstream elements of the gene (Gonzalez-Zulueta *et al.*, 1995). Mutation of p16 is infrequent in sporadic melanoma (Healy *et al.*, 1996), the predominant mechanism of inactivation was suggested as loss of heterozygosity. At least two different germline mutations in the coding region of p16 have been detected in some forms of familial melanoma (Liu *et al.*, 1995).

1.2.3.2 Cell Cycle Arrest

The detection and repair of low to moderate levels of cellular damage take place during normal 'housekeeping'. After high levels of damage the normal cell will stop cycling. The term 'arrest' is commonly used to describe this, although it erroneously implies permanent cessation. The cycling cell can be arrested at any point through the use of various inhibitors and cell cycle delays can be induced by DNA-damaging agents (Rowley, 1998). The importance of the cell cycle arrest can be illustrated by the function of p53. p53 is a DNA damage responsive protein and the most widely mutated gene in human cancers (Picksley and Lane, 1994; Bates and Vousden, 1996). p53 causes either G1 and G2 arrest or apoptosis (programmed cell death) after DNA damage is detected (Bates and Vousden, 1996; Schwartz *et al.*, 1997). Exposure of normal human skin to UVB sufficient to cause mild sunburn resulted in the rapid (within 2 hours) induction of p53 (Hall *et al.*, 1993). UVB irradiation of human melanocytes increased p53 expression (by protein stabilisation) up to ten-fold and was reported as a critical response for survival after UVB radiation (Loganzo *et al.*, 1994). p53 is a transcriptional activator of several genes including p21/WAF1 (Petrocelli *et al.*, 1996), cyclin G1 and G2 (Bates *et al.*, 1996) and GADD45 (Smith *et al.*, 1996). The regulation of the ability to transactivate target genes is not simply

correlated to the level of p53 protein and may feature a negative regulation element (Lu *et al.*, 1996).

Inactivation of p53 function removes the induction of the cellular checkpoint by p53 regulated genes and permits the unchecked replication of DNA. Transgenic mice carrying multiple copies of mutant p53 are highly susceptible to multiple squamous cell carcinomas (SCC) (Li *et al.*, 1995). UV-induced p53 mutations were found in 58% of invasive SCC (Brash *et al.*, 1991) and in 56% of basal cell carcinomas (BCC) (Ziegler *et al.*, 1993). The distribution of UV photoproducts show mutational 'hotspots' at pyrimidine clusters (Tornaletti *et al.*, 1993).

The most understood pathway of p53 induced cell cycle arrest is through the tumour suppressor gene p21 (Bates and Vousden, 1996), a universal inhibitor of CDKs (Xiong *et al.*, 1993). The level of p21 is widely varied in melanoma cells compared with normal melanocytes and, because most melanoma cells over express p53, this indicates an aberrant p53-independent regulation mechanism in melanoma cells (Vidal *et al.*, 1995). Of relevance to the work presented here is the observation that the regulation of p53 is disrupted by inorganic arsenic in lung cells by alteration of the methylation patterns of the promotor region.(Mass and Wang, 1997). It is unlikely that this phenomenon would be confined to the p53 gene only.

1.2.3.3   The repair of oxidative damage and alkali labile lesions

As indicated above, the integrity of DNA prior to replication and subsequent cell division is of paramount importance in the maintenance of genomic stability. There exist several repair mechanisms to detect and repair DNA damage and ensure that genomic integrity is maintained between generations.

The repair of DNA damage is of prime importance (Hanawalt, 1998; Demple and Harrison 1994) but a comprehensive review of DNA damage repair is beyond the scope of this

discussion, which will be confined to the repair of the lesions measured by the form of the assay employed in this thesis i.e. SSB and alkali labile lesions.

1.2.3.3.1 SSB repair

SSB rejoining is a rapid process with a half time for repair of a few minutes in normal cells (Cridland and Saunders, 1994; Collins *et al.*, 1995). The strand breaks themselves can differ, however: SSB induced by 365 nm UVA and 405 nm UVA/VIS appear to be different lesions as evidenced by different alkaline elution profiles (Peak *et al.*, 1991; Peak and Peak, 1989). Furthermore, lesions induced by 365 nm UVA and H_2O_2 were differently repaired: the 365-nm induced lesion repair process was slower than that observed for hydrogen peroxide (Peak *et al.*, 1991) and approximately 20% of the 365 nm-induced lesions appeared refractory to repair by (excision repair enzyme deficient) Xeroderma Pigmentosum cells (Peak *et al.*, 1991). SSB are also introduced into the DNA molecule as normal intermediates in the repair of other lesions (Halliwell and Aruoma, 1991). Thus a SSB with ends that match the normal repair-related excision would be rejoined rapidly and effectively while a SSB with ends that could not be recognised by the rejoining mechanism(s) may go unrepaired. The refractory-to-repair lesions described by Peak *et al.* (1991) may be of this type. It was also observed that the inactivation of fibroblasts by singlet oxygen (Tyrrell and Pidoux, 1989) was more pronounced at 365 nm than at 334 nm or 405 nm. Hence these two papers (Peak *et al.*, 1991;Tyrrell and Pidoux, 1989) provide evidence of at least two types of SSB:

(i)   A population of singlet oxygen mediated SSB (most evident after 365 nm irradiation) that have slow repair kinetics (some of which may be refractory to repair and thus potentially cytotoxic).

(ii)   A population of SSB/DSB induced by H_2O_2 and by 405 nm UVA/VIS that are repaired rapidly and effectively. This population may be heterogenous (i.e. the free ends of the strand breaks caused by hydrogen peroxide and 405 nm radiation may differ).

In unperturbed cells there is a steady state level of oxidative damage that represents an equilibrium between metabolically associated oxidative stress-induced damage and the enzyme activity that repairs it. It is reasonable to expect that this constant low level of oxidative damage might be repaired more effectively (i.e. the repair of SSB would be governed by the rate-limiting step in the enzymic sequence involved) than the sudden burst of strand breaks and oxidised bases introduced after UV irradiation (where the total repair of strand breakage may be governed by the number of strand breaks themselves i.e. the repair process may become saturated). However, it is also reasonable to expect that the constitutive level of repair is 'under-performing' at normal background levels of oxidative stress and could faithfully repair sudden higher levels of damage up to a certain threshold. Above this threshold, but close to it, the processes of mutagenicity and carcinogenicity would be initiated, while at higher levels of damage, the processes of apoptosis and cytotoxicity would be relevant.

1.2.3.3.2 Excision repair

Excision repair is the most general method of repairing damaged DNA. There are three types of excision repair (Friedberg *et al.*, 1995; Lindahl *et al.*, 1997)). Base excision repair (BER) is characterised by the removal of a damaged base by a specific repair enzyme - a DNA Glycosylase - that recognises and excises the damaged base (Friedberg *et al.*, 1995). Mismatch repair (MMR) is employed to correct a particular type of DNA damage - mispaired bases - and is executed through a number of pathways, including the BER pathway (Friedberg *et al.*, 1995). Nucleotide excision repair (NER) is responsible for the repair of generic damage, i.e. the enzymes involved recognise common features of types of DNA damage (rather than recognition of specifically damaged bases as in the BER pathway (Friedberg *et al.*, 1995). The repair process involves the removal of a short stretch of DNA on either side of the lesion; this gap is then filled in by DNA synthesis (Wilson and Singhal, 1998). This is usually referred to as 'unscheduled DNA synthesis',

UDS, (Friedberg *et al.*, 1995). The repair of oxidised bases and pyrimidine dimers (including the alkali labile lesions) are executed by the base excision and nucleotide excision repair pathways respectively. The excision repair of UVR induced DNA damage is executed more efficiently in some active genes (Bohr, 1995; Bohr *et al.*, 1985).

The repair of the DNA molecule is completed in all forms of excision repair by the action of DNA Ligases II and III (Tompkinson *et al.*, 1998).

The importance of DNA repair can be illustrated with two clinical conditions, Xeroderma Pigmentosum (XP) and Hereditary Non-Polyposis Colorectal Cancer (HNPCC).

XP is caused by one of a number of genetic defects in Nucleotide Excision Repair (NER) - the pathway responsible for repairing short wavelength (< 320 nm) UVR induced lesions. XP patients display extreme sensitivity to sunlight and with it a 2000 fold increased risk of skin cancer (Thompson, 1998; Kraemer *et al.*, 1994; Kraemer, 1996). HNPCC is caused by inherited mutations in the DNA Mismatch Repair (DMR) pathway. This pathway (Prolla *et al.*, 1998) is responsible for repairing mismatched or unpaired bases. These lesions arise spontaneously and in that it arose early in evolution, it is likely to be a very primitive pathway. Critically, DMR has evolved to permit an optimum level of mutation (to generate allelic variation and thus drive evolution). The normally 'safe' level of mutation that occurs normally is exceeded by some mutant alleles in the DMR pathway (Prolla *et al.*, 1998). In HNPCC mutations ever more rapidly accumulate and lead to the development of colorectal cancer at an average age of 42, 20 years earlier than a matched non-affected population (Liu, B *et al.*, 1995).

1.2.3.4 Apoptosis

Cells which have suffered excessive damage to the DNA are subject to what amounts to a viability check. During cell cycle arrest, the p53 protein effectively steers the cell down one of two courses- the repair pathways appropriate to the types of damage or, if the damage is too great to faithfully repair, the cell will be driven down the programmed cell

death pathway, apoptosis. This is the normal cellular process whereby 'unwanted' cells are removed, during for example development, releasing their contents in a controlled manner for the surrounding cells' uptake and metabolism. The control of apoptosis is a tightly regulated balance between the 'survival' genes and the 'suicide' genes of the Bcl-2 family (Farrow and Brown, 1996; Wyllie, 1995; Korsmeyer, 1995). Melanocytes constitutively express high levels of the pro-survival gene Bcl-2; this has been suggested as one of the reasons why melanoma is associated with sunburn episodes (i.e. they would survive a high dose of UVR at the cost of an increased probability of tumourigenesis) (Gilchrest *et al.*, 1999).

1.2.3.5   Immunosurveillance

The immune system continuously patrols the tissues of the body and will destroy tumour cells it detects (Janeway and Travers, 1994). In order for a tumour to develop, it must therefore elude the immune system. This can be accomplished in many ways but broadly, there are three categories (Janeway and Travers, 1994),

(i)   The tumour can evolve a low immunogenic profile, e.g. by not presenting abnormal peptides, by down regulation of MHC molecules or by not expressing co-stimulatory molecules.

(ii)   The tumour can stop expressing an antigenic peptide that has previously evoked an immune response

(iii)   The tumour can produce immunosuppressive substances (e.g. Transforming Growth Factor beta (TGF-β)).

For a more detailed description of the mechanisms involved, see Janeway and Travers, 1994. For an introduction on the immunology of melanoma and the current drive to develop immunotherapeutic vaccines see Dalgleish, 1996 or Mitchell, 1995.

42

1.3 THE EFFECTS OF ULTRA VIOLET RADIATION

1.3.1 Single cell gel electrophoresis

The effect of ultraviolet radiation-induced oxidative stress can be measured quantitatively by SSB of the sugar-phosphate backbone, thought to be caused by Fenton chemistry (Halliwell and Aruoma, 1991; Kielbassa *et al.*, 1997; Black 1987) taking place on the chromatin (de Mello Filho and Meneghini, 1985). This is discussed in greater detail below. SSB-induction by UVR is therefore an appropriate measure of UV-induced oxidative damage (Wenczl *et al.*, 1997). It is also a useful method of investigating photoprotective or radical scavenging effects of exogenous agents (Wenczl *et al.*, 1997; see also Chapter 6 of this thesis). Techniques used to measure SSB include immunochemistry (Wenczl *et al.*, 1997), alkaline-sucrose sedimentation (Peak *et al.*, 1987), alkaline elution (Peak *et al.*, 1989) and single cell gel electrophoresis or the 'comet' assay (McKelvey-Martin *et al.* 1993; Fairbairn *et al.*, 1995; Anderson *et al.*, 1998).

Single cell gel electrophoresis was first introduced by Ostling and Johanson in 1984 (Ostling and Johanson, 1984) who used a neutral pH lysis procedure to relax DNA supercoiling after ionising radiation-induced SSBs. Under more stringent conditions, up to 95% of protein could be removed from the DNA allowing the assay of double strand breaks (Anderson *et al.*, 1998). Alkaline single cell gel electrophoresis was developed from the Ostling and Johanson (1984) technique and techniques based on the denaturation of DNA by alkaline solutions (Tice, 1995). Under alkaline denaturing conditions, DNA duplex molecules containing SSBs lose their structure and the double stranded molecules become a population of single stranded, low molecular weight DNA fragments. These DNA fragments can be collected and assayed on the basis of their size by agarose electrophoresis. Two forms of the alkaline assay are commonly in use. These two forms of the assay were developed independently in separate laboratories (Singh *et al.* 1988, Olive *et al.* 1990). The assays based on the method of Singh *et al.* (1988) are especially

suited for detection of low numbers of strand breaks (Green *et al.*, 1996) whereas the assays based on the method developed by Olive *et al.* (1990) are especially suited for the detection of drug resistant sub-populations in tumours (Olive and Banath, 1993; Olive, 1998). The term 'comet assay' encompasses both these forms in the outline below The assay itself ("rapid, simple, visual and sensitive" (Anderson *et al.*, 1998)) is now in widespread use (for reviews see McKelvey-Martin *et al.*, 1993; Fairbairn *et al.*, 1995, Tice, 1995, Anderson *et al.*, 1998).

The principle of the assay is as follows. High molecular weight (i.e. unbroken) DNA migrates through an agarose gel at a slower rate than low molecular weight DNA when an electrical field is applied across the gel. Thus if single cells are embedded in agarose and the non-DNA contents are removed prior to applying the electrical field, unbroken DNA will remain in the peri-nuclear cavity while broken DNA will migrate towards the anode. Microscopic examination of the (stained) DNA produces a comet-like structure and hence the popular name for the comet assay (See Figure 2.3 in Chapter 2).

The amount of DNA in the comet tail is a function of DNA damage (Fairbairn *et al.*, 1995), and there are several parameters used for the measurement of DNA damage. These fall into three categories. The initial category employed was based on the physical parameters of Comet Area, Comet length and Tail length (Fairbairn *et al.*, 1995). These measurements have a linear relationship to DNA damage at low doses, but at higher doses the relationship breaks down, i.e. the comets do not get longer as DNA damage increases. It appears that the maximum Comet length is defined more by electrophoresis conditions than by dose (Fairbairn *et al.*, 1995). The second category is based on the DNA content of the heads and tails of the comets, as measured by staining intensity. But it is worth noting that whereas the total DNA content of a comet is a function of the position in the cell cycle of the cell that produced it, the fraction of DNA in the tail is a linear function of dose. The third group of parameters are the tail and comet 'moments' based on an engineering term (Ashby *et al.*, 1995) to describe the product of a physical quantity and its directed distance

44

from an axis. The 'Tail Moment' is a product of the distance between the centres of mass of the comet head and tail and the fraction of DNA in the tail (Olive *et al.*, 1990; Olive and Banath, 1993; Huang *et al.*, 1998). The 'Comet Moment' is based on the mathematical definition of the moment of inertia of a plane figure (Kent *et al.*, 1995). The Tail Moment and the Comet Moment have a linear relationship with dose (Kent *et al.*, 1995) and have a close relationship with each other (Kent *et al.*, 1995), but the linear dose response of the Tail Moment fails when the centre of the original nucleus is no longer the brightest point in the comet (Green *et al.*, 1996). The Comet Moment was formulated to overcome this and is independent of the head-tail relationship (Kent *et al.*, 1995).

However, the simplest method of measuring DNA damage by the comet assay is to assign comets to categories based on their appearance and allocating a score to the categories (Green *et al.*, 1996; Collins *et al.*, 1995). A mean or accumulated score can then be calculated when sufficient numbers of comets have been categorised. Images have also been measured and assessed using photography (McCarthy *et al.*, 1997), microautoradiography (Klaude *et al.*, 1996), fluorescent in situ hybridisation (McKelvey-Martin *et al.*, 1998), video enhanced laser scanning microscopy (Fairbairn *et al.*, 1994) and direct microscopy by use of a calibrated eyepiece (Hooghe *et al.*, 1995). The applications of the assay are widespread: the review by Anderson (1998) reviewed comet assay data on over 200 carcinogens and suspect carcinogens alone. The comet assay measures strand breaks in DNA. The measurement of lesions, howsoever caused, depends on the conversion of the lesion into a strand break. The lesions induced by UVR measured by the assay as employed in this work are discussed below.

1.3.2 SSB caused by direct absorption of short wavelength UVR by DNA

1.3.2.1 Alkali-labile lesions

The total Xe lamp spectrum contains UVB, UVA, Visible light and infra-red components, and will not only induce SSB by formation of active oxygen species, but also the UVB

component and to some extent the 405 nm component (Peak and Peak, 1989) will induce strand breakage via directly formed alkali-labile lesions. These alkali-labile lesions are an heterogeneous population of UVR-induced lesions which are thought to arise from apurinic or apyrimidinic (AP) sites that render the sites susceptible to hydrolysis of the sugar-phosphate DNA backbone (Cridland and Saunders, 1994; Cadet, 1994). While a complete understanding of the nature of alkali-labile sites is currently lacking, important information is available and is summarised below.

Relative yields of far-ultra violet radiation photoproducts have been determined in naked, double-stranded DNA (Table 1.1, redrawn from Cadet, 1994)

Table 1.1 Relative yields of far-ultra violet radiation photoproducts determined in naked, double-stranded DNA (Cadet, 1994)

Photoproduct	Relative yield
Cyclobutadipyrimidines	1
Pyrimidine (6-4) pyrimidones (alkali labile)	0.4 - 0.6
Cytosine photohydrate	~ 0.1
Thymine photohydrates	$< 10^{-3}$
Adenine - adenine adducts	$< 10^{-3}$
Thymine-adenine adducts	$< 10^{-3}$
DNA strand breaks	$< 10^{-3}$

The Pyrimidine (6-4) pyrimidone photoproduct (the' 6-4' photoproduct) is alkali-labile (Cadet, 1994) and may be formed (like the cyclobutane pyrimidine dimers (CPD)) by the photodimerisation of adjacent pyrimidines and may be thymine-thymine, cytosine-cytosine or thymine-cytosine (but cytosine methylation at C5 inhibits 6-4 photoproduct formation with thymine (Friedberg *et al.*, 1995)).

The 6-4 photoproduct has an absorption maximum at either 310 nm (Cridland and Saunders, 1994) or at 320 nm (Cadet, 1994; Clingen *et al.*, 1995) with a resultant photoisomerisation at these or intermediate wavelengths producing the Dewar valence isomer (Cridland and Saunders, 1994; Cadet, 1994; Friedberg *et al.*, 1995). The Dewar valence isomers are more labile to alkali than the corresponding 6-4 photoproduct (Cadet, 1994). Exposure of human mononuclear cells to natural sunlight demonstrated that virtually all 6-4 photoproducts were converted to the Dewar valence isomer (Clingen *et al.*, 1995). Cytosine and its related nucleosides also undergo a photoisomerisation involving transient formation of a Dewar compound (Cadet, 1994) but no information was given about its alkali-lability. Alkali-labile sites are also formed by hydroxyl radicals (Friedberg *et al.*, 1995) as demonstrated by the observation that irradiation in the presence of oxygen results in a four fold increase in the number of alkali-labile sites (Friedberg *et al.*, 1995).

1.3.3 *Oxidative stress induced by long wavelength UVR*

1.3.3.1 Introduction

The oxygen species that are generated from UVR are of several types (Halliwell and Aruoma, 1991; Cadenas, 1995, Black, 1987). The major reactive oxygen species superoxide anion radical ($\bullet O_2^-$), hydrogen peroxide (H_2O_2) and hydroxyl radical ($\bullet OH$) are derived from the one-, two-, and three-electron reduction of molecular oxygen respectively (Figure 1.3 redrawn from Black, 1987)

Figure 1.3   The four electron reduction of ground state oxygen to water

$^3O_2 \xrightarrow{\quad +e^- \quad} \bullet O_2^- \xrightarrow{+e^-} H_2O_2 \xrightarrow{\quad +e^- \quad} \bullet OH \xrightarrow{\quad +e^- \quad} H_2O$

The excited state species singlet oxygen ($^1O_2$) is produced by absorption of photons by a photosensitiser and subsequent energy transfer to ground state triplet oxygen ($^3O_2$). The reaction sequence superoxide ($\bullet O_2^-$) to hydrogen peroxide (H_2O_2) to hydroxyl radical ($\bullet OH$) is spin forbidden and proceeds very slowly unless catalysed by enzymes and by heavy ions (Figure 1.4., redrawn from Black, 1987). Additionally, there are cellular chromophores that absorb UVR or visible light, become electronically excited and subsequently transfer this excitation energy to DNA thus causing damage. This can occur directly (a Type I photosensitisation) or indirectly via energy transfer to ground state oxygen to form singlet oxygen (a Type II photosensitisation) (Foote, 1991)

Figure 1.4   Enzymic means of reactive species detoxification (Black, 1987)
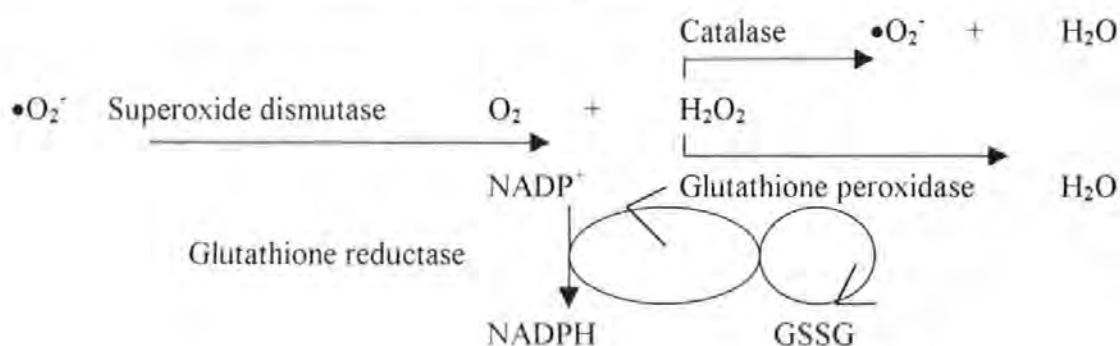
Hydroxyl radical ($\bullet OH$) is produced by the transition metal catalysed Haber-Weiss and Fenton reactions. Lipid peroxidation is initiated by free radical attack upon polyunsaturated acids (PUFA) in cell membranes which then participate in chain reactions with adjacent PUFA.

1.3.3.2   The radical anion superoxide ($\bullet O_2^-$) and its conjugate acid $\bullet HO_2$.

Superoxide is generated by one electron reduction of molecular oxygen and is the primary radical formed in the reduction of molecular oxygen to water (Black, 1987). $\bullet O_2^-$ reduces iron (III) to iron (II) in the Haber-Weiss cycle (see below) and can be reformed during iron (II) auto oxidation (Black, 1987). Superoxide is formed in the mitochondrial respiratory

48

chain by autooxidation of cytochrome b and NADH (Black ,1987) and by photooxidation of NADH or NADPH (Friedberg *et al.*, 1995). It is not a highly reactive molecule and does not react with bases at all (Wiseman and Halliwell, 1996). Superoxide is converted by spontaneous dismutation and by the enzyme superoxide dismutase (SOD) into hydrogen peroxide and molecular oxygen. SOD has three forms: cytosolic, extra-cellular and mitochondrial (Przedborski and Schon 1998) and it is unlikely that $\bullet O_2^-$ escapes from the mitochondrion into the cytosol although hydrogen peroxide is freely diffusable (Black, 1987).

1.3.3.3   Ground state molecular hydrogen peroxide (H_2O_2).

Hydrogen peroxide is the most prevalent mutagen to which human DNA is exposed (Green *et al.* 1996). Hydrogen peroxide is formed from many sources including normal physiological processes such as oxidative phosphorylation and the inflammatory cell respiratory burst (Rodriguez *et al.*, 1997). UVR produces hydrogen peroxide in mammalian cells (Peak and Peak , 1990; Tyrrell, 1995; Peak *et al.*, 1991); photooxidation of tryptophan (Tyrrell and Pidoux, 1989) or of NADH or NADPH (Friedberg *et al.*, 1995) produces hydrogen peroxide.

H_2O_2 destruction is catalysed by catalase ($6 H_2O_2 \Rightarrow 3 O_2 + 6 H_2O$) and the importance of this enzyme is reflected in the fact that it has one of the highest specific activities (i.e. catalytic turnover) known (Voet and Voet, 1990). Glutathione peroxidase is a selenium-containing enzyme that is the major enzyme involved in removing intra-cellularly generated lipid peroxides but also has an important role in removal of hydrogen peroxide (Iizawa *et al.* 1994). Glutathione is the unique hydrogen donor to glutathione peroxidase and depletion of glutathione strongly sensitises fibroblasts to UVA (Applegate *et al.* 1992). H_2O_2 may react with DNA directly (specifically the adenine moiety (Cadet, 1994) but it also produces hydroxyl radicals through the interaction with superoxide in the Haber-Weiss and Fenton reactions (Wiseman and Halliwell, 1996). This idea is supported by the

evidence that chelating iron in an inactive complex with o-phenanthroline completely eliminated H_2O_2-induced strand breakage (Melho-Filho and Meneghini, 1984; Jornot *et al.*, 1991). Hydrogen peroxide induces both SSB and double strand breaks (DSB) (Friedberg *et al.* 1995) in mammalian cells and is certainly responsible for some of the strand breaks reported in this study.

1.3.3.4 Hydroxyl radical ($\bullet$OH)

Hydroxyl radical ($\bullet$OH) can be generated by the transition metal-catalysed Haber-Weiss reaction from H_2O_2 and $\bullet O_2^-$ thus

$$Fe^{2+} \quad + \quad H_2O_2 \quad \longrightarrow \quad Fe^{3+} \quad + \quad OH^- \quad + \quad \bullet OH \quad \text{Eqn 1}$$

$$Fe^{3+} \quad + \quad \bullet O_2^- \quad \longrightarrow \quad Fe^{2+} \quad + \quad O_2 \quad \text{Eqn 2}$$

$$\bullet O_2^- \quad + \quad H_2O_2 \quad \longrightarrow \quad OH^- \quad + \quad O_2 \quad + \quad \bullet OH \quad \text{Eqn 3}$$
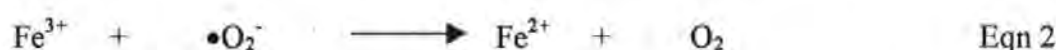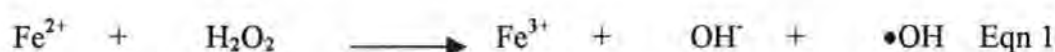
The sum of reaction (1) and (2) is reaction (3) (the Haber-Weiss reaction). The hydroxyl radical is extremely reactive (Halliwell and Aruoma 1991). The formation of hydroxyl radicals in close proximity to DNA can result in a large number of strand breaks (Peak and Peak, 1990). Protein-iron and DNA-iron complexes can participate in Fenton-type reactions and DNA strand breakage by hydroxyl radicals occur on the chromatin (Mello Filho and Meneghini 1984, Mello Filho and Meneghini 1985). Hydroxyl radicals also produce alkali labile sites (Freidberg *et al.* 1995) and base hydroperoxides (Cadet, 1994).

1.3.3.5 The electronically excited oxygen molecule, singlet oxygen ($^1O_2$).

Singlet oxygen is produced by absorption of photic energy by ground state (triplet) oxygen. The excitation energy required to produce singlet oxygen is extremely low at ~ 90 kJ mol^{-1} (Cridland and Saunders, 1994) corresponding to a wavelength of ~ 1300 nm. This implies that singlet oxygen will be produced from many different sources in vivo.

50

This molecule has been clearly implicated in damage to cellular macromolecules including proteins, lipids, and nucleic acids (Cridland and Saunders 1994; Vile and Tyrrell 1995; Halliwell and Aruoma 1991; Tyrrell 1995; Runger et al. 1995;). $^1O_2$ selectively attacks guanine (Halliwell and Aruoma 1991) and is responsible for fibroblast inactivation by 365 nm, 334 nm, and 405 nm radiation (Tyrrell and Pidoux 1989).

The cellular response to singlet oxygen includes the activation of heme oxygenase (Basu-Modak and Tyrrell 1993) and the activation of the transcription factor AP-1 (Grether-Beck et al. 1996). Singlet oxygen produces SSB in DNA (Halliwell and Aruoma, 1991) by a Type II photosensitisation reaction (Pflaum et al., 1994), i.e. singlet oxygen is generated by UV interaction with endogenous Type I photosensitisers. In this respect, porphyrins (with an absorbance peak at 405 nm (Tyrrell, 1995)) are good candidates as a source of strand breakage via a Type II photosensitised reaction.

A more complete account of the effects of singlet oxygen can be found in the reviews by Cerutti (1985); Tyrrell (1994), Chen et al. (1995) or Wiseman and Halliwell (1996).

1.3.3.6 Lipid Peroxidation

Free radical (•R) attack upon polyunsaturated acids (PUFA) yields lipid radicals (PUFA•)

$$•R \ + \ PUFA \longrightarrow PUFA• \ + \ RH$$
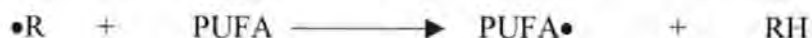
The PUFA radical can react with molecular oxygen to form peroxy radicals and by self-propagating chain reactions with adjacent PUFA form hydroperoxides.

$$PUFA• \ + \ O_2 \longrightarrow PUFA \ + \ PUFA\text{-}O\text{-}O \longrightarrow PUFA\text{-}O\text{-}OH \ + PUFA•$$
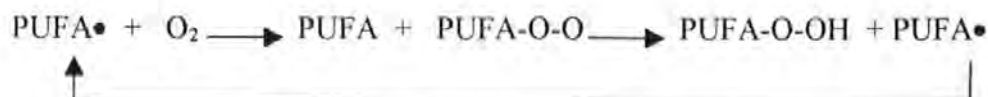
Lipid peroxidation is also caused by derivatives of the essential fatty acid arachidonic acid via UVR-activation of phospholipase A_2 by the same general reaction scheme.

Termination reactions include, for example, the Russell-type interaction between two

peroxyl radicals to form non-reactive end products (Burcham, 1998) or interactions with chain breaking antioxidants (Black, 1987; Burcham, 1998).

Of direct relevance to this work, millimolar amounts of hydrogen peroxide are generated by UVR (Tyrell and Pidoux, 1989) and cause extensive lipid peroxidation in rat hepatocytes (Pitot and Dragan 1991), lipid peroxidation is a likely cellular consequence of singlet oxygen generation and is an early event in UV-irradiated skin (de.Gruijl 1995). Lipid peroxides and hydroperoxides cause DNA strand breaks in human lymphocytes and fibroblasts (Burcham, 1998).

1.4   SUMMARY OF CONTENTS

The Thesis is structured as follows. Chapter 1 outlines the background processes of melanomagenesis and oxidative damage. The principles of the assay employed in the investigation, single cell gel electrophoresis (the 'comet assay') and the formation and nature of the lesions it measures (SSB) are introduced. Chapter 2 describes the various methods (and their development) employed in this work. Chapter 3 describes the results of *in vitro* melanocyte culture and includes a previously unreported technique for the potential culture of cells from an explanted naevus. Chapter 4 describes the dose responses of normal and tumour cells to low levels of UVA and UVB and to higher levels of unfiltered Xe lamp radiation. These data are discussed in Chapter 5. Chapters 6 and 7 report and discuss the modulation of the cells' responses to oxidative stress by prior exposure to prooxidant and antioxidant molecules. Chapters 8 and 9 describe the effects on DNA repair by inorganic arsenic, a skin carcinogen. The first section of Chapter 10 discusses the two readback systems employed in this work: a simple visual technique and an image analysis method. The second part of Chapter 10 introduces a new image analysis parameter – the Area Moment. This parameter appears more suited to the measurement of low dose phenomena than existing parameters and its use enabled the achievement of

statistical significance in one borderline experiment, where existing parameters failed in this respect (Section 10.2.4).

2 CHAPTER 2.

MATERIALS AND METHODS

2.1 ULTRAVIOLET IRRADIATION AND DOSIMETRY

The focus of this work was the study of the effects of Ultra Violet Radiation (UVR) in

cultured mammalian cells. The UVR source was a 150 W XBO xenon arc lamp (Applied

PhotoPhysics Ltd. UK). It was purchased second hand from Glynn Research Laboratories

(Bodmin, UK) and without an operating visual or technical information, hence it was

necessary to characterise this lamp as a radiation source. The irradiation array for the

delivery of UVR to the cells under test was designed, constructed and developed as part of

the work described in this thesis. This process is described in Appendix A.

2.1.1 The construction of the irradiation array

A schematic cartoon of the irradiation array is given in Figure 2.1. The array was

comprised of the lamp power pack upon which rested the lamp housing itself. An X-Y

plotter was placed immediately in front of the power pack and directly below the light

beam. A concave mirror (from an old spectrophotometer) was clamped in the centre of the

light beam focusing the beam onto a plywood lid that had been made to fit the X-Y plotter.

The lid had a 20 mm hole bored approximately 1/3 of the length and 1/2 of the width,

making it reversible. In the first position the light beam travelled 30 cm from the exit slit,

in the second position, 40 cm. The lid was made to be removable to facilitate the placing

of a cell culture plate onto the bed of the X-Y plotter. The position of the irradiation beam

was marked onto the black card. The sample to be irradiated was placed centrally on this

mark.

Figure 2.1

The construction of the irradiation array
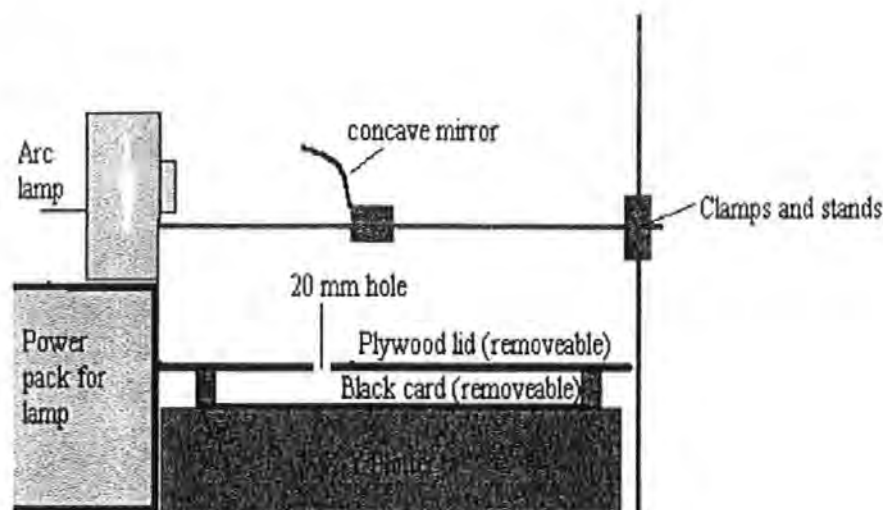
2.1.2   Delivery of unfiltered radiation

The delivery of unfiltered radiation was effected in two ways.

Either by placing the sample to be irradiated

(1)   below the 20 mm hole in the lid in which case a small circle of

approximately 25 mm in diameter could be irradiated or,

(2)   above the hole in which case an area of up to 25 cm^2 could be

irradiated.

2.1.3   Delivery of narrow band pass filtered radiation

Narrow band pass filters (Coherent-Ealing Ltd. UK) were used to transmit only 405 ± 5 nm

or 310 ± 5 nm radiation. The delivery of narrow band pass filtered radiation was effected

by the placing of an appropriate filter immediately above the hole with the sample to be

irradiated directly below. The non-linear nature of the radiation source would be expected

to result in a non-uniform radiant intensity over the irradiating area. This was measured by

radiometry after 405 nm narrow band pass filtering in 8 areas of the irradiation bed. The

use of narrow band pass interference filters permit the transmission of a narrow bandwidth

of radiation. The nature of the filters means that transmitted radiation is usually attenuated to between 10 and 15 % of the incident radiation of the desired wavelength. The wavelengths chosen for the initial investigations were 405 nm (UVA / violet) and 310 nm (UVB). The transmitted radiant intensities were measured by radiometry.

2.1.4 Radiometry

2.1.4.1 The MP200 radiometer

The MP200 Intellirad (Micropulse, UK) radiometer is a radiometer attachment for use with a Psion pocket computer. It has the facility of removable and interchangable sensors. It is powered by battery and is thus portable. It was used to provide rapid assessment of the XBO lamp output at the irradiating wavelengths prior to exposing the cells the radiation source. It was compared with actinometric measurements and found to be in close accord (Section 11.2.3.1.5).

2.1.4.2 The MP-231 UV-B sensor and the MP240 violet sensor

The MP-231 UV-B (Micropulse, UK) sensor and the MP-240 (Micropulse, UK) violet sensor are precision devices designed to measure UVR between 280 nm to 330 nm (MP-231) and visible radiation between 400 nm and 420 nm (MP-240). They are used with the MP-200 IntelliRad radiometer. Design accuracy is ± 5% of indicated readings and repeatability is better than ± 1% of indicated readings. Temperature dependence is ± 0.25% per °C from 0 °C to 40 °C. The response spectra for these two radiometer sensors are given in Figure 2.2.

Figure 2.2. The response curves of the MP-231 UV-B sensor (top) and the MP 240

Violet sensor (bottom)
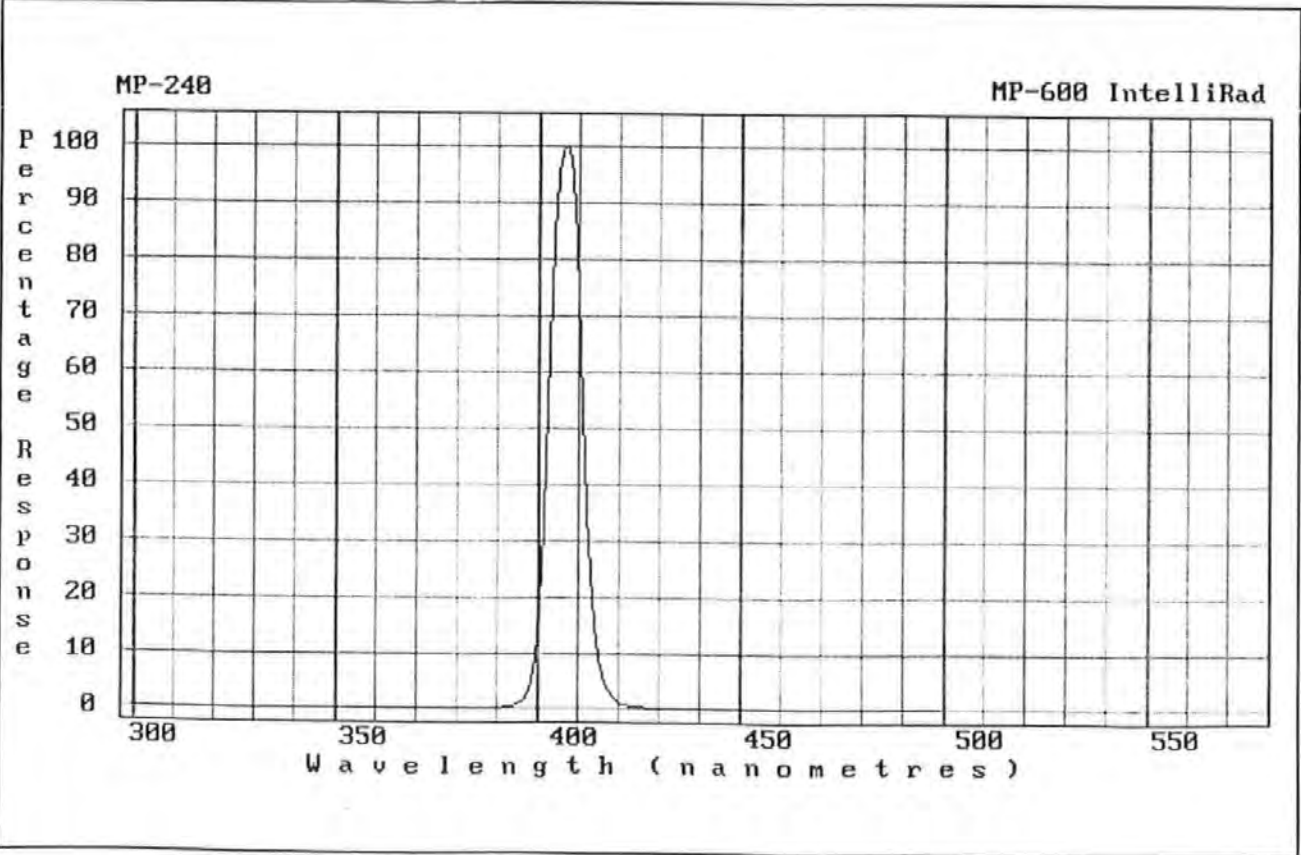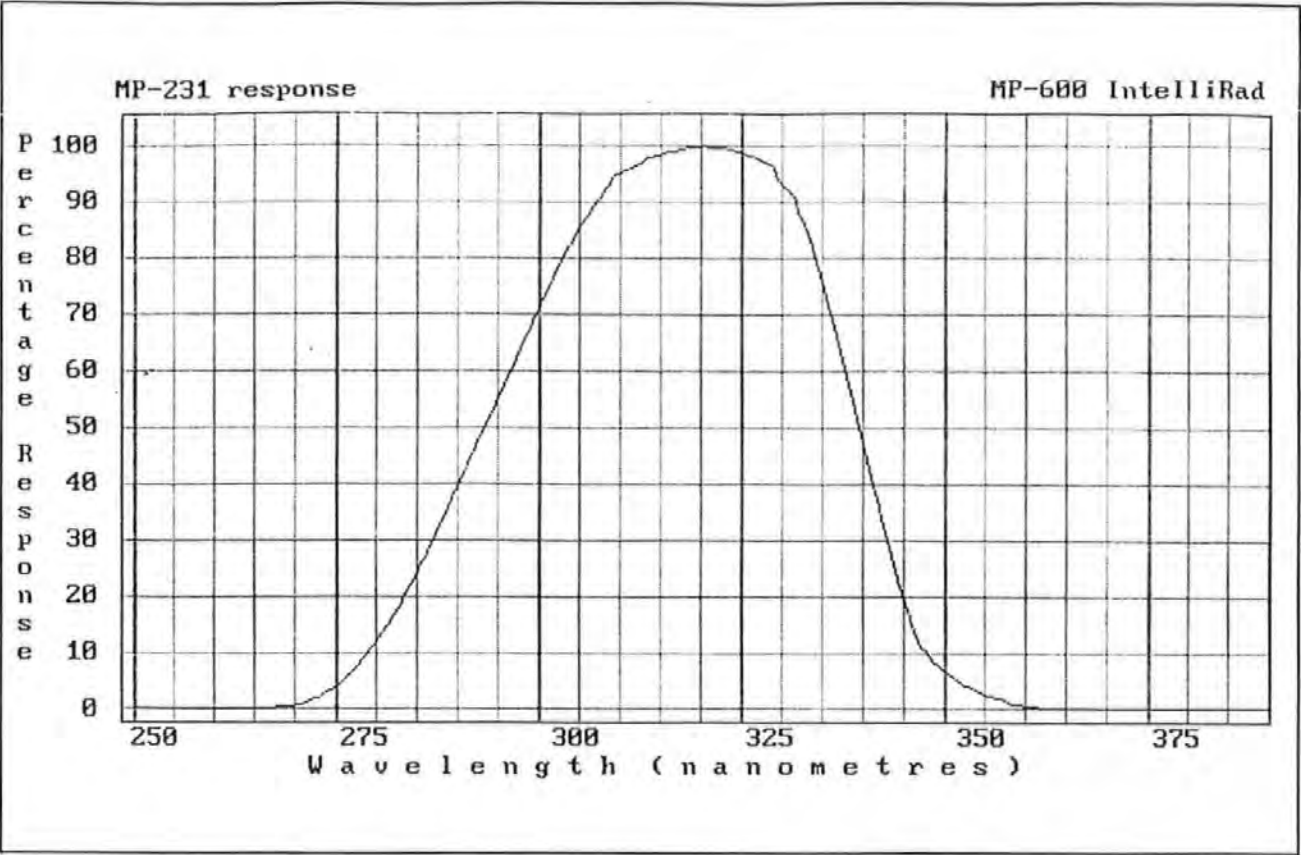
2.2 CELL CULTURE

2.2.1 Culture routines

2.2.1.1 Maintenance

All manipulations of cells were carried out in a class II laminar flow cabinet (Bio 2+,

Envair Ltd, England UK.). 10 ml and 1 ml sterile disposable pipettes were used once and

discarded into a 10% Chloros (supplied by the PHLS as part of the leasing arrangements)

solution. Sterile tissue culture flasks (Corning) of the non-vented type in sizes: 25 cm^2

(T25), 75 cm^2 (T75) and 150 cm^2 (T150) were used. Where multiwell plates were used for

cell culture they were incubated in a 5% carbon dioxide-in-air mix (BOC special gases,

UK), 100% humidity atmosphere inside a sealed plastic container. Exhausted medium and

'washings' were discarded into 20% Chloros by a vacuum aspirator. Incubation at 37 °C

was carried out in a dry incubator (Gallenkamp) at 37 ± 0.5 °C. Sterile technique was

practised at all times.

Normal (MRC 5) and Simian Virus transformed (MRC5 SV2) foetal lung fibroblasts,

A2058 metastatic melanoma cells, PUTKO hybrid leukaemia cells and DOK (Dysplastic

Oral Keratinocyte) cells were obtained from European Collection of Animal Cell Cultures,

Porton Down, UK. MRC5 were obtained in passage 18. All cells were grown to sufficient

numbers, and stocks were preserved in liquid nitrogen in the laboratory. A2058, MRC5,

and MRC5 SV2 were maintained in Dulbecco's Modified Eagles Medium (DMEM)

supplemented with 4 mM L-Glutamine (L-Glu) and 10% Fetal Calf Serum (FCS). The

concentration of L-Glu was raised to 4 mM as the slow turnover of media in the laboratory

could have resulted in nutrient starvation due to the decomposition of L-Glu during

storage. MRC 5 cells were, on average, split 1/3 once weekly. MRC 5 SV2 cells were, on

average, split 1/10 twice weekly. A2058 cells were, on average, split 1/8 weekly. DOK

were maintained in the above media but with the necessary addition of 5 μg/ml

hydrocortisone and were split 1/6 approximately weekly. PUTKO were maintained in RPMI (Roswell Park Memorial Institute) 1640 medium supplemented with 10% FCS + 4 mM L-Glu and were split 1/10 approximately 2-3 times weekly. Antibiotics were not used in routine culture in this laboratory.

2.2.1.1.1 Maintenance of adherent cells

Adherent cells were passaged as follows. When the cell monolayer was fully confluent, the monolayer was washed twice in PBS(t) and 1 ml of 0.25% trypsin/ EDTA added to the flask. The monolayer was incubated for 1 minute at 37 °C, after which time the trypsin/EDTA was removed. The flask was incubated (the activity of trypsin is temperature dependent) for a further 2 minutes (A2058) or 6 minutes (MRC5, MRC5 SV2) or 15 minutes (DOK). These times had been found to be the minimum times that would separate the cells from the culture flask. The trypsinisation reaction was arrested by the addition of 10-12 ml DMEM + 10% FCS. The cell suspension was then split as required into separate flasks, with surplus cell suspension disposed of by pipetting into a 10% Chloros solution. The flasks were then topped up with the appropriate culture medium to 10 ml (for a 25 cm^2 flask), 25 ml for a 75 cm^2 flask or 60 ml for a 150 cm^2 flask. The air in the flask was replaced with a 5% carbon dioxide-in-air mix and the cells returned to the 37 °C incubator .

2.2.1.1.2 Suspended cells

The suspension cell line PUTKO was passaged in a similar manner to adherent cells (Section 2.2.1.1.1) with the exception that the trypsinisation stage was omitted as the cells were already a single cell suspension, the cells were split 1/10 directly from the culture flask.

2.2.1.2 Human cell cultures used in this study

2.2.1.2.1 MRC5

MRC5 fibroblasts were established from the normal lung tissue of a 14 week male foetus

They are contact inhibited and senesce after approximately 60 population doublings. They

have a normal diploid karyotype (ECACC data sheet).

2.2.1.2.2 MRC5 SV2

MRC5 SV2 were derived from MRC5 by transformation with the SV40 virus. They are

not contact inhibited and they do not senesce. They have a hyperdiploid karyotype with a

modal number of chromosomes between 60 and 80 (ECACC data sheet).

2.2.1.2.3 A2058

A2058 metastatic melanoma cells were established from a lymph node deposit in a 76-

year-old male. They are not contact inhibited and they do not senesce. The cells produce

melanin (ECACC data sheet).

2.2.1.2.4 PUTKO

PUTKO were created by fusion of two human cell lines: K562 (isolated from the pleural

effusion of a 56 year old female with chronic myelogenous leukaemia in terminal blast

crisis) and P3-HR1 (clonally derived from the cell line JIYOYE which was derived from

the ascitic fluid of an African boy with Burkitts Lymphoma). PUTKO carry the Epstein-

Barr Virus genome (approximately 26 copies per cell). They do not senesce (ECACC data

sheet).

2.2.1.2.5 DOK

DOK (Dysplastic Oral Keratinocyte) were established from the tongue of a 57 year old man who was a heavy smoker. The cells are not contact inhibited and display some stratification in culture. They are aneuploid (ECACC data sheet).

2.2.1.2.6 OLL1M (Old Lady's Leg, donor 1, Melanocytes)

OLL1M normal human melanocytes were cultured in this laboratory from a benign naevus on the leg of a 75 year old lady. The cells displayed motility in explant culture (Section 3.2).

2.2.1.2.7 MMB4L (Middle aged Man's Blood, donor 4, Lymphocytes)

MMB4L normal human lymphocytes were obtained from whole blood taken from a 38 year old male.

2.2.1.2.8 YLB7L (Young Lady's Blood, donor 7, Lymphocytes)

YLB7L normal human lymphocytes were obtained from whole blood taken from a 23 year old female.

2.2.1.2.9 YBF15F and YBF15M (Young Boy's Foreskin, donor 15, Fibroblasts and Melanocytes)

YBF15F normal human fibroblasts and YBF15M normal human melanocytes were cultured by the trypsin dissaggregation method (Section 2.2.1.3.1) from the foreskin of a young (prepubescent) boy.

2.2.1.2.10 YBF14M (Young Boy's Foreskin, donor 14, Melanocytes)

YBF14M normal human melanocytes were cultured by the epidermal / dermal separation method (Section 0) from the foreskin of a young (prepubescent) boy.

2.2.1.2.11 YBF17M (Young Boy's Foreskin, donor 17, Melanocytes)

YBF17M normal human melanocytes were cultured by the epidermal / dermal separation method (Section 0) from the foreskin of a young (prepubescent) boy.

2.2.1.3 Preparation of primary cultures

Three methods of tissue culture were used to generate primary cell cultures. Clinically normal skin from various surgical procedures at Treliske Hospital was obtained from the donor (or the donor's representative) after informed and written consent. Skin samples were collected in ice-cold PBS(t) and stored for no more than 2 hours at 4 °C.

2.2.1.3.1 Trypsin dissaggregation (ECACC 1996; E.Corley, personal communication)

The skin sample was cut into 1 cm x 2 cm pieces and twice washed in PBS(t). A 0.5% trypsin / 0.1% D-glucose solution was made up in Hams F12 medium and brought to pH 7.45 by the addition of 3.0 M sodium hydroxide solution. The washed skin sample was placed into a 60 mm tissue culture dish containing 5 ml of the trypsin / glucose solution and chopped into very small pieces using stainless steel tissue culture scissors. The sample was transferred to a 50 ml centrifuge tube, the remaining cells were collected from the dish in a further 5 ml of trypsin / glucose solution and added to the centrifuge tube. 20 ml of trypsin / glucose solution was added to the tube and vigorously shaken. The tube was incubated for 2 hours at 37 °C with vigorous shaking every 15 minutes. After 2 hours the cell / tissue suspension was disaggregated through a 50 mesh cell dissociation sieve into a sterile 60 mm dish. The resulting cell suspension was transferred to a fresh 50 ml centrifuge tube. The dish and sieve were washed with 10 ml DMEM + 10% FCS, this was then added to the centrifuge tube. A further 20 ml of DMEM + 10% FCS was added and the cells were pelleted by centrifugation. The cell pellet was washed twice in 20 ml DMEM + 10% FCS, resuspended in the appropriate growth medium and plated into a T25. The flask was gassed with 5% CO_2 and incubated at 37 °C. After 24 hours the liquid in the

flask containing non-attached cells and tissue debris was tipped into 10% Chloros. The adherent cells were gently washed in PBS(t) and 6 ml of fresh medium added. The medium was changed again after 3 days.

2.2.1.3.2 Epidermal separation (Hedley *et al.* 1996)

The skin sample was trimmed of excess fat and cut into 0.75 cm x 0.75 cm pieces and washed twice in PBS(t). A 0.1% trypsin / 0.1% D-glucose solution was made up in PBS(t) and adjusted to pH 7.45 with 3.0 M sodium hydroxide; 5 ml of this trypsin solution was added to 60 mm tissue culture dishes. Two pieces of skin were added to each dish and placed in the fridge (4 °C) overnight. After an incubation period of approximately 18 hours the skin samples were transferred to a dish containing 2 ml MCDB 153 medium + 10% FCS. The epidermis and the dermis were separated with forceps. The basal side of the epidermal sheet and the upper side of the dermis were gently scraped into the media with a scalpel blade. The dermis and epidermis were then washed in 2 ml of MCDB 153 + 10% FCS. The cell suspension was transferred to a 50 ml centrifuge tube. This process was repeated for each piece of the skin sample. The cell suspensions were pooled and centrifuged; the resulting cell pellets were pooled, counted and plated in 6 ml of medium at a density of approximately 2×10^6 cells in a T25. The flask was gassed with 5% CO_2 and incubated at 37 °C for 24 hours. The liquid in the flask containing non-attached cells and tissue debris was tipped into 10% Chloros. The adherent cells were gently washed in PBS(t) and 6 ml of fresh medium added. The medium was changed again after 3 days.

2.2.1.3.3 Explantation (based on a method in Burt 1996; ECACC 1996)

Small (0.75 cm x 0.75 cm) pieces of skin were trimmed of fat and washed in PBS(t). The explant was placed in a drop of FCS and placed epidermal side up in a 25 cm^2 tissue culture flask. This flask was inverted and incubated for 3 hours at 37 °C. 1 ml of growth medium was added so that the edges of the explant were surrounded by medium with the epidermal surface at the gas/liquid interface. The air in the culture flask was replaced with

a 5% carbon dioxide in air mix and incubated at 37 °C. The media was changed after 7

days. The culture was incubated for a further month. For histological examination the

specimen was lifted, washed in PBS, fixed in formalin and routinely processed. It was

stained in Haemotoxylin and Eosin and Masson-Fontana and was stained for S-100 protein

using standard immunohistochemistry (R. Marshall, histology report, Specimen 'DG1',

Treliske Hospital, 1998).

2.2.1.4   Types of media used for the culture of melanocytes

2.2.1.4.1   M1669

This is a commercially available medium manufactured by Sigma. It is a modified version

of MCDB 151 and MCDB 104, and is supplemented with bovine pituitary extract, foetal

bovine serum, bovine insulin, bovine transferrin, basic fibroblast growth factor,

hydrocortisone, heparin and phorbol 12-myristate 13-acetate. The concentration of these

reagents is withheld as a trade secret. It was variously supplemented in this laboratory

with the antimycotic Nystatin (10 IU / ml) and the antibiotics Penicillin (100 IU / ml) +

Streptomycin (100 µg / ml) and 4 mM L-Glu as required.

2.2.1.4.2   MC1x

MC1x is the name given in this laboratory to the melanocyte growth medium developed by

S. Hedley at the University of Sheffield (Hedley *et al.* 1996; S.Hedley, personal

communication). (MC2x is the same medium with a 2-fold increase in growth

supplements and was developed and used in this laboratory in an attempt to improve

plating efficiency of melanocytes from elderly donors.) MC1x is a growth medium based

on MCDB 153 and supplemented with the following: 2% FCS, 25 µg/ml bovine pituitary

extract, 10 µg/ml bovine insulin, 10 µg/ml human apo-transferrin, 2.8 µg/ml

hydrocortisone, 6 mM L-Glutamine, 100 IU/ml penicillin, 100 µg/ml streptomycin,

10 U/ml nystatin, 10 nM phorbol 12-myristate 13-acetate, 0.6 ng/ml basic Fibroblast Growth Factor.

The supplements were made up into stock solutions and aliquots of the stock solution were stored in Eppendorf tubes at -20 °C. These aliquots of the stock solutions were subsequently diluted to working solutions as necessary. Aliquots of the working solutions were added to the basal medium to make up the final concentrations. The stock solutions were made up as follows:

5 mg bovine pituitary extract was dissolved in 1 ml 0.85% sodium chloride, aliquots of 500 µl were added to 100 ml of media or stored at -20 °C. Insulin was dissolved in 50 mM hydrochloric acid to a concentration of 50 mg / ml, aliquots of 20 µl were added to 500 ml of media (4 µl to 100 ml of media) or stored at -20 °C. Apo-transferrin was dissolved in PBS(t) to a concentration of 50 mg / ml, aliquots of 20 µl were added to 500 ml of media (4 µl to 100 ml of media) or stored at -20 °C. Hydrocortisone was dissolved in denatured ethanol to a concentration of 4 mg / ml, aliquots of 70 µl were added to 100 ml of media or stored in aliquots of 100 µl at -20 °C. 1 mg phorbol 12-myristate 13-acetate (PMA) was dissolved in 811 µl denatured ethanol to a concentration of 2 mM. Aliquots of 100 µl were stored at -20 °C. A working solution was made up by the dilution of 100 µl stock solution in 20 ml PBS(t) to a concentration of 10 µM; aliquots of 100 µl of this 10 µM working solution were added to 100 ml of media or stored at -20 °C. 25 µg basic fibroblast growth factor was dissolved in 1 ml PBS(t); aliquots of 25 µl were diluted in 1 ml PBS(t). 100 µl of this working solution were added to 100 ml of medium or stored at -20 °C. Nystatin was suspended at a concentration of 10^5 IU / ml. Aliquots of 10 µl were added to 100 ml of medium as required or stored in aliquots of 1 ml, 500 µl and 100 µl at -20 °C. L-glutamine was supplied as a 200 mM stock solution; aliquots of 3 ml or 2 ml were added to 100 ml medium to give a final concentration of 6 mM or 4 mM respectively. Penicillin

and streptomycin were supplied (or made up in tissue culture grade sterile water) as a 100x mixture; 5 ml of this mixture was added to 500 ml of media as required.

2.2.1.5 Normal human melanocytes: trypsin dissaggregation method.

The cell suspension generated by trypsin dissaggregation (Section 2.2.1.3.1) was centrifuged and resuspended in 6 ml of melanocyte growth medium. The medium was replaced after 72 hours and once weekly after that. The culture was otherwise left undisturbed for 7 weeks.

2.2.1.6 Normal human melanocytes: epidermal separation method.

The epidermal cell suspension generated by this method was centrifuged and plated out in 6 ml of melanocyte growth medium. The media was changed at 24 hours and at 3 days. The cells were subsequently fed twice weekly by replacing 3 ml of the medium in the flask with 3 ml of fresh medium. Cells were split 1/2 at the first passage (after approximately one month in culture). Fibroblast contamination of melanocyte cultures was treated as follows. Cells in passage 1 were split 1/3 into a T25 and incubated for 24 hours in DMEM + 10% FCS + 4 mM L-Glu + Nystatin (10 IU / ml) + Penicillin (100 IU / ml) + Streptomycin (100 µg / ml). This medium was then replaced by DMEM + 10% FCS + 4 mM L-Glu + Nystatin (10 IU / ml) + Penicillin (100 IU / ml) + Streptomycin (100 µg / ml) supplemented with 200 µg / ml geneticin sulphate and incubated for a further 5 days. The medium was then removed and the remaining cells washed twice with PBS(t). 6 ml of melanocyte growth medium was added and the cells fed twice weekly thereafter. It was necessary to repeat this treatment for some cultures because some fibroblasts remained; sometimes leading to the loss of entire melanocyte cultures.

2.2.1.7 Indirect Immunofluorescence

The culture of melanocytes by the cell culture methods described above was verified by fixed cell immunofluorescence (Normal operating procedure, PHLS procedures manual)

66

in situ fluorescence (based on Herbold *et al.* 1996). Mouse IgG anti S-100 (β-subunit) was used to identify melanocytes, a pool of clones containing mouse IgG anti-cytokeratins was used to identify keratinocytes, mouse IgG anti-actin was used as a positive control, FITC conjugated goat anti-mouse IgG (whole molecule) was used as the secondary antibody.

2.2.1.7.1 Fixed cell immunofluorescence

Fixed cell immunofluorescence was performed using 15 well slides designed for the purpose. A2058 melanoma cells, DOK keratinocytes and MRC5 SV2 fibroblasts were lifted by minimal trypsinisation, washed in DMEM + 10% FCS, centrifuged and resuspended at a cell density of approximately 1 million cells per ml. 20 μl aliquots of each cell suspension were added to a different column (3 wells) of the 15 well slides and air dried in the class II cabinet (see Table 2.1). When fully dried the slides were immersed in acetone for 10 minutes. The slides were washed in PBS and wrapped back-to-front in silver foil and stored at -20 °C until use.

Fixed cell immunofluorescence was performed on melanocyte cultures after geneticin sulphate treatment to remove fibroblasts. The monolayer was lifted with minimal trypsinisation, washed in DMEM + 10% FCS, centrifuged and resuspended at a cell density of approximately 100,000 cells per ml. 20 μl aliquots of this cell suspension were added to 5 of the remaining 6 wells of the prepared 15 well slide and air dried. The slide was then immersed in acetone for 10 minutes and washed in PBS. The prepared slide was placed in the 37 °C incubator until completely dry. The primary antibodies were applied to the prepared slide in rows. 20 μl of each antibody solution was pipetted onto each of the cell types in the same row (see Table 2.1). The slide was then placed into a closed container containing damp tissues and incubated at 37 °C for 1 hour. The slide was then washed twice in PBS and dried in the incubator as before. 20 μl of the secondary antibody solution was applied to each well and incubated in the closed container for 1 hour. The

slide was then twice washed in PBS and examined under the fluorescence microscope

(Section 2.3.4.2.1). Images were captured by the image analysis equipment (Section

2.3.4.2.1).

Table 2.1 The prepared slides for immunofluorescence. The wells of the 15-well slide were prepared for fixed cell immunofluorescence by the application of the cell types indicated in the top line of each section. Primary antibodies (indicated in the bottom line of each section) were applied to each well as indicated.

A2058	DOK	MRC5 SV2	Cell culture	Cell culture
α S-100	α S-100	α S-100	α S-100	α S-100
A2058	DOK	MRC5 SV2	Cell culture	Cell culture
α cytokeratin	α cytokeratin	α cytokeratin	α cytokeratin	α cytokeratin
A2058	DOK	MRC5 SV2	Cell culture	Cell culture
α actin	α actin	α actin	α actin	2° Ab only

2.2.1.7.2 In situ fluorescence

In situ fluorescence was used to confirm the presence of growing melanocytes in culture.

A proliferating melanocyte culture (i.e. after geneticin sulphate treatment) was selected. In

the class II cabinet the medium was removed and the cells washed in PBS. A fresh layer

of PBS was added to the flask for protection during the following procedure. The

monolayer was exposed by cutting the upper face away from the flask using a hot nail.

The cells were washed twice in PBS and 0.5 ml of primary antibody (α S-100 β subunit)

solution was added to the cells and left in the class II cabinet for 2 hours. The cells were

washed twice in PBS and 0.5 ml of diluted secondary antibody (FITC conjugated goat α

mouse IgG (whole molecule)) added to the cells and left in the class II cabinet for 2 hours.

The cells were then washed twice in PBS and examined with the fluorescence microscope

68

(Section 2.3.4.2.1). The images were captured by the image analysis equipment (Section 2.3.4.2.1).

2.2.1.8 Cryopreservation and resuscitation (ECACC 1996)

Cells to be cryopreserved were grown to confluence and then split 1/2 into 2 x T25s. The flasks were grown until 80-90% confluent, lifted with trypsin/EDTA and resuspended in DMEM + 10% FCS. The cell suspension was centrifuged and resuspended in 1 ml cryopreservation media (DMEM + 20% FCS + 10% DMSO + Penicillin (100 IU / ml) + Streptomycin (100 µg / ml) at 4 °C and placed into a 1.5 ml cryopreservation vial. The vial was labelled with cell line, passage number and date of preservation. The vial was then wrapped in multiple (>20) layers of tissue and placed at -80 °C over night. It was transferred to liquid nitrogen the following day and a record made of its location. Cells were resuscitated thus. The vial was retrieved from liquid nitrogen and placed into the 37 °C incubator and thawed as quickly as possible. When thawed, the vial was wiped with IMS and allowed to dry. The contents of the vial were then transferred to a T25 containing the resuscitation growth medium (DMEM or RPMI + 20% FCS + Penicillin (100 IU / ml) + Streptomycin (100 µg / ml)) that had been previously gassed with 5% CO_2 and incubated at 37 °C for 1 hour. The flask was re-gassed and incubated for a further 3 hours. For adherent cells, the medium was then carefully removed and replaced with the normal growth medium with antibiotics for that cell type, gassed and incubated at 37 °C. (For suspension cells, the resuscitation medium was removed during passage.) The flask was labelled with the cell line, passage number and date of resuscitation before being returned to the incubator.

2.2.1.9 Trypan blue exclusion test for cell viability

Counting of viable cells was performed thus. The cells to be counted were suspended in a carefully measured amount of liquid (either media or PBS depending on the application).

69

A 50 µl aliquot of this suspension was removed and added to one well of a 96 well plate. Using a fresh pipette tip, 50 µl of trypan blue stock solution was added to this well and mixed. Both chambers of a silvered haemocytometer were filled with this mixture. The cells were counted using an inverted microscope. The squares etched into the haemocytometer have a volume of 10^{-4} cm^3. At least 200 cells were counted per chamber, and the mean number of cells per square calculated. This number was multiplied by the trypan blue dilution factor (2) to give the cell density (in cells / ml) of the cell suspension. The total number of cells was calculated from the known volume of the suspension if necessary.

Trypan blue does not immediately penetrate viable cells but non-viable cells are stained blue. The ratio of unstained cells to total cells gave a measure of culture viability and was used to calculate seeding numbers. It was necessary to include non-viable cells in the count for the preparation of comet assay slides: non-viable cells still produced comets and failure to take this into account resulted in overcrowding and the loss of sensitivity of the assay (Section 2.3).

<u>2.2.1.10 Cytotoxicity</u>

<u>2.2.1.10.1 Growth kinetics and cell survival</u>

Cells were counted in triplicate prior to treatment and viability recorded. After treatment, the cells were counted and a record made of viability. Percent viability was recorded against treatment regime. Alternatively, viable cells were counted by Trypan blue exclusion in triplicate at a number of time points during serial culture of the cells. A comparison was made between treated and non-treated cells.

<u>2.2.1.10.2 Cytotoxicity in situ</u>

MRC5 normal fibroblast cells were seeded into separate T25 flasks and grown to either semi-confluence (to test for cytotoxic effects on dividing cells) or to full confluence (to test

for cytotoxic effects on non-dividing cells). MRC5 cells were chosen as these cells display contact inhibition of growth (ECACC data sheet). The cytotoxic agent under test was applied to these flasks at a range of doses. The range was initially based on values suggested by the literature (for example in Applegate *et al.* 1996; Lavker and Kaidbey 1997, Cridland and Saunders 1994) , and subsequently at experimentally-derived concentrations or doses.

The cytotoxicity-in-situ method was used to study the effects of UVR in two ways. Firstly, by placing a flask of cells directly over the irradiation aperture, it was possible to irradiate an entire T25 monolayer with unfiltered radiation. The 405 nm narrow band pass filter (50 mm x 50 mm) was approximately the same size as the growth area of a T25 and hence it was therefore possible to treat a whole T25 monolayer with 405 nm radiation. (It was not possible to do this with the 25 mm circular 310 nm filter.) Secondly, by placing the flask of cells under the 20 mm hole it was possible to treat a defined area of the monolayer (an approximately 25 mm diameter circle) with unfiltered or 405 nm or 310 nm narrow band pass filtered radiation. Overlapping these circles enabled the examination of combinations of the irradiating wavelengths and doses and the inclusion of the chemical modulants (e.g. arsenic, Chapter 8) in the culture flasks made it possible to examine the cells for indications of additive or synergistic effects of UVR and the modulant.

After these combination treatments and at the end of the testing period, the monolayer was washed twice in PBS and examined for a range of cytotoxic effects as follows. First, the monolayer was examined for 'holes' in the confluent sheet and compared to the untreated cells. Second, the monolayer was examined under an inverted microscope for morphological abnormalities. Third, 500 µl trypan blue stock solution was applied to the monolayer for two minutes. The monolayer was rinsed twice in PBS, and the flask was examined by eye and by microscopy. Finally, a semi-quantitative estimate of cytotoxicity was made using the above three parameters.

2.3 SINGLE CELL GEL ELECTROPHORESIS (THE 'COMET ASSAY')

2.3.1 Assay techniques

2.3.1.1 Overview of Comet assay procedure

Single cell gel electrophoresis is a highly sensitive and versatile assay for the measurement of clastogenicity at the single cell level (Section 2.3.1.1.1). In this work the assay was employed in various forms. In overview, cells to be assayed were either embedded in agarose gel before irradiation, or they were irradiated as a single cell suspension or a monolayer before embedding in agarose. The reasons for the variation in methodology are explained in the sections below. After treatment, agarose embedded cells were lysed in situ, and (after the naked DNA had been allowed to unwind in a highly alkaline buffer) electrophoresed. High molecular weight DNA was trapped in the peri-nuclear space whereas low molecular weight DNA migrated towards the anode. After staining and visualisation by fluorescence microscopy the DNA resembles a comet (Figure 2.4). The 'comets' referred to throughout this thesis are the products of the above procedure for a single cell.

2.3.1.1.1 Comet assay procedure: slide preparation (Green et al. 1996)

The method is an adaptation of the method developed by Singh et al. (1988). In overview, the cells to be analysed were plated out in a T75 tissue culture flask two or three days before the assay was due to be performed. They are seeded at a density such that the monolayer was confluent and the media in good condition when the assay was performed. The whole assay was performed under safelight conditions.

The assay slide base layer agarose (0.6% Type I agarose in DMEM without phenol red) was prepared immediately before the cells were lifted. The top layer agarose (1.2% LMP agarose in DMEM without phenol red) was prepared at the same time and stored in the 37 °C incubator. The base layer was applied by pipetting 100 μl of the molten base layer

72

agarose down a 20 mm x 20 mm cover slip onto a warm, dry, fully frosted microscope slide (Chance Propper Ltd. UK). The base layer was allowed to set at room temperature. The slides were labelled with a waterproof black marker pen.

The cells were lifted by minimal trypsin/EDTA treatment, washed in serum-containing media, washed twice in cold PBS and resuspended in PBS at a density of 6.25 x 10^5 cells/ml. Equal volumes of cell suspension (PBS) and top layer agarose (DMEM) were mixed. The cover slip was removed from the base layer and 65 μl of the top layer mixture applied to the base layer as before. The slide was placed on ice to set. The top layer thus consisted of a cell suspension in 0.6% LMP agarose in PBS/DMEM containing approximately 20,000 cells.

2.3.1.1.2 Comet assay procedure: lysis and electrophoresis

After treatment (see below, various sections) the assay slides were placed in ice cold lysis buffer (2.5 M NaCl, 100 mM Na_2EDTA, 10 mM Tris, NaOH to pH 10.0; 10% DMSO v/v and 1% v/v Triton X-100 were added immediately before use) for between 1 and 2 hours. They were then transferred to an electrophoresis tank where they rested in electrophoresis buffer (300 mM NaOH, 1 mM Na_2EDTA, pH 12.6) to allow the DNA to unwind and the residual lysis buffer and the electrophoresis buffer to equilibrate. After 30 or 40 minutes unwinding time the slides were electrophoresed at 20 V for 24 or 30 minutes. The slides were then neutralised with 2 ml of neutralisation buffer (400 mM Tris-HCl, pH 7.4) for 5 minutes followed by a further 1 ml for 5 minutes. The slides were then dried and stained with ethidium bromide (80 μg/ml), before being analysed by fluorescence microscopy. Comets were scored according to the methods described below.

2.3.1.1.3 Modulation of dose responses to UVR by exogenous chemicals

The cells were lifted by minimal trypsin/EDTA treatment, washed in serum-containing medium, and then resuspended in culture medium without serum to which any modulants

had been added or not. The cells were incubated in this media for the required time at 37 °C before being washed twice in cold PBS and resuspended in PBS at a density of 6.25 x 10^5 cells/ml. The cells were then assayed by one of the methods described below.

2.3.1.1.4 Statistical analysis of comets

The distribution of comets after treatment and single cell gel electrophoresis does not necessarily follow a Normal (Gaussian) Distribution, but the means of the distribution do. Hence for each experiment, at least 60 comets were analysed per slide and the mean value calculated for a number of parameters. To compare the effects of treatments, assays were performed in replicate (2-, 3-, or 6-fold) and the means for each replicate were calculated. These means and sample standard deviations were analysed by student t-test. The variances were analysed by f test and the appropriate form of the t-test employed. For some experiments which were not replicated, the distribution of comets at each dose or treatment were analysed by χ^2 test.

2.3.2 Irradiation procedures for the measurement of UVR-induced responses

2.3.2.1 Irradiation of cells suspended in agarose

The cells were lifted, washed, resuspended in agarose and applied to the base layer as described above. For irradiation, the coverslip was removed and the slide irradiated. The slide was then placed immediately into the lysis buffer (to measure SSB, Section 2.3.3.1) or treated further (to measure the repair kinetics, Section 2.3.3.2) and the lysis and electrophoresis procedure followed as above.

2.3.2.1.1 The fingerprick method of slide preparation.

This technique uses a suspension mixture of whole blood in LMP agarose as a top layer. A volunteer's finger is wiped with a sterile swab and a small prick is made in the finger using a sterile needle and fingerpricking device (Boehringer Mannheim) available 'over-the-

counter' for the purpose. 10 μl of the blood is removed by pipette from the surface of the skin and added to a 0.5 ml Eppendorf tube containing a heparin bead and 50 μl RPMI medium without phenol red that has been incubated at 37 °C. This process is repeated until enough cells have been collected. 10 μl of whole blood contains sufficient cells to make 2 assay slides. 60 μl of top layer (1.2% LMP agarose in RPMI without phenol red) is added to the tube and a top layer of 60 μl is applied to the slide. The cells were then treated and placed into lysis and the above lysis and electrophoresis procedure followed. This technique is quick and does not require cells cultured in vitro. It was used as a positive control for the apparatus in the first instance, and occasionally when cultured cells were not available for assay.

2.3.2.2 Irradiating cells suspended in a liquid

It was necessary to develop a protocol for irradiating single cell suspensions in tissue culture plates. It became apparent that the irradiation of individual slides could only be performed if the irradiation times were short (< ~ 2 minutes): to irradiate for longer would mean that the first slides irradiated would be in the lysis buffer for longer than the allowed 1 to 2 hours. The protocol was adapted based on the method of Klaude *et al.* (1996) such that after irradiation the damaged cells were suspended in LMP agar and placed in the lysis buffer when set (Section 2.3.3.1.2).

2.3.3 Assayed lesions of UVR-treated cells and the repair kinetics of the lesions

2.3.3.1 Assay of SSB of cellular DNA after UVR-treatment

The size of the nucleotide precursor pool in the experimental cells allows repair of cellular DNA and thus in order to measure low UVR dose phenomena a protocol had to be developed to take this into account. Repair could have been inhibited in a number of ways: incubation with aphidicolin has been reported (McKelvey-Martin *et al.* 1993), incubation on ice (McKelvey-Martin *et al.* 1993) also. These two methods permit excision but not the

rejoining of the induced strand breaks and they give a measurement of all excisable lesions, alkali-labile lesions and frank strand breaks. Protocols were developed which were judged most likely to give a measurement of SSB (Noz *et al.* 1996) including alkali labile lesions, independent of cellular repair processes, except where this was being measured.

2.3.3.1.1 Assays of lesions produced in cells suspended in agarose

The cells were lifted, washed, resuspended in agarose and applied to the base layer as described above. For treatment, the coverslip was removed and the slide irradiated. The slide was then immediately immersed into the lysis buffer and the lysis and electrophoresis procedure followed as above. This minimised repair times to around 8 to 10 seconds per slide.

2.3.3.1.2 Assays of lesions produced in cells suspended in liquid

The cells were lifted by minimal trypsin/EDTA treatment, washed in serum-containing medium, washed twice in cold PBS and then resuspended at a density of 6.25×10^5 cells/ml. Aliquots of these suspensions were pipetted into separate 24-well or 96-well tissue culture plates and placed at 4 °C until irradiated. Immediately after irradiation, the tissue culture plates were placed on ice, an equal volume of top layer 1.2% LMP agarose was added to the cell suspension, mixed and immediately applied to the base layer. The prepared slide was placed on ice and into lysis as soon as it had set.

2.3.3.2 Repair of UVR-induced SSB in cellular DNA

The repair of SSB is a rapid process with a half time of a few minutes (Collins *et al.* 1995). The SSB protocols described above were adapted to measure the SSB repair kinetics. This simply allowed a time of repair after irradiation, i.e. the repair process was arrested by placing the slide into the lysis buffer and the rest of the lysis and electrophoresis procedure followed (Section 2.3.1.1.2).

76

2.3.3.2.1 Repair of UVR-induced SSB in cells suspended in agarose

The cells were lifted, washed, resuspended in agarose and applied to the base layer as described above. For treatment, the coverslip was removed and the slide irradiated. The lamp shutter was closed after the irradiation period and the slide was allowed to repair for between 10 and 240 seconds at room temperature. The slide was then immersed into the lysis buffer at the end of the repair period and the lysis and electrophoresis procedure followed as above.

2.3.3.2.2 Repair of UVR-induced SSB in cells suspended in liquid

The cells were lifted by minimal trypsin/EDTA treatment, washed in serum-containing medium, washed twice in cold PBS and then resuspended in DMEM without phenol red at a density of 6.25×10^5 cells/ml. Aliquots of these suspensions were pipetted into separate 24-well (1 ml aliquots) or 96-well (150 μl aliquots) tissue culture plates and kept at room temperature until irradiated. Immediately after irradiation, the lamp shutter was closed and repair was allowed to take place at room temperature. After a repair period of between 10 and 240 seconds, 50 μl of the cell suspension was removed and added to 50 μl 1.2% LMP agarose, mixed and immediately applied as a top layer. The prepared slide was placed on ice and into lysis as soon as it had set.

2.3.3.3 Repair of UVR-induced excisable lesions in cells suspended in agarose

The comet assay protocol for the measurement of SSB repair described above was adapted for the study of excision repair kinetics up to repair times of 2 hours. After the top layer (containing the cells) had set, 100 μl of DMEM without phenol red was pipetted onto the layer and a cover slip applied. The slides were placed onto several layers of damp tissue inside a shallow box. The box was then placed in the incubator for the repair period. For every half-hour of repair time, the cover slip was removed and 100 μl DMEM without phenol red was added as before. At the end of the repair period the coverslip was removed

and the slide placed immediately into lysis. The lysis and electrophoresis procedure was performed thereafter as above.

2.3.4 Readback systems for the Comet Assay

2.3.4.1 The 6-category comet scoring system.

Comets were categorised according to their appearance. The scoring system was based on the 5-category method of Collins *et al.* (1995) but was modified in that 6 categories rather than 5 were finally decided upon (after several months experimentation, including assessment against an image analysis system (Section 2.3.5.1)). These 6 categories were chosen to approximate to the generally used parameter of Comet Moment (see below, Section 2.3.4.2.2). The 6th category (bottom, Figure 2.2) was utilised to accommodate a type of comet seen frequently but which the image analysis system could not satisfactorily analyse. These comets appear in high numbers after irradiation at high doses and after incubation in conditions of nutritional stress. Figure 2.2 shows computer-captured images of typical comets from each of the final 6 categories. They range from an undamaged cell (type 1, top, Figure 2.3) through to an extreme type of damage (type 6, bottom, Figure 2.3). At least 60 comets were categorised per slide and the mean comet value calculated. The number of comets in each category was recorded and used as an additional means of assessment.

Figure 2.3 The 6-category comet scoring system

Type 1

Type 2

Type 3

Type 4

Type 5

Type 6
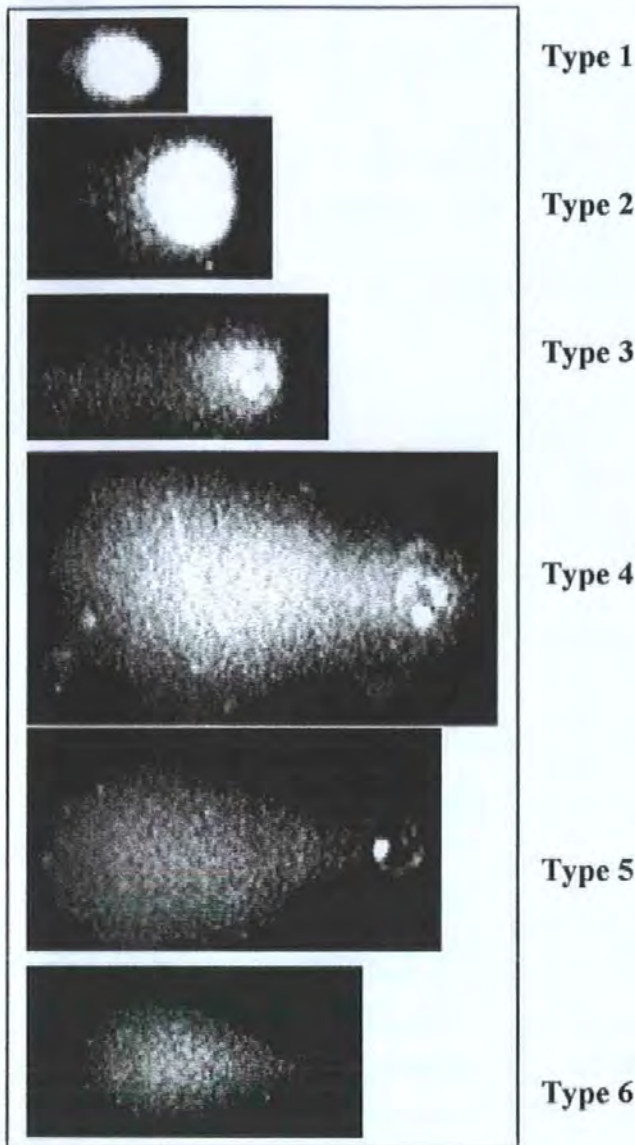
2.3.4.2 Image analysis of comets

2.3.4.2.1 Equipment

The fluorescence microscope used in this work was a Leitz Laborlux K fitted with a trinocular tube and camera mount. Two excitation filters were used: a green transmitting one (Leitz, N.2.1)-for the visualisation of ethidium bromide stained samples and a blue transmitting one (Leitz I.2) for the visualisation of FITC stained samples. Objectives

available were of 10x, 25x, 40x and a 50x water immersion type. Eyepieces were 10x magnification.

Images were captured by a frame grabber and stored on a custom built personal computer (VisionBase, UK) dedicated to the microscope and fitted with a CD writer. The image analysis software was Optimas version 6.1 and the comet assay software version 2.3.

2.3.4.2.2 Parameters used for the analysis of comets

The parameters that were used for analysis of results were the Comet Area, the Tail Moment as calculated by the method of Olive (Fairbairn *et al.* 1995), and the Comet Moment as calculated by the method of Kent *et al.* (1995).

Olive's Tail Moment is calculated from the product of % DNA in tail and displacement between the centre of mass of the head and the centre of mass in the tail (see Figure 2.4 **(Fttot / Fhtot + Fttot)(100) x l4)**. Kent's Comet Moment is based on the mathematical definition of the moment of inertia of a plane figure and is calculated from the measurement of fluorescence at over 200 points in the comet (see Figure 2.4 **Σ(0->n) ({F(l5) x l5} + {F(l6) x l6}) / Fhtot +Fttot).**

Figure 2.4. Image Analysis of Comet Formation
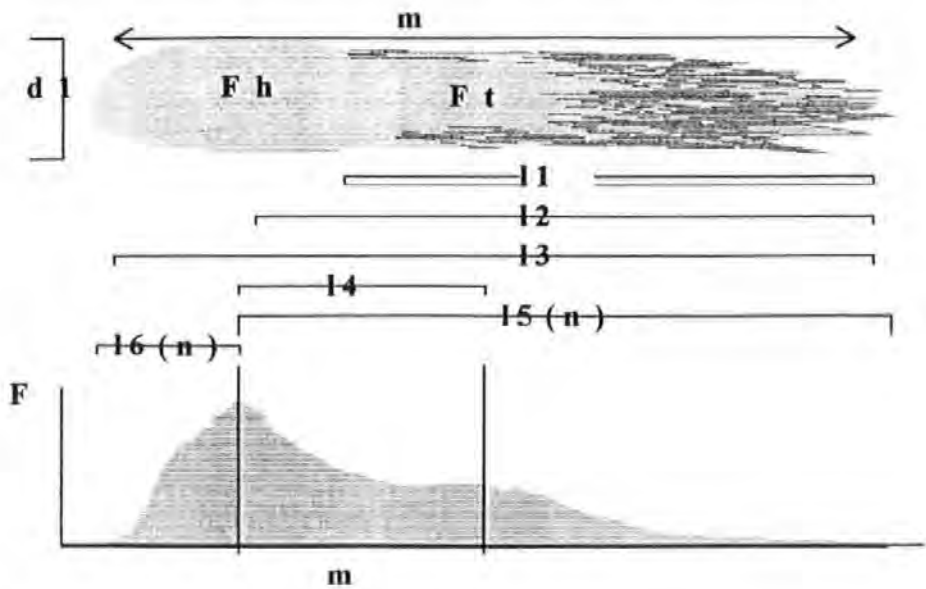
Where:-

m is the migration of the DNA to form the whole comet, as detected by the image capture equipment

d1 is the diameter of the comet head

F is the relative fluorescence of the various parts of the comet measured as an integral across the comet

Fh is the centre of mass of the comet head (fluorescence peak)

Ft is the centre of mass of the comet tail (fluorescence peak)

Fhtot is the total fluorescence of the comet head

Fttot is the total fluorescence of the comet tail

l1 is the length of the tail, measured from the distal end of the head

l2 is the length of the tail, measured from the centre of mass of the head

l3 is the length of the tail, measured from the proximal end of the head

l4 is the length of the tail, measured between the two centres of mass

l5 is the length of the tail, measured from the head's centre of mass to a number of points at regular intervals along the line l2 (n >= 80)

l6 is the distance from the centre of head mass to the proximal end of the head: a 'negative tail' value.

The Tail and Comet Moments are dimensionless numbers based on the fluorescence intensity of the comet head versus the comet tail and the size of the comet tail, and which takes into account that the comet assay is cell cycle sensitive.

2.3.5 A comparison of the readback systems

2.3.5.1 Method and results

To compare the visual (Section 2.3.4.1) and image analysis (Section 2.3.4.2) systems of assay readback, a 405 nm dose response was performed in two fold replicate on MRC5 SV2 fibroblasts. The assay was scored back visually and the data recorded. The slides were coded and given to the 'Optimas' technical team to be analysed in a blinded comparison. One set of replicates was not analysed.

The two readback systems were compared as follows. The visually derived comet value (between 1 and 6) was multiplied by a factor of 15 to enable direct comparison (on the same graph) with other values (e.g. mean tail lengths were between 50 -80 μm and the Tail and Comet Moments had values between 10 and 25) The image analysis-derived dose response and the visually derived dose response were plotted against dose. The results for Comet Area were plotted against a secondary axis and scaled to separate the dose response curve from the others. The two readback systems were in close accord (Figure 2.5).

The digitised images of the comets (n = 599) were assigned to a comet category from their appearance on the computer screen using a dictaphone to record the image number and the corresponding category. The image analysed parameters of each comet were plotted against the category assigned to it. The mean value of the parameters was calculated for each of the comet categories. These parameters were comet length (Figure 2.6), tail length (Figure 2.7), Comet Area (Figure 2.8), total DNA (Figure 2.9), % DNA in the comet head (Figure 2.10), Olive's Tail Moment (Figure 2.11) and Kent's Comet Moment (Figure 2.12).

82

Figure 2.5 The comparison of the two readback systems. A 405 nm dose response was performed in two fold replicate on MRC5 SV2 fibroblasts. The assay was scored back visually and by image analysis in a blinded comparison. One set of replicates was not analysed. The visually derived comet value was multiplied by a factor of 15 to enable direct comparison with the other values. The results for Comet Area were plotted against a secondary axis and scaled to separate the area dose response curve from the others. The image analysis-derived dose response and the visually derived dose response were seen to be in close accord.
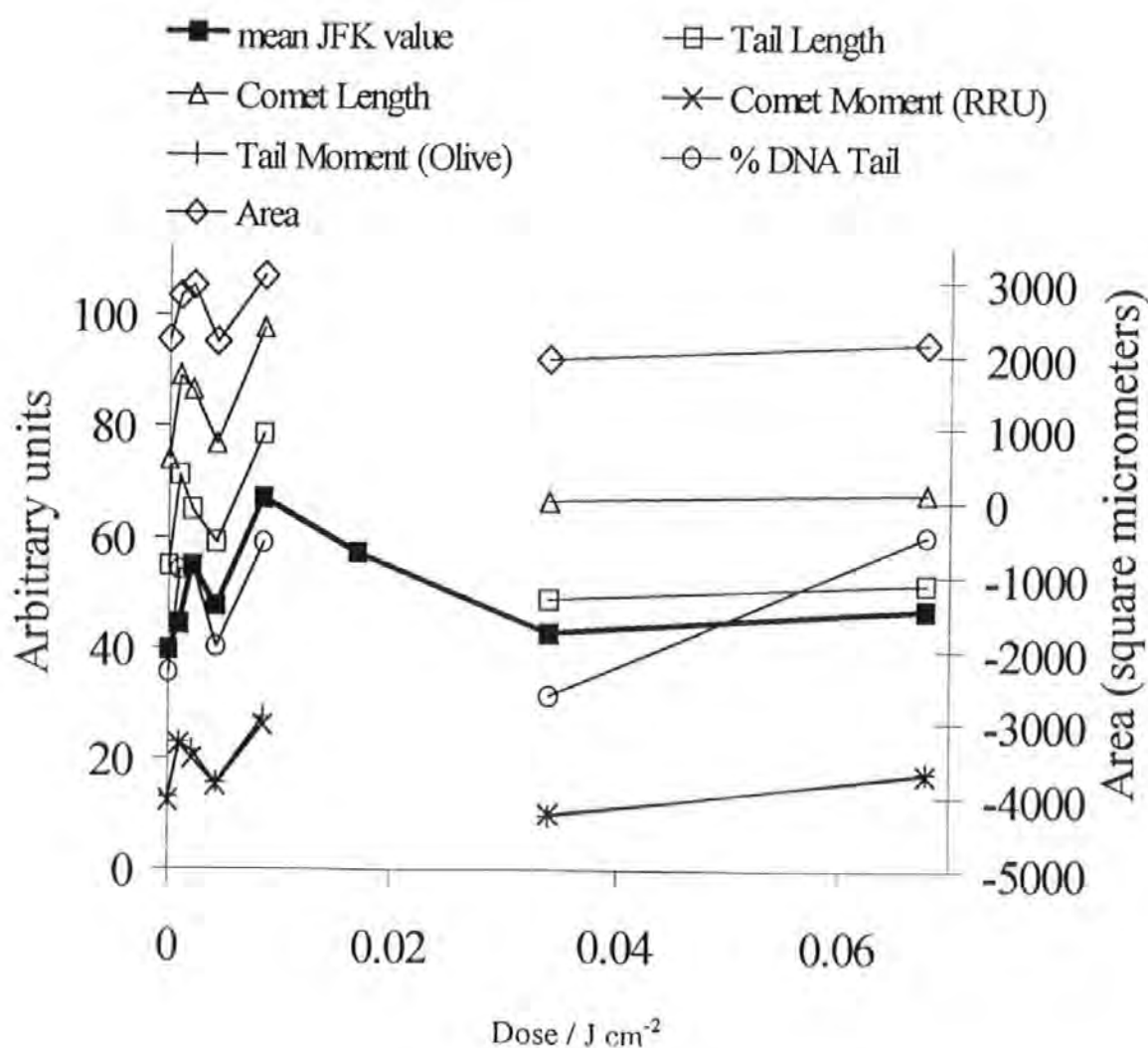
Figure 2.6 The relationship between comet length and the comet categories.
Digitised images of comets (n = 599) were assigned to a comet category from their
appearance on a computer screen. The image-analysed parameter of each comet was
plotted against the category assigned to it (•). The mean value of the parameter was
calculated for each of the comet categories and plotted against the category (solid
line).
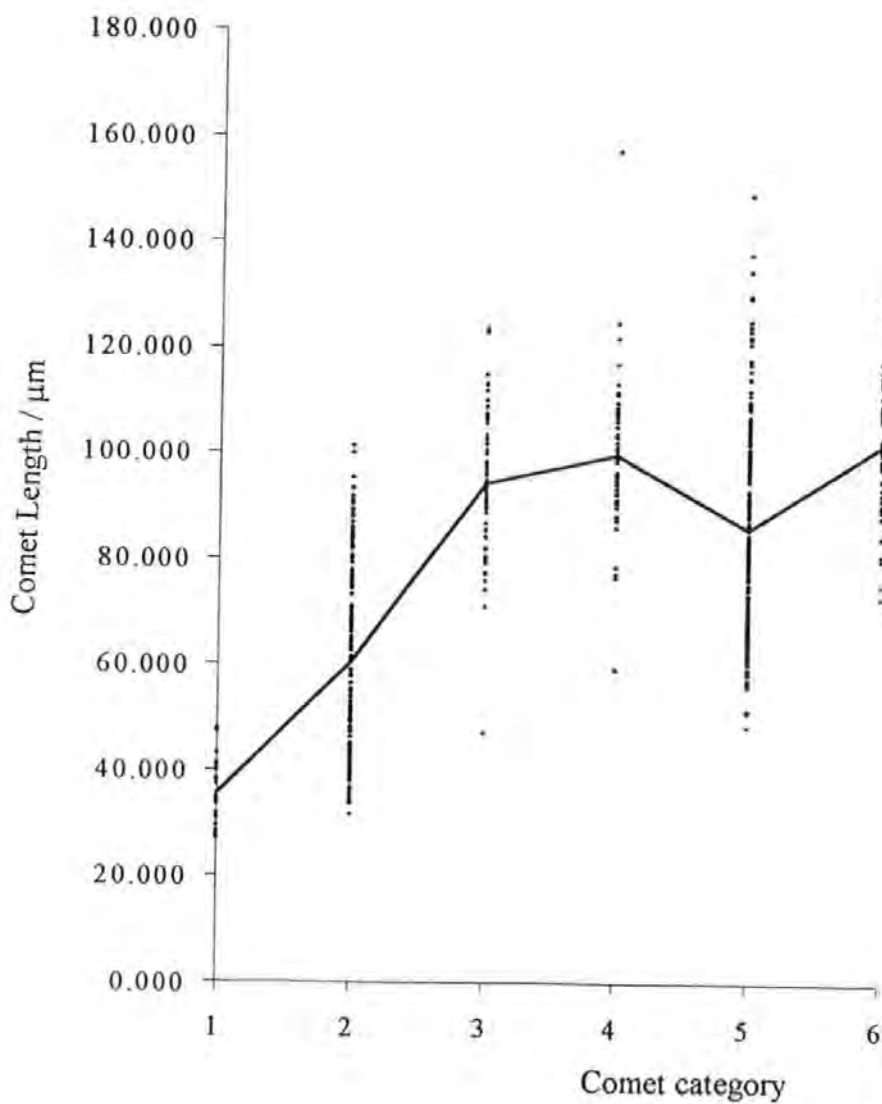
Figure 2.7 The relationship between tail length and the comet categories. Digitised

images of comets (n = 599) were assigned to a comet category from their appearance

on a computer screen. The image-analysed parameter of each comet was plotted

against the category assigned to it (•). The mean value of the parameter was

calculated for each of the comet categories and plotted against the category (solid

line)
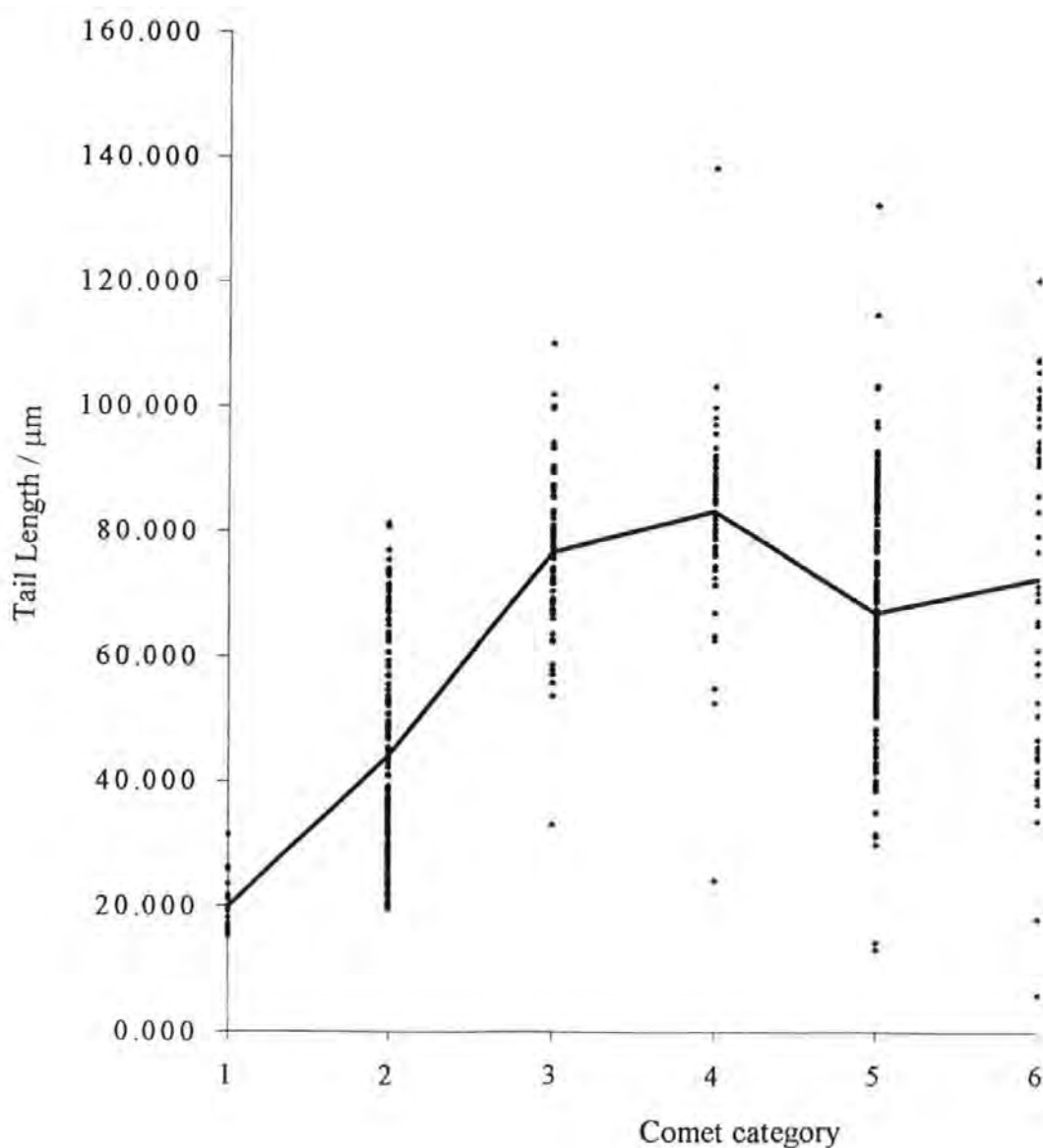
Figure 2.8 The relationship between Comet Area and the comet categories. Digitised images of comets (n = 599) were assigned to a comet category from their appearance on a computer screen. The image-analysed parameter of each comet was plotted against the category assigned to it (•). The mean value of the parameter was calculated for each of the comet categories and plotted against the category (solid line).
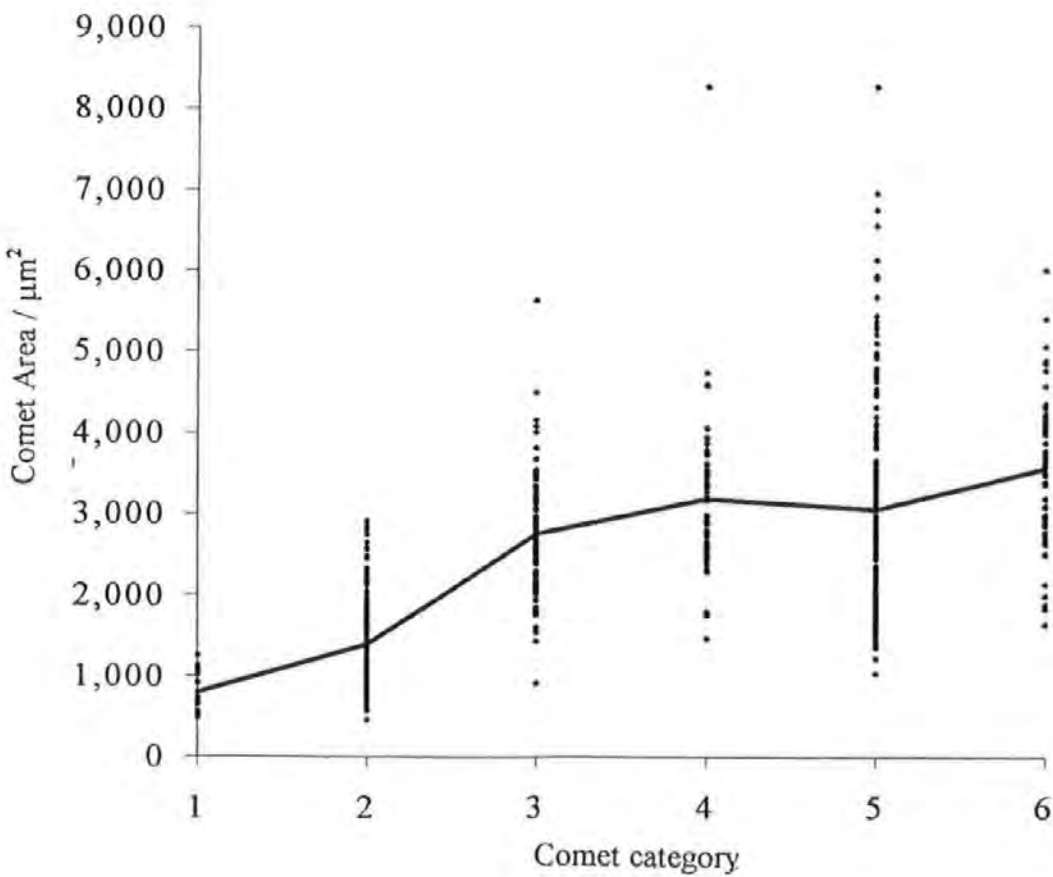
Figure 2.9 The relationship between the measurement of total DNA and the comet categories. Digitised images of comets (n = 599) were assigned to a comet category from their appearance on a computer screen. The image-analysed parameter of each comet was plotted against the category assigned to it (•). The mean value of the parameter was calculated for each of the comet categories and plotted against the category (solid line).
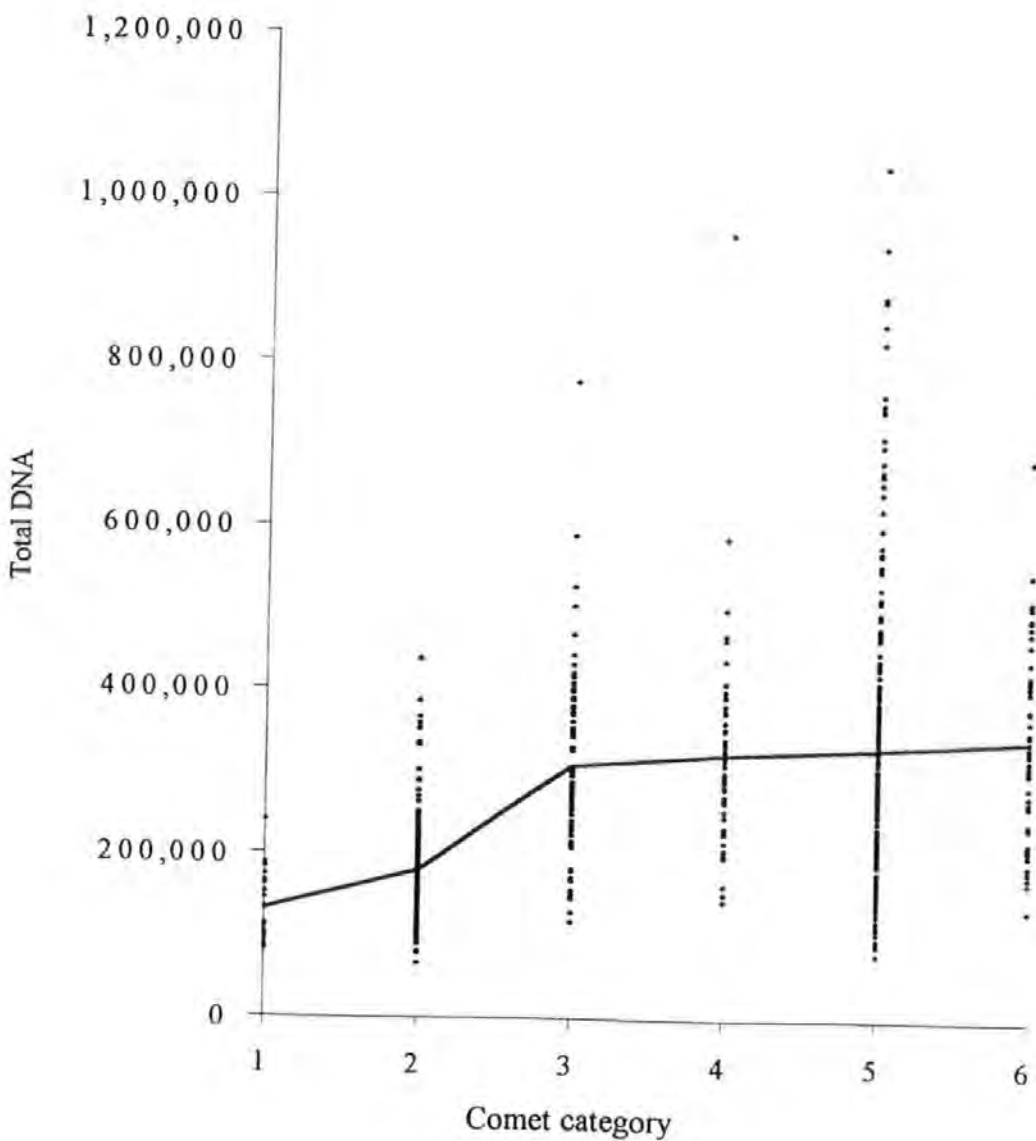
Figure 2.10 The relationship between the measurement of the fraction of total DNA in the comet head and the comet categories. Digitised images of comets (n = 599) were assigned to a comet category from their appearance on a computer screen. The image-analysed parameter of each comet was plotted against the category assigned to it (•). The mean value of the parameter was calculated for each of the comet categories and plotted against the category (solid line).
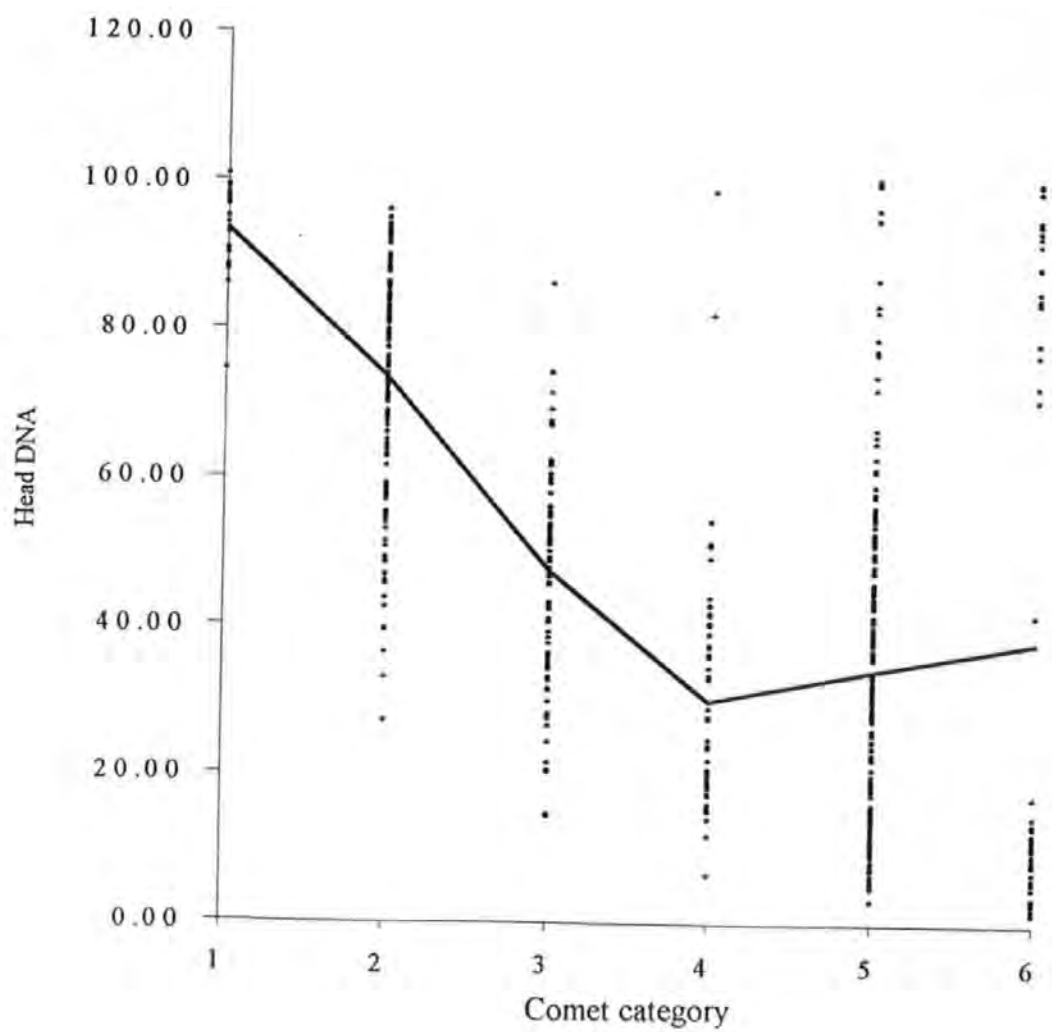
Figure 2.11 The relationship between Olive's Tail Moment and the comet categories. Digitised images of comets (n = 599) were assigned to a comet category from their appearance on a computer screen. The image-analysed parameter of each comet was plotted against the category assigned to it (•). The mean value of the parameter was calculated for each of the comet categories and plotted against the category (solid line).
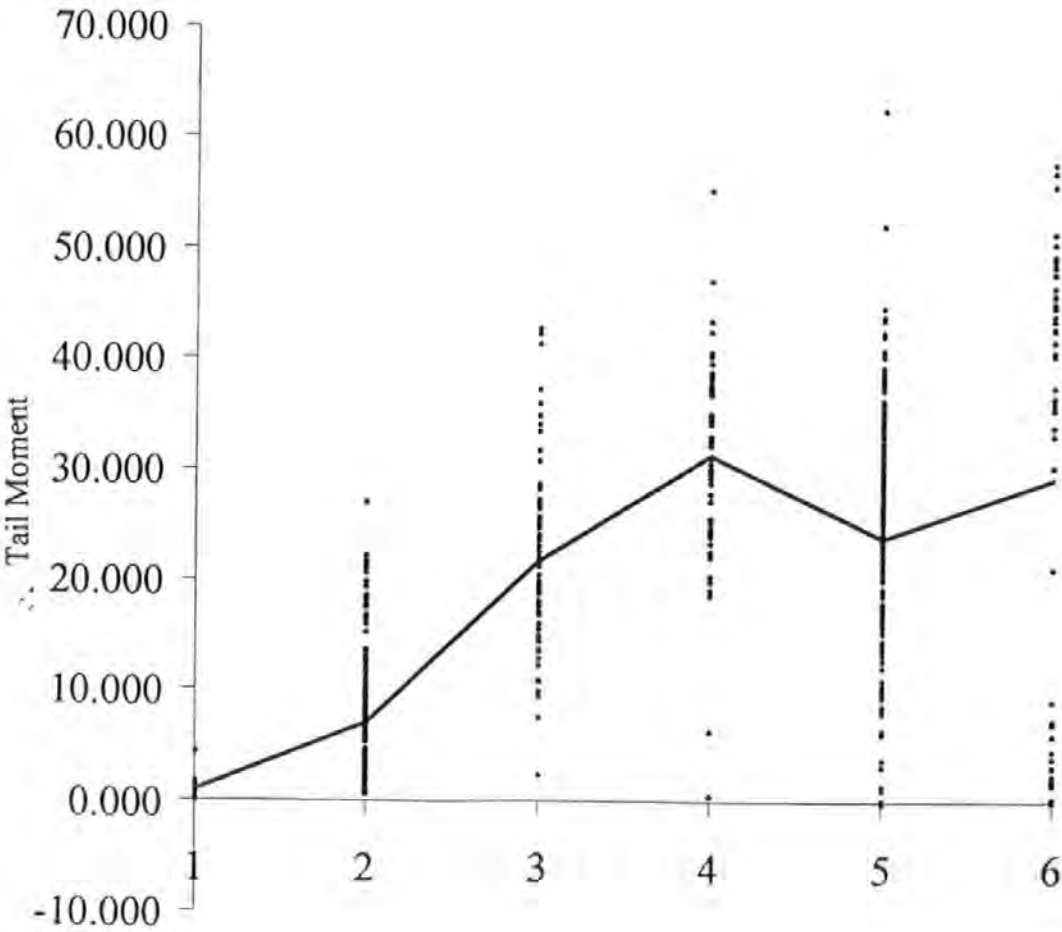
Figure 2.12 The relationship between Kent's Comet Moment and the comet categories. Digitised images of comets (n = 599) were assigned to a comet category from their appearance on a computer screen. The image-analysed parameter of each comet was plotted against the category assigned to it (•). The mean value of the parameter was calculated for each of the comet categories and plotted against the category (solid line).
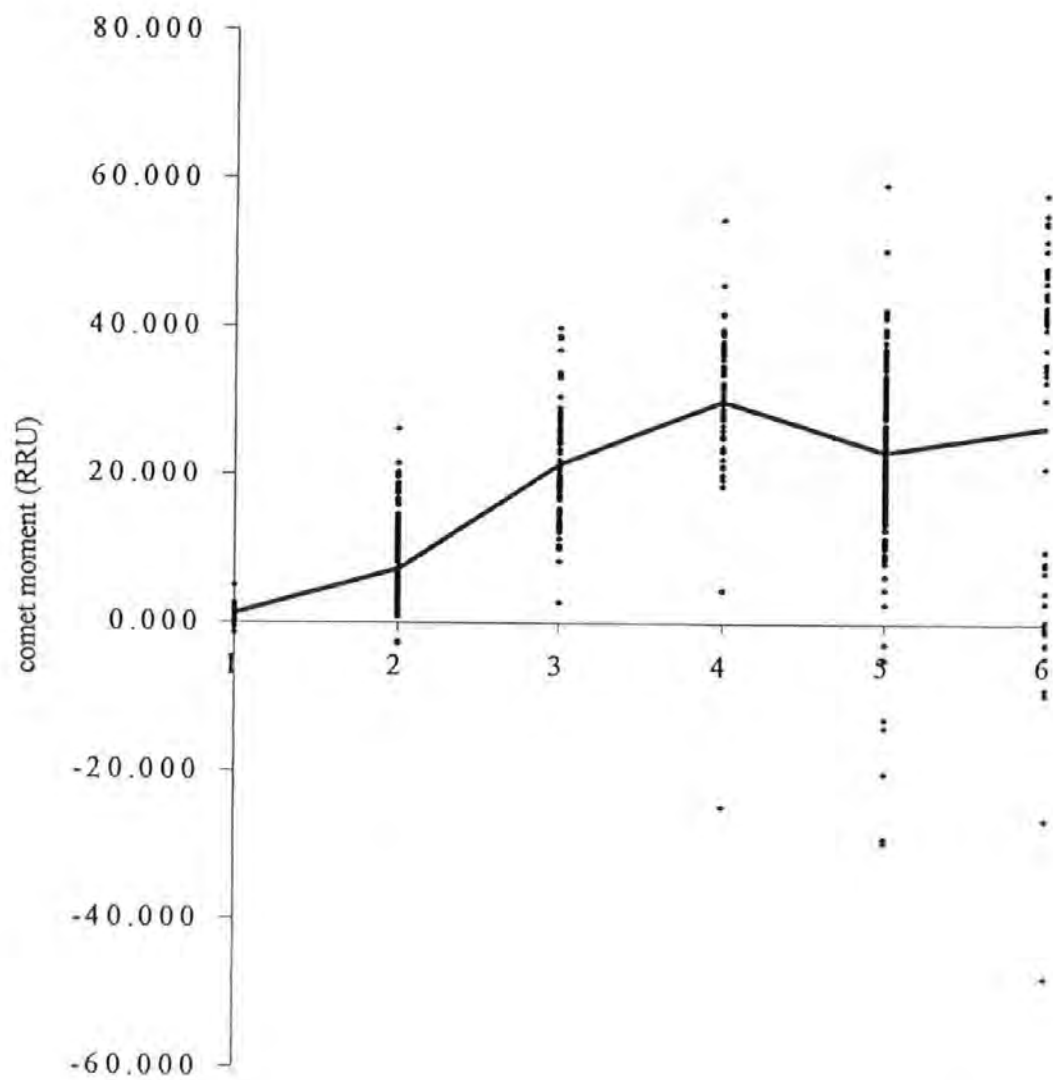
2.3.5.2 Physical parameters: Comet Length, Tail Length and Comet Area

The physical parameters of Comet and Tail Length (Figures 2.6 and 2.7) correlated with the comet categories 1 to 3, but not with the higher categories. The use of length as a readback parameter was used in the early history of the assay but was unsatisfactory as comet and tail length are only related linearly at low doses. An approximately linear relationship was observed between Comet Area and comet category (Figure 2.8).

2.3.5.3 DNA content

The image analysis system analyses fluorescence intensity as a measure of DNA content. Figures 2.9 and 2.10 indicate that the relationship between DNA content and the comet categories is complex. A quiescent cell with tightly packed DNA is more resistant to DNA damage than a replicating cell with partially unwound DNA; additionally, the DNA content in a replicating cell can be up to twice the amount of a quiescent cell. If there is a high DNA content in the comet head, the high intensity will cause the image analysis software to be 'saturated' and the DNA content to be underestimated. These two factors are linked and can be seen in Figures 2.9 and 2.10.

The data obtained indicated that the comets from cells with a high total DNA content (Figure 2.9) tended to be in the higher categories. Figure 2.9 displays a plateau above category 3, the DNA content at this plateau probably represents the mean amount of DNA in the cells. (MRC5 SV2 are heterogenous with respect to their polyploidy.) The lower mean values for comets in categories 1 and 2 are, therefore, probably underestimates due to the saturation of the equipment.

The amount of DNA in the head (Figure 2.10) was negatively correlated with comet category (as tail DNA is positively correlated (Figure 2.11)). The relationship was almost linear up to category 4, but above this category there was no correlation. The difficulty that the image analysis system has with responding to the intensity signal from the higher

category comets is clearly illustrated in Figure 2.10 where the % head DNA calculated for the type 5 comets ranged from less than 5% to 100%.

2.3.5.4 Olive's Tail Moment and Kent's Comet Moment

Comet Moment and Tail Moment are calculated from the physical parameter of length combined with the ratio of head to tail DNA. The relationship between the first 4 comet categories and Comet or Tail Moment was approximately linear, but this relationship did not hold for the higher comet values.

2.4 MODULATING REAGENTS

2.4.1 Production of stock solutions

2.4.1.1 Beta-carotene

Beta-carotene is insoluble in water (Roche Ltd., vitamins division, personal communication) and only sparingly soluble in ethanol (Sigma Technical Services). For use in the work reported here a saturated solution of synthetic beta-carotene powder was made up in denatured ethanol: 0.0017 g of beta-carotene was partially dissolved in 50.0 ml of denatured ethanol by warming at 37 °C and sonication. The bright orange solution was removed by pipette, the residual beta-carotene and solution was dried in the incubator and reweighed. The concentration of this solution was calculated by subtraction of the mass of undissolved beta-carotene from 0.0017 g. The saturated beta-carotene solution was diluted in denatured ethanol to various concentrations and absorbance at 453 nm was plotted against concentration. To create a stock solution, beta-carotene was dissolved in denatured ethanol as above. The stock solution was sterile-filtered through a 0.2 μm filter to remove clumps of undissolved beta-carotene and aliquots of 1 ml were stored at -20 °C. Aliquots of this stock solution were added to 20 ml of incubating media. The concentrations of the stock solution (and therefore the incubating solutions) were calculated by taking the

absorbance of three pooled aliquots at 453 nm and by subsequent reference to the calibration curve. The measured concentration of the stock solution was 27.5 ± 2.5 μM over the period of study.

2.4.1.2   The beta-carotene, vitamin C and vitamin E cold water dispersible matrix (ACE)

The insolubility of beta-carotene in water necessitated the use of a 10 % cold water soluble form of beta-carotene: 0.2 μm crystals of beta carotene held in a water soluble matrix which also contained antioxidant vitamins C and E as beta-carotene is a prooxidant. This was a gift of the vitamins division at Roche Pharmaceuticals Ltd. The 10 % CWS beta-carotene contained 100 mg / g beta-carotene, 40 mg / g vitamin C and 15 mg / g vitamin E. A stock solution was made up by adding 0.3236 g of the matrix to 500 ml of DMEM without phenol red and sonicated for 15 minutes. The concentration of the vitamins in the stock solution was calculated. The final incubating concentrations were beta-carotene 6.47×10^{-2} mg / ml (121 μM), vitamin C 2.5947×10^{-2} mg / ml (147 μM), vitamin E 9.7147×10^{-3} mg / ml (23 μM).

2.4.1.3   o-phenanthroline

0.1 M stock solution of o-phenanthroline was made up by adding 2.018 g o-phenanthroline to 102.0 ml denatured ethanol. Aliquots of 500 μl were stored at -20 °C.

2.4.1.4   Arsenic

0.1 M stock solution of sodium arsenate was made up by adding 3.154 g $Na_2HAsO_4.7H_2O$ (ACS Reagent, Sigma UK) to 101.0 ml of PBS(t). Aliquots of 500 μl were stored at -20 °C. A sterile standard incubation medium was made by the addition of 15.75 g $Na_2HAsO_4.7H_2O$ to 500 ml of RPMI 1640 medium.

A stock solution of 0.1 M sodium arsenite was made by adding 1.304 g $NaAsO_2$ (> 90% purity, Sigma UK) to 100 ml of PBS(t). This stock solution was discarded immediately after use.

3 CHAPTER 3.

THE CULTURE OF NORMAL HUMAN MELANOCYTES

3.1 INTRODUCTION

Melanocyte culture *in vitro* was first reported in 1982 by Eisinger and colleagues (Eisinger *et al.* 1982) using a human epidermal separation method to generate a single cell suspension. This suspension was then plated out in the presence of phorbol ester and cholera toxin which promoted the growth of melanocytes while suppressing the keratinocyte population. Their method was modified in 1984 by Halaban and Alfano who used a toxic geneticin sulphate treatment to eliminate dividing fibroblasts. Dorothy Bennett first reported the cloning of human melanocytes in 1985 (Bennett *et al.* 1985). Since then normal human melanocytes have been cultured *in vitro* using epidermal cell suspensions and usually generated by separation of the epidermis from the dermis (thus exposing the basal layer within which the melanocytes are dispersed). The melanocytes are then dislodged by scraping the two exposed surfaces and plated out in a number of ways: basically either by the use of a feeder layer of non-dividing fibroblasts or directly onto normal tissue culture plastic at a high cell density. Both of these methods have drawbacks, viz that (i) the use of feeder layers requires that the melanocyte culture is rendered homogenous before use, usually by media that is selectively toxic to the contaminating cells. (ii) Plating at high cell density can provide conditions which encourage keratinocyte growth and again requires the use of selective media. In this laboratory, melanocytes were cultured from clinically normal skin (removed during surgery) by the epidermal separation method, and plated directly onto tissue culture plastic (Section 2.2.1.6). They were treated with geneticin sulphate to kill proliferating fibroblasts.

The melanocyte:keratinocyte equilibrium in human epidermis is largely independent of the skin's pigmentary characteristics, thus excluding areas containing naevi, the ratio of keratinocytes to melanocytes is maintained at approximately 30 to 1. If contact with neighbouring cells is lost, for example during wound healing, cycles of cell division are initiated to restore tissue continuity. Hyperproliferation of keratinocytes during wound healing is accompanied by melanocyte migration and proliferation to maintain homeostasis. In order to study this and similar phenomena, a method of culturing keratinocytes from explants was developed in 1986 by Coulomb and colleagues (Coulomb *et al.* 1986). The explant-culture of human melanocytes was first reported in 1994 when Le-Poole *et al.* used an organotypic model to study melanocyte migration. This was a short term (7 day) culture in which the migration of melanocytes from within punch biopsies and into explant-cultured keratinocytes from the same biopsies was observed. Organotypic cultures are more variable than monolayer cultures due to the great increase in the complexity of the cultures, and reproducibility is thus more difficult; however, the organotypic methods more closely represent the situation *in vivo* and thus findings are more likely to be clinically relevant. Their culture method used 3mm punch biopsies cultured on nitrocellulose/cellulose acetate filters. The object of the study was to compare vitilligenous and normal melanocyte migration. Mitotic melanocytes were observed in these culture conditions for at least 5 weeks.

Section 3.2 reports the culture of naevus cells from an explanted naevus in this laboratory. Small pieces of skin containing naevi were cultured *ex vivo* and treated as explants using melanocyte-selective media. The naevi underwent an immediate (<48 h) pigmentary change. Keratinocytes were observed to grow out from the explant within a fortnight and melanocytes similarly within 28 days. The latter cells were shown to be melanocytic in origin, they were induced to proliferate and subsequently to migrate out of their tissue compartment (see Figures 3.1 to 3.4). Some of the experiments were repeated using

different selective media (Sigma 'M1669') and 6 mm punch-biopsied naevi from different sources, although only pigmentary changes were observed.

The culture of human melanocytes from epidermal suspensions was performed by trypsin dissaggregation (Section 2.2.1.5) and by epidermal separation (Section 2.2.1.6)

3.2 EXPLANT METHOD

3.2.1 Results

A pronounced increase in pigmentation took place in the naevus within 48 hours of culture. During the first fortnight of culture epidermal cells were observed to grow out from the explant. These cells subsequently died and were not replaced. During this period and afterwards an area of pigmentation appeared which extended from the naevus to one of the edges of the explant. Microscopic examination of the specimen *in situ* revealed cells of melanocytic morphology at the edges of the explant; these cells eventually migrated onto the culture flask surface.

The specimen was lifted, washed in PBS and examined histologically. The darkly pigmented cells of the original lesion were still present at the centre of the specimen (Figure 3.1). Pigmented cells were also seen along the base of the squamous epithelium extending out to one margin (Figure 3.2). Staining for S100 protein was carried out. This produced strong staining of the central lesion (Figure 3.3) and also cytoplasmic staining of the cells along the basal layer out towards the margin (Figure 3.4). There was no staining of other cells in the specimen.

3.3 EPIDERMAL SEPARATION METHOD

3.3.1 Results

The culture of melanocytes from elderly donors from skin removed during amputative surgery was attempted on a number of occasions, which proved satisfactory with regard to the initial number of melanocytes that attached to the culture flask. These melanocytes did

not proliferate to sufficient numbers for assay and generally died within an estimated 2 or 3 population doublings.

The converse was true for the culture of melanocytes from punch biopsies taken from middle aged donors. The melanocytes proliferated readily in 96 well plates (one biopsy per well) for several generations. This was, however, insufficient to provide enough cells for assay.

The culture of melanocytes from foreskins did prove successful in providing sufficient cells. Three cultures were made from foreskins. One culture (YBF14M) was used to verify the presence of melanocytes by fixed cell immunofluorescence. A second (sparse) culture (YBF17M) was used to verify the presence of attached (i.e. viable) melanocytes by indirect fluorescence in situ. The third culture (YBF15E) was used to assay the modulating effects of the ACE mixture (Section 6.2.3.2).

Figure 3.1 The explant culture of a human naevus: haemotoxylin and eosin staining (low power) showing original naevus with migrating cells
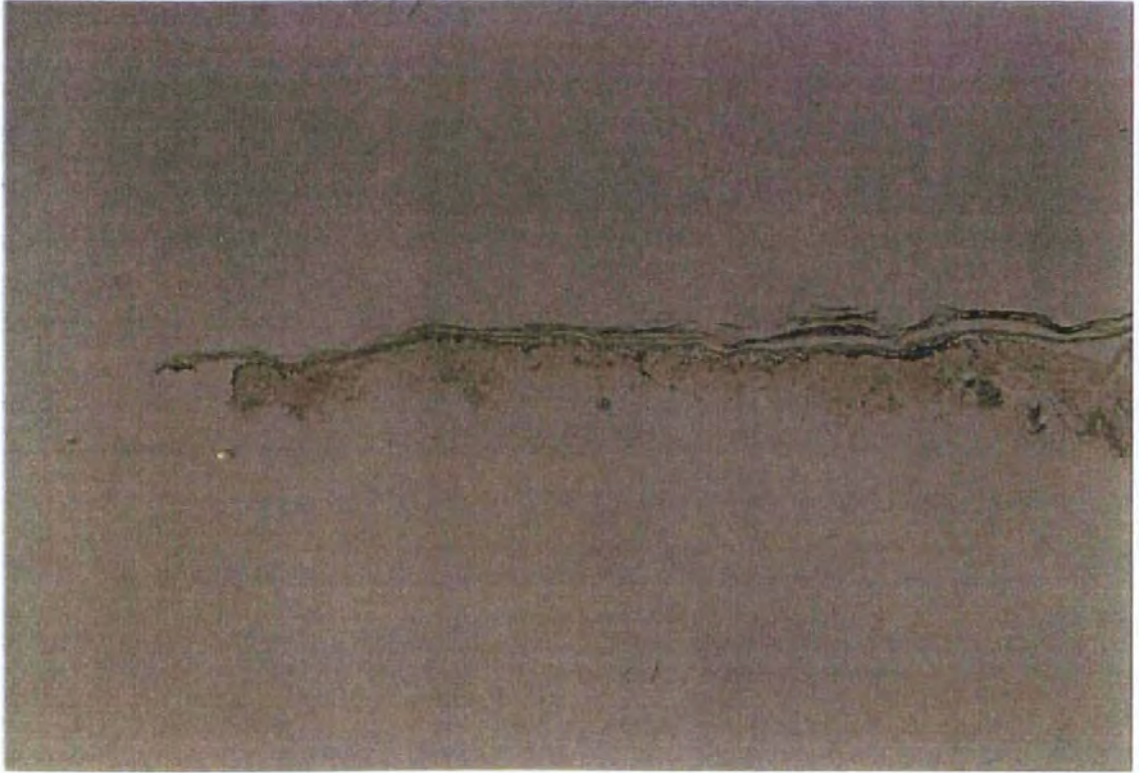
Figure 3.2 The explant culture of a human naevus: haemotoxylin and eosin staining (high power) showing edge of explant with migrating cells
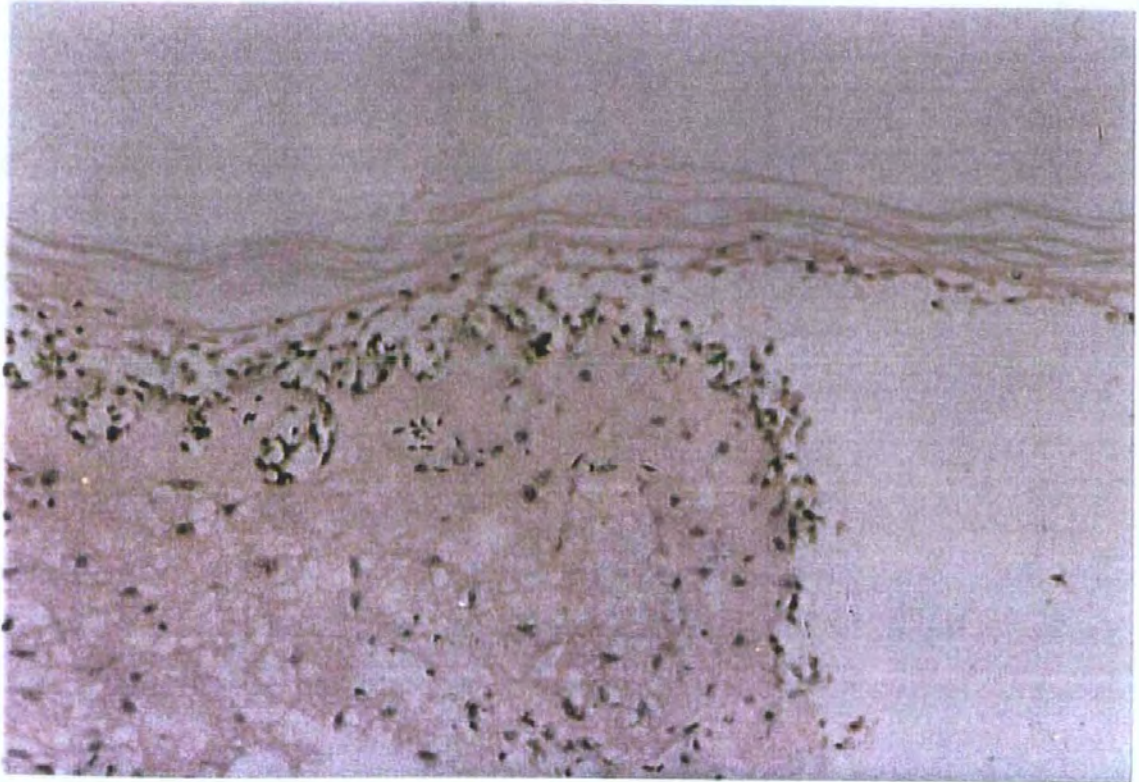
Figure 3.3 The explant culture of a human naevus: immunochemical staining for S-100 (high power) showing the central lesion
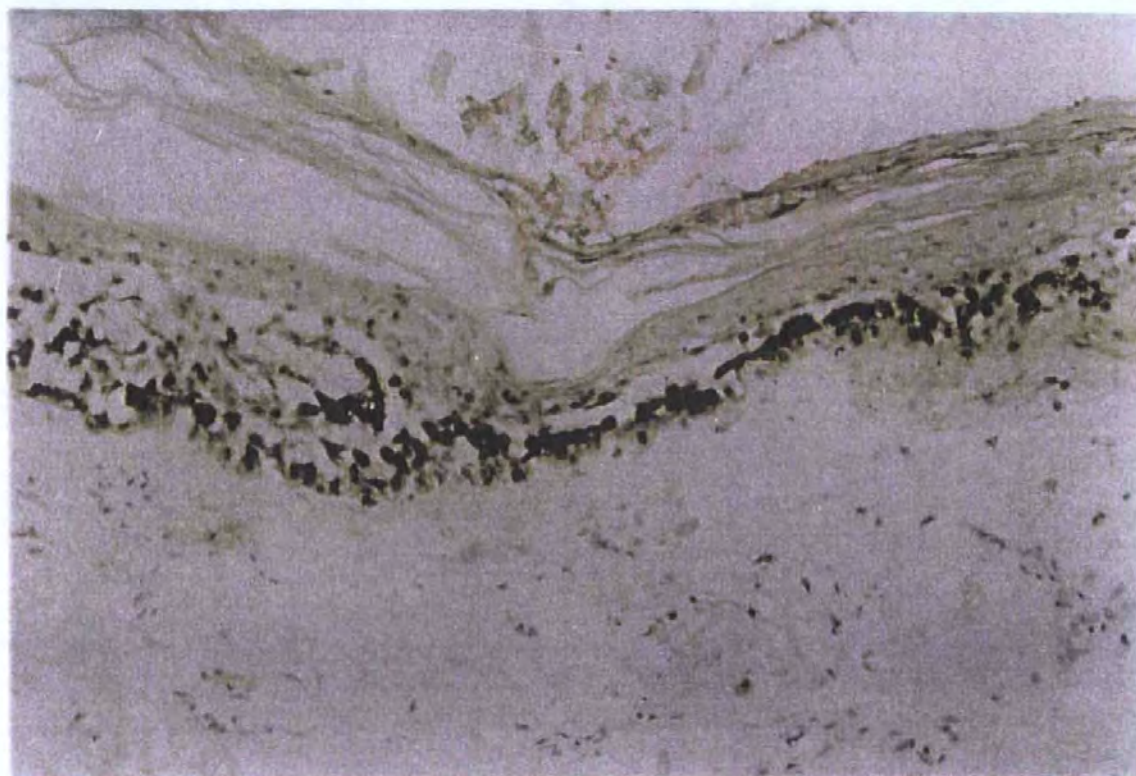
Figure 3.4 The explant culture of a human naevus: immunochemical staining for S-100 (high power) showing edge of explant with migrating cells

3.3.1.1 Fixed cell immunofluorescence

The successful culture of melanocytes was confirmed by fixed cell immunofluorescence. The cultures were tested against a panel of antibodies that recognised epitopes on keratinocytes (cytokeratin), melanocytes (S-100) and a general cell marker (actin). Table 3.1 presents a summary of the observations. Representative images were captured using the image analysis equipment and are presented in Figure 3.5

Table 3.1 Fixed cell immunofluorescence of melanocyte cultures

A2058	*DOK*	*MRC5 SV2*	*Cell culture*	*Cell culture*
α S-100 positive	α S-100 negative	α S-100 negative	α S-100 positive	α S-100 positive
A2058 α cytokeratin negative	*DOK* α cytokeratin positive	*MRC5 SV2* α cytokeratin negative	*Cell culture* α cytokeratin negative	*Cell culture* α cytokeratin negative
A2058 α actin weakly positive	*DOK* α actin weakly positive	*MRC5 SV2* α actin weakly positive	*Cell culture* α actin v. weakly positive	*Cell culture* 2° Ab only negative

The results of the fixed cell immunofluorescence were ambiguous, in that the signal from the anti-melanocyte antibody indicated the presence of melanocytes, but at lower numbers than the controls, even though equal numbers of cells were applied to the immunofluorescence slide. This indicated that non-melanocytic cells were present and as the anti-cytokeratin antibody gave a strong signal on keratinocytes, the contaminating cells were judged to be fibroblasts. The anti-actin antibody failed to give a strong signal in the controls and in the cultures although a positive signal was observed. (The amplitude of

this signal was below the detection limits of the camera and therefore the blank images are not included in Figure 3.5; the anti-actin/melanocyte culture image is included for completeness).

Figure 3.5 Fixed cell immunofluorescence of melanocyte cultures. Left column: anti S-100 (i.e. melanocyte marker), right column anti-cytokeratin (i.e. keratinocyte marker).Top row: A2058 melanoma cells. Middle row: DOK kerainocyte cells. Bottom row: melanocyte cultures.
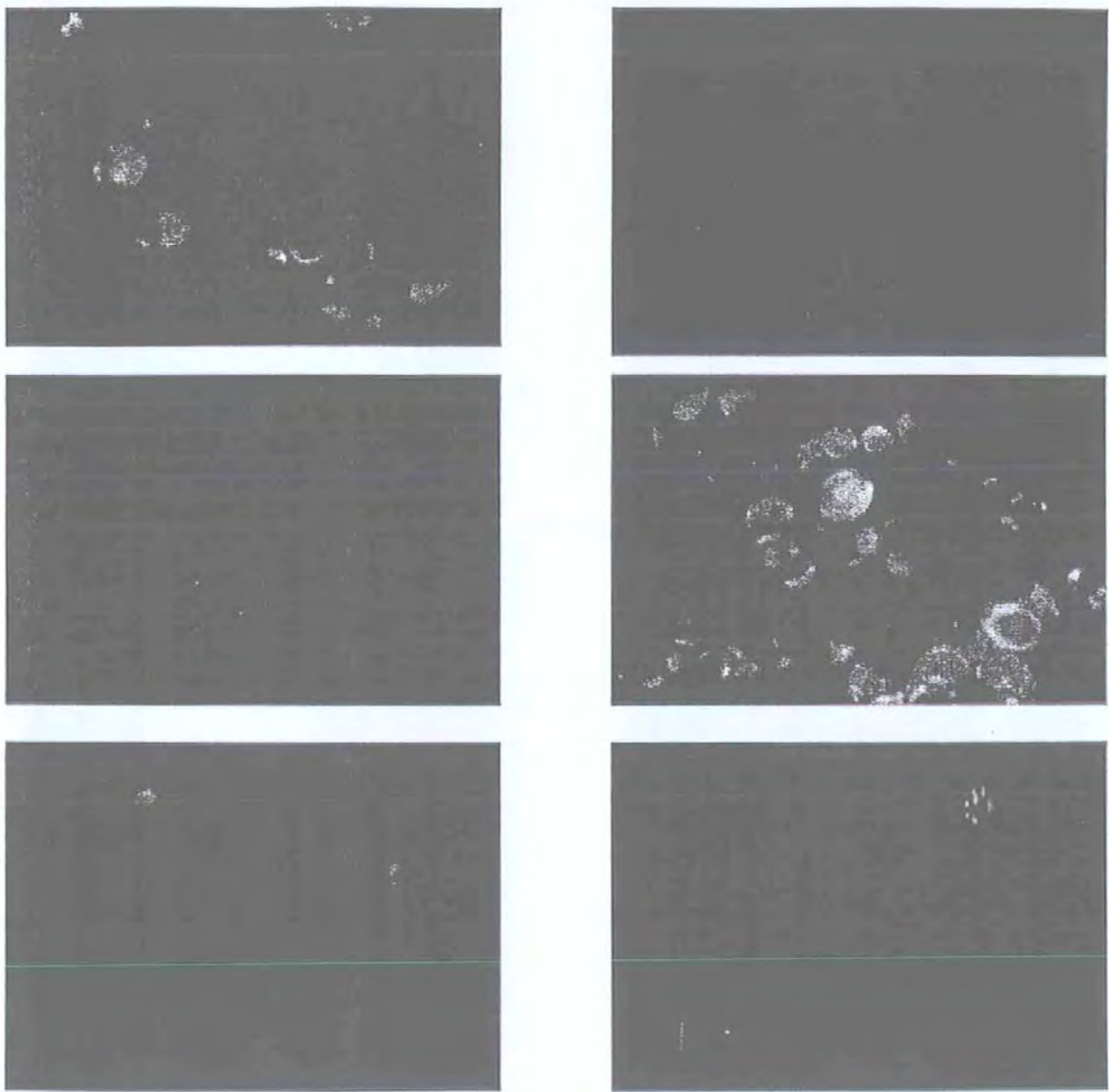
3.3.1.2 Indirect immunofluorescence in situ

The presence of viable melanocytes was confirmed by indirect immunofluorescence *in situ*. A typical image of a melanocyte in culture, stained in situ for S-100 is given in Figure 3.6

Figure 3.6 A normal human melanocyte in culture, stained for S-100 protein.
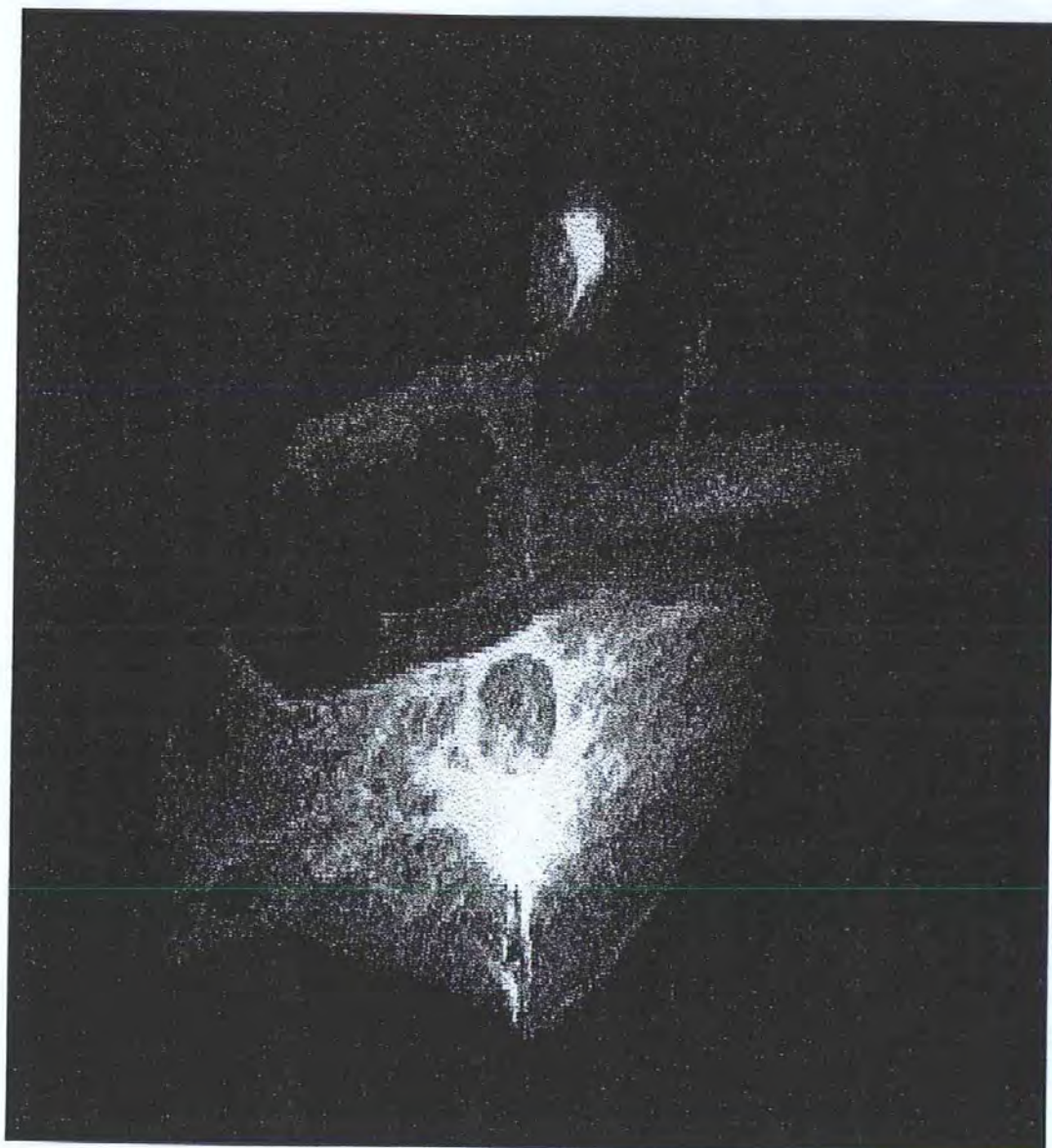
CHAPTER 4.

NORMAL RESPONSES OF HUMAN CELLS TO LOW DOSES OF

310 NM AND 405 NM UVR AND VISIBLE RADIATION

RESULTS

4.1 INTRODUCTION

Oxidative stress is cytotoxic, clastogenic and carcinogenic to human cells (Przedborski and

Schon, 1998; Lavker and Kaidbey, 1997; Spencer *et al.*, 1996; Halliwell and Aruoma

1991; Morin *et al.* 1998; Picardo *et al.* 1996; Wiseman and Halliwell, 1996; Guyton and

Kenzler, 1993).

UVR exerts an oxidative stress on living cells (Cerutti, 1985; Wenczl *et al.*, 1997; Cridland

and Saunders, 1994; Green *et al.*, 1993; Morin *et al.*, 1998; Coohill *et al.*, 1987; Pflaum *et

al.*, 1994; Peak and Peak, 1990; Peak *et al.*, 1987; Black, 1987; Kielbassa *et al.*, 1997;

Tyrrell and Pidoux, 1988; Applegate *et al.*, 1996). SSB are one manifestation of oxidative

stress and in this work the comet assay was used to monitor their formation. (A review of

the roles of oxidative stress and ultraviolet radiation in carcinogenesis will be found in the

General Introduction to this thesis (Section 1.3)). The comet assay employed in this work

is based on the method of Singh *et al.* (1988) with minor modifications. Two variants of

the assay were employed, one to assay direct SSB and the other to assay excision repair-

induced SSB, these are described below.

UV-irradiation was carried out at room temperature and direct SSB was measured in the

first variant by performing the assay immediately (less than 10 s) after irradiation (Noz *et

al.*, 1996). This method gave a measure of direct SSB plus alkali-labile lesions (see

Section 1.3.2 of the General Introduction) and was employed to assess the UVR dose

responses of the cells described in the second Section of this chapter. The second variant

permitted repair of the UVR-induced lesions by delaying the assay procedure while repair

took place. Because SSB repair is a very rapid process (Collins *et al.*, 1995), conducting the assay at a lower (room) temperature slowed the repair process down and allowed for more data on the repair kinetics to be gathered before the repair process is complete. Two systems of comet readback were employed: initial studies were carried out using a visual categorisation method based on that of Collins *et al.* (1995, Section 2.3.4.1) and later studies were carried out using Comet Assay v2.3 software operating under the Optimas v6.1 image analysis software (VisionBase Ltd. UK, formerly Optimas UK). The two readback systems were compared before purchase (Section 2.3.5). The consistency of readback data by either the visual or the automated systems was assessed by repeating some of the early experiments and comparing the assay results. The dose responses reported in Section 4.2.2.3.1 were found to be very similar by both readback systems. In particular, the Comet Area and the mean 'visual' comet value (see methods, Section 2.3.4) were found to be in very close agreement.

The following three Sections discuss the comet assay data obtained using the methods described above. The first Section (Section 4.2.1) addresses the issue of the cytotoxic effects of the UVR delivered to the cells. In essence, as discussed in the second Section the doses delivered to the cells were sub-cytotoxic. Section 4.2.2.3 describes the 405 nm UVR dose responses in 6 cell lines (normal and transformed fibroblasts and lymphocytes and a melanoma cell line) measured by image analysis and visual inspection. The image analysis equipment returns several parameters for analysis; of these, the parameters chosen for interpretation were the Comet Area, Comet Length, Tail Length, Olive's Tail Moment and Kent's Comet Moment. (In later experiments (described in Chapters 6 and 8) and based on the results of the experiments described in this Chapter (Chapter 4), the parameters analysed were the Comet Area and the two Moments.) A manuscript is in preparation that describes the suitability of these parameters for the measurement of low dose phenomena. The dose responses measured by all five parameters have therefore been reported in this Chapter (Chapter 4). Section 4.2.2 also describes 310 nm (Section 4.2.2.4)

105

and total Xe lamp (Section 4.2.2.5) radiation dose responses (measured by image analysis) of the normal lymphocytes and the transformed lymphocyte line. Section 4.2.3 describes the repair of 405 nm-induced SSB in normal fibroblasts and the repair of total Xe lamp radiation-induced SSB in normal lymphocytes.

N.B. A phenomenon in the dose responses was repeatedly observed during this work and has been referred to throughout as a 'peak' of SSB. The peaks are transitory increases in assayed SSB, but owing to the uncertainty attached to their origin, they have been given a non-specific descriptive title. It is important that the term is not confused with the same term that is used to describe a feature in radiation spectra when used in conjunction with a wavelength descriptor. This is brought to the attention of the reader as the term '405 nm peak', used herein to indicate a high level of assayed SSB induced by 405 nm radiation, could equally apply to the high output at 405 nm observed in the Xe lamp radiation spectrum. The two uses are easily distinguished by their context.

4.2 RESULTS

4.2.1 Cytotoxicity of UVR on human cells

The doses of UVR delivered to the cells under test were tested for cytotoxicity by a number of methods (Section 2.2.1.10). In general, the doses delivered to the cells, and especially those delivered during the comet assay procedures, were non-cytotoxic. The cytotoxicity of the radiation delivered to the cells was assessed using the fibroblast cell line MRC5 and the pigmented cell line A2058. The cytotoxic effects were estimated in a number of ways (see methods, Section 2.2.1.10, for full details). A summary of findings is presented in Table 4.1 (MRC5) and Table 4.2 (A2058). It can be seen from these Tables that the doses below ~500 J cm^{-2} were sub-cytotoxic with a few exceptions. The cytotoxicity thresholds presented in these tables were compared to values that have been reported in the literature. The cytotoxic doses delivered in this laboratory were approximately 1 or 2 orders of magnitude higher than were reported by Tyrrell and Pidoux

(1989) in a study of fibroblast cytotoxicity and Applegate *et al.* (1996) in a study of melanoma cytotoxicity. This is probably due to the higher fluences delivered to the cells in these two studies. Tyrrell and Pidoux (1989) used a 2.5 kW Hg/Xe lamp (fluence not reported) and Applegate *et al.* (1996) used a UVASUN 3000 (delivering 30 W cm^{-2} of UVA). The 150W XBO lamp used in these studies delivered a 405 nm fluence of ~ 75 µW cm^{-2}, effectively a 400,000 fold lower fluence than that used by Applegate *et al.* (1996). This lower level of stress would undoubtedly be easier for the irradiated cells to survive, resulting in a lower cytotoxic effect dose for dose. Slight mitogenicity was noted after some irradiations; this was probably due to the mitogenic effect of oxygen free radicals generated during irradiation (Murrell *et al.* 1990). Morphological change (a granular appearance and / or elongation) was noted in some cells after some of the higher doses. Some of these may have been due to direct effects of the radiation (e.g. membrane perturbation or enhanced mitogenicity) but in the absence of detailed microscopy they will not be discussed further.

Some experiments were performed under natural (sunlight) irradiation. For these experiments the fluences at 310 nm and 405 nm were measured by radiometry on a clear May morning (18/5/98) and again one week later (28/5/98), a cloudy and wet morning. The 405 nm fluence was plotted against the UVB fluence (Figure 4.1). This figure also presents the 310 nm and 405 nm fluences of the Xe arc lamp before and after narrow band pass filtering.

The cytotoxicity data taken in conjunction with Figure 4.1 confirmed that the doses delivered to the cells in the laboratory were indeed physiologically relevant.

Table 4.1 The cytotoxic effects of the Xe arc lamp radiation on MRC5 fibroblasts.

Cells	Radiation	dose / mJ cm^{-2}	Method	Comments / Effects
MRC5	310	21	Irradiated in suspension. Immediate trypan blue exclusion.	Viability 94% of controls. Slight cytotoxicity (+).
		83	Irradiated in suspension. Immediate trypan blue exclusion.	Viability 84% of controls. Cytotoxicity (+).
	Total	3.60E+05	Irradiated in situ. Incubated 14 days	Non-cytotoxic
		7.20E+05	Irradiated in situ. Incubated 14 days	Slight cytotoxicity (+)
		7.20E+05	Irradiate in situ. Incubate 1 hr. Trypan blue exclusion	Slight cytotoxicity (+)
		7.20E+05	Irradiate in situ. Incubate 60 hrs. Trypan blue exclusion	Slight cytotoxicity (+)
		1.08E+06	Irradiated in situ. Incubated 14 days	Slight cytotoxicity (+)
		1.20E+06	Irradiate in situ. Incubate 1 hr. Trypan blue exclusion	Slight cytotoxicity (+)
		1.80E+06	Irradiated in situ. Incubated 14 days	Cytotoxicity (++)
		2.20E+06	Irradiated in situ. Incubated 14 days	Substantial cytotoxicity (+++)
		2.40E+06	Irradiate in situ. Incubate 60 hrs. Trypan blue exclusion	Cytotoxicity (++)
		2.50E+06	Irradiated in situ. Incubated 14 days	Substantial cytotoxicity (+++)
		2.60E+06	Irradiate in situ. Incubate 1hr 37 °C	Slight cytotoxicity
		2.90E+06	Irradiated in situ. Incubated 14 days	Substantial cytotoxicity (+++)

Table 4.2 The cytotoxic effects of Xe arc lamp radiation on A2058 melanoma cells

Cells	Radiation	dose / mJ cm^{-2}	Method	Comments / Effects
A2058	405	17.1	Irradiated in media. Incubated 14 days.	Lower fluence Xe bulb. Slight mitogenic effects
A2058	405	47	Irradiated in situ. Incubated 14 days	Non-cytotoxic
A2058	405	1.35E+02	Irradiated in media. Incubated 14 days.	Lower fluence bulb. Slight mitogenic effects
A2058	405	2.70E+02	Irradiated in media. Incubated 14 days.	Lower fluence bulb. Slight mitogenic effects
A2058	Total	1.60E+04	Irradiated in situ. Incubated 67 hrs	Higher fluence bulb. Slight mitogenicity.
A2058	Total	2.50E+04	3 hrs incubation at 37 °C. Trypan blue exclusion	Higher fluence bulb. Viability ~72% of controls
A2058	Total	1.30E+05	Irradiated in situ. Incubated 67 hrs	Higher fluence bulb. Slight mitogenicity.
A2058	Total	1.72E+05	3 hrs incubation at 37 °C. Trypan blue exclusion	Higher fluence bulb. Viability ~59% of controls
A2058	Total	2.40E+05	Irradiated in situ. Incubated 14 days	Slight cytotoxicity. Morphological change
A2058	Total	3.60E+05	Irradiated in situ. Incubated 14 days	Non cytotoxic. Morphological change
A2062	Total	5.40E+05	Irradiated in situ. Incubated 14 days	Non cytotoxic. Morphological change

Figure 4.1 The fluence levels of the natural (sunlight) radiation delivered to the cells outside this laboratory. The fluence at 310 nm and 405 nm was taken by radiometry on a clear May morning and again one week later, a cloudy and wet morning. The 405 nm fluence was plotted against the UVB fluence. This figure also presents the fluences of the Xe arc lamp at 310 nm (approximately 22 μW cm^{-2}) and 405 nm (approximately 75 μW cm^{-2}) before and after narrow band pass filtering (nbpf) (see text for details).
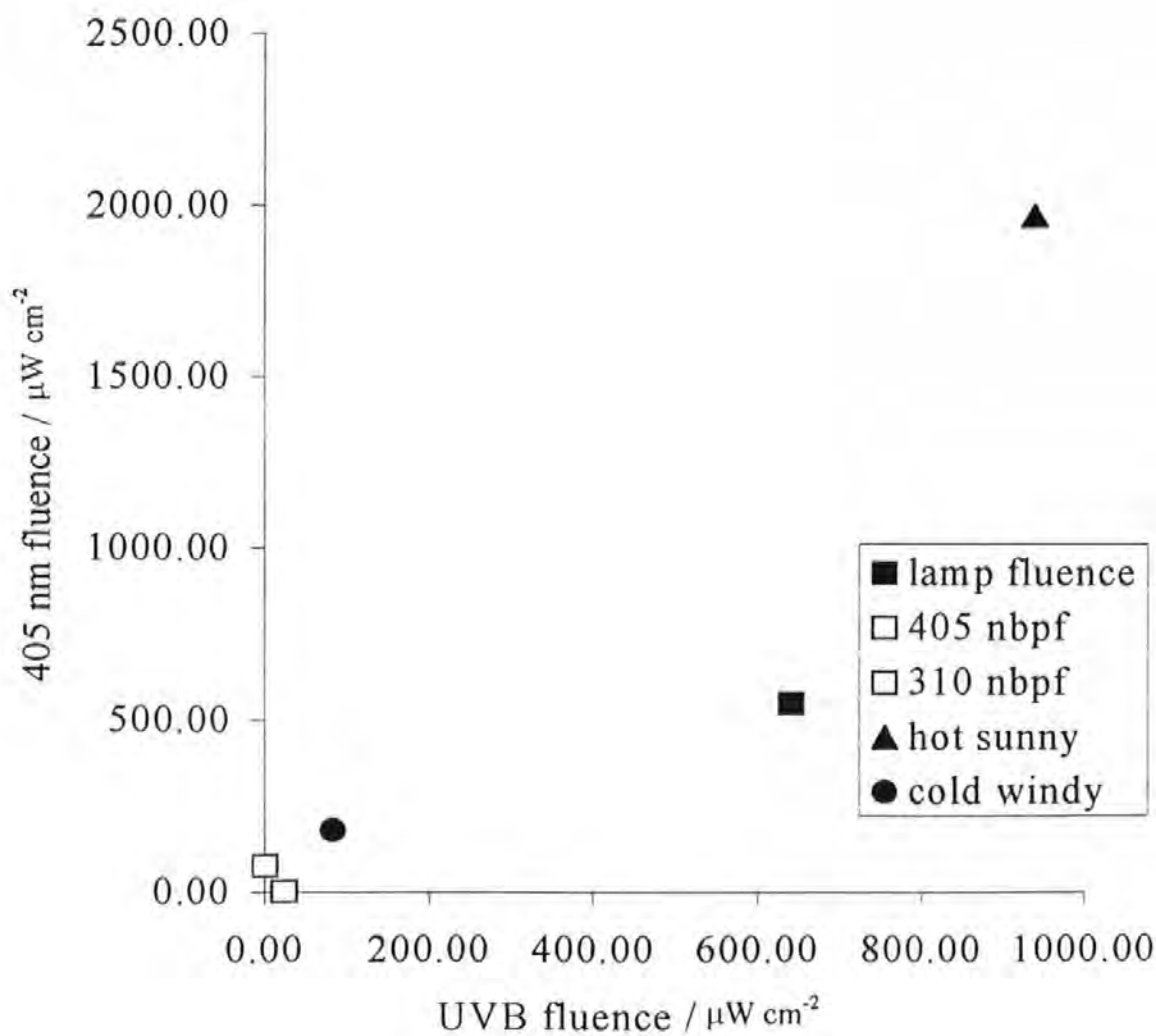
4.2.2 Direct SSB induced by UVR in human cells

4.2.2.1 Introduction

SSB induced by 405 nm narrow band radiation, 310 nm narrow band radiation and total Xe

lamp radiation were measured in a variety of cell types. Cells were embedded in 0.6%

LMP agarose made up in DMEM without phenol red (Section 2.3.1.1.1) and irradiated for

times between zero and 320 s using the 'embedded' protocol (Section 2.3.2.1). Cells were

immediately placed into ice-cold lysis mix and electrophoresed for 24 minutes at   20 V.

SSB were assayed by both the visual inspection (Section 2.3.4.1) and image analysis

(Section 2.3.4.2).

SSB was measured in normal lymphocytes from a male donor (MMB4L) and from a

female donor (YLB7L) using whole blood and the fingerprick method (Section 2.3.2.1.1)

SSB was also measured in the lymphocyte cell line PUTKO (created by the fusion of a

male and a female lymphocytic tumour (ECACC data sheet)), Simian Virus 40-

transformed fibroblasts (MRC5 SV2) and melanoma cells (A2058) by the embedded +

media protocol (Section 2.3.2.1). At higher doses SSB were measured in the normal

fibroblast cell line MRC5 by the suspended + PBS protocol (Section 2.3.2.2).

In general, SSB were observed to increase for the first few minutes of irradiation. This

increase was transient in the cases of the low fluence 405 nm radiation (~75 μW cm^{-2}) and

the 310 nm radiation (~20 μW cm^{-2}) despite continued irradiation, reflecting an effective

cellular SSB repair mechanism, but the increase in SSB at the much higher fluence level of

the unfiltered radiation (~ 2 mW cm^{-2}) was observed to be dose-dependent. In the last

mentioned case, although some SSB repair was observed at around 2 minutes of irradiation

time, this was not adequate to overcome the high rate of SSB-induction. Two peaks of

SSB (i.e. an increase in SSB followed by a decrease in SSB) were seen throughout the

experimental series. A small peak within 20 to 60 s of starting irradiation ('Peak 1') and a

large peak at 80 to 120 s of irradiation time ('Peak 2')

The results are presented below in tabular form. The following key applies to the whole of

this Section.

Figure 4.2 The key to the tables in Section 4.2.2

	405		310		Total	
	Peak 1	Peak 2	Peak 1	Peak 2	Peak 1	Peak 2
Cell type	Magnitude	Magnitude	Magnitude	Magnitude	Magnitude	Magnitude
	Time	Time	Time	Time	Time	Time

Time is measured in s from the start of irradiation time in all experiments.

Magnitude is assessed thus:

-     Peak not detectable

±   Peak detectable as a point of inflection

+   Peak just detectable

++   Peak clearly seen

+++   Peak is the highest assayed value

The Data Sets are grouped by either cell type or irradiation wavelength and displayed graphically by data set, in order to allow direct comparisons between sets to be made. The Data Sets obtained are summarised in Table 4.3 and are numbered from 1 to 7 such that the same source data (i.e. the same comets) are given the same number. The analysis of that data by different parameters is given a letter from a to e. The reorganisation of the data for intracellular comparison is numbered in parentheses, indicating that the analysed data are used again. The results are discussed in Chapter 5 (Section 5.2).

Table 4.3 SSB was measured in the cell types MRC5 (normal fibroblast), MRC5 SV2 (transformed fibroblast), A2058 (melanoma), MMB4L (normal lymphocyte), YLB7L (normal lymphocyte) and PUTKO (hybrid transformed lymphocyte). The wavelengths employed were 405 nm, 310 nm and total Xe lamp radiation..

| | | Data Sets | | | | | |
| | | Lymphocyte | | | Melanoma | Fibroblast | |
λ	Parameter	PUTKO	MMB4L	YLB7L	A2058	MRC5	MRC5 SV2
405	Area / comet value	1 (7a)	1 (6a)	1	1	2	1
	Tail length	3a (7b)	3a (6b)	3a			3a
	Comet length	3b (7c)	3b (6c)	3b			3b
	Tail Moment	3c (7d)	3c (6d)	3c			3c
	Comet Moment	3d (7e)	3d (6e)	3d			3d
310	Area / comet value	4a (7a)	4a (6a)				
	Tail length	4b (7b)	4b (6b)				
	Comet length	4c (7c)	4c (6c)				
	Tail Moment	4d (7d)	4d (6d)				
	Comet Moment	4e (7e)	4e (6e)				
Total	Area / comet value	5a (7a)	5a (6a)				
	Tail length	5b (7b)	5b (6b)				
	Comet length	5c (7c)	5c (6c)				
	Tail Moment	5d (7d)	5d (6d)				
	Comet Moment	5e (7e)	5e (6e)				

4.2.2.3 SSB induced by 405 nm narrow band radiation

The observations summarised below are discussed in Chapter 5 of this thesis.

SSB induced by 405 nm radiation was measured in transformed fibroblasts (MRC5 SV2)

and melanoma cells (A2058) using the visual inspection method. SSB induced by 405 nm

radiation was measured in transformed fibroblasts (MRC5 SV2), normal lymphocytes

(MMB4L and YLB7L) and hybrid lymphocytes (PUTKO) by image analysis (I.A.) using

the parameter of Comet Area for direct comparison with the visual inspection method (see

also Section   ). The data are summarised in Table 4.4 and displayed in Figure 4.3.

The increase in comet values after 320 s irradiation observed in A2058 cells is an artefact

of the readback system under development at the time of the assay. The higher dose

comets (from both the A2058 and the MRC5 SV2 cells) had a different appearance, often

with the nucleus in the middle of the comet. In the early stages of assay development these

comets were given a high value to linearise the dose response (based on the current

literature, a linear dose response was expected). This weighting of comets was successful

(in that the regression line paralleled the later parts of the dose response) but was not

developed further when it became clear that the phenomenon of 'peaks' was reproducible

and reflected a cellular response. The successful prediction of high dose comet values did

demonstrate, however, that the appearance of these distinctive comets was a function of

dose.

From Table 4.4 and Figure 4.3 the following observations can be made.

(i)   The dose responses to 405 nm radiation in MRC5 SV2 cells read back by the visual

        inspection method and the image analysis parameter of Comet Area were found to

        be in very close accord. The two systems are therefore immediately comparable

        with respect to this parameter.

(ii)   The dose responses in the cells from male donors (MRC5 SV2, A2058, MMB4L)

        displayed a large (maximum) peak at 80-90 s of irradiation time, whereas the cells

from a female donor (YLB7L) displayed a very small peak. The hybrid cells which contained both male and female elements displayed an intermediate peak.

(iii)   The dose response to 405 nm radiation in A2058 cells readback by the visual inspection method was less than that of the matched dose response in MRC5 SV2 cells. This may be due to the photoprotective pigment melanin produced by A2058 but not MRC5. To test this, MRC5 and A2058 were assayed after 20 s 405 nm irradiation in six-fold replicate. The two dose responses differed significantly ($p < 0.05$) by one-tailed t-test.

Table 4.4. 405 nm-induced SSB in 6 cell types, measured by Comet Area (image analysis) or comet value (visual).

	Irradiation time / secs	Readback method	405 nm	
			Peak 1	Peak 2
MRC5 SV2	0 – 320	Visual	++	+++
			20	80
MRC5 SV2	0 – 320	I.A.	++	+++
			20	80
A2058	0 – 320	Visual	++	+++
			40	80
MMB4L	0 – 240	I.A.	-	+++
			-	90
YLB7L	0 – 240	I.A.	+	+
			15	90
PUTKO	0 – 240	I.A.	+	+
			75	105

Figure 4.3   SSB induced by 405 nm radiation measured in transformed fibroblasts

(MRC5 SV2) and melanoma cells (A2058) using the visual inspection method (open

symbols). SSB induced by 405 nm radiation measured in transformed fibroblasts

(MRC5 SV2), normal lymphocytes (MMB4L and YLB7L) and hybrid lymphocytes

(PUTKO) by image analysis (solid symbols) using the parameter of Comet Area for

direct comparison with the visual inspection method. Error bars have been omitted

for clarity.
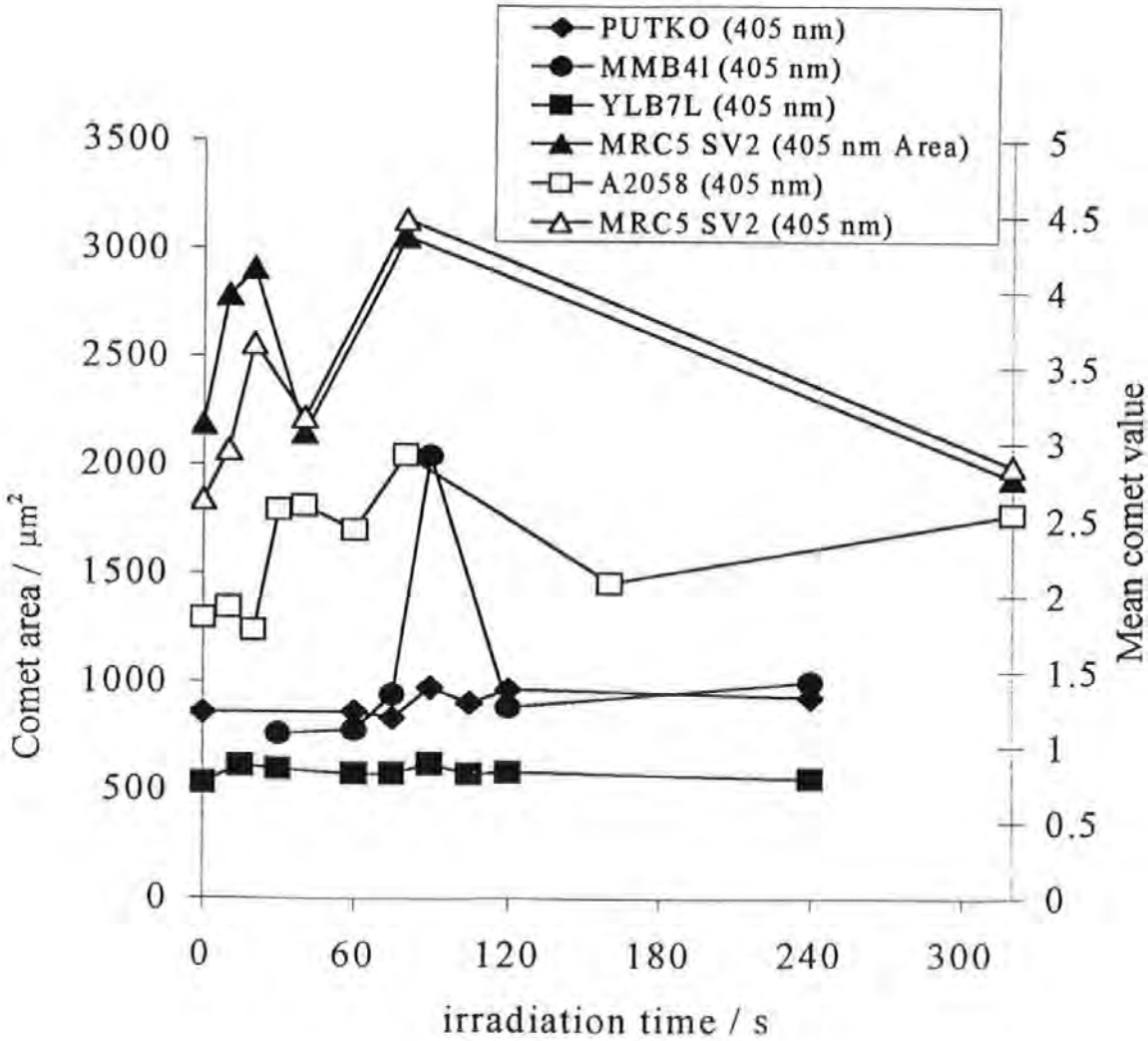
4.2.2.3.2 Data set 2. SSB induced by 405 nm radiation in MRC5 fibroblast cells

SSB induced by 405 nm radiation was also measured in MRC5 normal fibroblasts. These data were gathered as part of the investigations into repair responses of these cells to UVR-induced DNA damage. The data have therefore been gathered by a different methodology (see Section 4.2.2.1) and can not be directly compared to the previous figure. The data set comprises 41 independent determinations of SSB after a range of irradiation times from zero to 15 minutes ($0 - \sim 70$ mJ cm^{-2}). The data were gathered by irradiation for a total UV dose and not for a total irradiation time. The doses recorded have been converted to irradiation times by back-calculating from the average output of the lamp during this period. This is reflected in the X error bars which represent the mean $\pm 8\%$ of the lamp output measured by radiometry (see Section 11.2.3.1.6). These data are presented in Figure 4.4 and summarised in Table 4.5. The following observations were made.

(i)   The dose response of MRC5 normal fibroblasts to 405 nm radiation in the dose range 0-70 mJ cm^{-2} shows two peaks which were observed to occur at ~ 140 s and ~ 350 s.

(ii)   The dose response resembles those from the previous figure (Figure 4.3) in that a transitory increase in SSB was followed by a period of repair despite continued irradiation.

Table 4.5. 405 nm-induced SSB in MRC5 fibroblast cells.

	Readback	405 nm	
		Peak 1	Peak 2
MRC5	Visual	++	+++
		~140	~350

Figure 4.4 SSB was measured in MRC5 normal fibroblasts by the 'suspended' protocol as part of the investigations into repair responses of cells to UVR. The data set comprises 41 independent determinations of SSB after a range of irradiation times from zero to 15 minutes. This figure can be compared to Figure 4.3 which was generated using the 'embedded' protocol. (It is possible that the first peak is actually a 'peak 2', see text for details.) Y error bars represent one standard deviation of the mean, X error bars represent the error inherent in the back-calculation of irradiation times (see text for details).
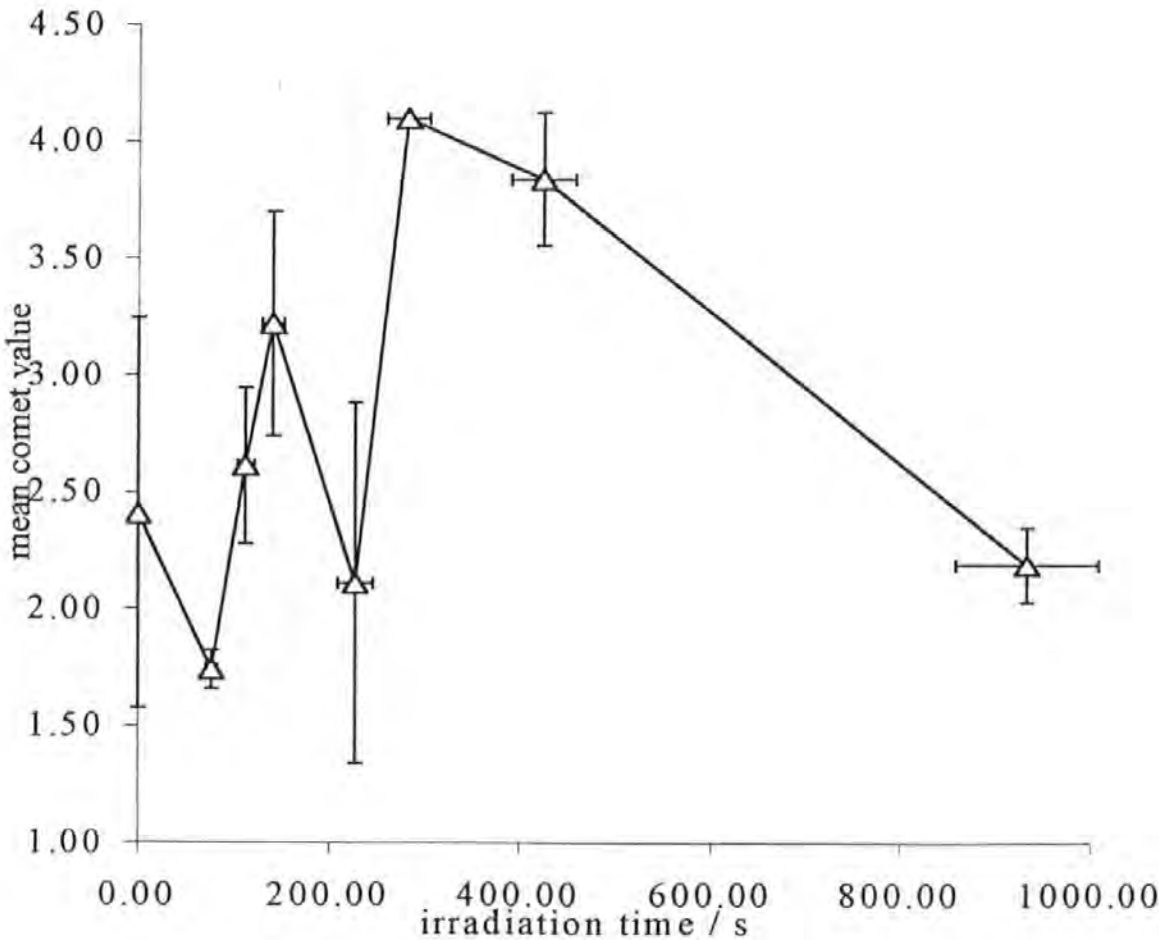
<u>4.2.2.3.3 Data set 3: A comparison of SSB induced by 405 nm radiation in 4 cell lines,</u>

<u>measured by image analysis.</u>

The observation that a large peak was induced by 405 nm radiation in male cells but not in cells which contained a female element was subjected to further analysis. In order to do this, SSB induced by 0-240 s (0-18 mJ cm^{-2}) 405 nm radiation were measured in transformed fibroblasts (MRC5 SV2), normal lymphocytes (MMB4L and YLB7L) and hybrid lymphocytes (PUTKO). The parameters of Comet length (Table 4.6, Figure 4.5), Tail length (Table 4.7, Figure 4.6), Tail Moment (Olive) (Table 4.8, Figure 4.7) and Comet Moment (Kent) (Table 4.9, Figure 4.8) were measured by image analysis.

The dose responses of each cell type were all measured using the 'embedded' protocol and obtained independently of each other. This enabled inter-cell comparison. Figures 4.5 to 4.8 are analyses of the same experimental data using the different comet assay parameters listed above. These figures (and the figures in the following experiments) also provide an assessment of the suitability of each parameter for the further investigations planned for this study (see also chapters 6 and 8). The MRC5 SV2 cell is a physically large cell and so the dose response of this cell line has been plotted on a secondary axis. This optimises the details of the other dose responses (compare, for example, Figure 4.5 with Figure 4.3).

The following observations were made.

(i)   The second peak was observed in all four cell types, but to a greater extent in the male cells than in the female cells. A peak intermediate between these two was observed in the hybrid cells.

(ii)   The first peak was observed in the cell types which were successfully assayed at very early time points.

(iii)   The detection, magnitude and timing of the observed peaks were very much dependent on the comet assay parameter used.

(iv)   The physical parameters of Comet Area (Figure 4.3) Comet length (Figure 4.5) and Tail length (Figure 4.6) successfully detected peak 2 in all 4 cells and peak 1 in cells assayed at 10-15 s.

(v)   The Tail Moment (Figure 4.7) detected peak 2, sometimes at different times to the physically-based parameter-measured peaks: in the MMB4L cells the peak was assayed earlier (75 secs), whereas in the YLB7L and PUTKO cells it was assayed later (105 secs). The Tail Moment clearly detected peak 1 in the early points (10-15 secs) assayed and showed a downward slope in the MMB4L cells at 30-60 secs, indicating (perhaps) that this was the downward slope of peak 1.

(vi)   Kent's Comet Moment detected peak 2 in all cells. It detected peak 1 in MRC5 SV2 cells but not in YLB7L cells. It detected peak 1 in PUTKO cells and reported a downward slope during the 30-75 second period, suggesting that maybe this was evidence of peak 1.

4.2.2.3.3.1   Data set 3a: Comet length (Figure 4.5)

Table 4.6. 405 nm induced SSB in 4 cell lines, assayed by Comet length.

	405 nm	
	Peak 1	Peak2
MRC5 SV2	++	+++
	20	80
MMB4L	-	+++
	-	90
YLB7L	+	+
	15	90
PUTKO	-	++
	-	90

4.2.2.3.3.2   Data set 3b: Tail length (Figure 4.6)

Table 4.7. 405 nm induced SSB in 4 cell lines, assayed by Tail length

	405 nm	
	Peak 1	Peak2
MRC5 SV2	++	+++
	20	80
MMB4L	-	+++
	-	90
YLB7L	+++	+
	15	90
PUTKO	-	+
	-	90

4.2.2.3.3.3   Data set 3c: Tail Moment (Olive) (Figure 4.7)

Table 4.8. 405 nm induced SSB in 4 cell lines, assayed by Olive's Tail Moment

Table 4.8	405 nm	
	Peak 1	Peak2
MRC5 SV2	++	+++
	20	80
MMB4L	++	+++
	75	240
YLB7L	+++	++
	15	90
PUTKO	-	+++
	-	90

123

4.2.2.3.3.4　Data set 3d: Comet Moment (Kent) (Figure 4.8)

Table 4.9. 405 nm induced SSB in 4 cell lines, assayed by Kent's Comet Moment

Table 4.9	405 nm	
	Peak 1	Peak2
MRC5 SV2	++	+++
	20	80
MMB4L	++	++
	30	90
YLB7L	-	+
	-	90
PUTKO	++	+++
	60	90

Figure 4.5 SSB induced by 405 nm radiation measured in transformed fibroblasts (MRC5 SV2), normal lymphocytes (MMB4L and YLB7L) and hybrid lymphocytes (PUTKO) by Comet length (Table 4.6).
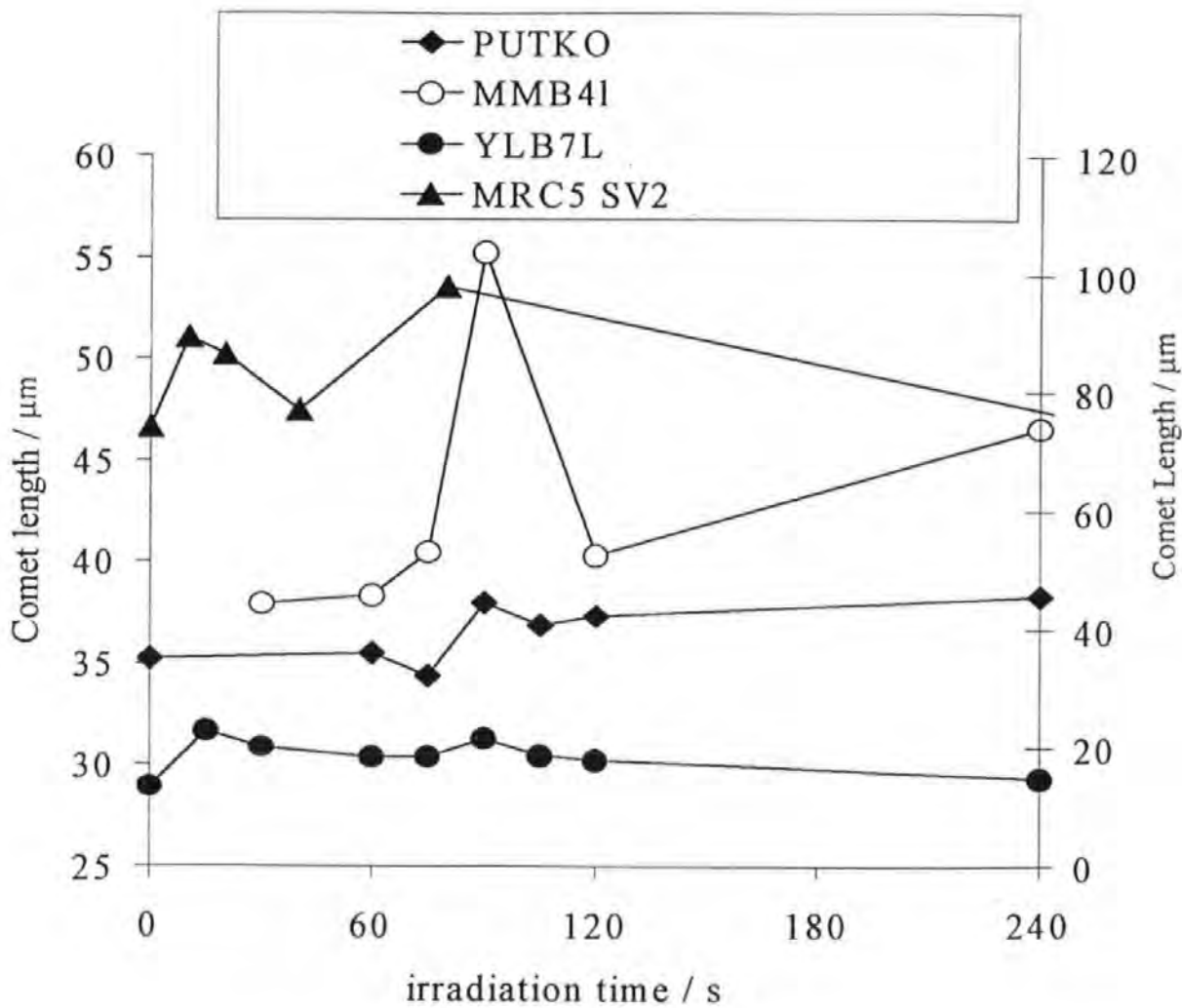
Figure 4.6   SSB induced by 405 nm radiation measured in transformed fibroblasts (MRC5 SV2), normal lymphocytes (MMB4L and YLB7L) and hybrid lymphocytes (PUTKO) by Tail length (Table 4.7)
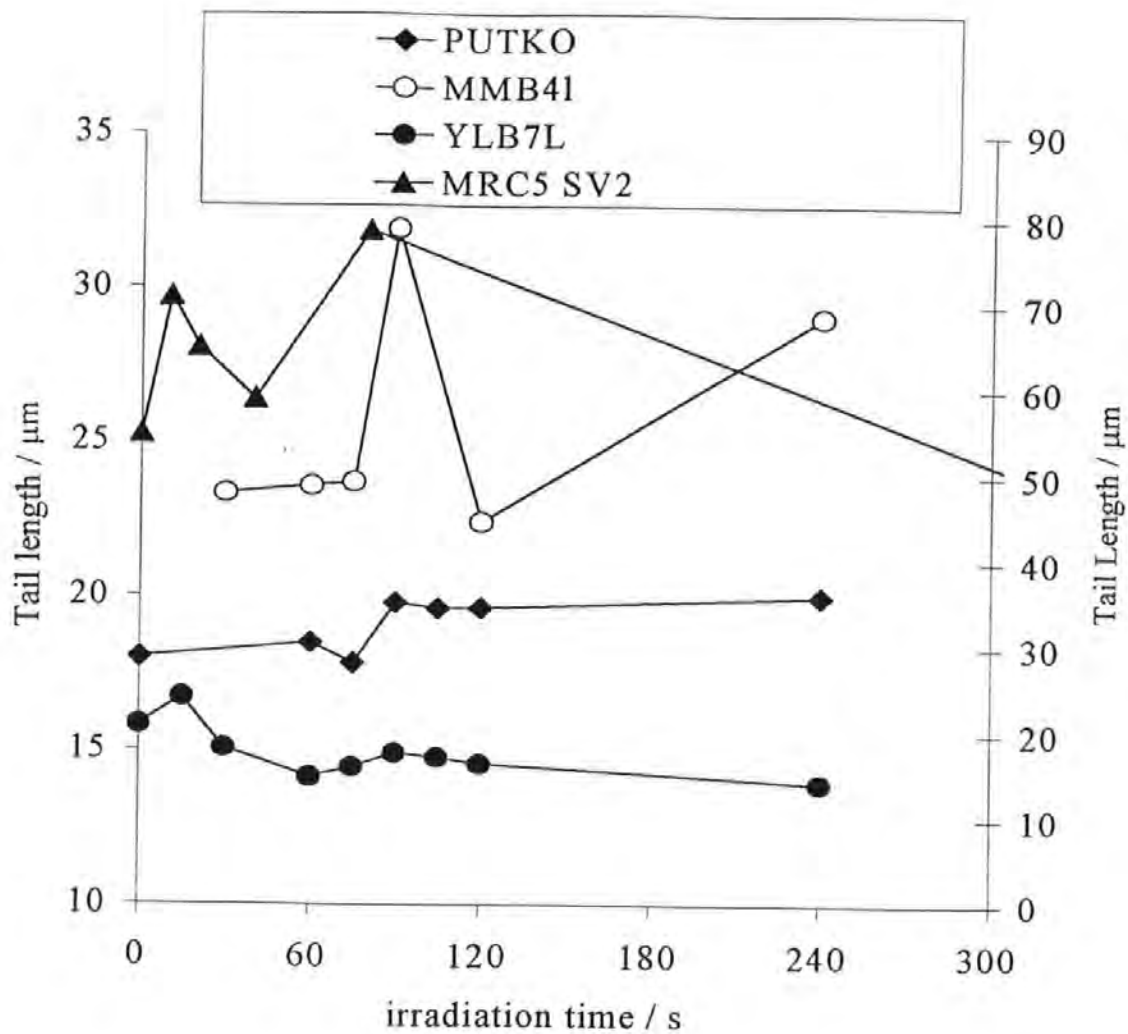
Figure 4.7   SSB induced by 405 nm radiation measured in transformed fibroblasts (MRC5 SV2), normal lymphocytes (MMB4L and YLB7L) and hybrid lymphocytes (PUTKO) by Olive's Tail Moment (Table 4.8)
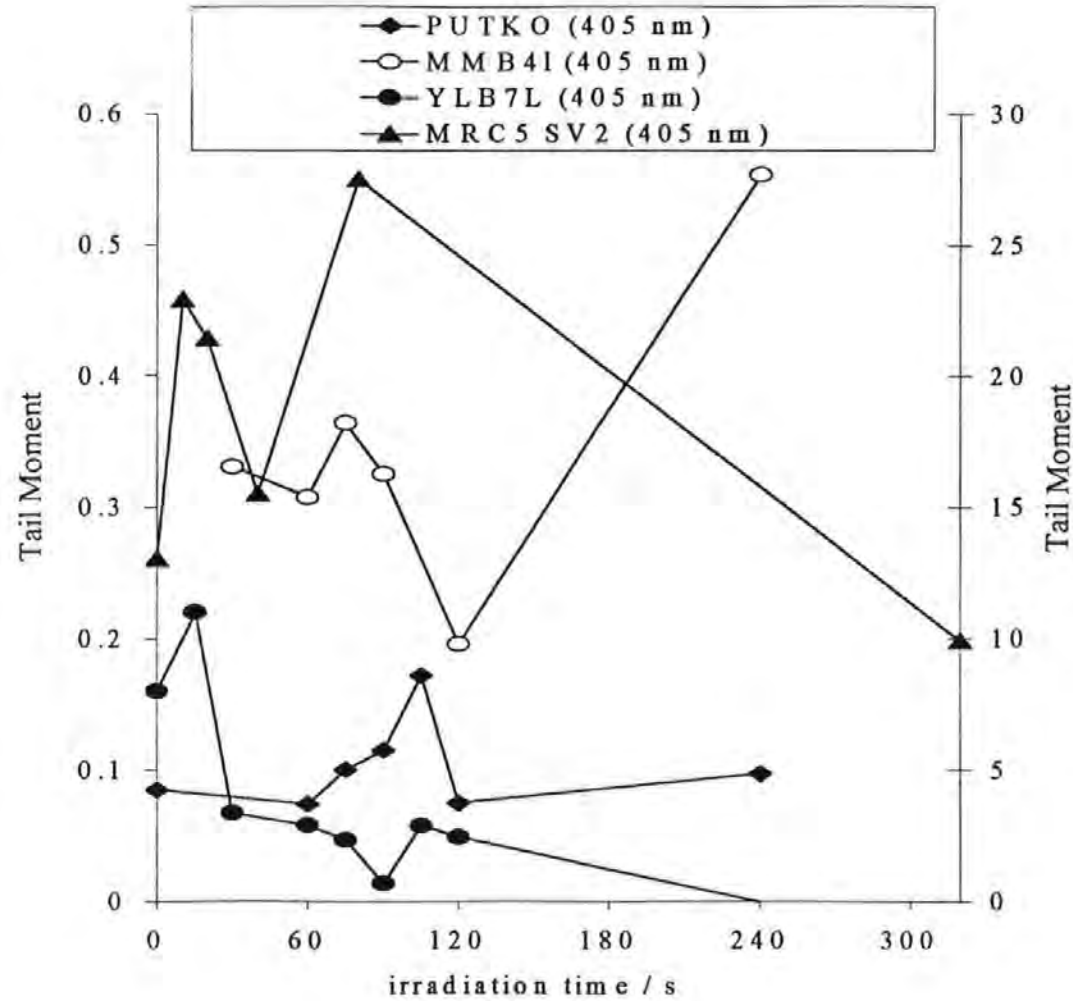
Figure 4.8 SSB induced by 405 nm radiation measured in transformed fibroblasts (MRC5 SV2), normal lymphocytes (MMB4L and YLB7L) and hybrid lymphocytes (PUTKO) by Kent's Comet Moment (Table 4.9)
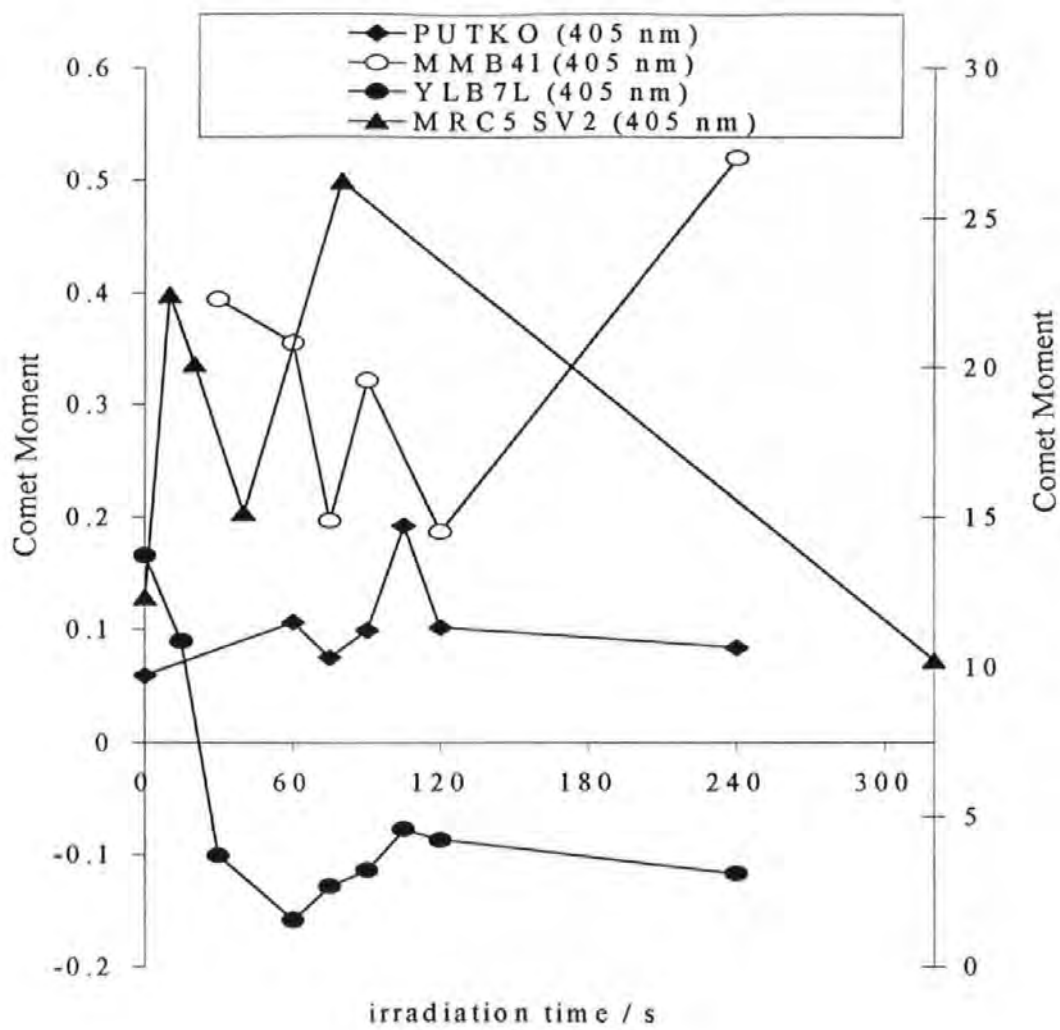
4.2.2.4 Data set 4: A comparison of 310 nm-induced SSB in lymphocytes.

To obtain more information about the two peaks observed in the 405 nm dose responses

the normal (male) lymphocytes (MMB4L) were compared with the hybrid lymphocytes

PUTKO in two parallel series of experiments - SSB induced by low fluence 310 nm

narrow band radiation (~20 μW cm^{-2})(this Section) and high fluence (~3 mW cm^{-2})

unfiltered Xe lamp radiation (Section 4.2.2.5).

SSB induced by 310 nm radiation was measured in normal (MMB4L) and hybrid

(PUTKO) lymphocytes by image analysis. The parameters measured were Comet Area

(Table 4.10, Figure 4.9), Comet length (Table 4.11, Figure 4.10), Tail length (Table 4.12,

Figure 4.11), Olive's Tail Moment (Table 4.13, Figure 4.12) and Kent's Comet Moment

(Table 4.14, Figure 4.13). The following observations were made.

(i)   Peak 2 was clearly detected as maxima in both cell lines by all five parameters.

Peak 2 was assayed at 90 s in MMB4L cells by all five parameters and at 120 s in

PUTKO cells by all five parameters.

(ii)   Peak 1 was detected in PUTKO cells at 60 s by Comet Area, Comet length and Tail

length and at 75 s by Olive' Tail and Kent's Comet Moments.

(iii)   Peak 1 was detected in MMB4L cells at 30 s by the two moments and as a small

peak at 30 s by Tail length. Peak 1 was indicated by a lessening of the gradient at

30 s by Comet Area and Comet length.

(iv)   The magnitude of Peak 2 in MMB4L cells was greater than that of Peak 2 in

PUTKO cells, measured by all five parameters.

(v)   The magnitude of Peak 1 was greater in PUTKO cells than in MMB4L cells when

measured by Comet Area, Comet length and Tail length; conversely Peak 2 was

greater in MMB4L cells than in PUTKO cells when measured by the two moments.

4.2.2.4.1 Data set 4a: Comet Area (Figure 4.9)

Table 4.10 SSB induced by 310 nm radiation in two cell types, measured by Comet Area

| Table 4.10 | 310 nm | |
	Peak 1	Peak2
MMB4L	±	+++
	30	90
PUTKO	++	++
	60	90

4.2.2.4.2 Data set 4b: Comet length (Figure 4.10)

Table 4.11 SSB induced by 310 nm radiation in two cell types, measured by Comet length

| Table 4.11 | 310 nm | |
	Peak 1	Peak2
MMB4L	±	+++
	30	90
PUTKO	++	+++
	60	120

4.2.2.4.3 Data set 4c: Tail length (Figure 4.11)

Table 4.12 SSB induced by 310 nm radiation in two cell types, measured by Tail length

Table 4.12	310 nm	
	Peak 1	Peak2
MMB4L	+ 30	+++ 90
PUTKO	++ 60	+++ 120

4.2.2.4.4 Data set 4d: Tail Moment (Olive) (Figure 4.12)

Table 4.13 SSB induced by 310 nm radiation in two cell types, measured by Olive's Tail Moment

Table 4.13	310 nm	
	Peak 1	Peak2
MMB4L	++ 30	+++ 90
PUTKO	++ 75	+++ 120

4.2.2.4.5 Data set 4e: Comet Moment (Kent) (Figure 4.13)

Table 4.14 SSB induced by 310 nm radiation in two cell types, measured by Kent's Comet Moment

Table 4.14	310 nm	
	Peak 1	Peak2
MMB4L	++ 30	+++ 90
PUTKO	++ 75	+++ 120

131

Figure 4.9   SSB induced by 310 nm radiation measured in normal (MMB4L) and hybrid (PUTKO) lymphocytes by Comet Area (Table 4.10)
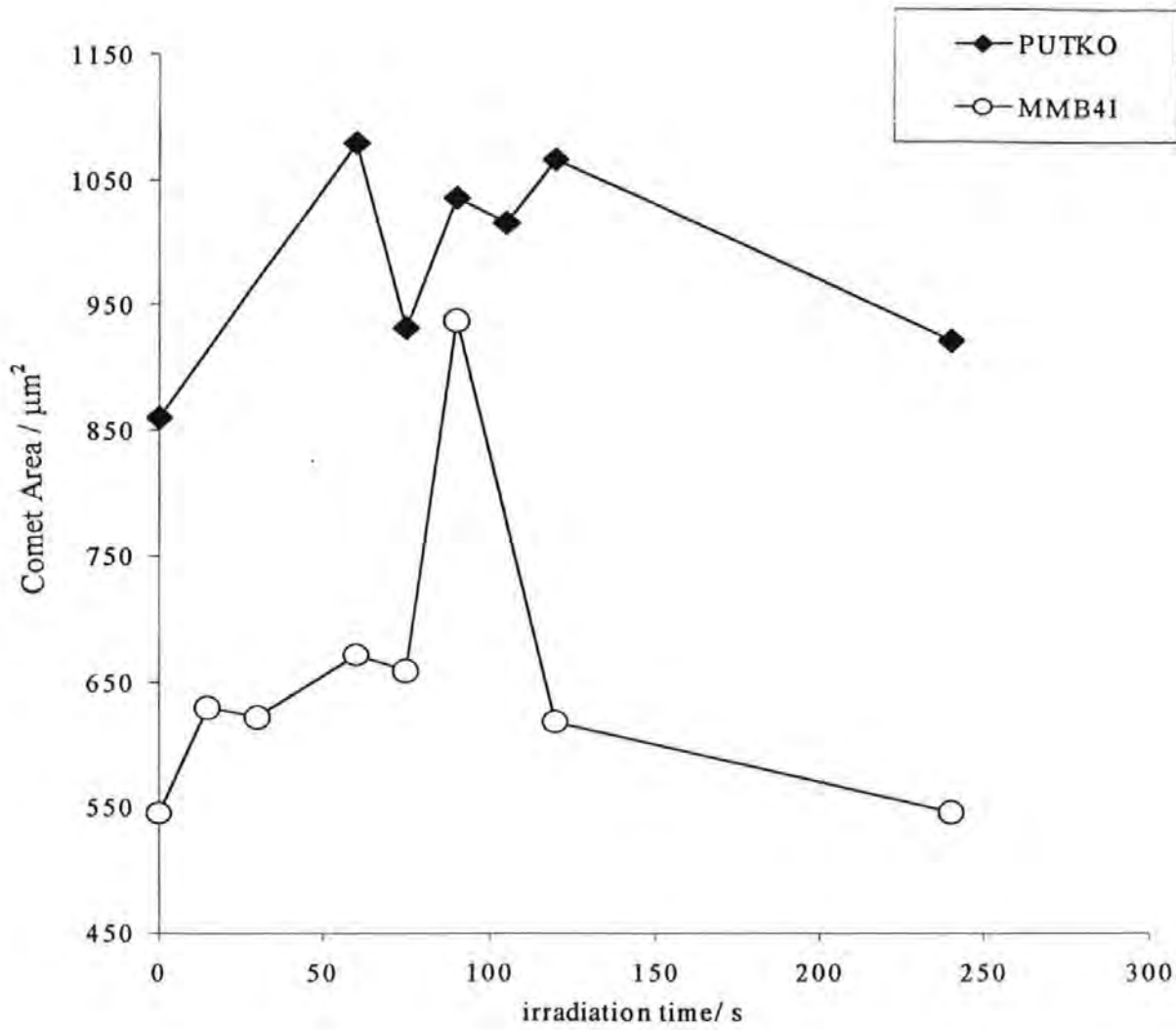
Figure 4.10   SSB induced by 310 nm radiation measured in normal (MMB4L) and hybrid (PUTKO) lymphocytes by Comet length (Table 4.11)
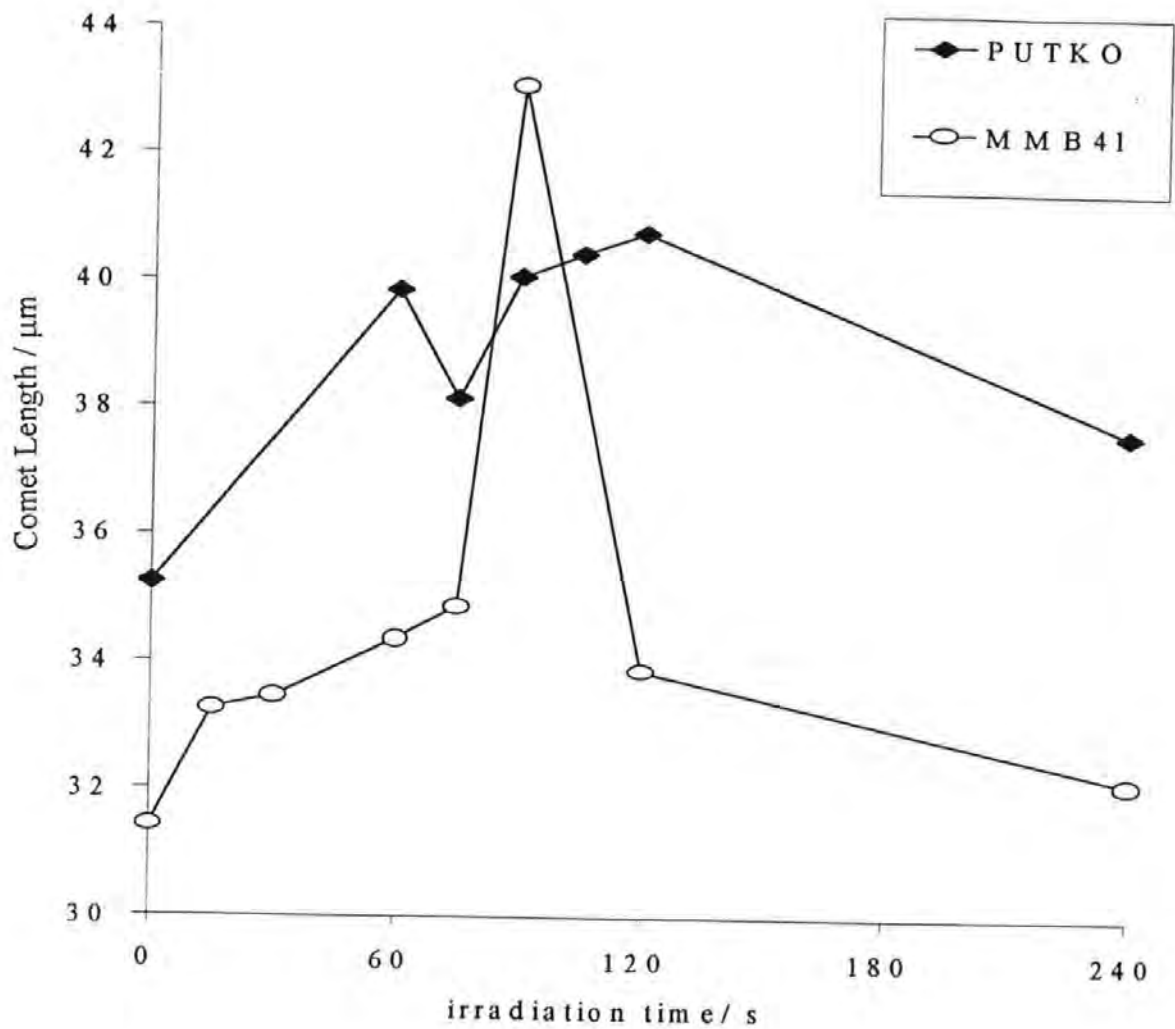
Figure 4.11   SSB induced by 310 nm radiation measured in normal (MMB4L) and hybrid (PUTKO) lymphocytes by Tail length (Table 4.12)
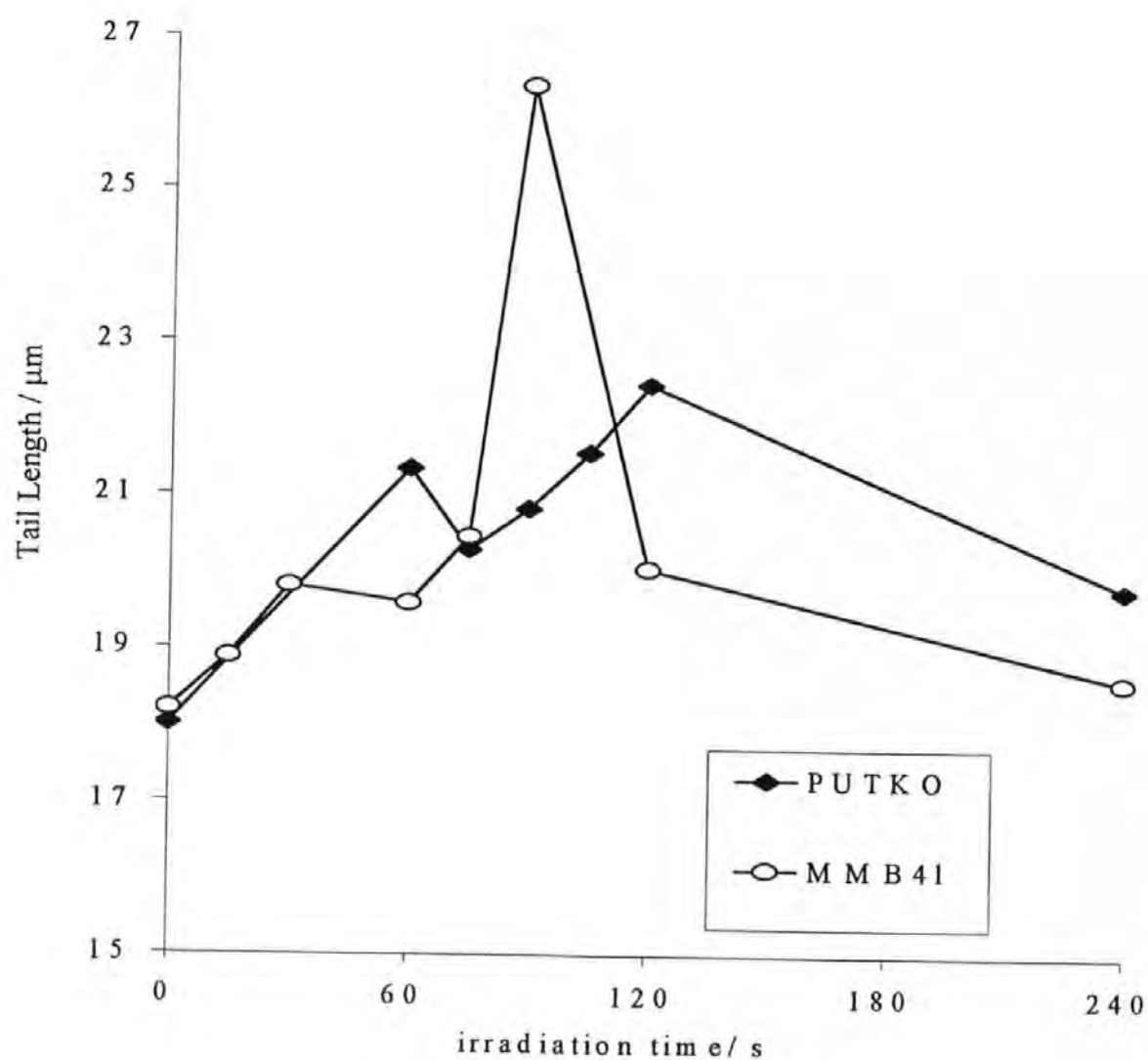
Figure 4.12   SSB induced by 310 nm radiation measured in normal (MMB4L) and

hybrid (PUTKO) lymphocytes by Olive's Tail Moment (Table 4.13)
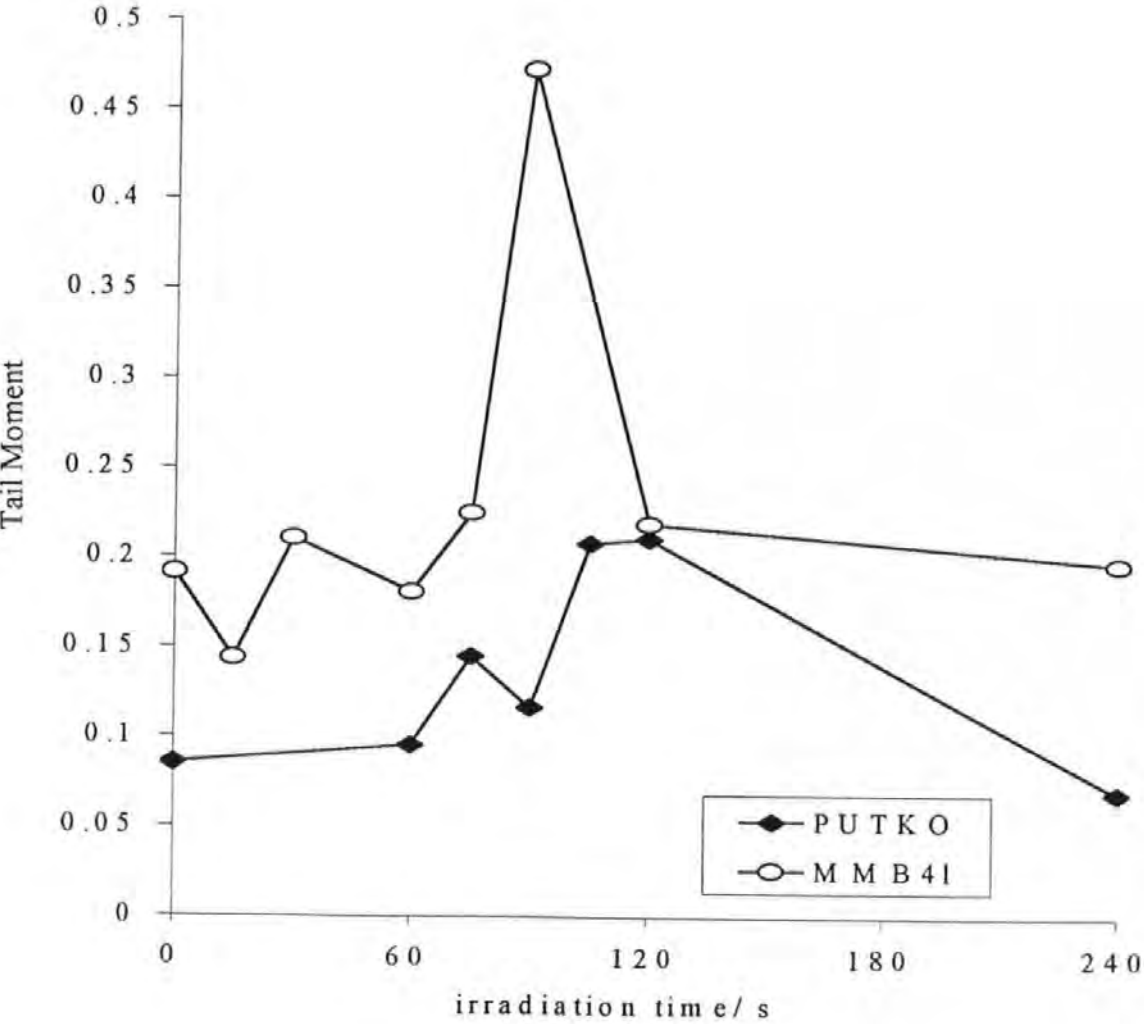
Figure 4.13   SSB induced by 310 nm radiation measured in normal (MMB4L) and

hybrid (PUTKO) lymphocytes by Kent's Comet Moment (see also Table 4.14)
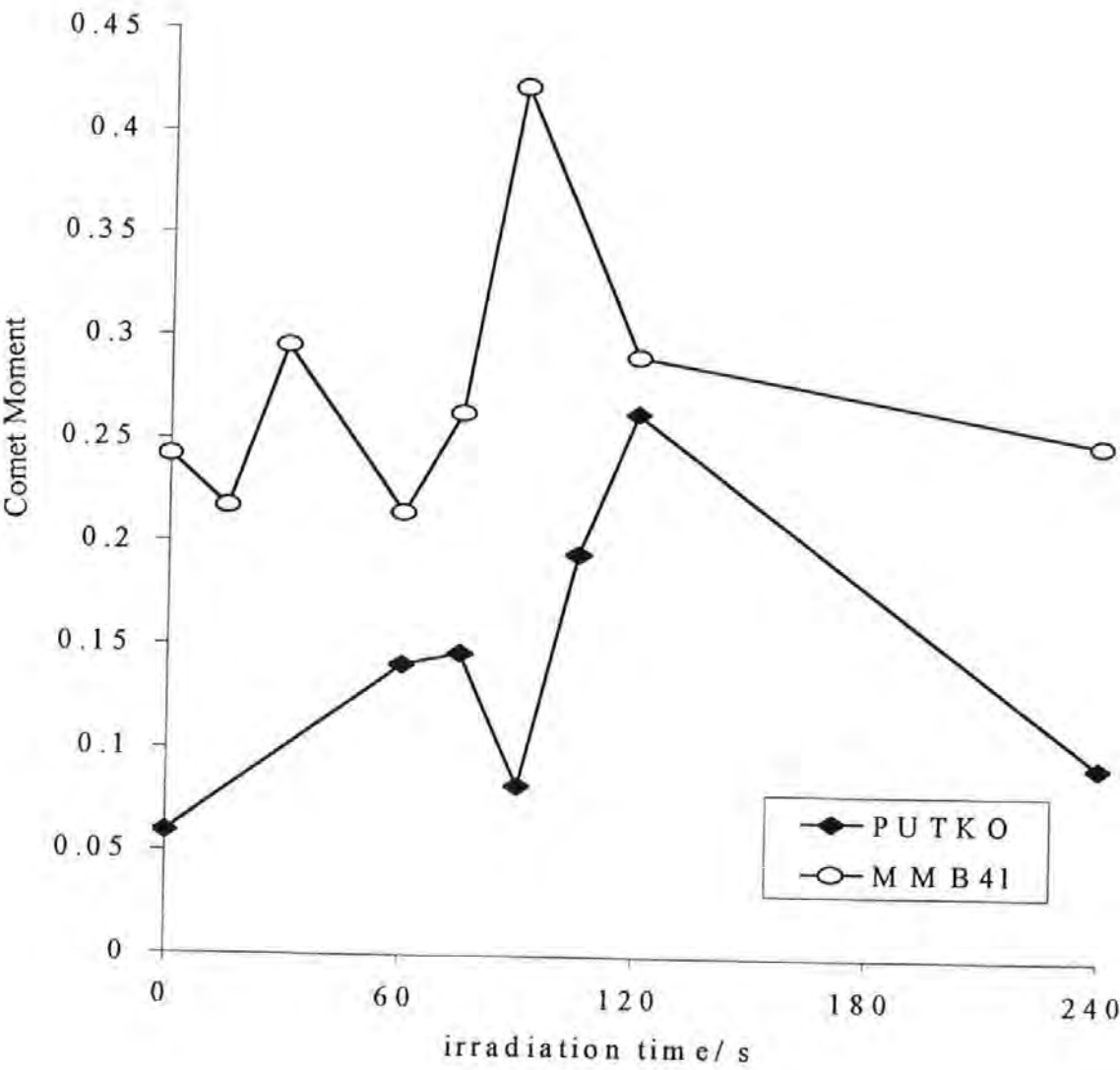
4.2.2.5 Data set 5: A comparison of total Xe lamp-induced SSB in lymphocytes.

SSB induced by unfiltered Xe lamp radiation was measured in normal (MMB4L) and

hybrid (PUTKO) lymphocytes by image analysis as in the previous Section. The

parameters measured were Comet Area (Table 4.10, Figure 4.14), Comet length (Table

4.11, Figure 4.15), Tail length (Table 4.12, Figure 4.16), Olive's Tail Moment (Table 4.13,

Figure 4.17) and Kent's Comet Moment (Table 4.14, Figure 4.18). The following

observations were made.

(i)   The dose response of MMB4L cells to unfiltered Xe radiation was linear over the

        range of irradiation times employed (0-240 s) when measured by all five

        parameters.

(ii)   The dose response of PUTKO cells to unfiltered Xe radiation was linear when

        measured by Comet Area, Comet length and Tail length. The dose response had

        sub-linear characteristics when measured by Tail Moment and Comet Moment.

(iii)   Peak 2 was detected at 105 s in PUTKO cells by all five parameters; Peak 1 was

        detected in PUTKO cells by the two moments at 75 s. Neither peak was a

        maximum or appeared to be super-linear in nature.

(iv)   Peak 1 at 60 s and Peak 2 at 120 s were just detectable in MMB4L cells by all five

        parameters, but were little more than slight deviations from linearity and the peaks

        would not be apparent to the uninformed eye.

4.2.2.5.1 Data set 5a: Comet Area (Figure 4.14)

Table 4.15 SSB induced by unfiltered Xe lamp radiation in two cell types, measured by Comet Area

Table 4.15	Total Xe lamp radiation	
	Peak 1	Peak2
MMB4L	±	-
	60	-
PUTKO	-	++
	-	105

4.2.2.5.2 Data set 5b: Comet length (Figure 4.15)

Table 4.16 SSB induced by unfiltered Xe lamp radiation in two cell types, measured by Comet Area

Table 4.16	Total Xe lamp radiation	
	Peak 1	Peak2
MMB4L	±	-
	60	-
PUTKO	-	++
	-	105

138

Table 4.17 SSB induced by unfiltered Xe lamp radiation in two cell types, measured

by Comet Area

Table 4.17	Total Xe lamp radiation	
	Peak 1	Peak2
MMB4L	±	-
	60	-
PUTKO	±	++
	75	105

4.2.2.5.4 Data set 5d: Tail Moment (Olive) (Figure 4.17)

Table 4.18 SSB induced by unfiltered Xe lamp radiation in two cell types, measured

by Olive's Tail Moment

Table 4.18	Total Xe lamp radiation	
	Peak 1	Peak2
MMB4L	++	+++
	30	90
PUTKO	++	+++
	75	120

Table 4.19 SSB induced by unfiltered Xe lamp radiation in two cell types, measured by Kent's Comet Moment

Table 4.19	Total Xe lamp radiation	
	Peak 1	Peak2
MMB4L	-	-
	-	-
PUTKO	++	++
	75	105

Figure 4.14 SSB induced by total Xe lamp radiation measured in normal (MMB4L) and hybrid (PUTKO) lymphocytes by Comet Area (Table 4.10)
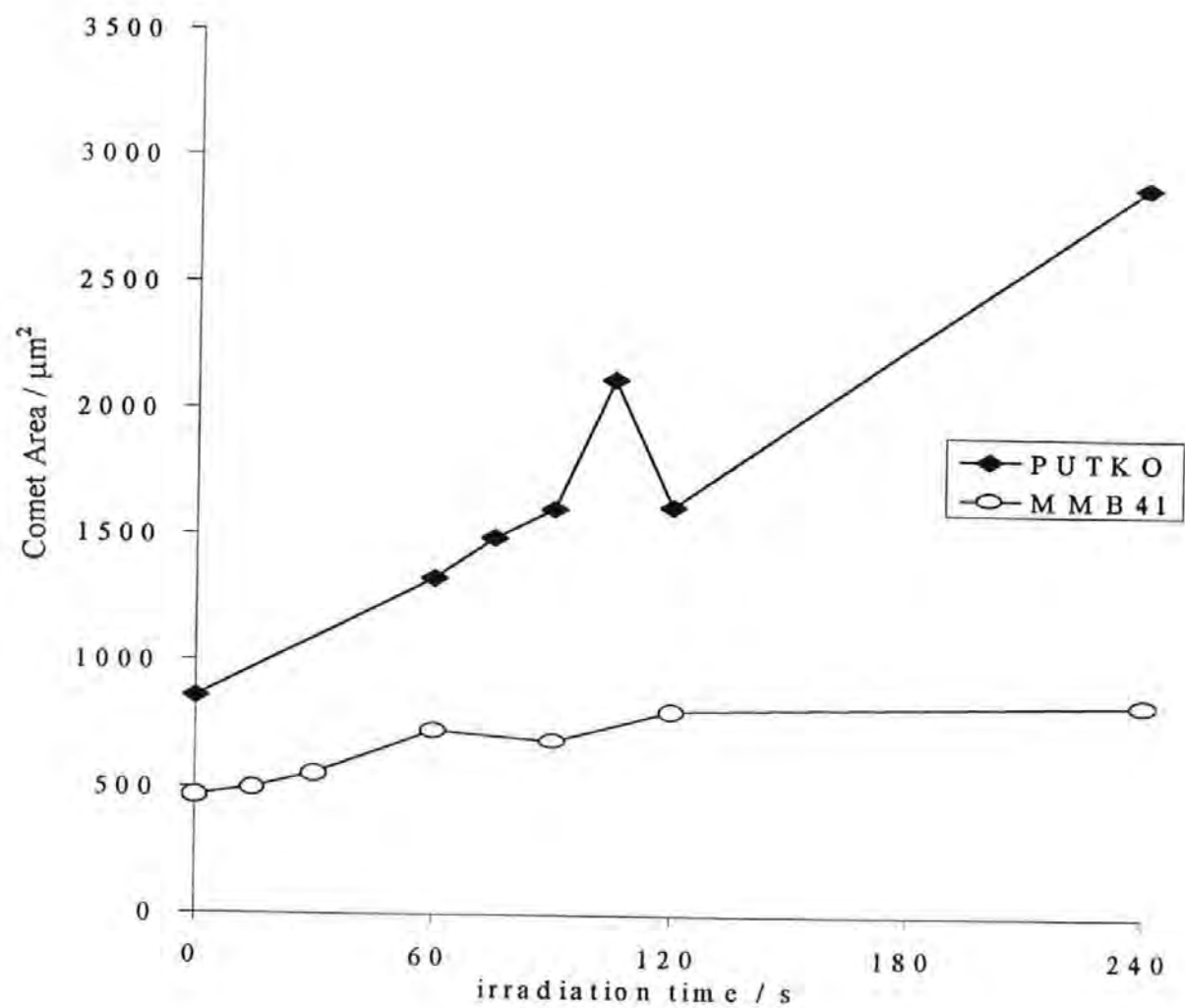
Figure 4.15   SSB induced by total Xe lamp radiation measured in normal (MMB4L)

and hybrid (PUTKO) lymphocytes by Comet length (Table 4.16)
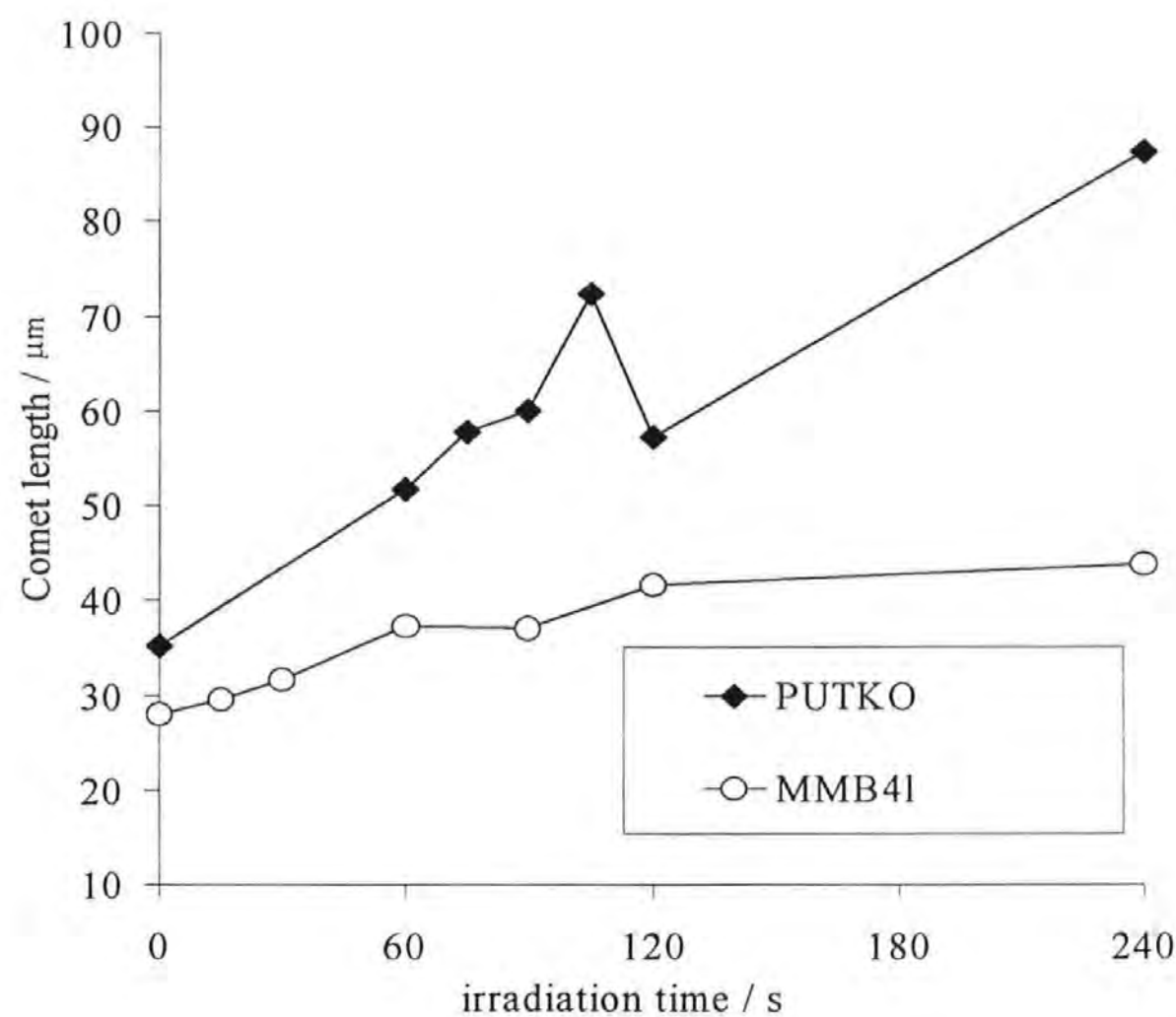
Figure 4.16   SSB induced by total Xe lamp radiation measured in normal (MMB4L) and hybrid (PUTKO) lymphocytes by Tail length (Table 4.17)
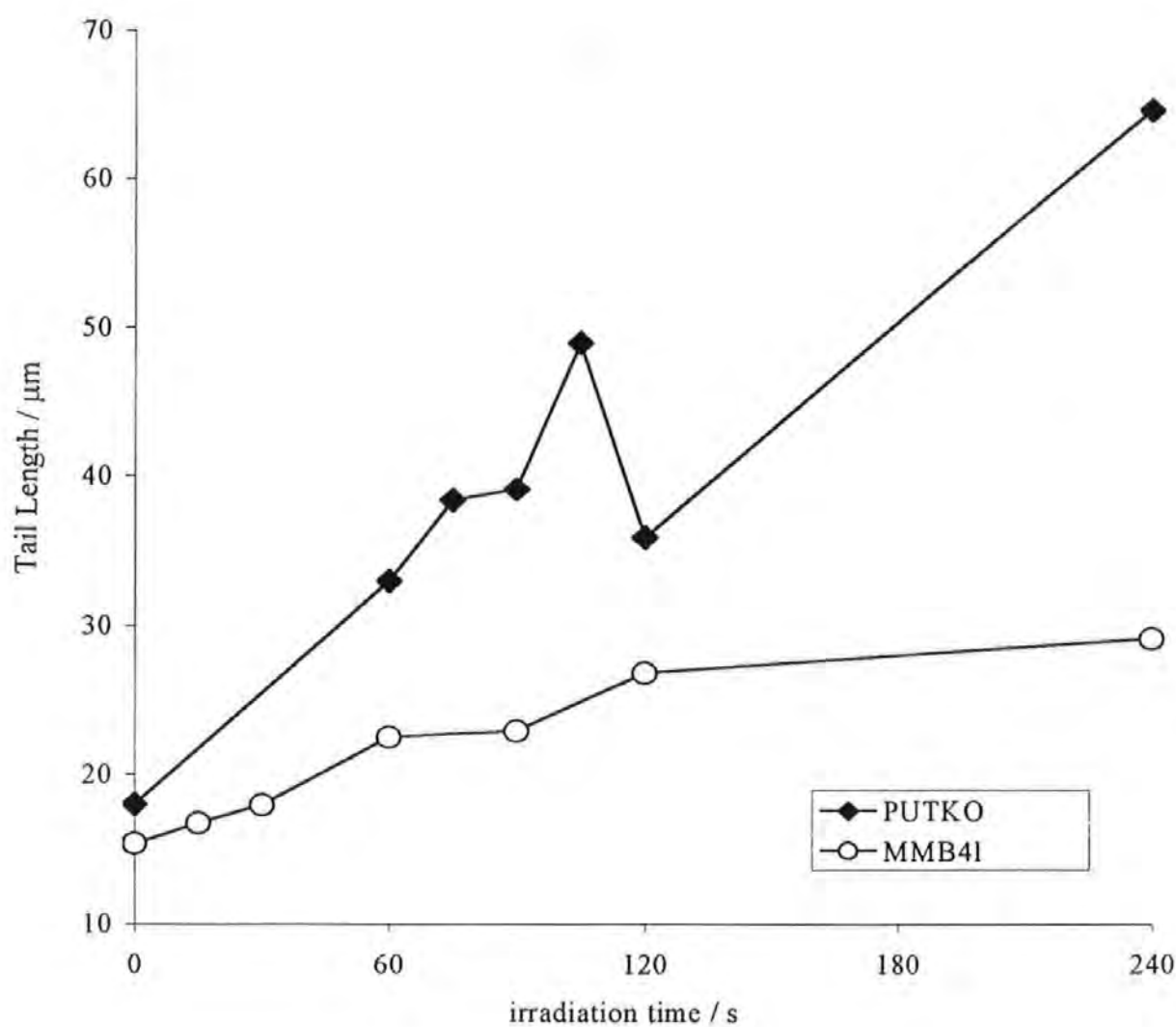
Figure 4.17   SSB induced by total Xe lamp radiation measured in normal (MMB4L) and hybrid (PUTKO) lymphocytes by Olive's Tail Moment (Table 4.18)
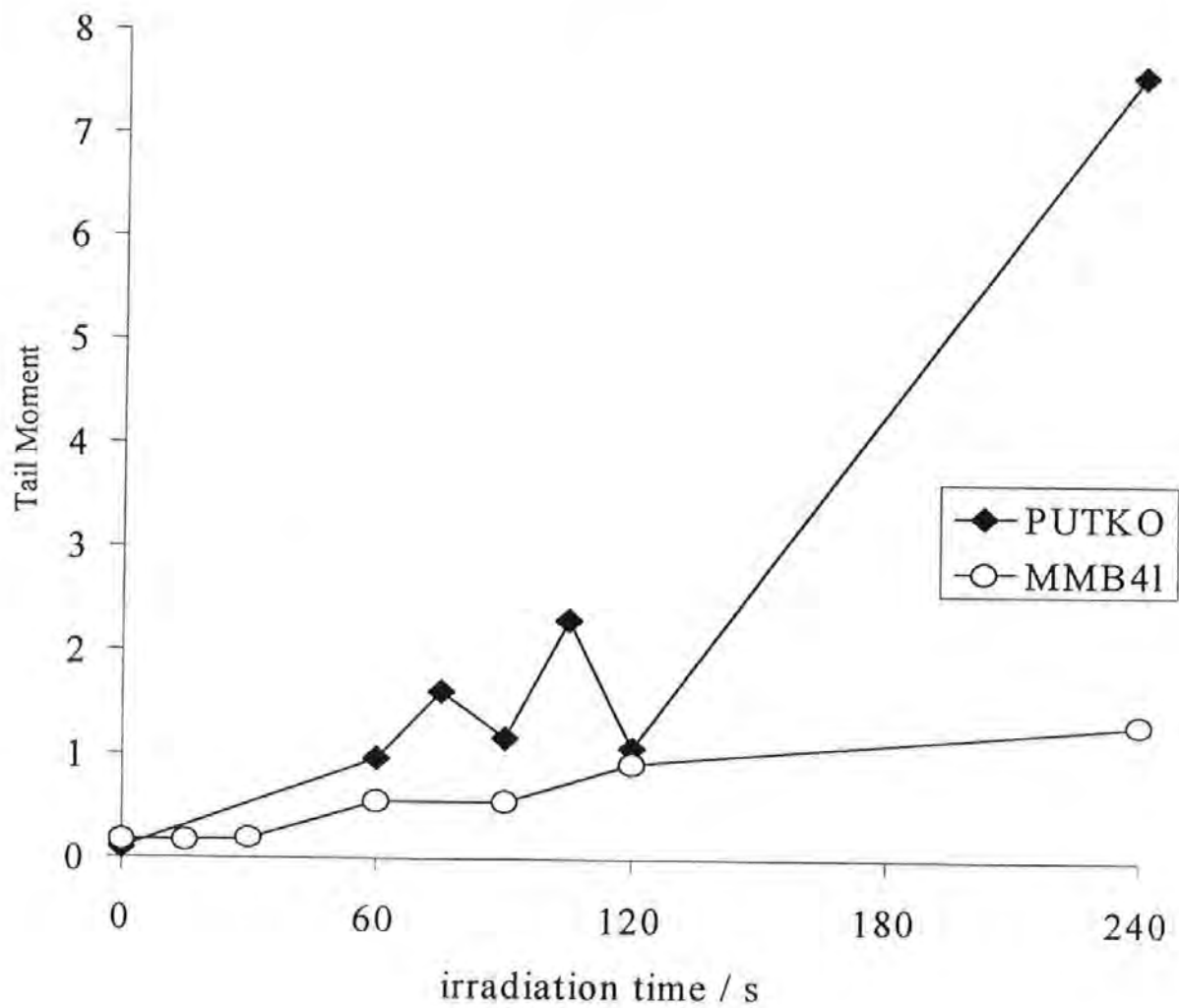
Figure 4.18   SSB induced by total Xe lamp radiation measured in normal (MMB4L) and hybrid (PUTKO) lymphocytes by Kent's Comet Moment (see also Table 4.19)
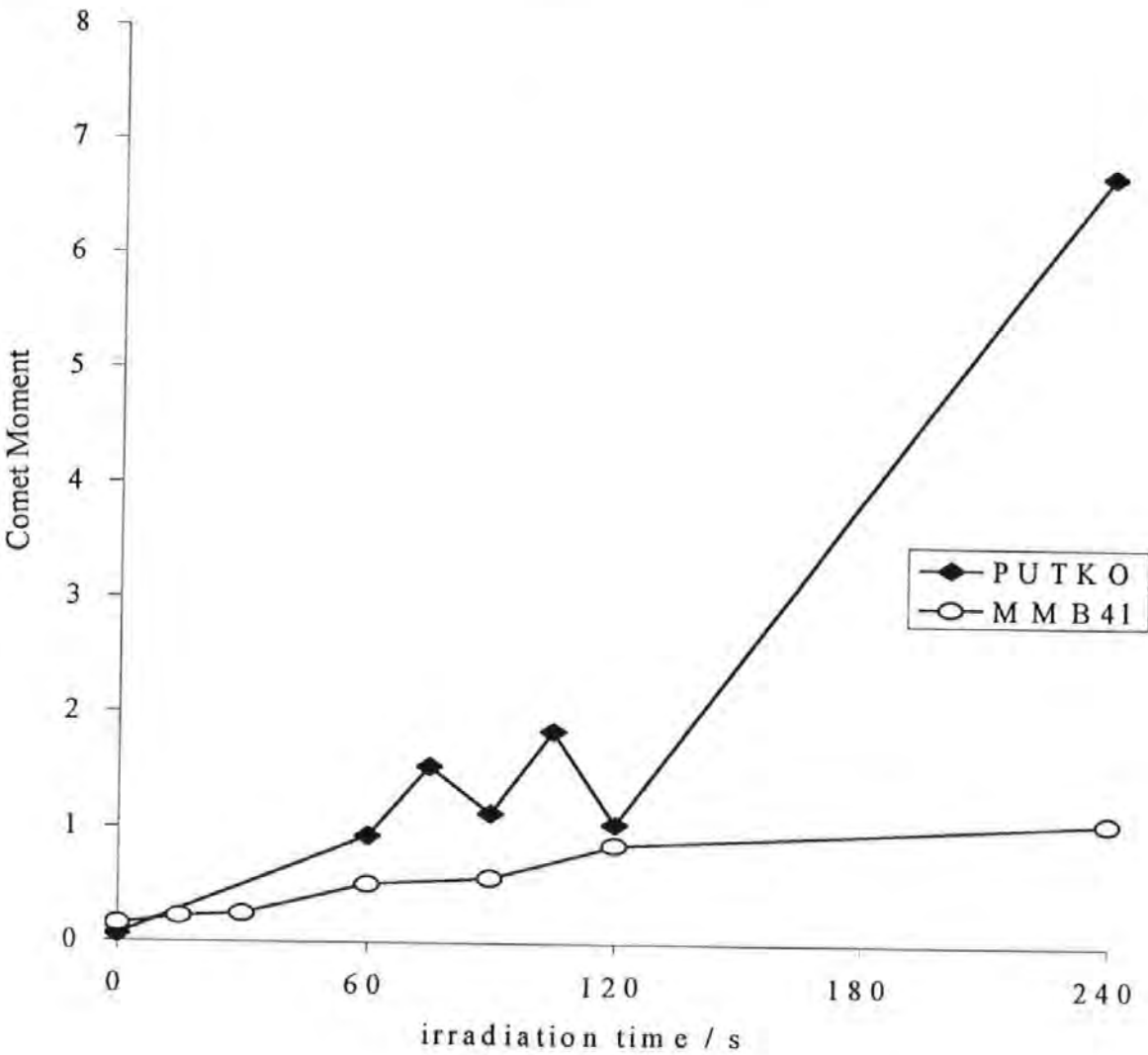
4.2.2.6   Data Sets 6 and 7: A comparison of SSB induced by 405 nm, 310 nm and total Xe

lamp radiation in normal lymphocytes MMB4L

The data for MMB4L and PUTKO cells from the preceding Section were reclassified by

cell type, thus enabling a comparison to be made between the effects of the irradiation

wavelengths employed. The following observations were made.

(i)   The magnitude of Peak 2 induced by 405 nm radiation was greater than that

induced by 310 nm radiation in MMB4L cells when measured by the Comet Area,

Comet length or Tail length but was of lesser magnitude when measured by the Tail

Moment and the Comet Moment.

(ii)   The magnitude of Peak 2 induced by 405 nm radiation was greater than, or at least

equal to that induced by 310 nm radiation in PUTKO cells.

(iii)   SSB induced by unfiltered radiation in PUTKO cells massively overshadowed that

induced by the narrow band radiation as measured by all five parameters.

(iv)   Conversely, in MMB4L cells the magnitude of the 405 nm radiation induced Peak

2 was greater than the unfiltered radiation dose response when measured by Comet

Area and when measured by Comet length or Tail length, but to a lesser extent.

4.2.2.6.1.1   Data set 6a: Comet Area (Figure 4.19)

Table 4.20 SSB in MMB4L lymphocytes induced by 405 nm, 310 nm or total Xe lamp

radiation as measured by Comet Area

Table 4.20	405		310		Total Xe radiation	
	Peak1	Peak 2	Peak1	Peak 2	Peak1	Peak 2
Magnitude	-	+++	±	+++	±	-
Seconds of irradiation	-	90	30	90	60	-

146

Table 4.21 SSB in MMB4L lymphocytes induced by 405 nm, 310 nm or total Xe lamp radiation as measured by Comet length

Table 4.21	405		310		Total Xe radiation	
	Peak1	Peak 2	Peak1	Peak 2	Peak1	Peak 2
Magnitude	-	+++	±	+++	±	-
Seconds of irradiation	-	90	30	90	60	-

4.2.2.6.3 Data set 6c Tail length (Figure 4.21)

Table 4.22 SSB in MMB4L lymphocytes induced by 405 nm, 310 nm or total Xe lamp radiation as measured by Tail length

Table 4.22	405		310		Total Xe radiation	
	Peak1	Peak 2	Peak1	Peak 2	Peak1	Peak 2
Magnitude	-	+++	+	+++	±	-
Seconds of irradiation	-	90	30	90	60	-

4.2.2.6.4 Data set 6d Tail Moment (Olive) (Figure 4.22)

Table 4.23 SSB in MMB4L lymphocytes induced by 405 nm, 310 nm or total Xe lamp radiation as measured by Olive's Tail Moment

Table 4.23	405		310		Total Xe radiation	
	Peak1	Peak 2	Peak1	Peak 2	Peak1	Peak 2
Magnitude	++	+++	++	+++	±	-
Seconds of irradiation	75	240	30	90	30	-

Table 4.24 SSB in MMB4L lymphocytes induced by 405 nm, 310 nm or total Xe lamp radiation as measured by Kent's Comet Moment

MMB4L	405		310		Total Xe radiation	
	Peak1	Peak 2	Peak1	Peak 2	Peak1	Peak 2
Magnitude	++	++	++	+++	±	-
Seconds of irradiation	30	90	30	90	60	-

Figure 4.19   SSB induced by 405 nm, 310 nm or total Xe lamp radiation measured in MMB4L normal lymphocytes by Comet Area (Table 4.20)
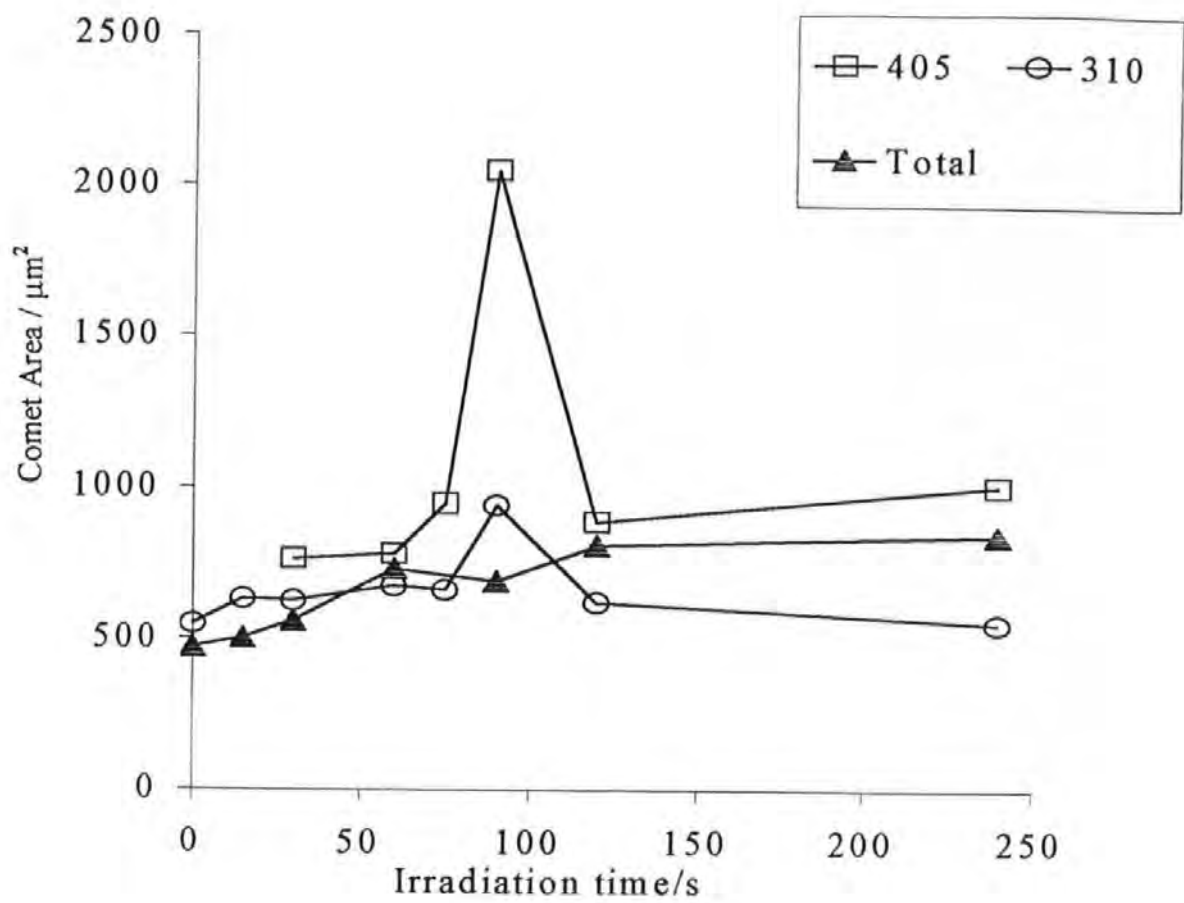
Figure 4.20   SSB induced by 405 nm, 310 nm or total Xe lamp radiation measured in MMB4L normal lymphocytes by Comet length (Table 4.21)
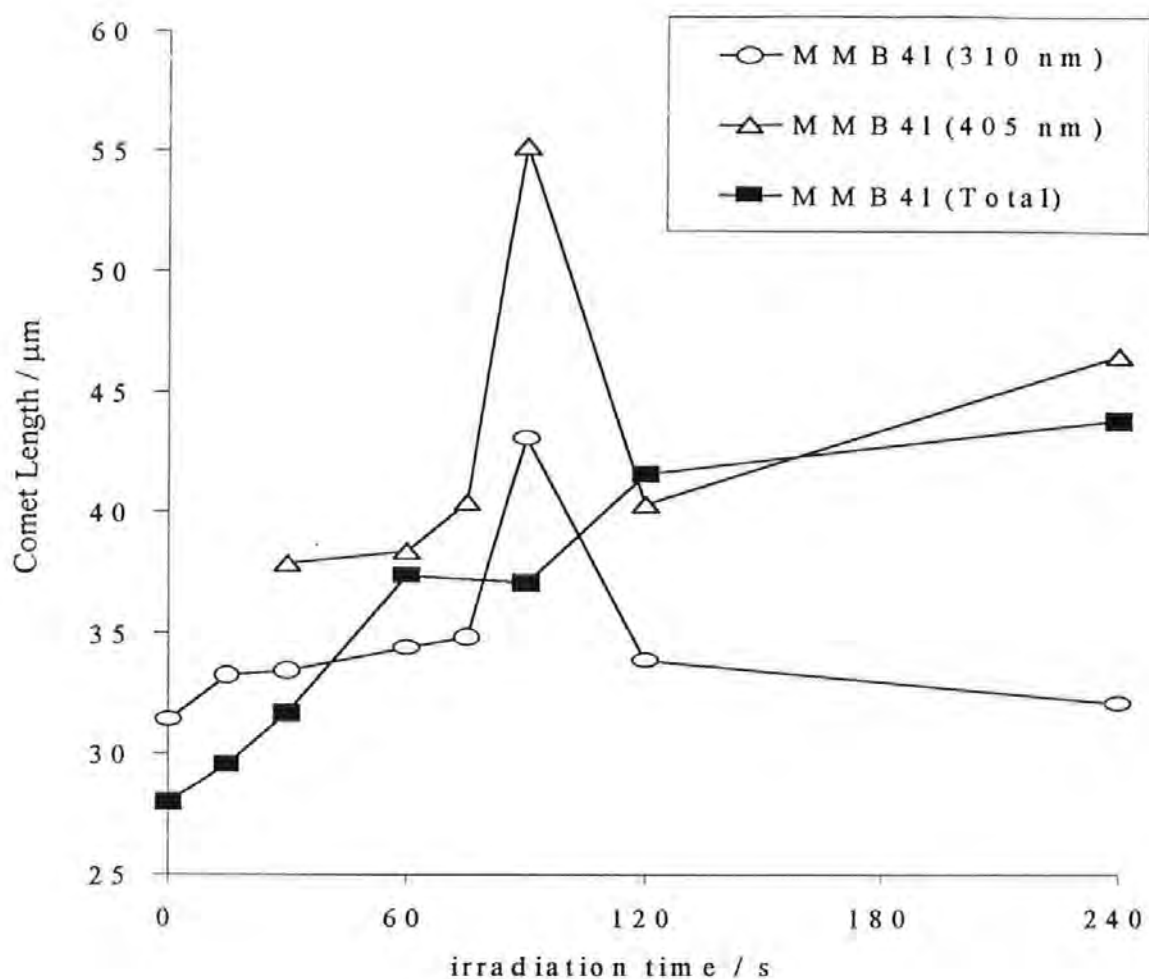
Figure 4.21   SSB induced by 405 nm, 310 nm or total Xe lamp radiation measured in MMB4L normal lymphocytes by Tail length (Table 4.22)
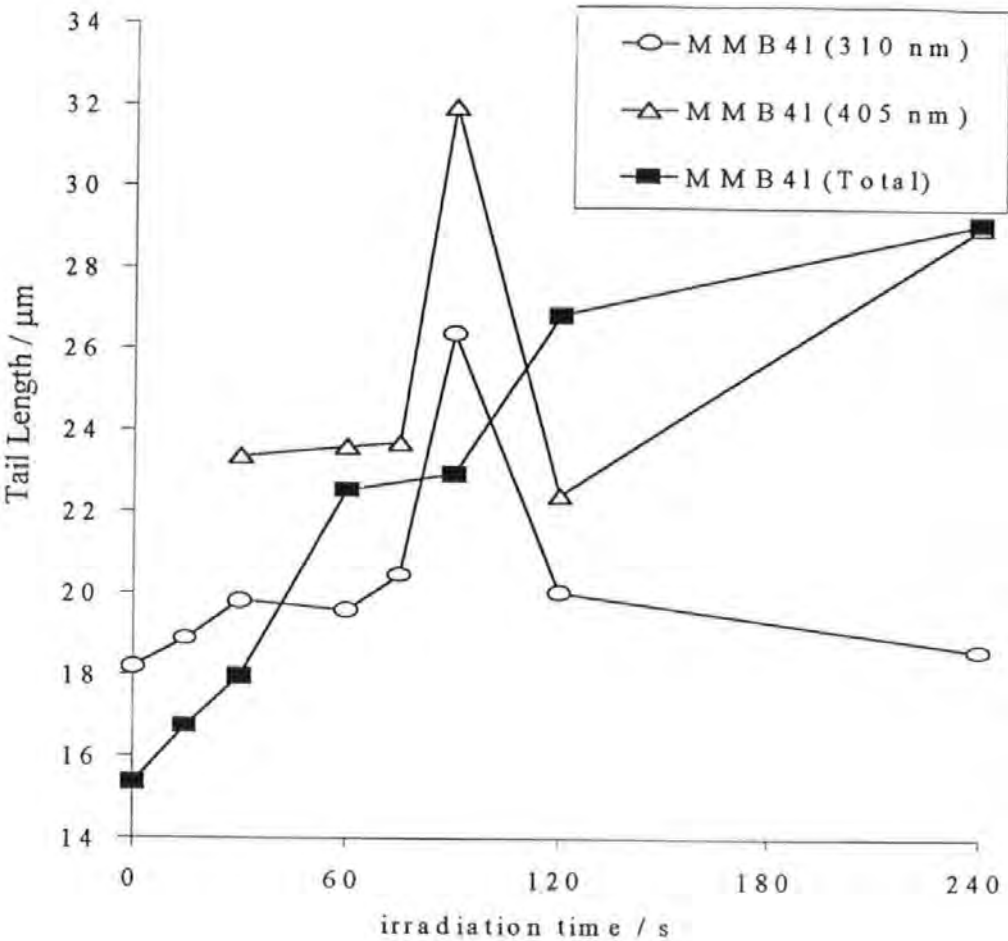
Figure 4.22   SSB induced by405 nm, 310 nm or total Xe lamp radiation measured in MMB4L normal lymphocytes by Olive's Tail Moment (Table 4.23)
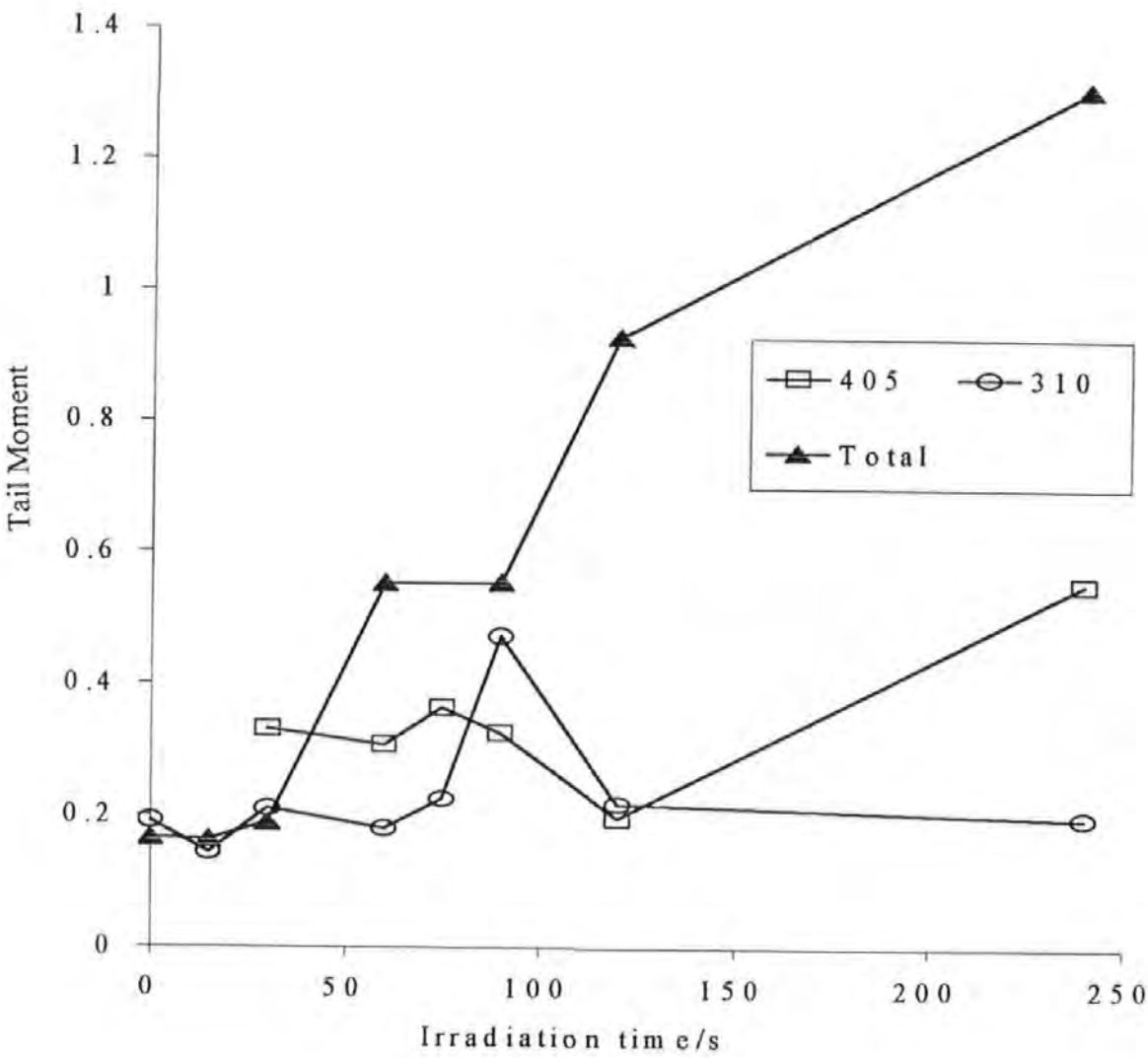
Figure 4.23   SSB induced by 405 nm, 310 nm or total Xe lamp radiation measured in MMB4L normal lymphocytes by Kent's Comet Moment (Table 4.24)
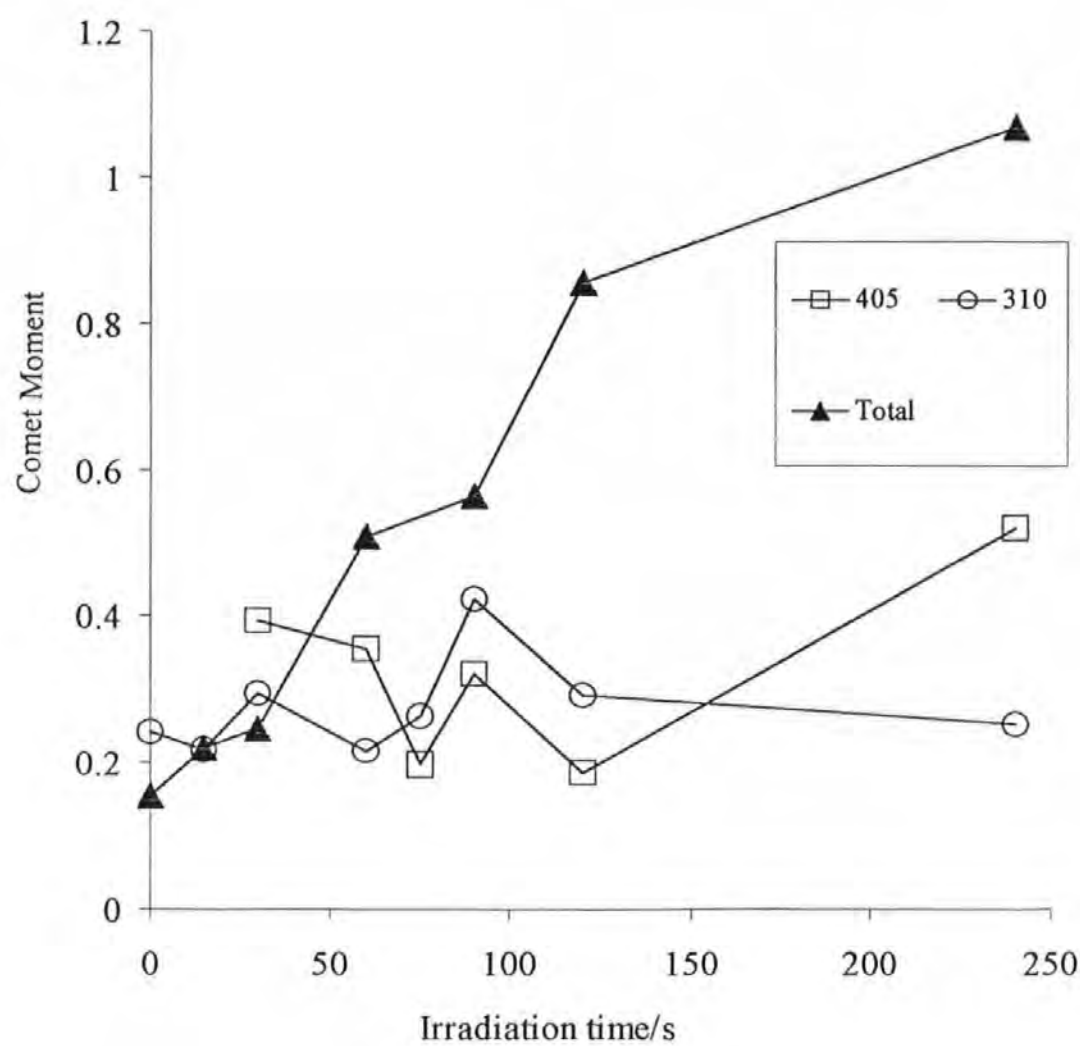
4.2.2.6.6 Data set 7: A comparison of SSB induced by 405 nm, 310 nm and total Xe lamp radiation in transformed hybrid lymphocytes PUTKO

4.2.2.6.7 Data set 7a: Comet Area (Figure 4.24)

Table 4.25 SSB in PUTKO hybrid lymphocytes induced by 405 nm, 310 nm or total Xe lamp radiation as measured by Comet Area

Table 4.25	405		310		Total Xe radiation	
	Peak1	Peak 2	Peak1	Peak 2	Peak1	Peak 2
Magnitude	+	+	++	+++	-	++
Seconds of irradiation	75	105	60	90	-	105

4.2.2.6.7.1 Data set 7b Comet length (Figure 4.25)

Table 4.26 SSB in PUTKO hybrid lymphocytes induced by 405 nm, 310 nm or total Xe lamp radiation as measured by Comet length

Table 4.26	405		310		Total Xe radiation	
	Peak1	Peak 2	Peak1	Peak 2	Peak1	Peak 2
Magnitude	-	++	++	+++	-	++
Seconds of irradiation	-	90	60	90	-	105

4.2.2.6.7.2 Data set 7c Tail length (Figure 4.26)

Table 4.27 SSB in PUTKO hybrid lymphocytes induced by 405 nm, 310 nm or total Xe lamp radiation as measured by Tail length

Table 4.27	405		310		Total Xe radiation	
	Peak1	Peak 2	Peak1	Peak 2	Peak1	Peak 2
Magnitude	-	+	++	+++	±	++
Seconds of irradiation	-	90	30	120	75	105

4.2.2.6.7.3   Data set 7d Tail Moment (Olive) (Figure 4.27)

Table 4.28 SSB in PUTKO hybrid lymphocytes induced by 405 nm, 310 nm or total

Xe lamp radiation as measured by Olive's Tail Moment

Table 4.28	405		310		Total Xe radiation	
	Peak1	Peak 2	Peak1	Peak 2	Peak1	Peak 2
Magnitude	-	+++	++	+++	++	+++
Seconds of irradiation	-	90	60	120	75	120

4.2.2.6.7.4   Data set 7e Comet Moment (Kent) (Figure 4.28)

Table 4.29 SSB in PUTKO hybrid lymphocytes induced by 405 nm, 310 nm or total

Xe lamp radiation as measured by Kent's Comet Moment

PUTKO	405		310		Total Xe radiation	
	Peak1	Peak 2	Peak1	Peak 2	Peak1	Peak 2
Magnitude	++	+++	++	+++	++	++
Seconds of irradiation	60	90	75	120	75	120

155

Figure 4.24 SSB induced by 405 nm, 310 nm or total Xe lamp radiation measured in PUTKO hybrid lymphocytes by Comet Area (Table 4.25)
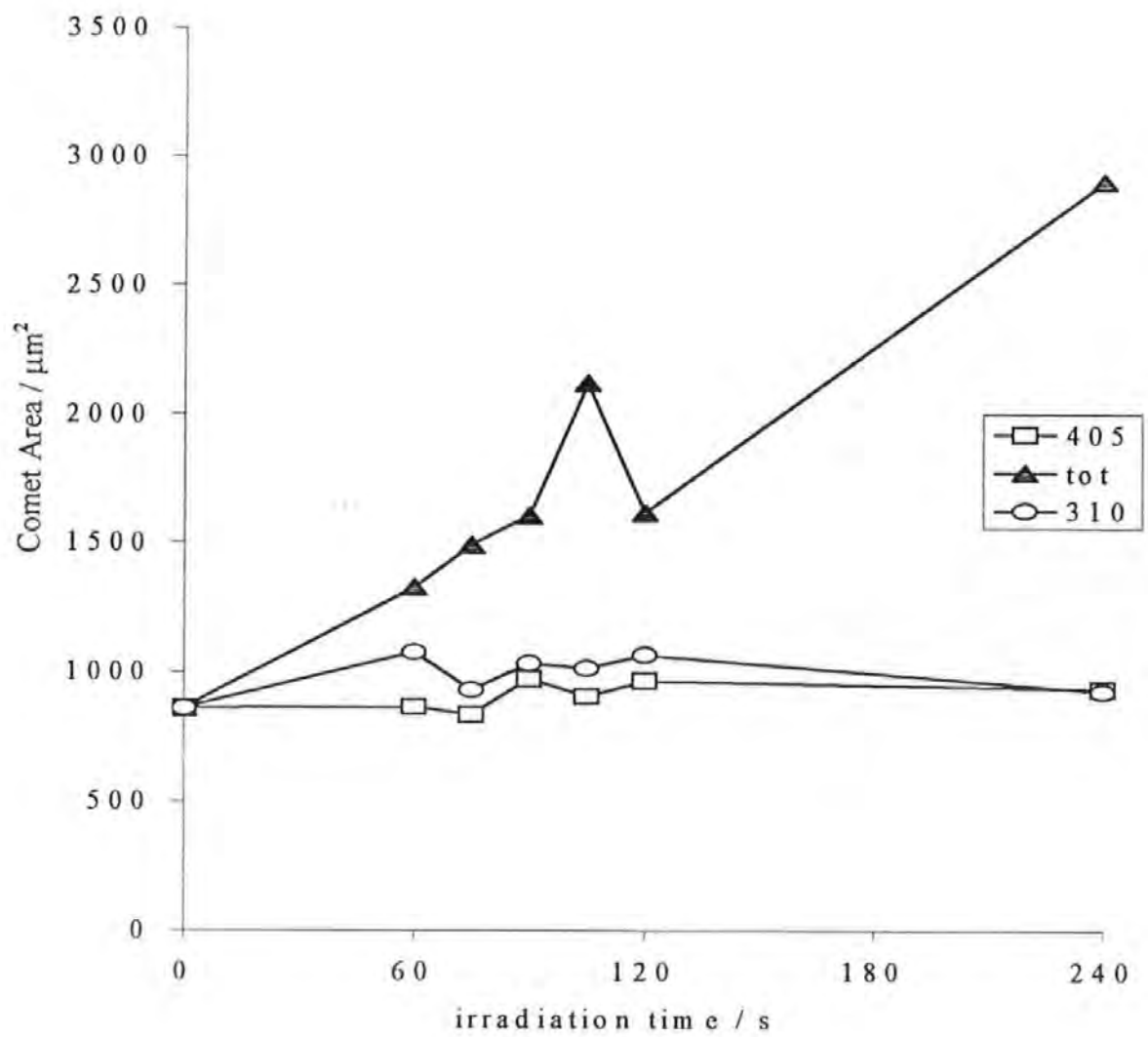
Figure 4.25   SSB induced by 405 nm, 310 nm or total Xe lamp radiation measured in PUTKO hybrid lymphocytes by Comet length (Table 4.26)
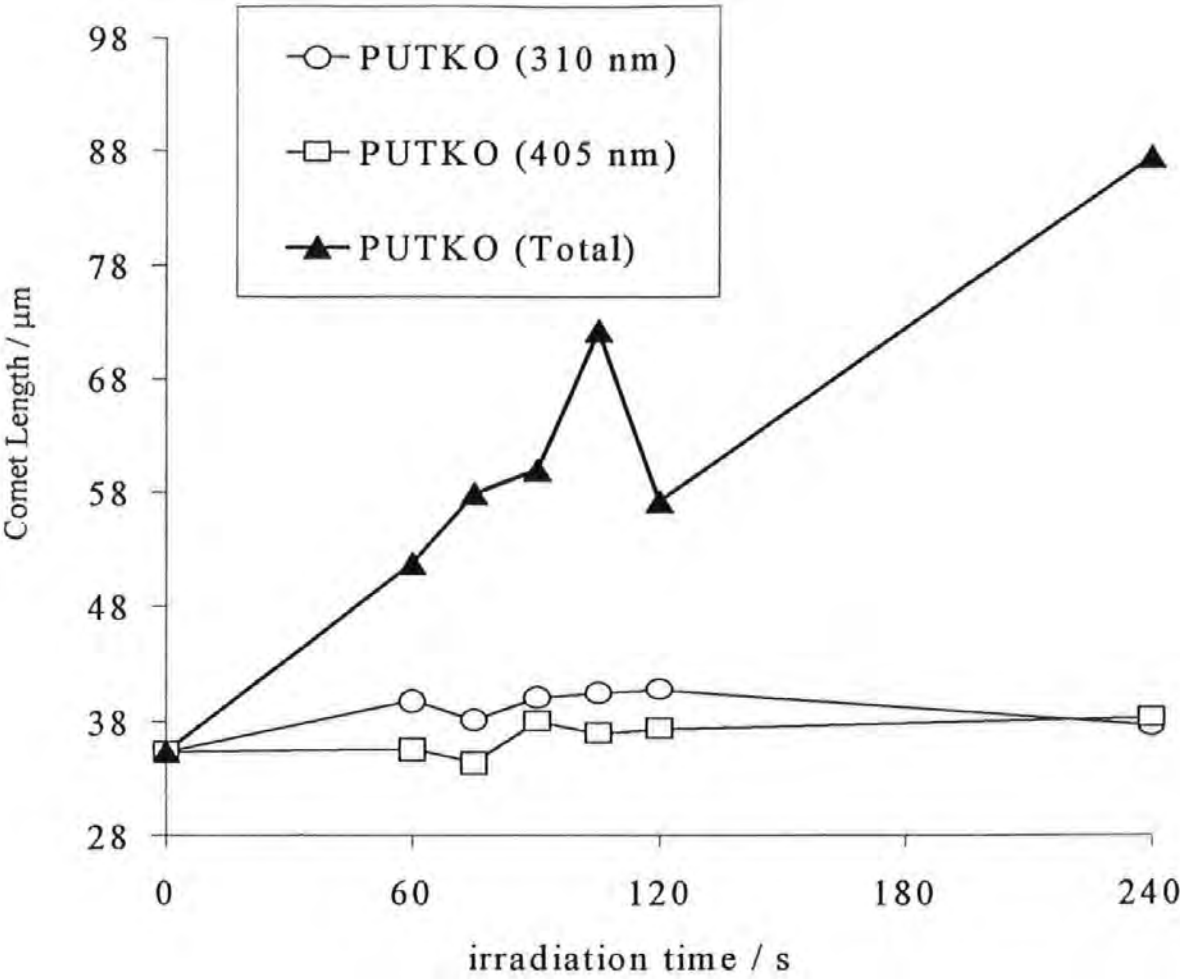
Figure 4.26   SSB induced by 405 nm, 310 nm or total Xe lamp radiation measured in PUTKO hybrid lymphocytes by Tail length (Table 4.27)
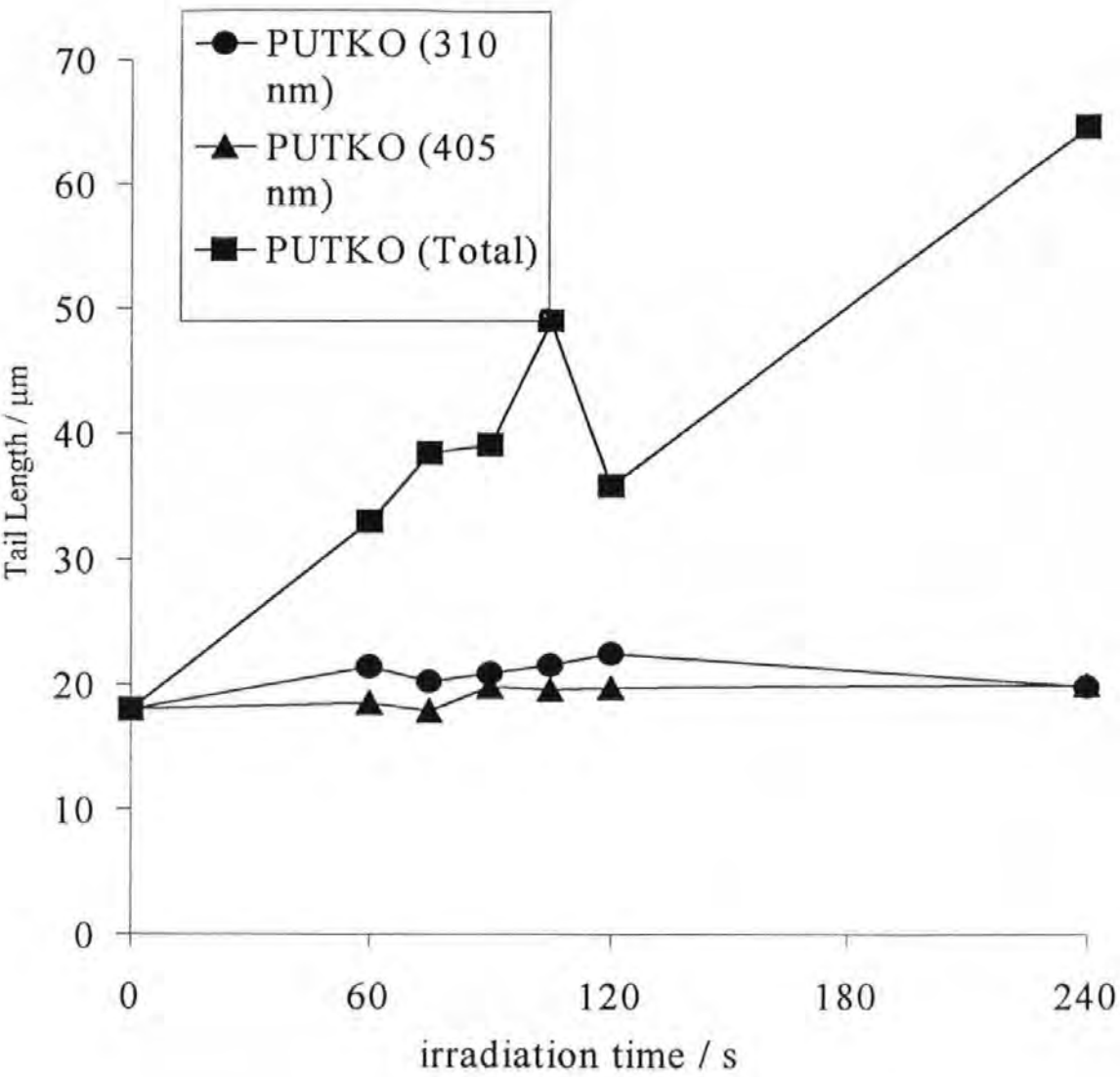
Figure 4.27   SSB induced by 405 nm, 310 nm or total Xe lamp radiation measured

in PUTKO hybrid lymphocytes by Olive's Tail Moment (Table 4.28)
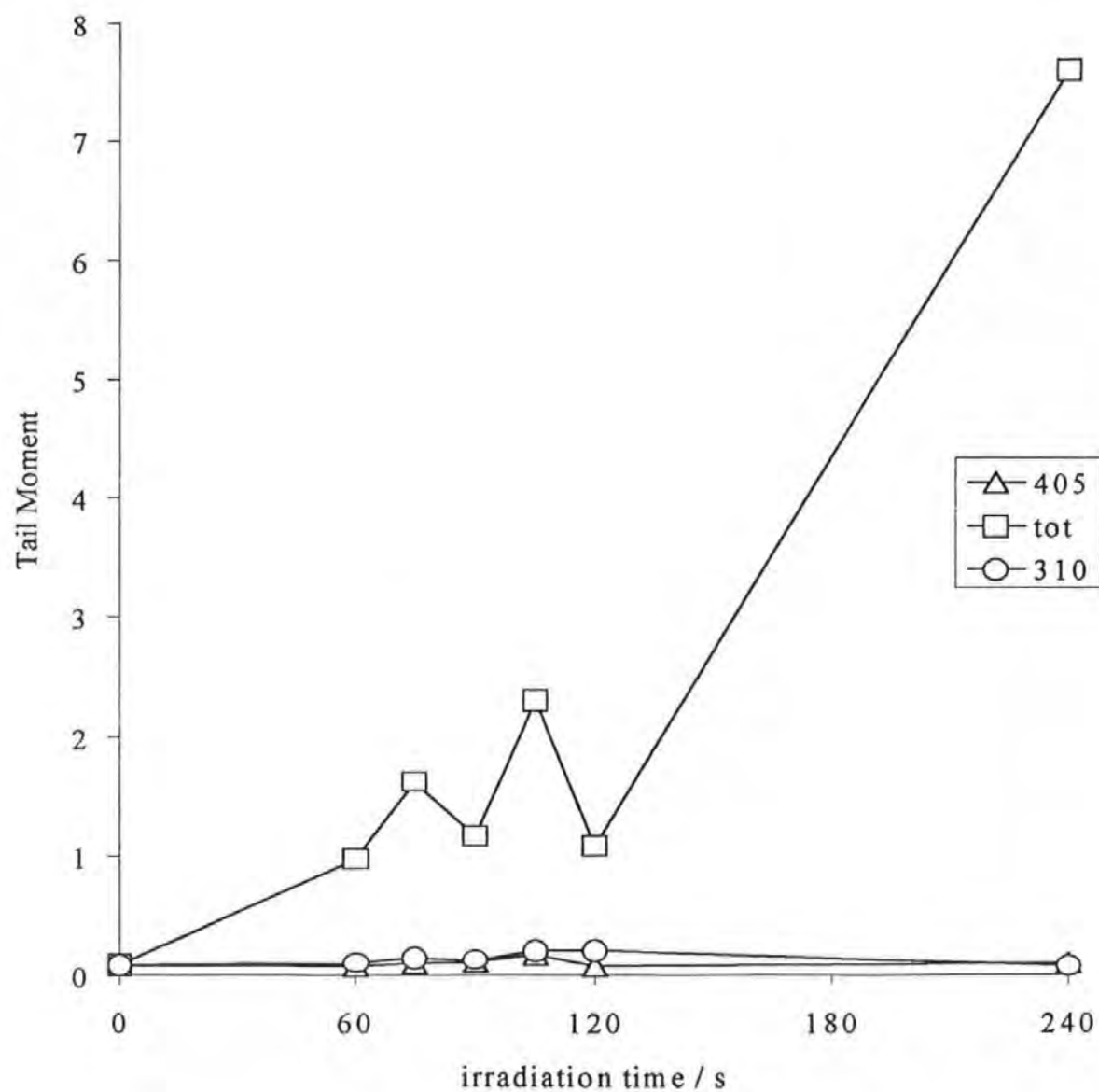
Figure 4.28   SSB induced by 405 nm, 310 nm or total Xe lamp radiation measured in PUTKO hybrid lymphocytes by Kent's Comet Moment (Table 4.29)
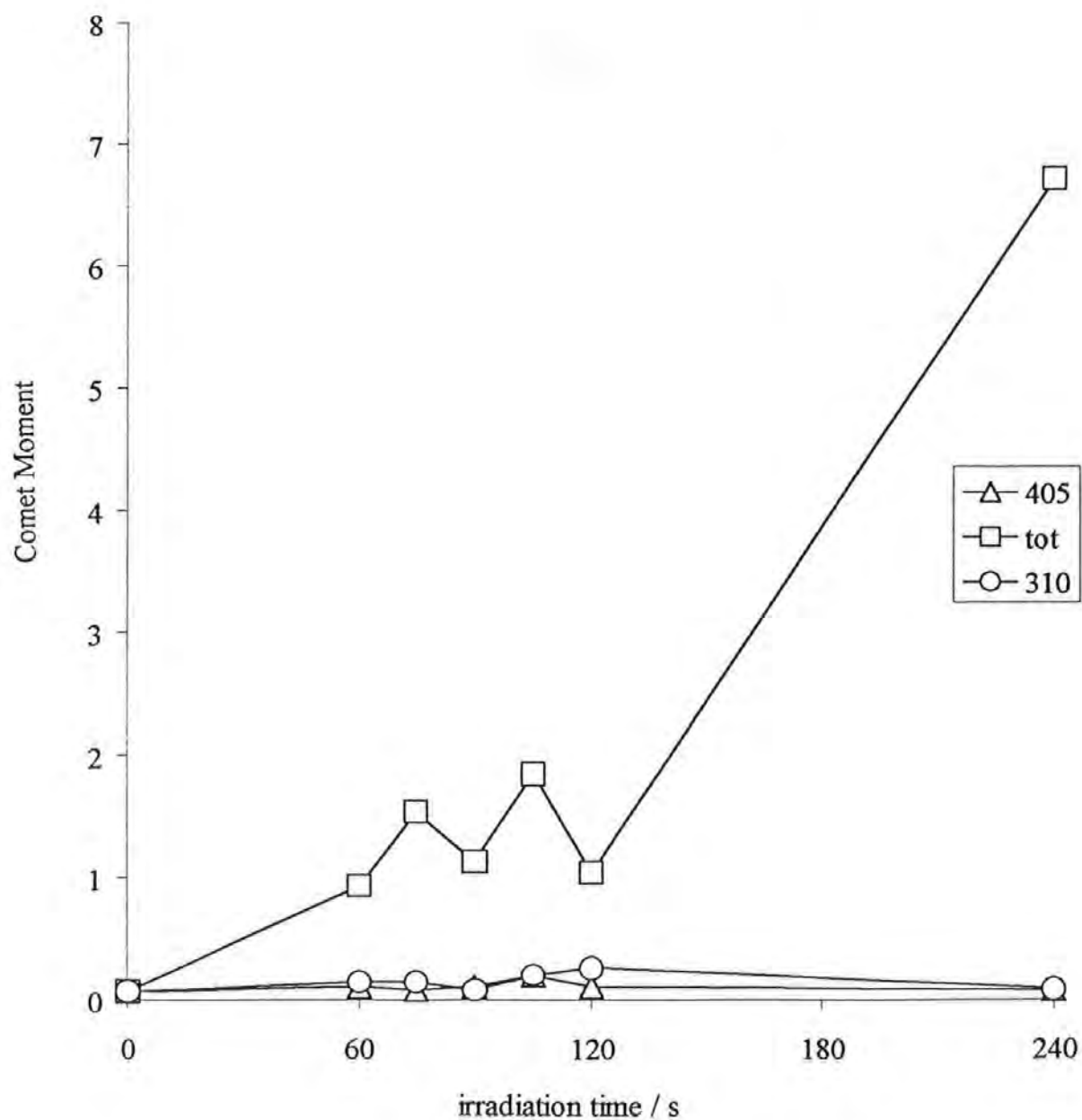
4.2.3   *The repair of SSB induced by UVR in human cells*

The dose responses described in the previous Section indicates that low fluence narrow band radiation is repaired effectively under continuous irradiation, but that the high fluence total Xe lamp radiation is not. This raised 3 points:

(i)   Was the rapid reversal of low fluence radiation-induced SSB due to a photochemical process or a cellular process?

(ii)   Were the lesions induced by high fluence total Xe lamp radiation of a different type (i.e. refractory to SSB repair) to the low fluence lesions rather than just being different in quantity?

(iii)   These two questions above posed a third question: what was the background rate of SSB repair at room temperature?

Two experiments were performed in response to these questions. It was thought that the data might be due to an experimental artefact. Hence, in order to test this further, it was decided to investigate the same repair process in normal cell types, using different protocols and after different radiation conditions. Hence, if the repair process was observed, the probability would be that the repair process was physiological and not an artefact of the experimental conditions.

First, MMB4L normal lymphocytes were irradiated with total Xe lamp radiation for 0, 15 or 30 s (designated Ti (Time of irradiation)) in Figure 4.29). Slides were then either irradiated for a further 30, 60, 90 or 210 s or allowed to repair at room temperature for the same time (Figure 4.29) in parallel. Secondly, MRC5 normal fibroblasts were 405 nm irradiated for 90 s (Figure 4.30) using the suspension protocol (Section 2.3.2.2). Comet assay slides were prepared from the cells while they were repairing the 405 nm-induced SSB. These slides were then placed onto ice to set and placed into ice cold lysis buffer after 2 minutes. In total, 11 slides were assayed over a repair period of approximately four minutes. Both assays were read back by image analysis of 60 comets per slide. The mean

Comet Area, Tail Moment and Comet Moment for each of the slides were plotted against the repair times.

The following observations were made.

(i)   SSB continued to increase for 60 s after 405 nm irradiation of the MRC5 fibroblasts and after total Xe lamp irradiation of the MMB4L normal lymphocytes.

(ii)   After the initial increase in SSB a reduction in SSB (i.e. a repair process) was clearly observed in both cell types.

(iii)   In the 405 nm irradiated normal fibroblasts a minimum in SSB was observed at ~180 s. This minimum was the start of a small peak at ~240 s. Due to the experimental structure (i.e. the time points of assay were determined beforehand and were designed to match the previously assayed time points (Section 4.2.2.5), it was not possible to observe these phenomena in the normal lymphocytes.

Figure 4.29   MMB4L normal lymphocytes were irradiated with total Xe lamp
radiation for 0, 15, or 30 s (designated Ti,: Time of irradiation). Slides were then
either irradiated for a further 30, 60, 90 or 210 s or allowed to repair at room
temperature for the same time. The mean value of 60 comets per slide were
calculated for the Comet Area, Tail Moment and the Comet Moment and plotted
against repair time.
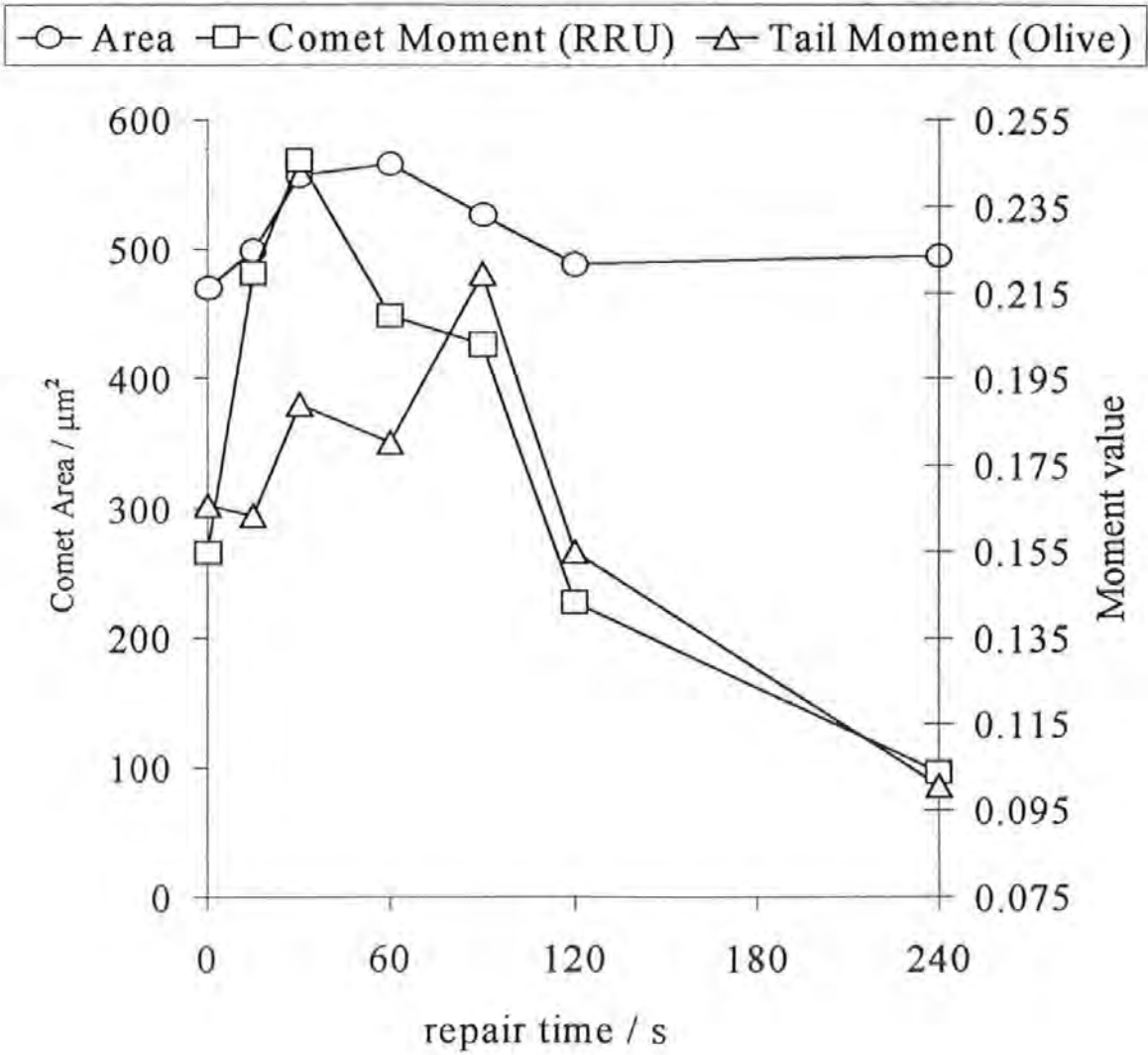
Figure 4.30 MRC5 normal fibroblasts were 405 nm irradiated for 90 s (Figure 4.30) using the suspension protocol. Comet assay slides were prepared from the cells while they were repairing the 405 nm-induced SSB. These slides were then placed onto ice to set and placed into ice cold lysis buffer after 2 minutes. In total, 11 slides were assayed over a repair period of approximately four minutes. The mean value of 60 comets per slide were calculated for the Comet Area, Tail Moment and the Comet Moment and plotted against repair time
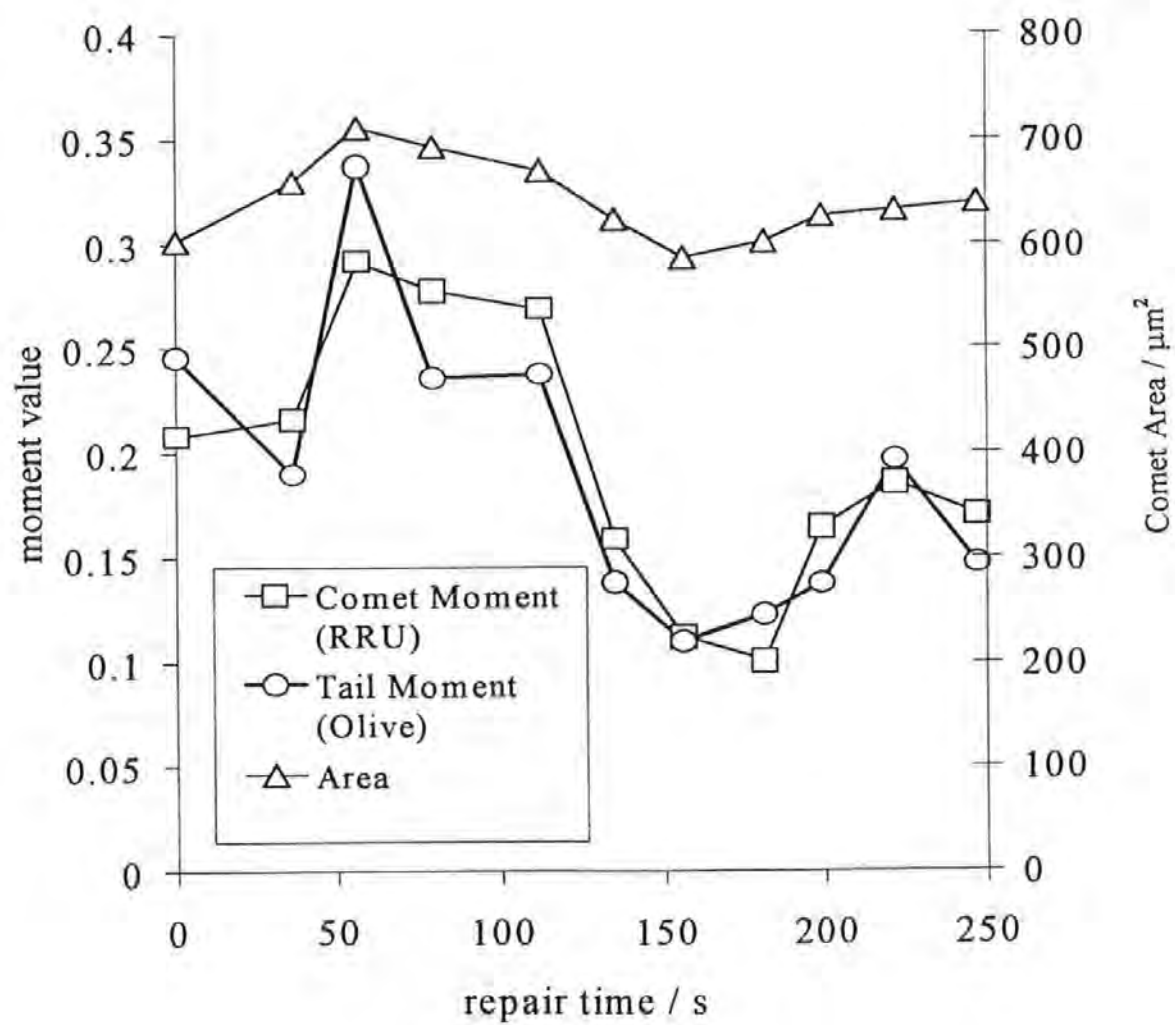
4.2.4 *Normal excision repair processes*

4.2.4.1 Normal repair responses of cells to cellular stress induced by UVR and cell

culture methods

The living cell is subject to a constant low level of DNA damage and the formation of

DNA adducts of all kinds. The repair of these lesions involves complex overlapping sets

of enzymatic reactions that continuously scan the genome and remove the lesions that are

found. The general steps involved in excision repair are thought to be (Bohr, 1994)

(i)   recognition of the lesion

(ii)   incision at the site of the lesion

(iii)   removal of the lesion and surrounding bases

(iv)   insertion and polymerisation of appropriate bases opposite the intact strand

(v)   ligation of the newly-synthesised patch of nucleotides into an intact double helix

These processes have been examined at the molecular level by many methods, including

the comet assay (Olive, 1998). The purpose of the following experiments was to identify

time points in the repair process that would be informative of the overall repair status

taking place in the cell at the time of assay. These time points could then be used, for

instance, to assess the modulating effects of arsenic on DNA repair.

This aim was approached in a number of ways. MRC5 fibroblasts were subjected to the

following treatments.

(i)   Non-irradiated cells were embedded in agarose and rested in the incubator for up to

one hour. These cells were assayed at 0, 5, 10, 15, 25, 35, 45 and 55 minutes of

resting time by the visual inspection method. A period of   excision activity was

observed at approximately 25 minutes (Figure 4.31).

(ii)   Cells were embedded in agarose and 405 nm irradiated for a) 100 s (10.6 mJ cm^{-2})

and allowed to repair (37 °C) for 0-40 minutes or b) 200 s and allowed to repair

(37 °C) for 20-90 minutes. The cells were assayed by the visual inspection method.

A period of excision activity was observed at 25-30 minutes (especially in the higher-dose cells) followed by a period of ligation activity. Two minor periods of repair activity were observed at approximately 45 minutes and 80 minutes in the higher-dose cells (Figure 4.32).

(iii)   Cells were suspended in media and 405 nm- or mock-irradiated for 15 minutes ($63.5 \ mJ \ cm^{-2}$) and allowed to repair for 0-180 minutes. A minor period of repair activity was observed at approximately 30 minutes and a major period of repair activity at approximately 60 minutes was observed in the mock irradiated cells. A major period of excision repair activity (a large increase in assay values) was seen between 60 minutes and 135 minutes followed by a period of rapid ligation (a corresponding decrease in assay values) in the 405 nm-irradiated cells as measured by Comet Area (Figure 4.33), Tail Moment (Figure 4.34), Comet Moment (Figure 4.35).

(iv)   Cells embedded in agarose made up with either PBS or DMEM without phenol red were 405 nm- or mock-irradiated for 30 minutes ($135 \ mJ \ cm^{-2}$). The cells were then either placed immediately into lysis or allowed to repair ($37 \ ^{\circ}C$) for a further 60 minutes. In both media and PBS suspended cells the irradiated cells displayed more SSB after 60 minutes repair than immediately after irradiation (Figure 4.36).

Figure 4.31 Non-irradiated MRC5 fibroblasts were embedded in agarose and rested in the incubator for up to one hour. These cells were assayed at 0, 5, 10, 15, 25, 35, 45 and 55 minutes of resting time before being assayed by the visual inspection method. A period of excision activity was observed at 25 minutes.
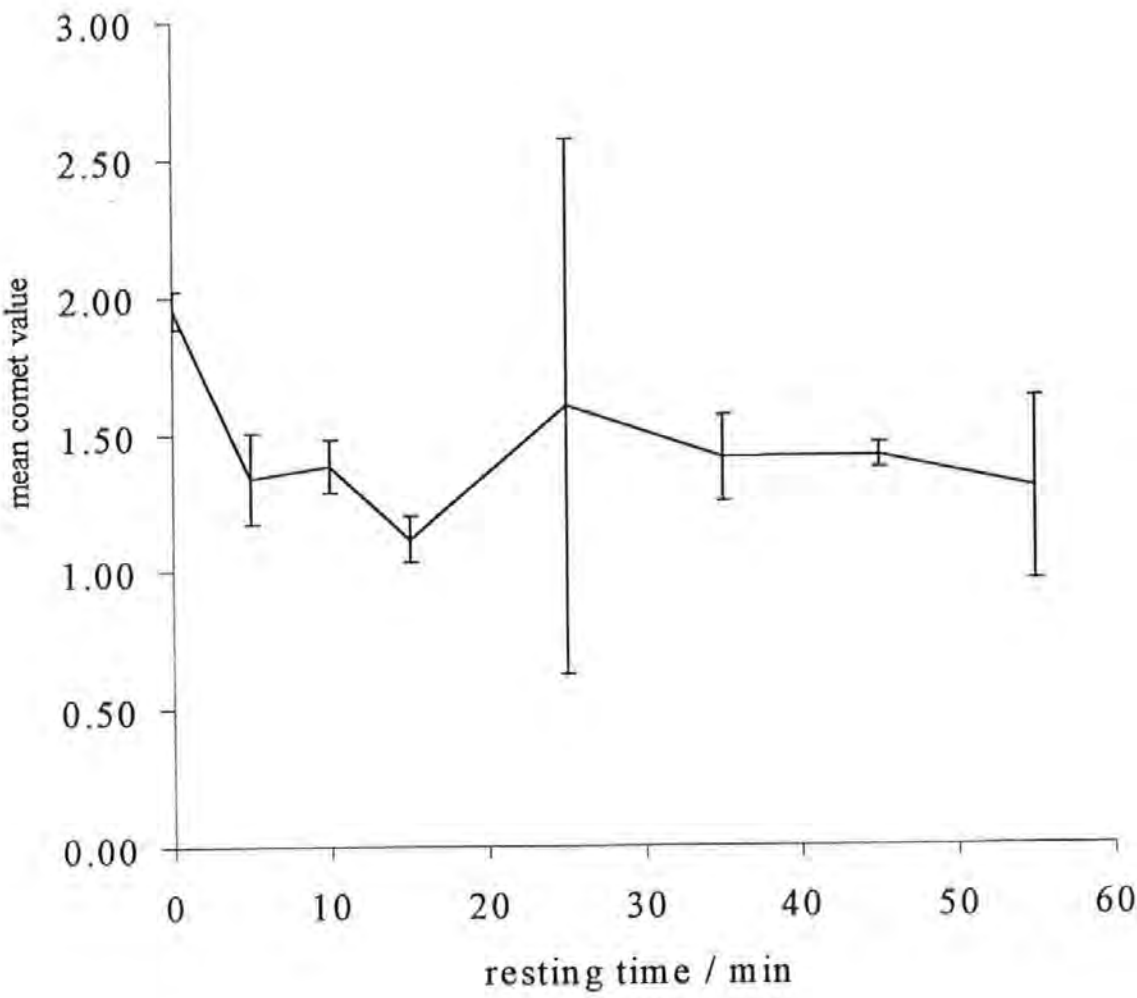
Figure 4.32 MRC5 fibroblasts were embedded in agarose and 405 nm irradiated for a) 100 s (10.6 mJ cm^{-2}) and allowed to repair (37 °C) for 0-40 minutes or b) 200 s (21.2 mJ cm^{-2}) and allowed to repair (37 °C) for 20-90 minutes. The cells were assayed by the visual inspection method. A period of excision activity was observed at 25-30 minutes (especially in the higher-dose cells) followed by a period of ligation activity. Two minor periods of repair activity were observed at approximately 45 minutes and 80 minutes in the higher-dose cells.
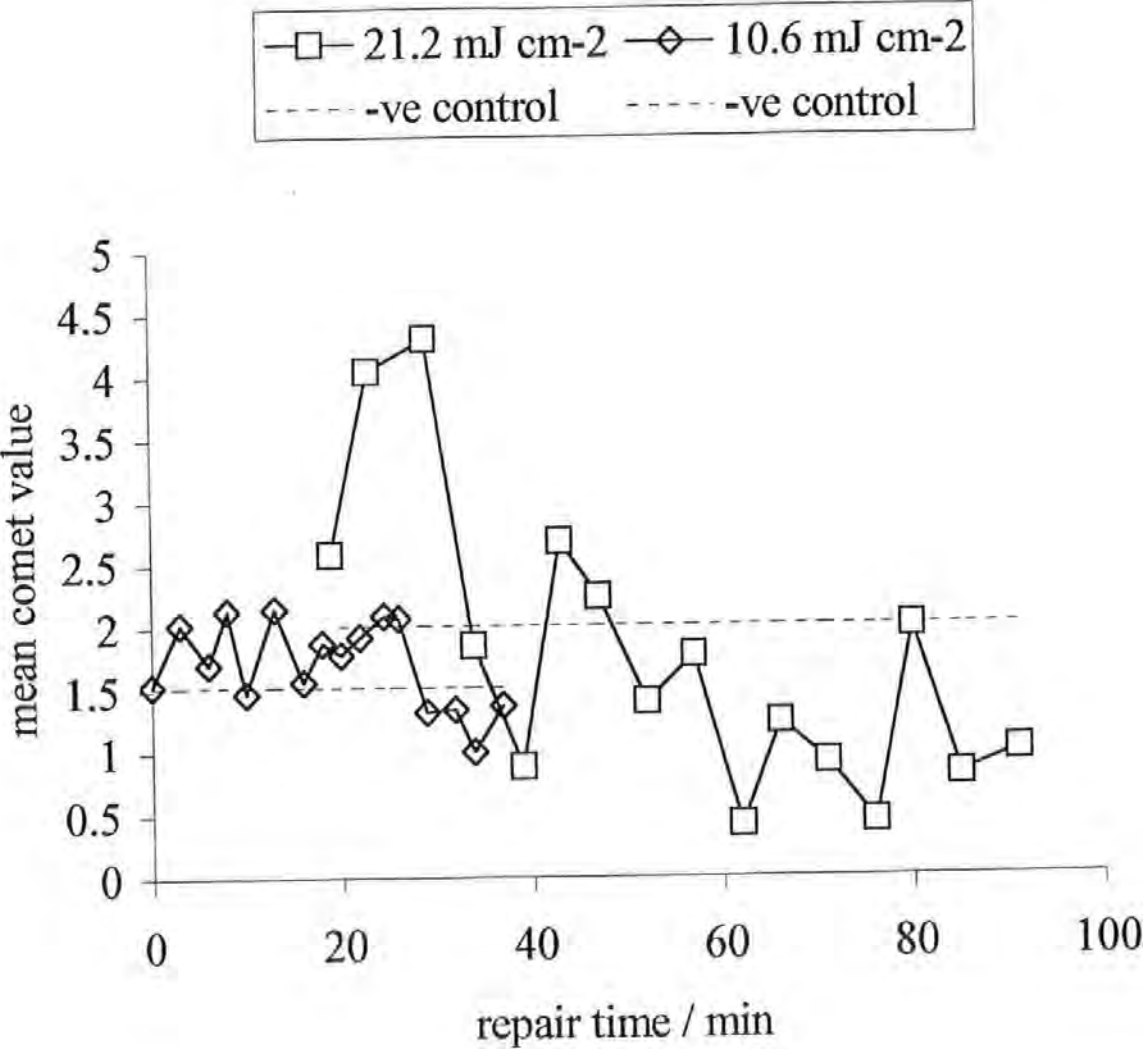
Figure 4.33 MRC5 fibroblasts were suspended in media and 405 nm- or mock-irradiated for 15 minutes (63.5 mJ cm^{-2}) and allowed to repair for 0-180 minutes before being assayed by image analysis using the parameter of Comet Area. A minor period of repair activity was observed at approximately 30 minutes and a major period of repair activity at approximately 60 minutes was observed in the mock irradiated cells. A major period of excision repair activity was seen between 60 minutes and 135 minutes followed by a period of rapid ligation in the 405 nm-irradiated cells.
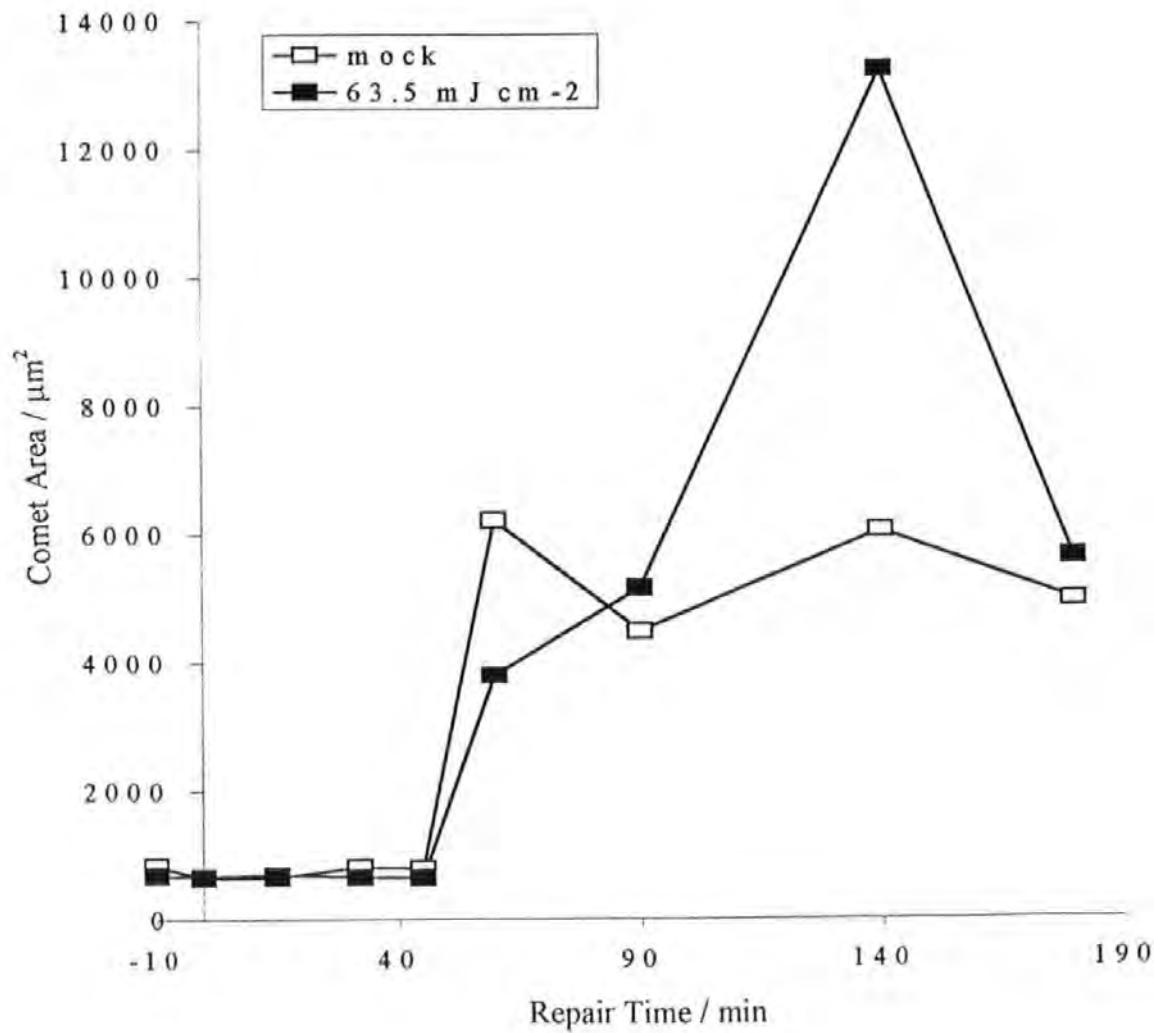
Figure 4.34 MRC5 fibroblasts were suspended in media and 405 nm- or mock-irradiated for 15 minutes (63.5 mJ cm^{-2}) and allowed to repair for 0-180 minutes before being assayed by image analysis using the parameter of Tail Moment. A period of repair activity at approximately 60 minutes was observed in the mock irradiated cells. A major period of excision repair activity was seen between 60 minutes and 135 minutes followed by a period of rapid ligation in the 405 nm-irradiated cells.
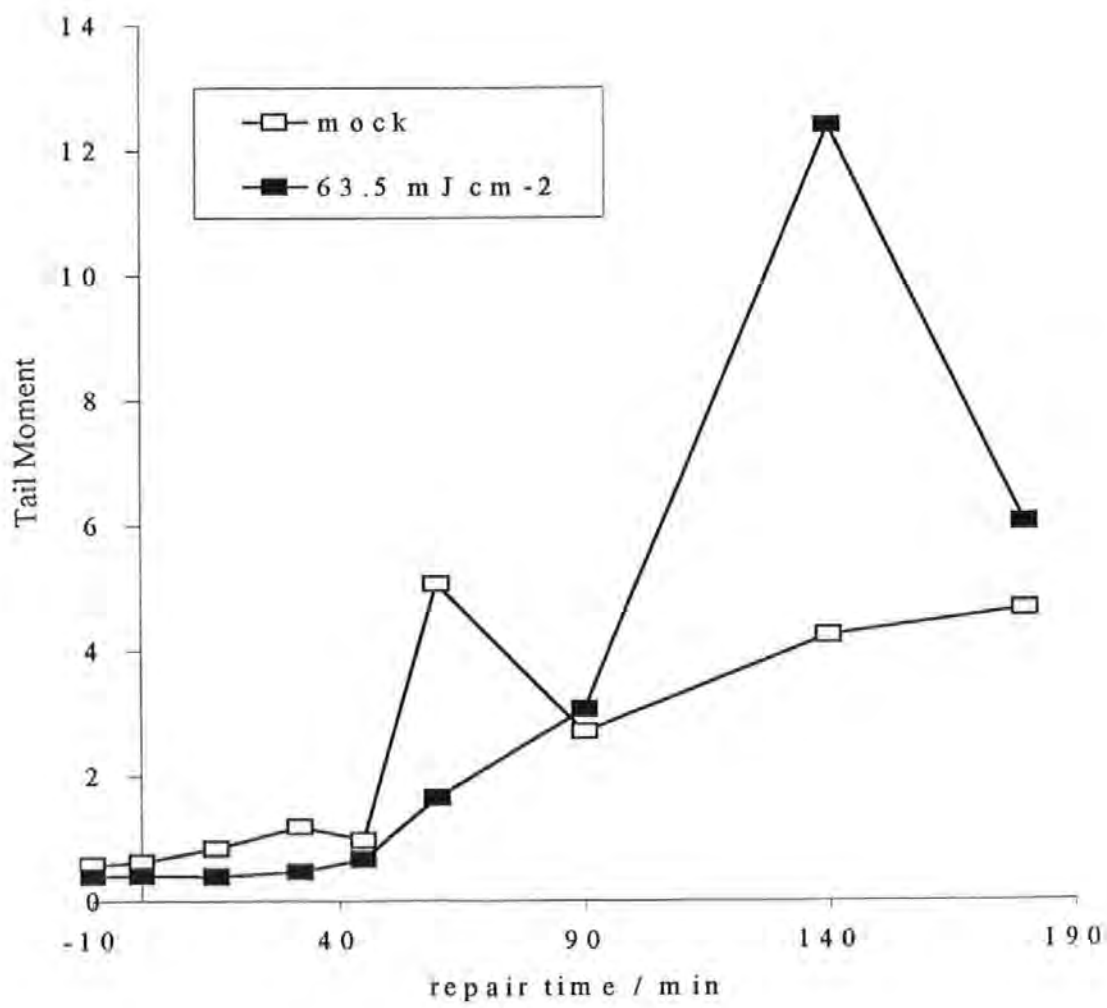
Figure 4.35 MRC5 fibroblasts were suspended in media and 405 nm- or mock-irradiated for 15 minutes (63.5 mJ cm^{-2}) and allowed to repair for 0-180 minutes before being assayed by image analysis using the parameter of Comet Moment. A minor period of repair activity was observed at approximately 30 minutes and a major period of repair activity at approximately 60 minutes was observed in the mock irradiated cells. A major period of excision repair activity was seen between 60 minutes and 135 minutes followed by a period of rapid ligation in the 405 nm-irradiated cells.
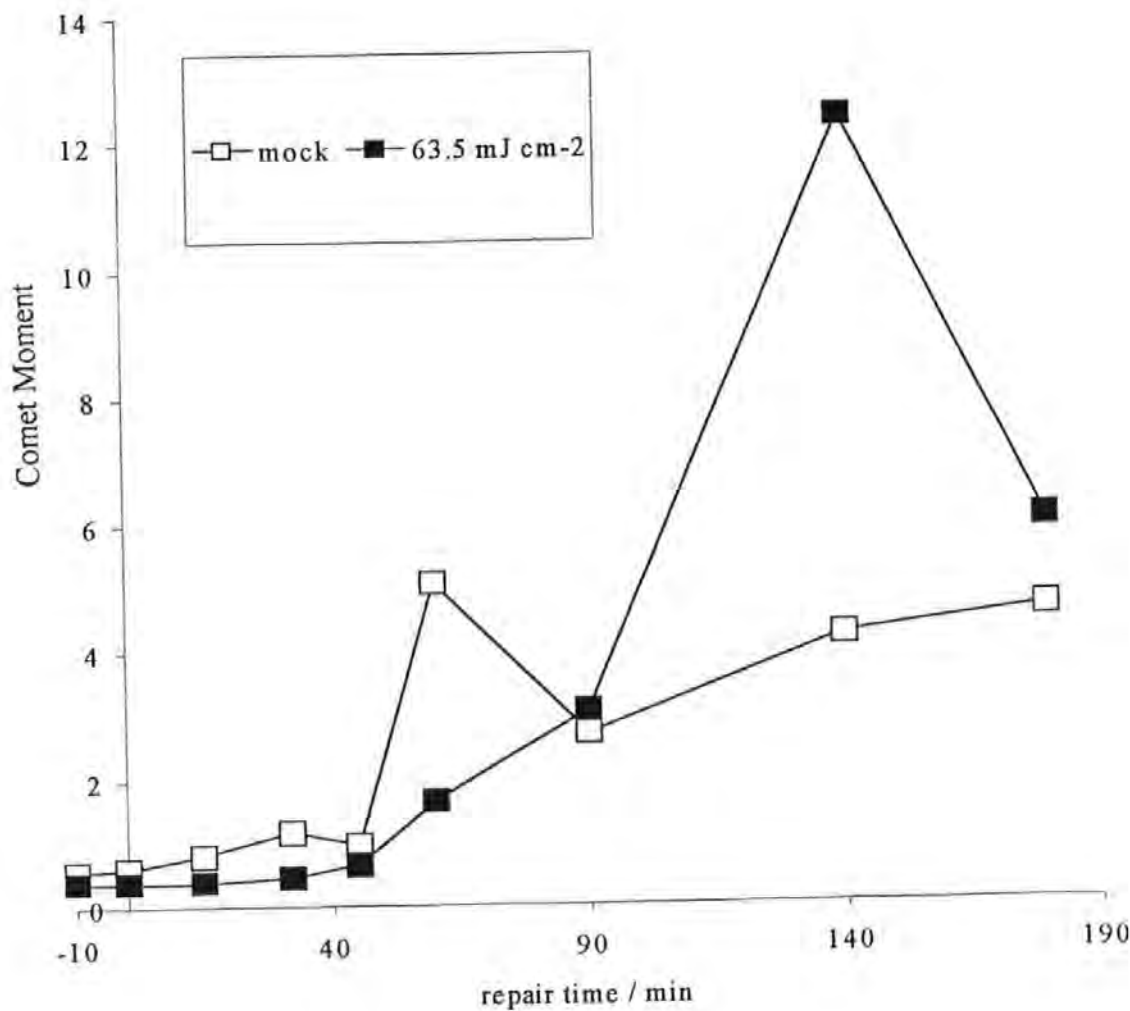
Figure 4.36 MRC5 fibroblasts were 405 nm- or mock-irradiated for 30 minutes (135 mJ cm^{-2}) embedded in agarose made up with either PBS or DMEM without phenol red. The cells were then either placed immediately into lysis or allowed to repair $(37 \text{ }^{\circ}\text{C})$ for a further 60 minutes. In both media and PBS suspended cells the irradiated cells displayed more SSB after 60 minutes repair than immediately after irradiation
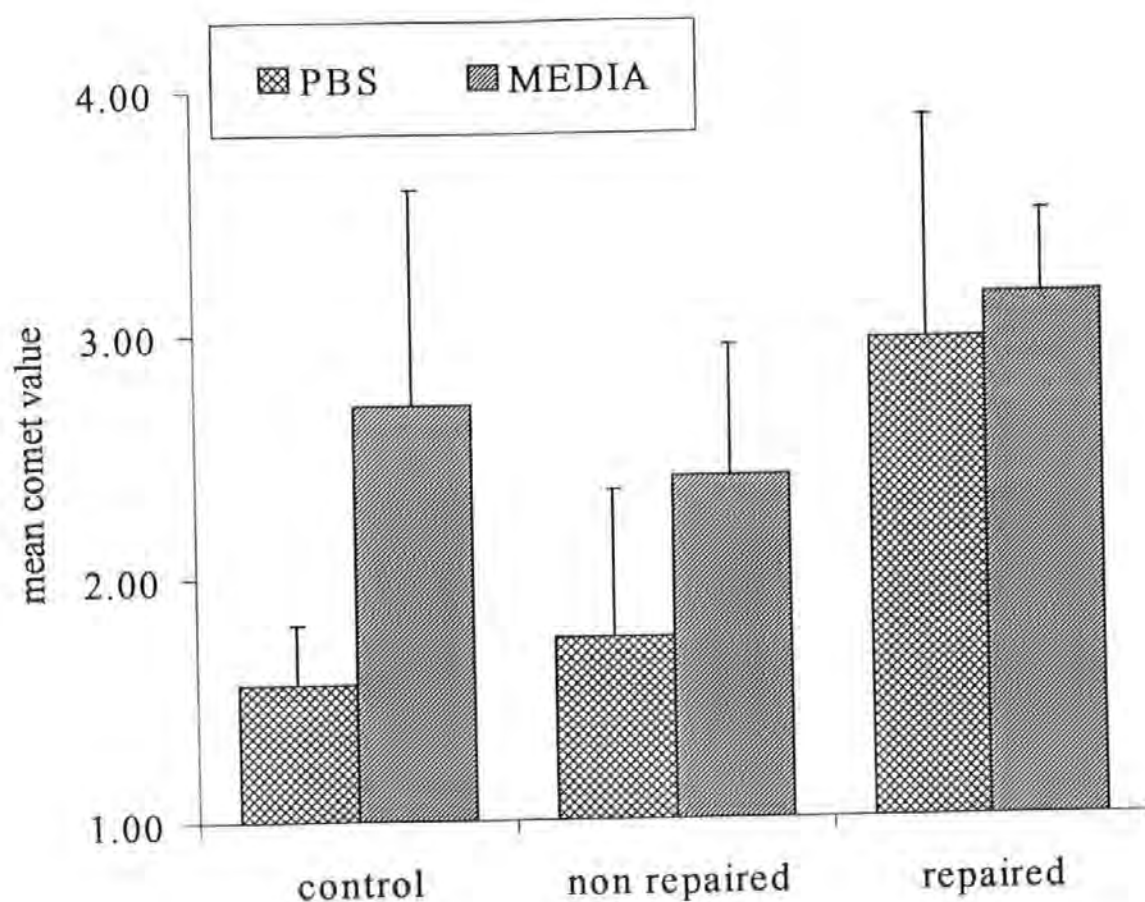
4.2.5 Summary

SSB dose responses to low fluence narrow band 310 nm and 405 nm radiation and high fluence total Xe lamp radiation have been obtained for a number of different human cells using the comet assay. Whilst differences between cell types were observed a general pattern of response was observed. The response to the low fluence narrow band filtered radiation (< 18 mJ cm^{-2}) was generally an increase in SSB for the first two minutes of irradiation. This was rapidly repaired to baseline levels whether under continued irradiation or not. Two peaks in SSB induction were regularly seen: an early peak at around 30 s and a second peak - usually a maximum - at around 90 s. This second peak appeared much-enhanced in cells which came from male donors only. An approximately linear dose response was obtained with the high fluence total Xe lamp radiation, although some of the characteristics of the low fluence (monochromatic) dose responses were observed. It was found, however, that the detection and measurement of the dose response phenomena was very much dependent on the parameter by which the comets were analysed. In this respect, the two 'moments' were more suited to the measurement of the higher fluence radiation induced SSBs while the Comet Area was particularly sensitive to the low fluence phenomena.

These data are discussed in the following chapter.

CHAPTER 5.

NORMAL RESPONSES OF HUMAN CELLS TO LOW DOSES OF
UVR AND VISIBLE RADIATION

DISCUSSION

5.1 INTRODUCTION

The comet assay has been developed in this work to assay SSB induced by long
wavelength UVR (405 nm) and the data obtained have been interpreted in this context.
Irradiation at three wavelengths (monochromatic 310 nm and 405 nm and unfiltered Xe
lamp radiation) produced an increase in strand breakage within half a minute or even less.
The amount of strand breakage increased with continuous irradiation for the first two
minutes. After this time, strand breakage induced by the low fluence narrow band (310 nm
and 405 nm) radiation decreased in spite of continued irradiation, clearly indicating a
repair process. Irradiation with total Xe lamp spectrum radiation produced an
approximately linear dose response with some characteristics of the low dose phenomena,
(namely the formation of a peak at 75-120 s from the start of irradiation), but the overall
extent of SSB induction appeared too great for the effects of repair to be observed. It is
unlikely that specific base excision has taken place in this time (see Section 4.2.4); rather,
given the nature of the xenon lamp emission spectrum in the UVB, it is more likely that the
increase in SSB is due to direct breakage of the DNA backbone (Noz *et al.*, 1996).
Differences in dose responses were seen with respect to cell type, fluence and comet assay
parameter.

The results described in the previous chapter will be discussed in two parts. First, the
sources of the SSB will be outlined and possible mediators of the phenomena described
will be discussed. The effects on the living cell of low levels of SSB will be outlined and
the differences between the image analysis parameters will be explained and reconciled.

The section will conclude with an estimate of SSB quantum yields. In the second part, the phenomena described in Chapter 4 will be discussed in the light of the first part. In particular, the causes of the two peaks will be discussed and a model of events presented. The implications of the male/female differences will also be discussed insofar as the limited data allow.

5.2 SSB INDUCED BY UVR IN HUMAN CELLS

5.2.1 The sources of the SSB

The SSB induced in DNA by the wavelengths employed in this study are from a number of sources (see the General Introduction, Section 1.3). Short wavelength UVR generates SSB by direct absorption of UVR by DNA (Peak *et al.*, 1987) while long wavelength UVR (Peak *et al.*, 1987) and visible light (Pflaum *et al.*, 1994) generate SSB by indirect mechanisms. These indirect mechanisms are considered more important biologically at long wavelength UVR and are usually oxygen dependent (Cridland and Saunders, 1994), (but see also Table 1.1 and Section 1.3.2.1 ,which covers alkali-labile sites). SSB are also formed from alkali-labile sites induced in human cells by direct absorption of UVR by DNA (Cridland and Saunders, 1995; Cadet, 1994) and by 405 nm radiation (Peak *et al.*, 1989). It is not possible to distinguish the origin of the strand breaks under the conditions of the comet assay employed in these studies. The term SSB is used for all classes of this type of lesion howsoever caused.

Two cell types (MMB4L normal lymphocytes and MRC5 normal fibroblasts) were used to examine repair. In MMB4L cells that had been irradiated with 30 seconds of total Xe lamp radiation and allowed to repair in the absence of further radiation, a peak in the Tail Moment value was observed at 90 s (Figure 4.29) although the cells had not been exposed to radiation for 60 s. This was observed in MRC5 fibroblasts, 60 s after stopping 405 nm-irradiation of the cells (Figure 4.30). The absence of photic energy during this time

implies that the repair is not a photochemical reversal of SSB induction, rather it is probably the direct rejoining of SSB.

The predominant mechanisms for SSB production operating at long wavelengths of UVR are indirect (photosensitisation) reactions (Cridland and Saunders, 1994) and are probably mediated by a mixture of porphyrins and flavin residues (Peak and Peak, 1995). The 405 nm-induced and the 310 nm-induced dose responses closely followed the same time course in MMB4L normal lymphocytes (Section 4.2.2.6) and the two narrow band dose responses were broadly similar in PUTKO cells (Section 4.2.2.6.6). This suggests that a similar mechanism of strand breakage is being induced by 310 nm and by 405 nm radiation. It is proposed that a reaction sequence is induced in human cells by 310 nm or 405 nm radiation which leads to a photosensitised (Type II, see General Introduction, Section 1.3.3.1) increase in oxidative stress resulting in DNA strand breakage. Based on the observation of an increase in SSB after irradiation, it is further proposed that this reaction sequence persists for approximately 60 s after irradiation has ceased and continues to exert the clastogenic effect, possibly through long-lived reactive species.

5.2.2 The structure and formation of 'comets'

The comet assay is a sensitive method of measuring DNA strand breakage at the single cell level (McKelvey-Martin et al., 1993; Fairbairn et al., 1995; Anderson et al., 1998). It is based on the differential migration of single stranded DNA fragments through an agarose gel according to size. SSB introduced into supercoiled DNA cause, first, relaxation of the DNA supercoils into large DNA loops; and second, at higher levels of strand breakage, DNA fragments that migrate more freely in the gel than loops (Ostling and Johanson, 1984). It is proposed that the occurrence of the peaks described in the previous chapter is due to unwinding of supercoiled DNA induced by low numbers of SSB followed by a rapid repair process.

5.2.2.1 Caveat

The phenomenon of 'saturation' due to the integration capabilities of the image analysis system (outlined in Section 2.3.5.3) has the result that the accurate measurement of 'total DNA' content will be sensitive to the signal to area ratio: a larger Comet Area will permit a higher proportion of the total DNA to be calculated. This is clearly demonstrated in Figure 5.1 where a peak value of total DNA content is measured in comets observed at the same irradiation time that gave a maximum value for Comet Area in MMB4L cells. Extreme caution must therefore be employed when using a calculation involving DNA content (or a fraction thereof) if the image analysis equipment has been 'saturated'; data should be compared with the parameters based on the physical characteristics (i.e. length and area) before firm conclusions can be made.

Figure 5.1 MMB4L normal male lymphocytes were 405 nm irradiated (~70 μW cm^{-2}) for between zero and 240 s. SSB was measured by the parameter of Comet Area; the total DNA content was calculated at each dose (based on the fluorescence signal) and was plotted on the same x-axis. The measured DNA content was observed to be sensitive to Comet Area.
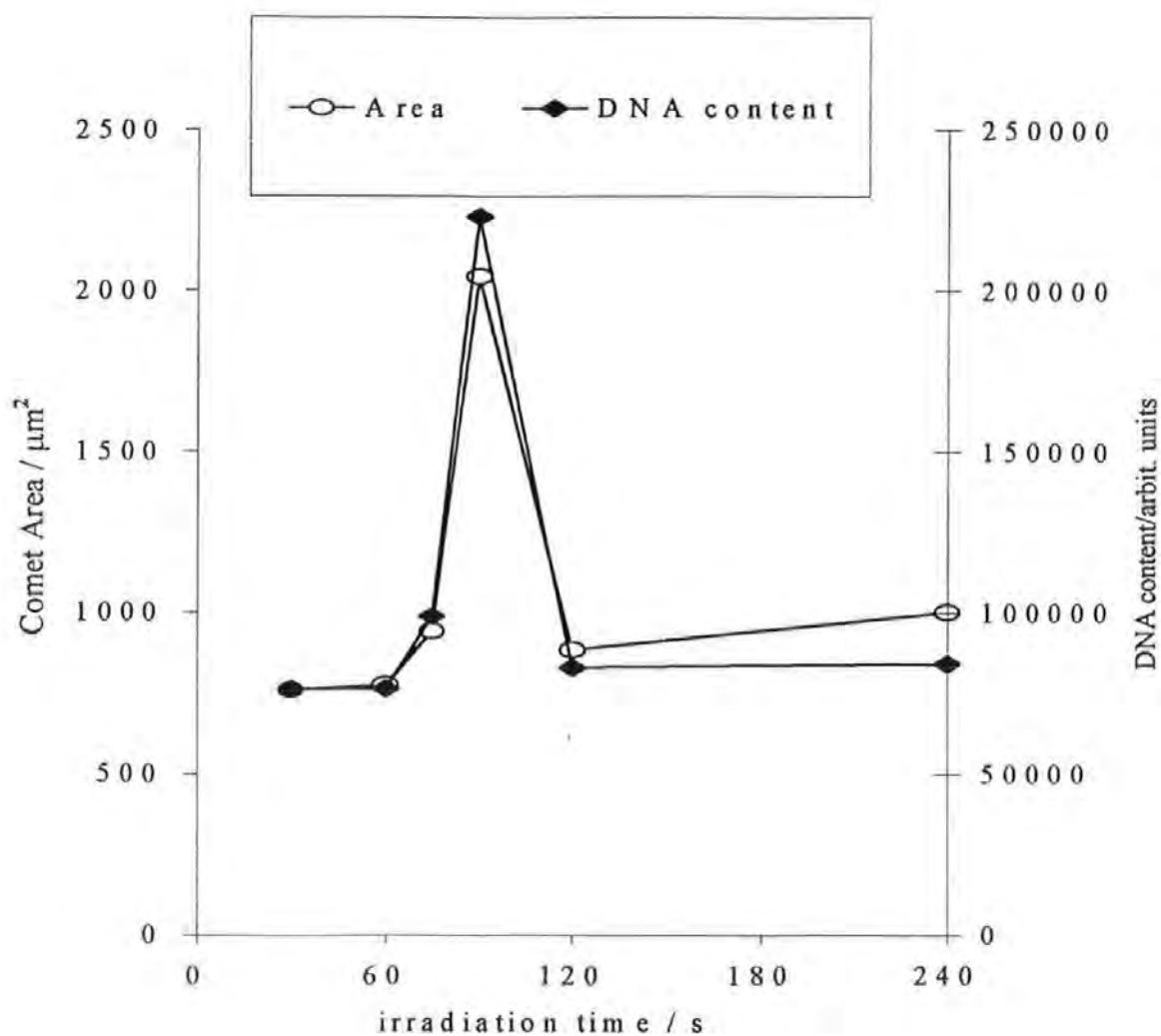
5.2.3 Estimates of absolute numbers of SSB

5.2.3.1 Introduction

In this study, the number of strand breaks induced by the low fluence radiation has not been directly quantified. However, using values obtained from the literature an estimate can be made. There are two ways this has been done,

(i)   Action spectra for SSB induction have been estimated from the data for 313 nm and 405 nm UVA (Peak *et al.*, 1987), broadband UVA and UVB (Wenczl *et al.*, 1997), UVR and visible light (Kielbassa *et al.*, 1997; Pflaum *et al.*, 1994). These action spectra have been extrapolated to the doses and wavelengths employed in this study.

(ii)   Migration characteristics of DNA in the comet assay have been extracted from the published literature and compared with values obtained in this study. The comet assay has arisen in an arbitrary manner (Ross *et al.*, 1995) and judgement was necessary when deciding how a particular laboratory's technique differed from the one reported in this work and how to incorporate other workers' results into this study.

Two assumptions have been made. These are that

(i)   The human genome contains 3×10^9 base pairs (Alberts *et al.*, 1989),

(ii)   The average molecular mass of one base pair is 660 Daltons (Voet and Voet, 1990b).

It must be emphasised that the values estimated in this work for the numbers of SSB induced by the extremely low fluence radiation are semi-quantitative at best.

5.2.3.2 Extrapolation of published action spectra (see Tables 5.1 and 5.2)

Peak *et al.* (1987) used alkaline elution to measure SSB induction by 313 nm and 405 nm monochromatic radiation . The yields of strand breakage they calculated from their figures were 3.6 SSB/10^8 Da / MJ m^{-2} (i.e. 0.7128 SSB / mJ cm^{-2} / cell) and 0.2 SSB/10^8 Da/MJ m^{-2} (0.040 SSB / mJ cm^{-2} / cell) for 313 nm and 405 nm radiation respectively. These figures extrapolate to 1.426 SSB / cell induced by 90 s of 310 nm radiation and 0.257 SSB / cell induced by 90 s of 405 nm irradiation for work performed in this laboratory. Peak and co-workers cite three other UVB studies for comparison with their data. The values given were 7.4 SSB/10^8 Da / MJ m^{-2} (Hirschi *et al.*, 1981), 14 SSB/10^8 Da / MJ m^{-2} (Rosenstein and Ducore, 1983), and 65 SSB/10^8 Da / MJ m^{-2} (Smith and Patterson, 1985). For 2 mJ cm^{-2} (or 90 s irradiation) these give values of 2.93 SSB / cell, 5.544 SSB / cell, and 25.74 SSB / cell respectively.

Table 5.1 Action spectra for 310 nm SSB

Author	Wavelength /nm	cells	SSB yield	Units as given	SSB / mJ / cm2 / cell	Approximate no SSB after 2mJ cm^{-2}
Peak *et al.* 1987	313 nm mono	P3 epitheliod	3.6	SSB / 1e8 Da / J m-2 (x 1e-6)	0.7128	1.426
Hirschi *et al.* 1981	313	human fibroblasts	7.4	SSB / 1e8 Da / J m-2 (x 1e-6)	1.465	2.93
Rosenstein and Ducore(a) 1983	313	human fibroblasts	14	SSB / 1e8 Da / J m-2 (x 1e-6)	2.772	5.544
Smith and Paterson 1982	313	human fibroblasts	65	SSB / 1e8 Da / J m-2 (x 1e-6)	12.87	25.74
Wenczl *et al.* 1997	UVB	human melanocytes	1.9	SSB / 1e10 Da / kJ m-2	3.762	7.524
Elkind and Ham 1978	UVB	HeLa	3.1	SSB / 1e10 Da / kJ m-2	6.140	12.28
Kielbassa *et al.* 1997	UVB	AS52 CHO	0.2	SSB / 1e6 bp / kJ m-2	6.00	12.00
Kielbassa *et al.* 1997	310	AS52 CHO	0.1	SSB / 1e6 bp / 20 kJ m-2	0.15	0.3

Table 5.2   Action spectra for 405 nm SSB

Author	Wavelength/ nm	cells	SSB yield	Units as given	SSB / mJ cm^{-2} / cm2 / cell	Approximate no SSB after 6.5 mJ cm^{-2}
Peak et al. 1987	405 nm mono	P3 epitheliod	0.2	SSB / 1e8 Da / 5J m-2 (x 1e-6)	0.040	0.257
Kielbassa et al. 1997	>360 nm	AS52 CHO	0.5	SSB / 1e6 bp / 200 kJ m-2	0.002	0.015
Kielbassa et al. 1997	>400	AS52 CHO	0.1	SSB / 1e6 bp / kJ m-2	3.00	19.5
Pflaum et al. 1994	VIS	L1210 mouse leukaemia	0.1	SSB / 1e6 bp / 450 / kJ m-2	44	286
Pflaum et al. 1994	VIS	L1210 mouse leukaemia	0	SSB / 1e6 bp / 16/ kJ m-2	540	3540
Wenczl et al. 1997	UVA	human melanocytes	0.07	SSB / 1e10 Da / kJ m-2	0.138	0.9
Roza et al. 1985	UVA	human fibroblasts	0.09	SSB / 1e10 Da / kJ m-2	0.178	1.158

Wenczl et al. (1997) used immunochemistry to quantify broadband UVA and UVB induced SSB in melanocytes. They calculated yields of 0.07 SSB / 10^{10} Da / kJ m^{-2} (0.138 SSB / mJ cm^{-2} / cell) for UVA and 1.9 SSB / 10^{10} Da / kJ m^{-2} (3.762 SSB / mJ cm^{-2} / cell) for UVB. These extrapolate to 0.9 SSB / cell for UVA and 7.524 SSB / cell for UVB. They cited additional studies for comparison with their data. The values quoted were 0.09 SSB / 10^{10} Da / kJ m^{-2} for UVA (Roza et al., 1985) and 3.1 SSB / 10^{10} Da / kJ m^{-2} for monochromatic 313 nm radiation (Elkind and Han, 1978). These extrapolate (90 s irradiation) to 1.158 SSB / cell (UVA) and 12.28 SSB / cell respectively. Kielbassa (1997) using alkaline elution showed values of 0.2 SSB/10^6 bp / kJ m^{-2} (6 SSB / mJ cm^{-2} / cell) for broadband UVB and 0.1 SSB/10^6 bp / 20 kJ m^{-2} (0.15 SSB / mJ cm^{-2} / cell) for monochromatic 310 nm UVB. These extrapolated (90 s irradiation) to 12.00 SSB / cell, and 0.3 SSB / cell for broadband UVB and 310 nm

monochromatic UVB respectively. A value of 0.05 SSB / 10^6 bp / 200 kJ m^{-2} was extracted from their figure for SSB induced by wavelengths > 365 nm. This extrapolates to a figure of 0.015 SSB / cell. A value of 0.1 SSB / 10^6 bp / kJ m^{-2} was extracted from their action spectrum for wavelengths ~ 400 nm. This extrapolated to 19.5 SSB / cell for the 405 nm peak.

Pflaum *et al.* (1994) also using alkaline elution and visible light estimated that wavelengths 400-450 nm were responsible for 44% of oxidative damage induced by UVR and visible light while accounting for only 3.5% of the total power delivered by the lamp (1.58 x 10^3 mJ cm^{-2}). From their figures an SSB yield was measured at 0.1 SSB / 10^6 bp / 450 kJ m^{-2}, this is a total induction of 300 SSB / cell. Taking into account the action spectrum described, an estimate of 0.19 SSB / mJ cm^{-2} / cell was made for wavelengths between 400 and 450 nm. This extrapolated to a 90 second 405 nm yield of 1.234 SSB / cell. However, if the chromophore(s) involved in the photosensitisation absorb at the longer end of the range; then the extrapolated value would be an overestimation of 405 nm induced SSB. Slowly developing (> 6hrs) alkali labile sites show an action spectrum with a broad peak that is at a maximum between 400 and 500 nm, whereas the action spectrum for SSB decreases with increasing wavelength (Peak and Peak, 1995). Oxidative damage induced by wavelengths shorter than 399 nm accounted for 10% of the total damage (Pflaum *et al.*, 1994). These figures are therefore subject to the compounded action spectra associated with polychromatic radiation. Extrapolation of the uncorrected data to a 240 second irradiation (i.e. by total Xe lamp radiation, as done in this thesis) was done in two ways: extrapolation from the SSB yield itself and by comparing the irradiation procedures. The SSB yield (0.19 SSB / mJ cm^{-2} / cell) extrapolated to 91.2 SSB / cell for a (total Xe) fluence of 2 mW cm^{-2} for 4 minutes irradiation. Pflaum *et al.* (1994) employed a 1000W halogen lamp; 20 minutes unfiltered irradiation produced 8045 SSB / cell as calculated (this work) from their figures. The work described in this thesis, employed a 150 W Xenon lamp, 4 minutes irradiation would

therefore deliver approximately 3.3% of the dose (subject to the spectral output of the 'halogen' lamp). This extrapolates to 241 SSB / cell.

5.2.3.3 Extrapolation from comet migration characteristics

Table 5.3   Extrapolation of SSB numbers from comet migration characteristics

| | Approximate no SSB induced | | | | | |
| | 60 secs | | 90 secs | | 240 secs | |
	Area	Tail length	Area	Tail length	Area	Tail length
MMB4L (310 nm)	926	1021	1295	1374	755	969
PUTKO (Total)	1831	1718	2215	2039	4005	3376

Peak et al. (1991) measured hydrogen peroxide-SSB by alkaline elution. They observed a threshold of 10 μM H_2O_2 below which no strand breakage could be detected. McKelvey-Martin et al. (1997) measured an almost linear (by Comet Area) dose response to 0-15 μM H_2O_2. The data from Peak et al. (1991) was extracted (in this work) from their figures and regressed against a linear model, constrained through the origin. An SSB yield of 167 SSB / μM H_2O_2 / cell was calculated and called variable f. This figure was used to estimate the number of strand breaks measured by McKelvey -Martin et al. (1997) at concentrations of 5 μM H_2O_2 (836 SSB / cell), 10 μM H_2O_2 (1672 SSB / cell) and 15 μM H_2O_2 (2508 SSB / cell). These values were then regressed (the regression coefficient being labelled f') against the increases in Tail length (25 μm, 35 μm, 40 μm respectively) or the increase (the regression coefficient being labelled f'') in Comet Area (800 μm^2, 1250 μm^2, 1700 μm^2 respectively) induced by these concentrations.

i.e. Δ SSB / Δ [H$_2$O$_2$] = f ; Δ Tail length / Δ [H$_2$O$_2$] = f' ; Δ Comet Area / Δ [H$_2$O$_2$] = f"

therefore Δ SSB / Δ Tail length = f / f' and Δ SSB / Δ Comet Area = f / f"

Thus an estimate of strand breakage to Tail length increase or to Comet Area increase was

obtained. This was calculated at 52.1SSB / μm (f / f') increase in Tail length and

1.38 SSB / μm^2 (f / f") increase in Comet Area. Taking the large 405 nm peak induced in

MMB4L cells these values extrapolate to an induction of 1768 SSB / cell and 469 SSB /

cell measured from the Tail length and the Comet Area respectively. SSB induced by 60 s

of total Xe lamp in PUTKO cells was calculated at 1718 SSB / cell and 1831 SSB / cell

from the increases in Tail length and Comet Area respectively. SSB induced by 240

second of total Xe lamp radiation was calculated from the Tail length and Comet Area at

3376 SSB / cell and 4005 SSB / cell respectively. The unwinding time allowed by

McKelvey-Martin *et al.* (1997) was half (20 minutes) that allowed in these studies

(40 minutes). Unwinding time is a critical assay parameter: Tail length increases with

unwinding time (Yendle *et al.*, 1997). Under the conditions employed in the two

laboratories, for an identical assay in all respects except this, it is likely that the comets

would be smaller under their laboratory's conditions. The estimated yield of SSB by this

method, therefore, is probably an overestimation; additionally, the multiple manipulations

of the original data render the whole estimate subject to an unknown error.

The two repair experiments performed in this work (Section 4.2.3) were used to check the

estimates involved. These two experiments are independent of each other. One

experiment measured the repair of a 405 nm induced peak in MRC5 fibroblasts

(Figure 4.30) and the other measured low levels of SSB induced by 30 s of total Xe lamp

radiation in MMB4L cells (Figure 4.29). These cells showed less SSB induced by total Xe

lamp radiation unlike PUTKO (see Section 4.2.2.5). The difference between the highest

values and lowest values were extracted for the Comet Area and Tail length from both

experiments. These values were used to calculate repair kinetics by the same formula used to estimate the Comet Area or Tail length relationship with H_2O_2-induced SSB.

i.e. $\dfrac{\Delta SSB}{\Delta t(s)} = \dfrac{\Delta Tail\ length}{\Delta t(s)} \times 52.1$ and $\dfrac{\Delta SSB}{\Delta t(s)} = \dfrac{\Delta Comet\ Area}{\Delta t(s)} \times 1.38$

The rate of repair obtained for MMB4L cells was 1.77 SSB s^{-1} or 2.55 SSB s^{-1} (an induction of 106 or 153 SSB) calculated from the Comet Area and Tail length respectively. The rate of repair obtained for the MRC5 fibroblasts was 1.74 SSB s^{-1} or 2.07 SSB s^{-1} an induction of 174 or 207 SSB) from the Comet Area and Tail length respectively.

Green *et al.* (1996) state that under their experimental conditions 1 Gy of ionising radiation induces 1000 SSB per mammalian cell and increases Comet length by 15 µm. This extrapolated to 1,156 SSB / cell and 777 SSB / cell induced during the 405 nm and the 310 nm peaks in MMB4L cells respectively; and 1,156 SSB / cell and 3,497 SSB / cell induced by 60 s and 240 s of total Xe lamp irradiation respectively. In this work, Electrophoresis was carried out at 17 ±1 °C and at 1.3 V / cm (not 15 °C and not 0.83 V / cm as described in their protocol) and hence, under the conditions employed in this thesis, therefore, the number of SSB calculated are slight overestimates.

In conclusion, although the number of strand breaks cannot be determined accurately, an order of magnitude estimate can be made. The alkaline elution technique is not as sensitive as the comet assay and gave a range of values that varied over an order of magnitude (Peak *et al.*, 1987). The data from Pflaum *et al.*, once corrected for spectral output as described above, gave a figure of 3540 SSB / cell for the 405 nm peak induced by the hypothetical 6.5 mJ cm^{-2} or 90 s irradiation time. This was much greater than the other values. The uncorrected data, however, produced a figure closer to the lower values obtained from the other data. Given that the total yield of SSB in the paper by Pflaum *et al.* was calculated (this work) at 8045 SSB / cell, it is possible that the low figures are closer to the true number of strand breaks. The SSB dose response may possibly be super-linear (i.e. the number of SSB may be higher than would be predicted by a linear model) at

experiments. These values were used to calculate repair kinetics by the same formula used to estimate the Comet Area or Tail length relationship with H_2O_2-induced SSB.

i.e. $\dfrac{\Delta SSB}{\Delta t(s)} = \dfrac{\Delta Tail\ length}{\Delta t(s)} \times 52.1$ and $\dfrac{\Delta SSB}{\Delta t(s)} = \dfrac{\Delta Comet\ Area}{\Delta t(s)} \times 1.38$

The rate of repair obtained for MMB4L cells was 1.77 SSB s^{-1} or 2.55 SSB s^{-1} (an induction of 106 or 153 SSB) calculated from the Comet Area and Tail length respectively. The rate of repair obtained for the MRC5 fibroblasts was 1.74 SSB s^{-1} or 2.07 SSB s^{-1} an induction of 174 or 207 SSB) from the Comet Area and Tail length respectively.

Green *et al.* (1996) state that under their experimental conditions 1 Gy of ionising radiation induces 1000 SSB per mammalian cell and increases Comet length by 15 µm. This extrapolated to 1,156 SSB / cell and 777 SSB / cell induced during the 405 nm and the 310 nm peaks in MMB4L cells respectively; and 1,156 SSB / cell and 3,497 SSB / cell induced by 60 s and 240 s of total Xe lamp irradiation respectively. In this work, Electrophoresis was carried out at 17 ±1 °C and at 1.3 V / cm (not 15 °C and not 0.83 V / cm as described in their protocol) and hence, under the conditions employed in this thesis the number of SSB calculated are overestimates.

In conclusion, although the number of strand breaks cannot be determined accurately, an order of magnitude estimate can be made. The alkaline elution technique is not as sensitive as the comet assay and gave a range of values that varied over 2 orders of magnitude (as noted by Peak *et al.*, 1987). The data from Pflaum *et al.*, once corrected for spectral output as described above, gave a figure of 1.2 SSB / cell for the 405 nm peak induced by the hypothetical 6.5 mJ cm^{-2} or 90 s irradiation time. The uncorrected data, however, produced a figure lower than the values obtained from the other data. Given that the total yield of SSB in the paper by Pflaum *et al.* was calculated (this work) at 8045 SSB / cell, it is possible that the low figures are closer to the true number of strand breaks. The SSB dose response may possibly be super-linear (i.e. the number of SSB may be higher than would be predicted by a linear model) at low doses, in which case the low

low doses, in which case the low figures would be underestimates. The estimation of very low numbers of SSB by the increase in Comet length would therefore appear to be the more reliable. It must be borne in mind, however, that only one SSB per supercoil is required to induce DNA unwinding and at these very low doses of UVR a SSB may have disproportionately large effects than it would when placed in the context of higher dose phenomena. In the light of these considerations it is proposed that both sets of figures are correct in part. The very low number of strand breaks induced by low fluence narrow band 405 nm or 310 nm radiation have a large SSB to 'effect' ratio whereas the high fluence total radiation has a lower SSB to 'effect' ratio. It is estimated, therefore, that the Peak 2 observed in the low fluence responses is caused by an induction of approximately 1000 SSB per cell. It is noted that the dose responses induced by low fluence radiation and low concentrations of hydrogen peroxide (McKelvey-Martin, 1997) are similar in principle. It is suggested that 90 s narrow band radiation under the conditions employed in this laboratory and 5μM H_2O_2 under the conditions employed by McKelvey-Martin *et al.* are equivalents. The calculated yields of SSB / 5 μM H_2O_2 (836) and the above estimates of a 405 or 310 nm peak support this idea.

The higher number of strand breaks induced by total Xe radiation obeyed an approximately linear relationship with dose and the dose response agreed with what would be predicted from the literature. It is proposed therefore that the irradiation of cells with total Xe radiation induces lesions resulting in strand breakage of the order of 10^4 to 10^5 lesions per cell.

5.2.3.4 Quantum Yields

Table 5.4   Summary of extrapolated data

	Number of points extrapolated	Mean of extrapolated points	Std err of mean (as %)	Quantum yield (SSB / photon)	Quantum efficiency
405 nm peak (6.5 mJ cm^{-2} or 90s)	10	341	62.5 (18.3%)	8.2×10^{-8}	0.25
310 nm Peak (2.0 mJ cm^{-2} or 90s)	11	319	50.2 (15.7%)	3.26×10^{-7}	1

An estimation of quantum yields of SSB induction by 405 nm narrow band radiation and 310 nm narrow band radiation were made from the mean of the extrapolated values described above (Table 5.4) assuming a cellular target of 314μm^2 (Alberts *et al.*, 1984). They were calculated as 8.2×10^{-8} SSB per 405 nm quantum and 3.26×10^{-7} SSB per 310 nm quantum. The relative effectiveness of UVB to 405 nm radiation in inducing SSB was four times greater. Cridland and Saunders (1994) estimate the relative effectivness at approximately 2 orders of magnitude.

5.3   THE CELLULAR RESPONSE TO LOW FLUENCE UVR

SSB dose responses to low fluence narrow band 310 nm and 405 nm radiation and high fluence total Xe lamp radiation have been obtained for a number of different human cells using the comet assay. Whilst differences between cell types were observed, however, a general pattern was seen. The response to the low fluence radiation was generally an increase in SSB for the first two minutes of irradiation. This was rapidly repaired to baseline levels whether under continued irradiation or not. Two peaks in SSB induction were regularly seen: an early peak at around 30 s and a second larger peak - usually a maximum - at around 90 s. This second peak appeared much enhanced in cells which came from male donors only. A linear dose response was obtained with the high fluence

total Xe lamp radiation, although some characteristics of the low fluence dose responses were observed. It was discovered that the detection and measurement of the dose response phenomena was very much dependent on the parameter by which the comets were analysed. In this respect, the two 'moments' were more suited to the measurement of the higher fluence radiation induced SSB while the Comet Area was particularly sensitive to the low fluence phenomena.

The possible mediators of the strand breaks were discussed in the previous section (Halliwell and Aruoma, 1991; Wiseman and Halliwell, 1996; Cadet, 1994; Cridland and Saunders, 1994; Friedberg *et al.*, 1995; Peak and Peak, 1995). The lesions induced by 405 nm radiation are primarily caused by hydroxyl radical attack on the DNA causing direct SSB, alkali labile lesions and base hydroperoxides. The upstream mediators probably include hydrogen peroxide, lipid peroxides, and lipid hydroperoxides. Singlet oxygen cannot be ruled out as a direct mediator, although the strand breaks induced in DNA by singlet oxygen appear to be qualitatively different from the lesions induced by 310 and 405 nm narrow band radiation (Peak *et al.*, 1991). The Type I photosensitisers, i.e. the primary chromophores responsible for the indirect effects are probably a mixture of porphyrins and flavins (Peak and Peak, 1995). The 310 nm effects are predominantly direct effects and will include a high proportion of dipyrimidine Dewar valence isomers. The following model (Figure 5.2) is proposed for the effects of low fluence radiation in these studies.

Figure 5.2   The effects of low fluence UVR in human cells
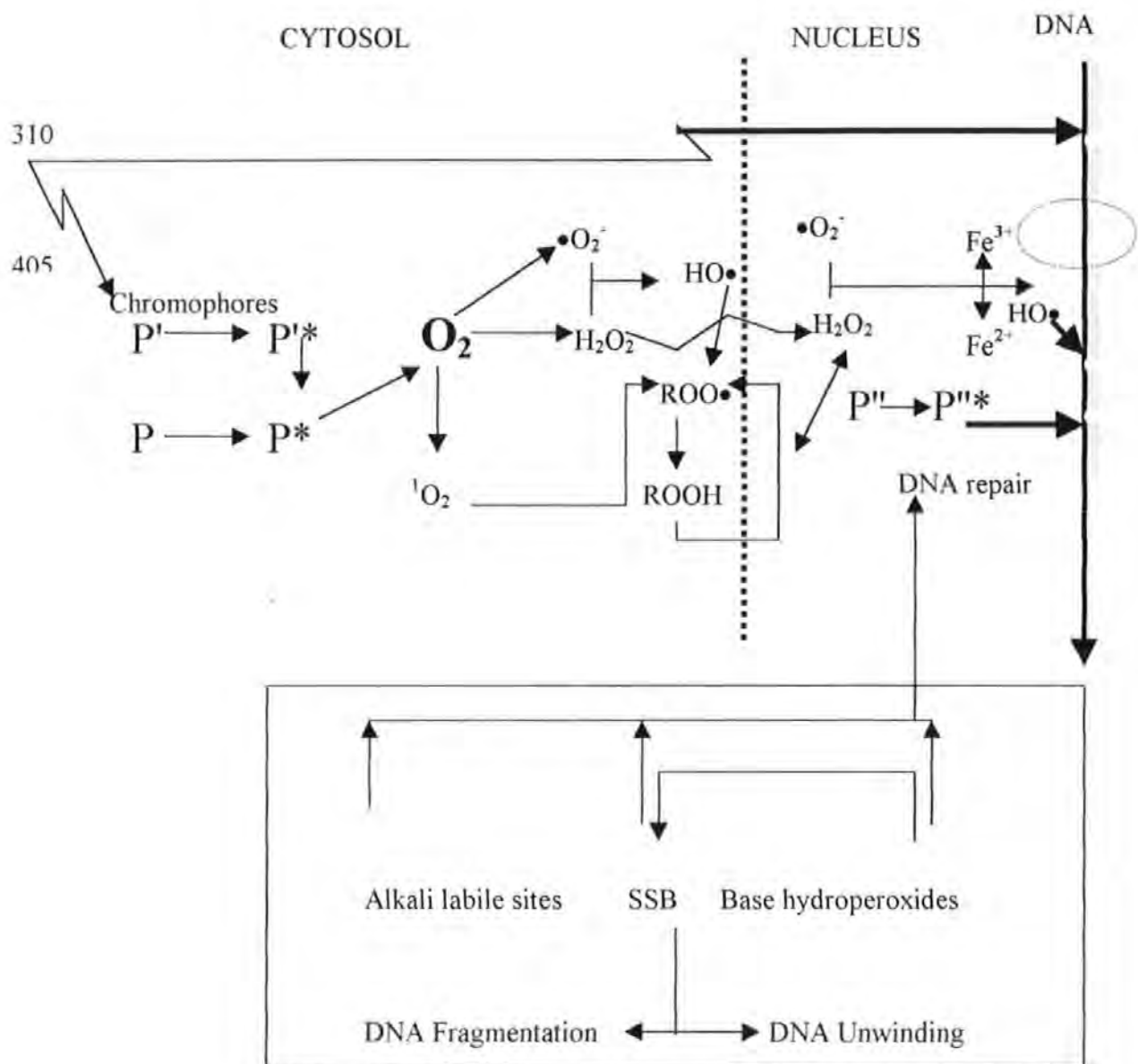
The effects of low fluence UVR summarised above are proposed to occur in the following

manner. 405 nm radiation is absorbed by the Type II photosensitisers P or P'. The excited

photosensitiser (P* or P'*) may then transfer this energy directly to ground state oxygen.

Alternatively, the photosensitiser may be Type I (P") and transfer the energy directly to

DNA. The reactive singlet oxygen, or the combination of superoxide, hydrogen peroxide

and free iron in close proximity to membranes will initiate lipid peroxidation chain

reactions crossing the lipid bilayer nuclear membrane either directly or by hydrogen

peroxide diffusion through the membrane . Lipid peroxidation will therefore occur on both

faces of the membrane. The lipid peroxides and hydroperoxides may generate diffusable peroxides to add to the Fenton reaction taking place on the chromatin and producing the lesions described.

The phenomenon of the two peaks may be a result of any or all of the following. Photobleaching (i.e. the effective destruction of the chromophore by absorption of radiation) of the cellular chromophore could allow repair to take place in the absence of further SSB, but the 310 nm-induced SSB are primarily direct effects and thus do not involve a chromophore. The dose responses to 310 nm and 405 nm radiation were very similar, and hence this has been interpreted as an underlying common mechanism. Photobleaching is therefore unlikely to be responsible for the reversal of the SSB, and could also be ruled out on the grounds of the extremely low fluence employed. It was noted in a very early experiment with the high fluence bulb that irradiation for 100 or 1000 s at 405 nm ($\sim$106 μW cm^{-2}) produced a plateau and not a peak. This implies that photobleaching is not responsible.

It was noted in the repair experiments that after stopping irradiation, that SSB continued to increase for a further 60 s before the repair process was able to reverse the increase in SSB. This implies delayed effects, and several possible explanations can be forwarded, any or all of which may be responsible.

(i)   The reactive species generated may continue to exert their effects for a further 60 s. However, it is unlikely that the lipid peroxidation would be sustained for this length of time, but the reactive base hydroperoxides resulting from UVR (Cadet, 1994) could be long lived enough to exert effects after 60 s (P. Burcham, personal communication).

(ii)   The delayed effects could also reflect the time taken for the diffusion of molecules. The phenomena of the two peaks could be explained by the existence of two populations of molecules, for example a nuclear population of active species (that cause SSB) responsible for peak 1 and a second cytosolic population that cause a

191

greater number of SSB (due either to greater reactivity towards DNA or a greater number of clastogenic molecules) that results in the second peak.

(iii)   Alternatively, the nature of the two populations of molecules may be repair-related; for example, if a limited nuclear population of metabolites limited the reversal of SSB (hence peak 1), a second larger cytosolic population might be fully effective and permit the reversal of SSB to pre-irradiation levels (and thus could be responsible for peak 2).

(iv)   The molecules could also be parts of a fast photosensitising pathway involving the P" Type II molecules (peak 1) and parts of a slow photosensitising pathway involving the P and P' Type II photosensitisers (peak 2).

(v)   A very different alternative is that the peaks reflect the unwinding and rewinding process over time and are manifestations of the release of torsional energy. The initial attack on the DNA backbone relaxes supercoiling, thus exposing more DNA to strand breakage. It is possible that the chromatin (and with it the iron) molecules are propelled clear of the DNA under the release of the supercoiling, thereby removing the hydroxyl attack. Once all available supercoils have been relaxed, the unwinding and exposure process will slow down and the DNA can be recoiled. However, the reduction in comet values may not be repair associated: the relaxed supercoils may be drawn by electrophoresis back into the comet head and if the comet head was already 'saturated' then this would pass undetected by the readback system.

The differences between the peaks in male only cells and those which came from female donors is unclear. They may reflect genuine y-linked or imprinted gene differences; if this is the case, then an explanation for the higher male incidence of some diseases, including melanoma, may be important. It could be a chance phenomenon, however; in this respect it is noted that if the probability of observing positive phenomena is 0.5 (i.e. a peak or no

peak)then the probability of observing peaks in 4/4 male cells and 0/1 female cells is 2^{-5} (<0.03). Interestingly, the hybrid cell displayed an intermediate peak.

5.4 PERSPECTIVE

The previous Chapter and this one laid the foundation for the following four Chapters contained in this thesis. Chapter 6 describes the modulation of the observed dose responses by prooxidant and antioxidant molecules, with a view to estimating the relative importance of the various active species. It was found that low concentrations of o-phenanthroline reduced (but by less than half) 405 nm-induced SSB, implying that the greater pathway is not the hydrogen peroxide-hydroxyl radical pathway. Beta-carotene, a powerful oxidant at atmospheric oxygen levels was found to increase SSB. The two reagents together appeared to synergise and greatly enhance Peak 2.

Malignant melanoma incidence in males (but not females) in the South-West of England is associated with high levels of environmental arsenic (Phillip et al., 1983). Chapter 8 describes the effects of arsenic on SSB repair. Although arsenic was found not to exert clastogenic effects in its own right, it was found that it partially inhibited the rejoining of SSB.

The final Chapter reviews the assay as employed in this thesis. The first Section (Section 10.1) discusses the two readback systems and the suitability of the existing image analysis parameters for the measurement of these low dose phenomena. The second part (Section 10.2) proposes and examines a new image analysis parameter-the Area Moment-that appears to be more suitable for the detection of low-dose-modulation.

6 CHAPTER 6.

THE MODULATION OF NORMAL CELLULAR RESPONSES TO UV RADIATION BY PROOXIDANT AND ANTIOXIDANT MOLECULES

RESULTS

6.1 INTRODUCTION

One of the objectives of this research project was to develop the comet assay to screen compounds for photoprotective or photosensitising properties within cells. Chemicals were tested at a range of concentrations, irradiation wavelengths and doses on a variety of human cells. Initially, the comet assay was assessed while investigating the prooxidant and antioxidant (Burton and Ingold, 1984; Birnboim, 1992; Cozzi *et al.*, 1997) properties of synthetic beta-carotene. Further studies of the effect of o-phenanthroline and beta-carotene plus o-phenanthroline were also undertaken. As a result of these experiments a mixture of the vitamin A precursor beta-carotene, vitamin C (ascorbic acid) and vitamin E (alpha tocopherol) (ACE) was also used as a modulant chiefly because this was a cold water dispersible system. A summary of the results from these experiments is given in Table 6.1.

Table 6.1 The effect of the prooxidant and antioxidant molecules.(b-car: beta-carotene, o-phen:o-phenanthroline) on UV irradiated cells

Modulant	Wave-length	Dose/ mJ cm^{-2}	Number of doses compared	Cell line	Readback Method	Effects / Comments
0.1 mg/ml b-car	310 405	10	4	MRC5SV2	Visual inspection	Photoprotective (p<0.05, χ^2.)
0.1 mg/ml b-car	405	0 - 8.5	5	MRC5SV2	Visual inspection	Photoprotective
0-92% stock ACE	Total Xe	120	4	YBF15F	Image Analysis	Slight concentration-dependent photoprotection
stock ACE	Total Xe	60 - 240	4	PUTKO	Image Analysis	Dose dependent photosensitisation (p< 0.001 t-test)
0.05 mg/ml b-car	405	0 - 35	7	MRC5 SV2	Visual inspection	Dose dependent photosensitisation
0-3 µg/ml b-car	405	10	6	MRC5 SV2	Visual inspection	Concentration dependent photosensitisation
700 nM b-car	Total solar radiation	Sunny or Raining	4	MRC5	Visual inspection	Photosensitisation
700 nM b-car	405	7	2	A2058	Image analysis	No modulation
700 nM b-car	405	7	2	A2058	Image analysis	Possible modulation
700 nM b-car	405	0 - 17	6	A2058	Visual inspection	No modulation
50 µM o-phen	405	0 - 17	6	A2058	Visual inspection	Photoprotective at low doses
700 nm b-car + 50 µM o-phen	405	0 - 17	6	A2058	Visual inspection	Photosensitisation at 8 mJ cm^{-2} (p< 0.05, t-test)
0 - 15 mM o-phen	Total Xe	120	5	PUTKO	Image Analysis	Concentration dependent photosensitisation

6.2 RESULTS

6.2.1 The modulating effects of beta-carotene.

6.2.1.1 Introduction

Beta-carotene is extremely hydrophobic and effectively insoluble in water (Vitamins division, Roche Pharmaceuticals, personal communication) although Sigma UK Ltd advised a maximum solubility of 0.1 mg beta-carotene per ml of water (186 μM) and a maximum solubility of 1 mg / ml beta-carotene in ethanol (1.86 mM) (Sigma Technical Services, personal communication). The low solubility of beta-carotene in water or ethanol resulted in very low experimental concentrations and correspondingly small effects. To overcome the lack of aqueous solubility a number of approaches were adopted. Two forms of beta-carotene were used: powdered synthetic beta-carotene (Sigma, 95% purity) and a 10% w/w cold-water-soluble form (that also contained vitamin C (4% w/w) and vitamin E (1.5% w/w) (Roche Pharmaceuticals). Both forms are heat and light sensitive (Sigma, UK). In this work solutions of synthetic beta-carotene were prepared in a number of ways: suspended in aqueous media (Cozzi *et al.*, 1997) and added to the LMP agarose before heating to ~ 100 °C, or added to media at 37 °C and sonicated for 15 minutes, or added to media and incubated for several days at 37 °C, or dissolved in ethanol and filtered through a 0.2 μm filter (Mathews-Roth, 1992). The advantages and disadvantages of each method are outlined in the relevant sections below and discussed in Chapter 7. The results described below are compared to data from the published literature and discussed in context, also in Chapter 7.

6.2.1.2 MRC5 SV2 transformed fibroblasts

The cell line MRC5 SV2 was used in the first set of experiments; this cell line was used in a repair study of UVA, UVB, and UVC induced lesions (Alapetite *et al.* 1996) and was

196

known to be repair proficient. The cell line is also very easy to culture with a short population doubling time, this made for large numbers of cells available for testing.

6.2.1.2.1 The effects of 310 nm, 405 nm and total Xe radiation on MRC5 SV2 fibroblasts in the presence of synthetic beta-carotene

Beta-carotene was added (or not added to the controls) to LMP agarose in DMEM without phenol red to make a final concentration of 0.1 mg / ml. The control agarose (non-beta-carotene-containing medium) mixture and the test agarose (beta-carotene-containing-medium) mixture were heated to ~ 100 °C for 15 minutes with agitation before warming at 37 °C for 30 minutes. This improved the solubility of the beta-carotene in cold or warm media, but heating the beta-carotene to this temperature may have altered its reactivity profile as beta-carotene is heat sensitive (Sigma, UK). MRC5 SV2 transformed fibroblasts were suspended in the two media under test and then 310 nm- (~ 10 mJ cm^{-2}), 405 nm- (~ 10 mJ cm^{-2}), mock-irradiated, or exposed to the unfiltered Xe lamp (>>200 mJ cm^{-2}). SSB induction was measured by the comet assay immediately after irradiation. The assay was read back visually and the percentage of comets in each category was calculated. The fractions of comets in each category was plotted against the treatment procedure (Figure 6.1). The beta-carotene-treated cells were protected from the low doses of the 310 nm radiation and the 405 nm radiation but unprotected against the high dose of unfiltered radiation. The comet distributions in the non-beta-carotene-treated and irradiated cells were significantly different to the unirradiated controls (p < 0.05, chi-squared test) but the comet distributions in the beta-carotene-treated and irradiated cells were not different from the controls. It was concluded that the cells irradiated in 0.1 mg / ml beta-carotene-containing media were afforded significant protection from the effects of low doses of UVR (Kendall *et al.*, 1998).

The photoprotective effect of beta-carotene observed above may have been due to,

(1)   Physical absorption of the radiation. Carotenoids absorb significantly in this region

and beta-carotene displays a maximum between 400 nm and 450 nm depending on

the solvent used (Dawson *et al.*, 1988);

(2)   Extra-cellular quenching of reactive oxygen species (ROS);

(3)   An altered reactivity profile of beta-carotene after the heating procedure.

An experiment was designed to address these three points. To rule out the possibility that

the beta-carotene was affected by heating, it was dissolved in the media by sonication. To

remove any extra-cellular beta-carotene and thus any extra-cellular quenching of ROS or

extra-cellular absorption of radiation, the cells were washed three times in PBS.

MRC5 SV2 transformed fibroblasts were incubated for one hour in either normal (DMEM

without phenol red) or 0.1 mg / ml beta-carotene-containing media, prepared by sonication

(to rule out point 3). The cells were then washed three times in PBS (to eliminate points 1

and 2) prior to 405 nm-irradiation at doses between 0 mJ cm^{-2} and 8.5 mJ cm^{-2}. The

experiment was performed in duplicate, read back visually and the mean comet values

were plotted against dose (Figure 6.2). None of the dose responses of the untreated or

treated cells were significantly different, by t-test, from the control cells, (possibly due to

the high variance (see Figure 6.2) of the assay results from the control cells) but the beta-

carotene-treated cells displayed less damage than the untreated cells. The beta-carotene

modulated responses to 2.1 and 8.5 mJ cm^{-2} radiation were significantly less than the

normal counterparts (p = 0.024 and 0.002 respectively, 1 tailed t-test, equal variance). The

overall trend in assayed SSB with increased dose was obtained by regressing the data to fit

the model y = mx + c. The untreated cells displayed an overall dose dependent increase in

SSB. This was not seen in the beta-carotene-treated cells, rather a slight downward trend

was seen. It was concluded that the photoprotective effects of beta-carotene were not due to extracellular absorption of UVR or extracellular quenching of ROS (there was no beta-carotene available outside of the cell itself) or an altered reactivity profile of beta-carotene due to heating (as the beta-carotene suspension had been prepared by sonication, not heating).

6.2.1.2.3   The effects of 405 nm radiation on MRC5 SV2 transformed fibroblasts after incubation with 0-3 µg / ml synthetic beta-carotene.

The photoprotective effects of beta-carotene evident at 0.1 mg / ml (Section 6.2.1.2.2) were not evident at lower concentrations. At some concentrations below 5 µg/ml beta-carotene appeared to photosensitise the cells (data not shown). MRC5 SV2 fibroblast cells were incubated for one hour in DMEM without phenol red that contained concentrations of beta-carotene in the range 0-3 µg / ml prior to receiving 10 mJ cm^{-2} 405 nm radiation. The experiment was performed in duplicate, read back visually and the mean comet value at each concentration was plotted against concentration (Figure 6.3). The photosensitisation effects of beta-carotene were observed to be concentration dependent although they failed to reach significance. The dose response appeared to have sigmoidal characteristics, but returned a high correlation coefficient ($r^2 = 0.8364$) when fitted to a linear model.

Figure 6.1 The photoprotective effects of beta-carotene. MRC5 SV2 transformed
fibroblasts were 310 nm- (~ 10 mJ cm^{-2} '310'), 405 nm- (~ 10 mJ cm^{-2} ,'405'), mock-
('neg') irradiated or exposed to the unfiltered Xe lamp (>>200 mJ cm^{-2} , 'pos') in
agarose made up with DMEM without phenol red which either did ('+') or did not ('-
') contain 0.1 mg / ml beta-carotene. SSB was measured by the comet assay
immediately after irradiation. The percentage of comets in each category was
calculated (vertical axis) and plotted against the treatment procedure. The
photoprotection was significant by χ^2 test (p<0.05).
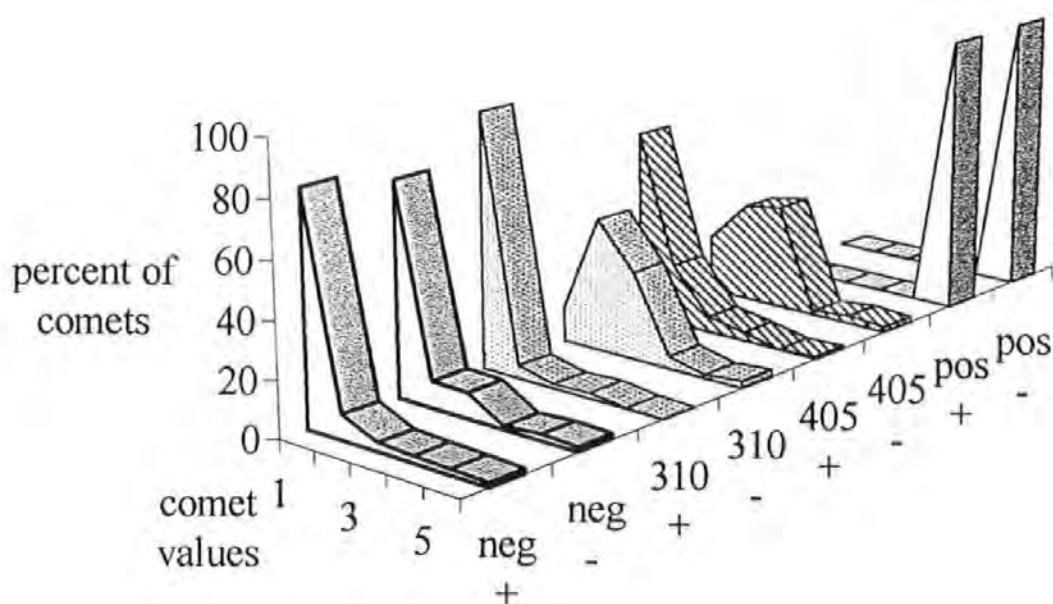
Figure 6.2 The photoprotective effects of beta-carotene. MRC5 SV2 transformed fibroblasts were incubated for one hour in either normal (DMEM without phenol red) or 0.1 mg / ml beta-carotene-containing media. They were washed thoroughly in PBS prior to 405 nm-irradiation at doses between 0 mJ cm^{-2} and 8.5 mJ cm^{-2}. The mean comet values of duplicates were plotted against dose. At all doses the beta-carotene treated cells displayed less damage than the untreated cells. The photoprotection was significant at 2.1 mJ cm^{-2}(p<0.05) and 8.5 mJ cm^{-2} (p<0.001) by 1-tailed t-test.
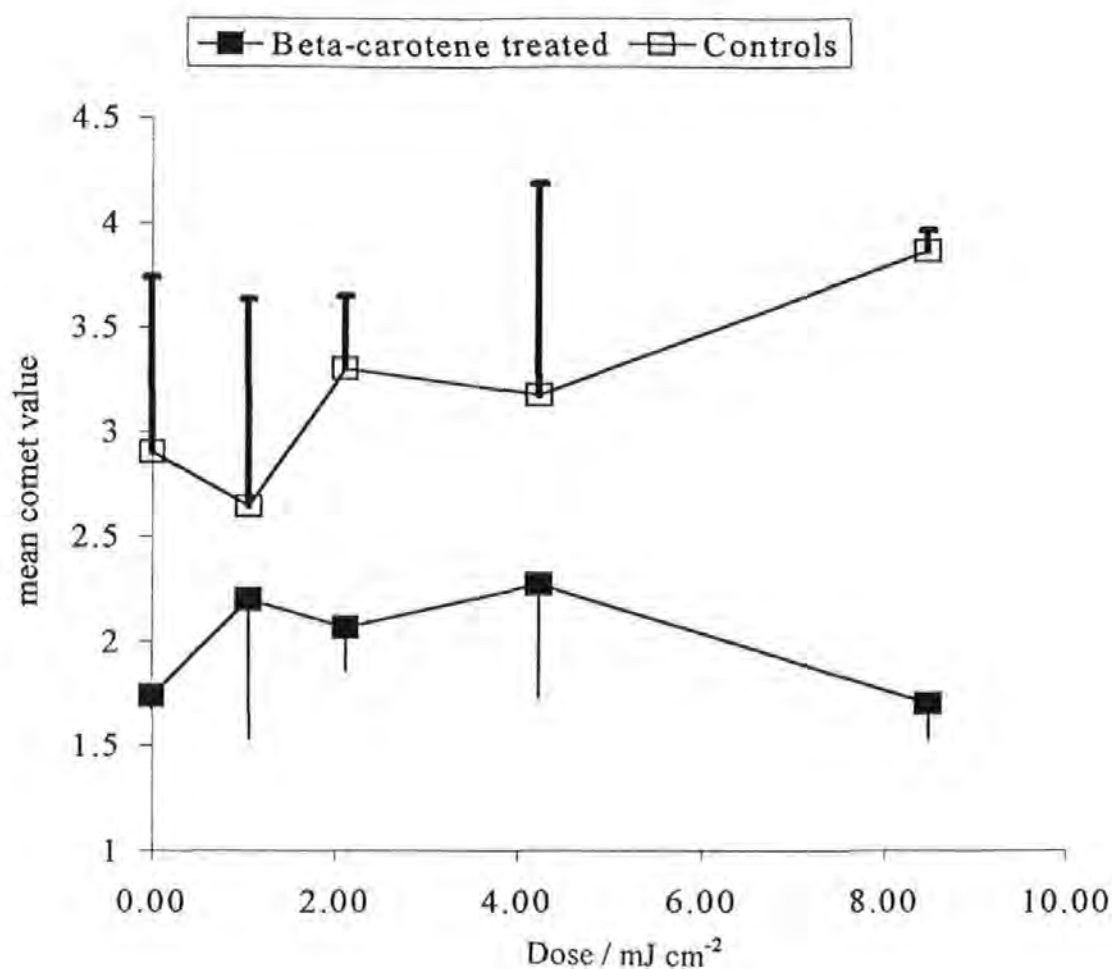
6.2.1.2.4 The effects of 405 nm radiation on MRC5 SV2 fibroblasts after incubation for three days with beta-carotene

The hydrophobicity of beta carotene was clearly evident in the aqueous media: the centrifuge tubes and culture flasks were stained orange and amalgamated clumps of beta-carotene powder (approximately 0.1 to 1 mm in diameter) could be seen floating on the surface and sticking to the sides of the vessels. It was possible that the cells could not take up enough beta-carotene in the time allowed (1 hour) from the beta-carotene available in the media to significantly modulate the responses to UVR. To rule out this possibility, MRC5 SV2 transformed fibroblasts were incubated in normal growth media or growth media containing 0.05 mg / ml beta-carotene for three days. This method allowed the cells under test to form a monolayer and to accumulate the beta-carotene from solution. The possible carotenoid-related upregulation of gap junctional communication (Yamasaki and Naus, 1996) between cells could also have aided the distribution of beta-carotene (and other antioxidant molecules) within the cell population. The drawback to this method was the high incidence of culture contamination due to the addition of non-sterile reagents. After 3 days, one non-contaminated culture from each of the (passage-matched) beta-carotene and control cultures was washed three times in PBS and 405 nm irradiated (embedded in agar) in the dose range zero to 35 mJ cm^{-2}. The assay was read back visually and the mean comet value of over 50 comets per slide plotted against dose (Figure 6.4). The beta-carotene treated cells appeared to be photosensitised to the extent that the early peak (~10 mJ cm^{-2}) was shifted to the left. This experiment was not replicated and so no indication of error can be made.

Figure 6.3 The concentration dependent photoprotective effects of beta-carotene.
MRC5 SV2 fibroblast cells were incubated for one hour in DMEM without phenol
red that contained between 0 and 3 µg / ml beta-carotene prior to washing in PBS and
10 mJ cm^{-2} 405 nm irradiation. The solid squares represent the mean of duplicate
determinations, the open triangle represents the mean of two determinations of non-
treated, non-irradiated cells. The error bars represent the mean plus or minus one
standard deviation. The photosensitisation effects of beta-carotene were observed to
be concentration dependent although not significantly so.

$$y = 0.4589x + 3.493$$
$$R^2 = 0.8364$$
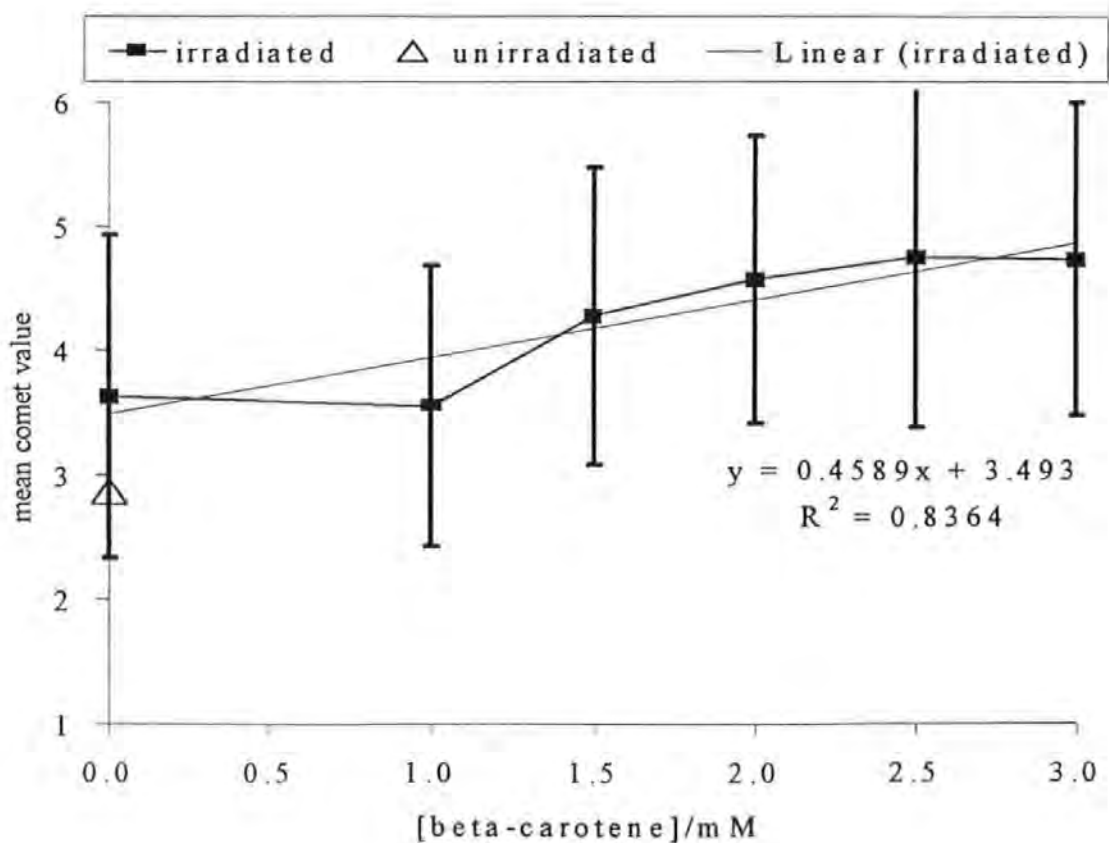
Figure 6.4 The photosensitising effects of beta-carotene. MRC5 SV2 transformed fibroblasts were incubated in normal growth media (open squares) or 0.05 mg / ml beta-carotene-containing growth media (solid squares) for three days prior to thorough washing in PBS and 405 nm irradiation in the dose range zero to 35 mJ cm^{-2} . The beta carotene treated cells appeared to be photosensitised to the extent that the early peak (~10 mJ cm^{-2}) was shifted to the left.
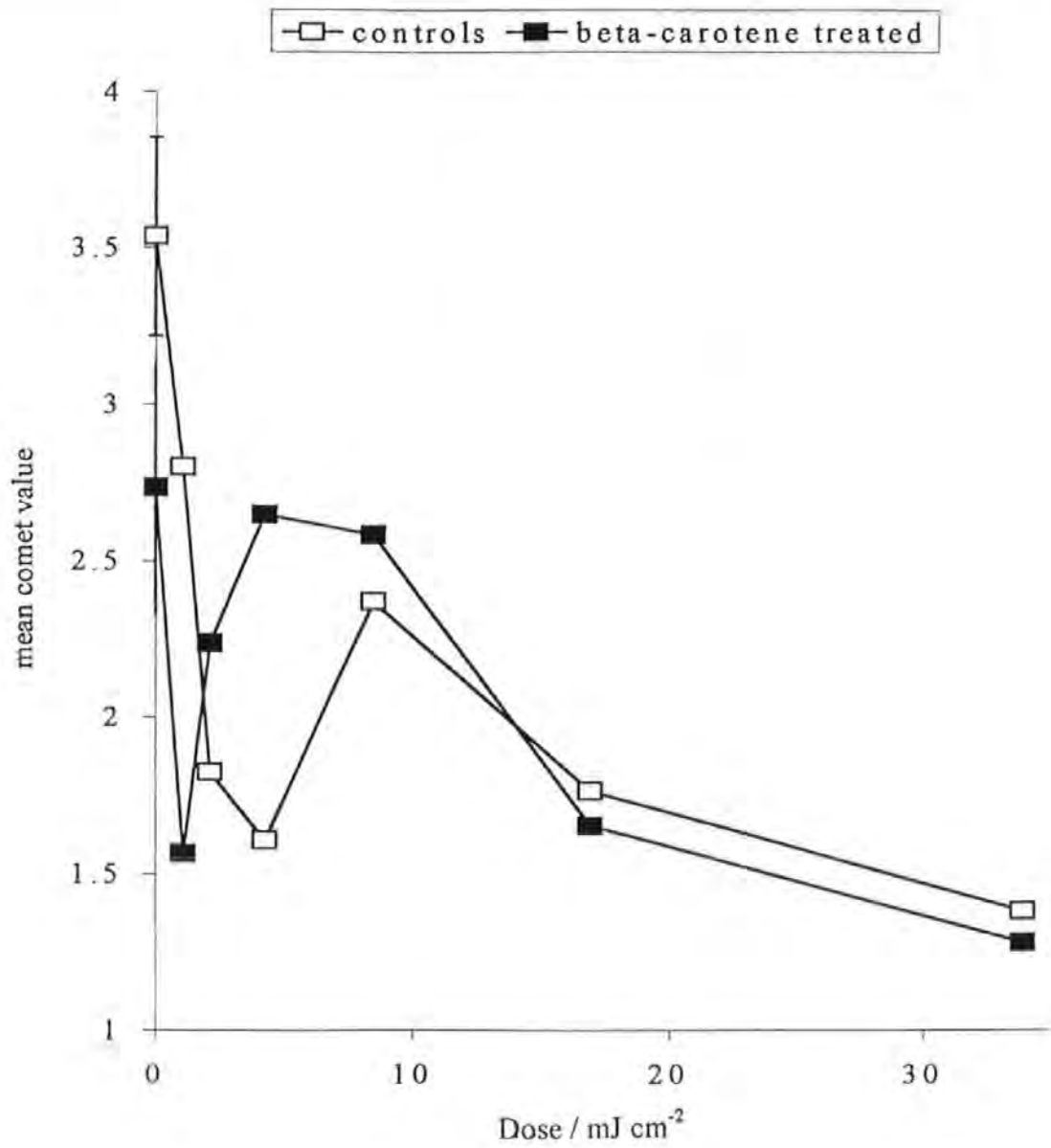
6.2.1.3   A2058 metastatic melanoma cells

The low solubility of beta-carotene in water resulted in unknown concentrations of beta-carotene in aqueous solution and thus available to the cells for uptake. This made quantification of the modulating effects unreliable with respect to beta-carotene concentration. It was decided to change the beta-carotene solvent from aqueous media (based on the method of Mathews-Roth, 1992) to denatured (i.e. containing methanol and iso-propanol to conform to Customs and Exise requirements) spectrophotometric grade ethanol after consultation with Sigma Technical Services. Accordingly, a saturated solution of synthetic beta-carotene in ethanol was made by several cycles of vigorous shaking, sonication and warming at 37 °C. The solution was sterile-filtered through a 0.2 μm filter and 1.0 ml aliquots of this solution were stored at -20 °C (Sigma UK). An accurately weighed amount of beta-carotene was made up into a sub-saturated solution in a similar manner and used to construct a standard curve to determine (via UV spectrophotometry) the concentration of the filtered beta-carotene stock solution (Section 2.4.1.1). It was decided to use the A2058 melanoma cell line as the cell line under test. The decision to change two variables (solvent and cell line) was taken for the following reasons. A2058 melanoma cells are metastatic and, owing to their reduced adhesion to the culture flask, require a shorter trypsin treatment to generate single cell suspensions, thus lowering the background level of damage induced by the trypsin treatment. A2058 has a more uniform morphology, cell volume and DNA content (ECACC data sheet) than MRC5 SV2 thus readback variation from the assay was reduced. A2058 has a longer population doubling time than MRC5 SV2, thus extrapolation of growth curves to predict confluence was more reliable. Both cell types were compared for their normal responses to 405 nm radiation and were seen to be very similar (Figure 4.3).

6.2.1.3.1 The potential cytotoxicity of beta-carotene in ethanol

The cytotoxicity of the beta-carotene in ethanol solution was investigated at a range of

ethanol concentrations from 30% (containing ~ 50 μM beta-carotene) to 0.3% (containing

~ 500 nM beta-carotene). T25 flasks were seeded with 10 ml of cell suspension containing

1.2×10^6 A2058 cells. The beta-carotene-in-ethanol solutions were added to the flasks to

make the concentration series. The flasks were gassed with 5% CO_2 and incubated at 37

°C for up to 24 hours. The highest concentration of ethanol that the cells could tolerate

was established by Trypan blue exclusion at 0.3% for 24 hours- although the cells could

tolerate 3% for one hour without evidence of cytotoxicity as measured by Trypan blue

exclusion.

6.2.1.3.2 The effects of 405 nm radiation on A2058 cells after incubation with 700 nM

beta-carotene

The effects of 405 nm radiation on A2058 cells after one hour incubation in 700 nM beta-

carotene (calculated from the known concentration of the filtered stock solution and

containing 0.5% ethanol) were investigated by two methods (see below).

6.2.1.3.2.1 Method 1: with cells embedded in agarose and analysed by image analysis

The cells were incubated for one hour in media which did or did not contain 700 nM beta-

carotene, and washed three times in PBS before resuspending in media without phenol red.

The cells were embedded in agarose and 405 nm-irradiated for 90 seconds (7 mJ cm^{-2}).

The experiment was conducted in duplicate and read back by image analysis. The beta-

carotene-treated cells appeared to be significantly photoprotected ($p < 0.05$, one tailed t-test,

equal variance) when analysed by the RRU moments, but no significant difference was

seen when the Olive moments were analysed by the same test (Figure 6.5). The

experiment was therefore repeated in 6-fold replicate to clarify this (Figure 6.6). The mean

values of the control cells and the beta-carotene-treated cells did not differ significantly

(p>0.05 one tailed t-test, equal variance) when analysed by Comet Area or either of the RRU moment or the Olive moment.

6.2.1.3.2.2   Method 2: cells suspended in PBS and assays read back visually

The variation in the lamp output over the irradiating area was measured at approximately $\pm$ 8% (see Appendix A, Section 11.2.3.1.6). The irradiation of single slides in situ thus resulted in the delivery of higher doses of radiation to one half of the slide compared to the other half, raising assay variance and introducing a readback bias. (This latter was especially important if the slide contained a high density of comets when the required number of comets may have been found in one small area of the slide.) In a second approach, the A2058 melanoma cells were irradiated suspended in PBS. This modification was made for the following reasons. Photooxidation of some media constituents (in particular tryptophan (Hiraku *et al.* 1995)) can generate hydrogen peroxide and lead to a high background level of SSB, (compare, for example, the two mean comet values after irradiation of MRC5 cells suspended in media or PBS, Section 4.2.4). Hence, the effect of the variation in lamp output could be increased by the different concentrations of hydrogen peroxide generated by different fluences over the irradiating area. In this respect, the PBS suspension method had two potential benefits. First, irradiation of the cells in PBS eliminated extracellular hydrogen peroxide generation. Second, the cell suspension was mixed with the LMP agarose after irradiation thus the differently irradiated cells were more evenly distributed over the assay slide, eliminating readback bias. The drawback to this method was that some SSB repair would take place during slide preparation (see Section 4.2.3)

A2058 melanoma cells were incubated for one hour in DMEM without phenol red that did or did not contain 700 nM beta-carotene prior to 405 nm irradiation for doses of 0, 1.4, 2.9, 5.8, 8.5 and 17.1 mJ cm^{-2}. The investigation was performed in duplicate over three independent experiments as part of a beta-carotene/ o-phenanthroline investigation. The

assay was read back by the visual inspection method. The mean comet value was normalised to the negative controls in each experiment, thus providing an internal standard. Mean comet values were analysed by t-test as before: there was no significant modulation of the dose response by beta-carotene. The mean comet values were plotted against dose (Figure 6.7). The modulated dose response was seen to be in close agreement with the unmodulated response. It was noted that the 10 mJ cm^{-2} peak had been shifted to the left, appearing at around 3 mJ cm^{-2}, representing a time span of one minute and approximately the time taken for slide preparation after irradiation suggesting that the early peak was indeed a time-related phenomenon and not a dose-related one (as discussed in Chapter 5). This protocol was subsequently modified for the measurement of direct SSB on the basis that the repair period introduced the kinetics of SSB repair as an unnecessary variable. For measurement of SSB by this protocol the cells were irradiated and slides prepared on ice, at which temperature DNA repair is slowed down (but not arrested altogether (Bock *et al.* 1998)).

6.2.1.4 MRC5 Normal human fibroblasts

The failure of the technique to reproducibly measure significant modulation of the dose response was attributed to three main causes.

(1) The concentrations of beta-carotene obtainable in solution were thought to be too low to produce a modulation of sufficient magnitude.

(2) The variance associated with the non-linearity of the lamp was thought to be masking the small changes that were produced.

(3) The assay is cell cycle sensitive and it was thought that the use of constitutively cycling cells was also increasing assay variance. The first of these issues was addressed by using a cold water dispersible form of beta-carotene (Section 6.2.3 below). The second and third issues were addressed together.

Contact inhibited MRC5 normal human fibroblasts were grown to confluence and incubated for 5 days as a monolayer to arrest cell division. The cells were lifted, resuspended and incubated for one hour in media which did or did not contain 700 nM beta-carotene. The cells were washed three times in PBS and resuspended in PBS. They were then placed on ice and exposed to total solar radiation (which is effectively linear) for 10 minutes on a clear sunny May morning (18/5/98) or for 30 minutes on a cloudy and wet morning one week later (28/5/98) at exactly the same time of day (11.30 am). Figure 6.8 represents the mean of triplicate determinations for the unexposed non-treated cells, unexposed beta-carotene-treated cells, exposed non-treated cells and exposed beta-carotene-treated cells. For both beta-carotene-treated and untreated cells, the exposed cells differ significantly ($p < 0.05$ 1 tailed t-test, equal variance) from the unexposed cells under both weather conditions. The difference between exposed beta-carotene treated cells and the exposed untreated cells only approaches significance (clear and sunny, $p<0.12$; cloudy and wet, $p<0.08$).

6.2.2 Conclusions on the use of synthetic beta-carotene as a photomodulant

It was concluded that although beta-carotene appeared to have clear photosensitising properties, the failure of the technique to reproducibly produce statistically significant modulation was primarily due to the small magnitude of the changes as a result of low concentrations of beta-carotene obtainable in aqueous solution. It was also concluded that, secondary to this and compounding the problem, the small changes that were produced were overshadowed by a high assay variance, caused by a number of factors but chiefly the non-linearity and low intensity of the narrow band radiation.

Figure 6.5. The possible modulation of the dose response by 700 nM beta-carotene.
A2058 melanoma cells were incubated for one hour in medium which did or did not
contain 700 nM beta-carotene, and washed three times in PBS before resuspending in
media without phenol red. The cells were embedded in agarose and 405 nm-
irradiated for 90 seconds (7 mJ cm^{-2}). The experiment was conducted in duplicate
and read back by image analysis. The beta-carotene-treated cells appeared to be
significantly photosensitised ($p<0.05$, one tailed t-test, equal variance) when analysed
by the Comet Moments, but no significant difference was seen when the Tail
Moments were analysed by the same test.
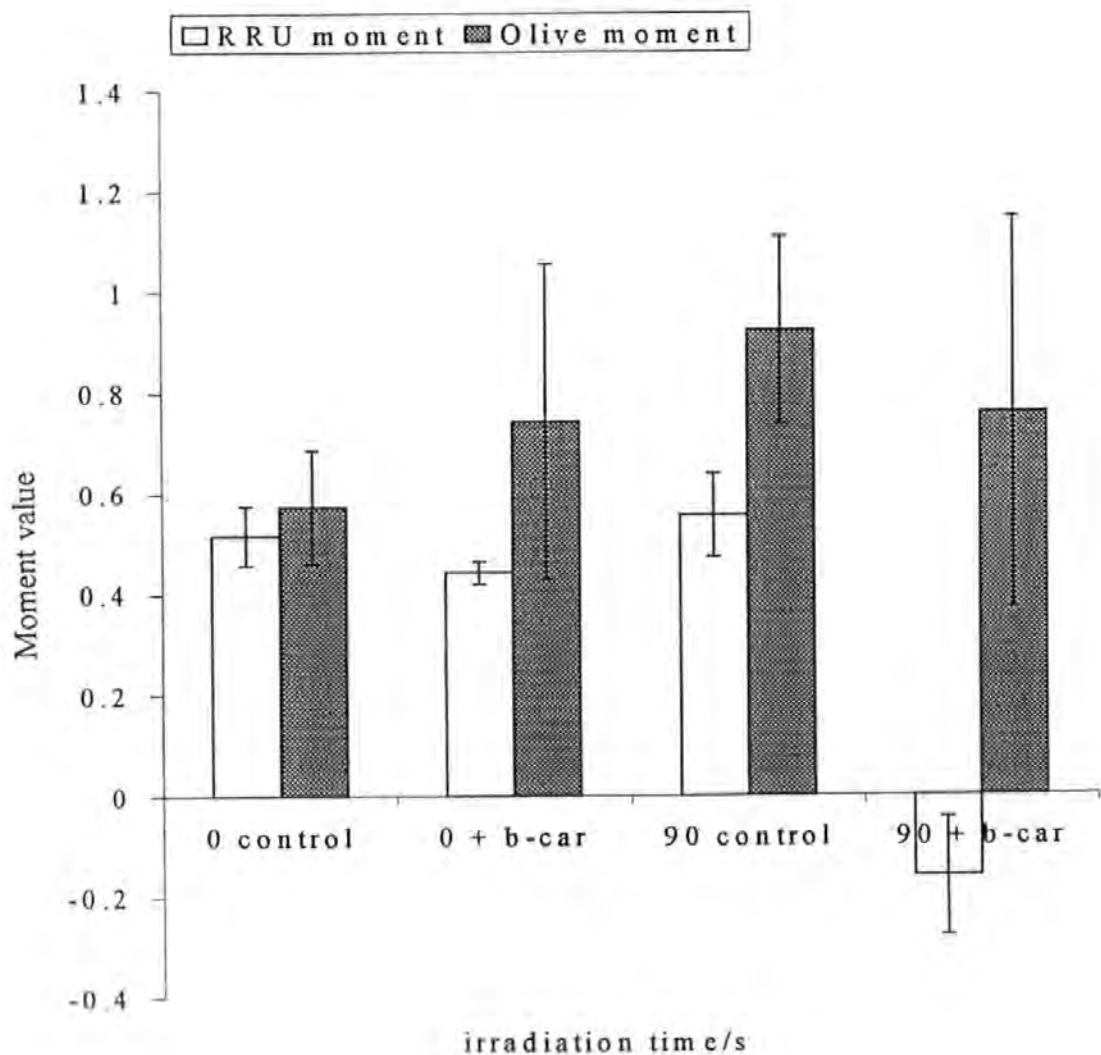
Figure 6.6 Non-significant photosensitisation effects of beta-carotene. A2058 melanoma cells were incubated for one hour in medium which did or did not contain 700 nM beta-carotene, and washed three times in PBS before resuspending in media without phenol red. The cells were embedded in agarose and 405 nm-irradiated for 90 seconds (7 mJ cm^{-2}). The experiment was conducted in 6-fold replicate and read back by image analysis. There was no significant modulation of the dose response when measured by either the Comet Moment or the Tail Moment.
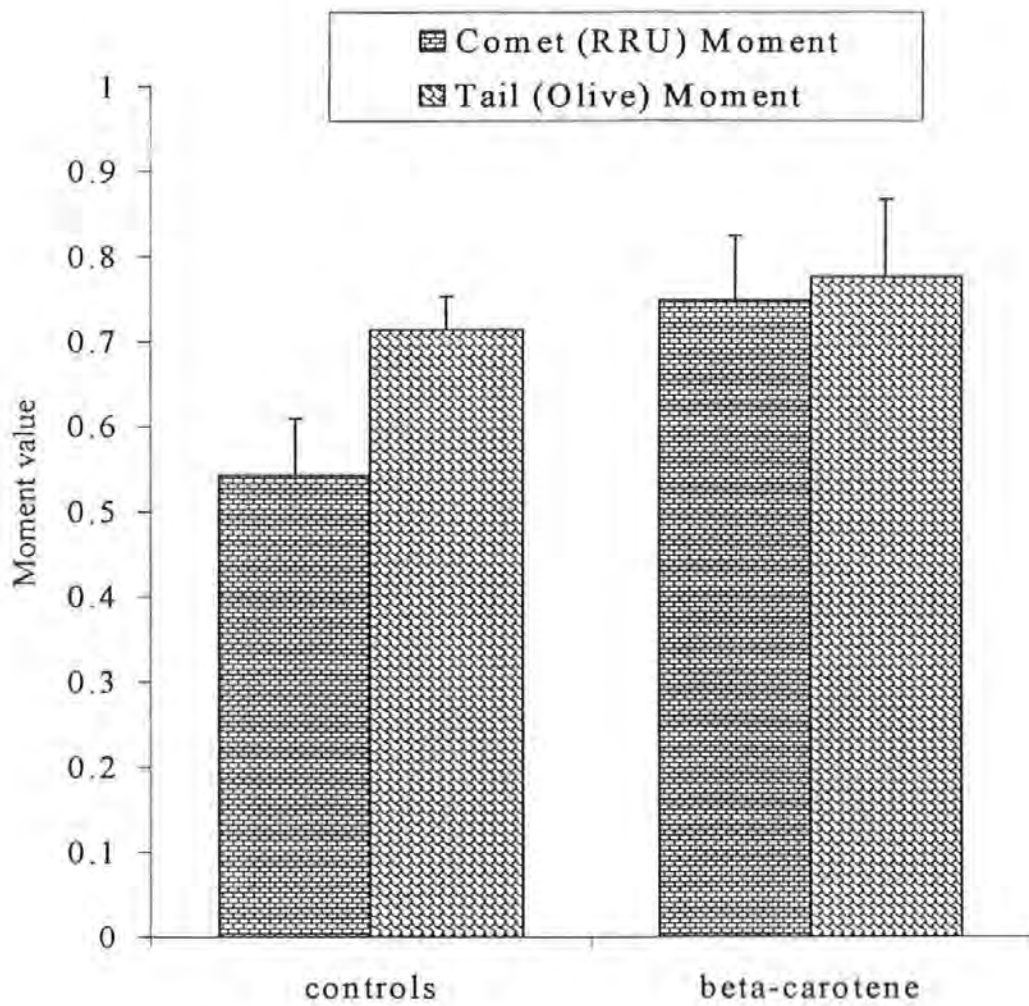
Figure 6.7 The normal and beta-carotene-modulated responses to 405 nm radiation.
A2058 melanoma cells were incubated for one hour in DMEM without phenol red
that did (solid squares) or did not (open circles) contain 700 nM beta-carotene prior
to 405 nm irradiation for doses in the range 0 mJ cm^{-2} to 17 mJ cm^{-2} in duplicate.
The figure is a composite of 3 experiments (see text for details). Error bars have been
omitted for clarity.
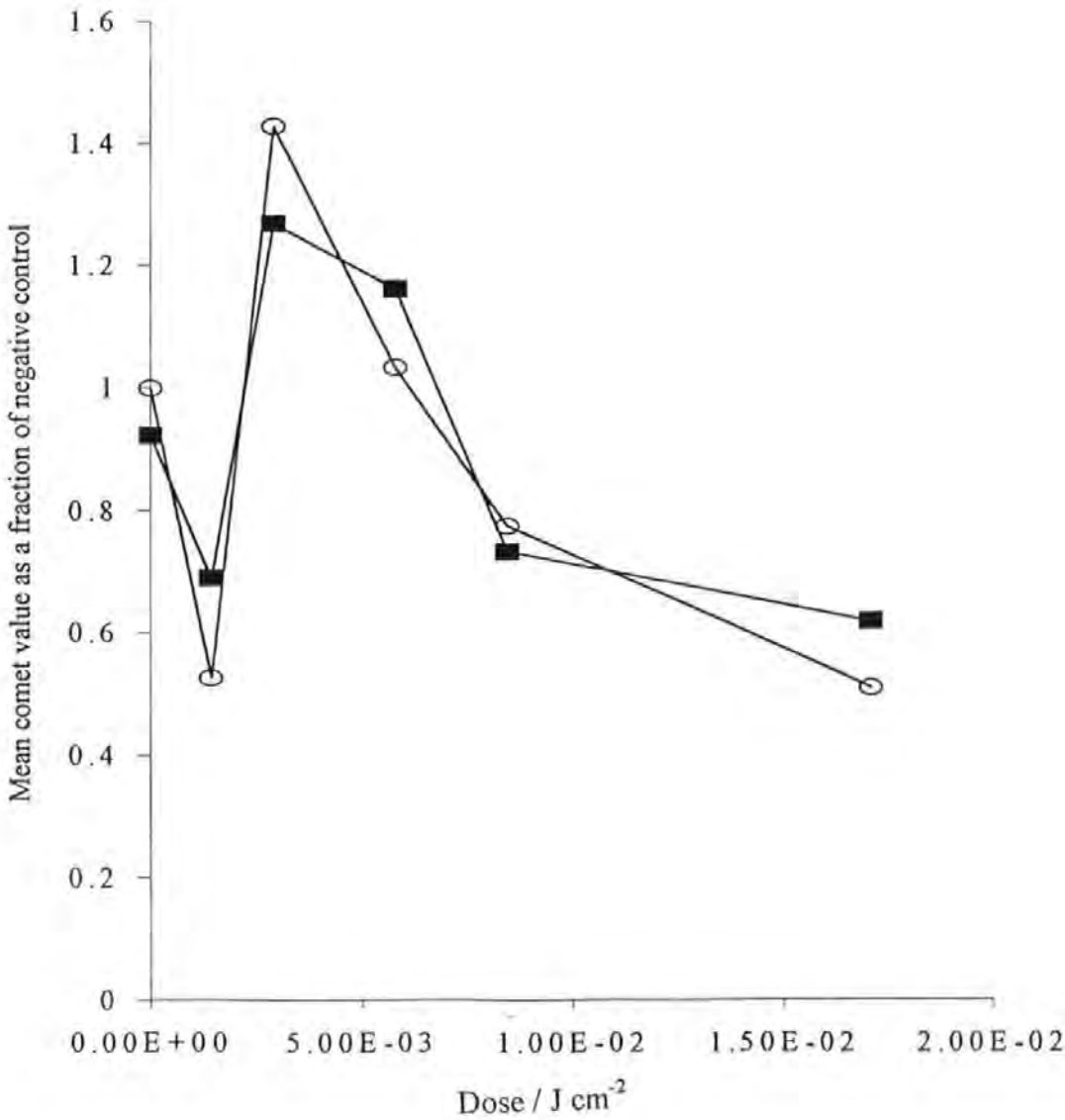
Figure 6.8 The normal and beta-carotene- modulated effects of total solar radiation. MRC5 fibroblasts were incubated for one hour in DMEM without phenol red that either did or did not contain 700 nM beta carotene. The cells were exposed (on ice) to total solar radiation for 10 minutes on a clear sunny May morning or for 30 minutes on a cloudy and wet morning one week later at the same time of day (11.30 am). The figure represents the mean of triplicate determinations for the unexposed non-treated cells (open columns), unexposed beta-carotene-treated cells (dark shading), exposed non-treated cells (light shading) and exposed beta-carotene-treated cells (diagonal stripe)
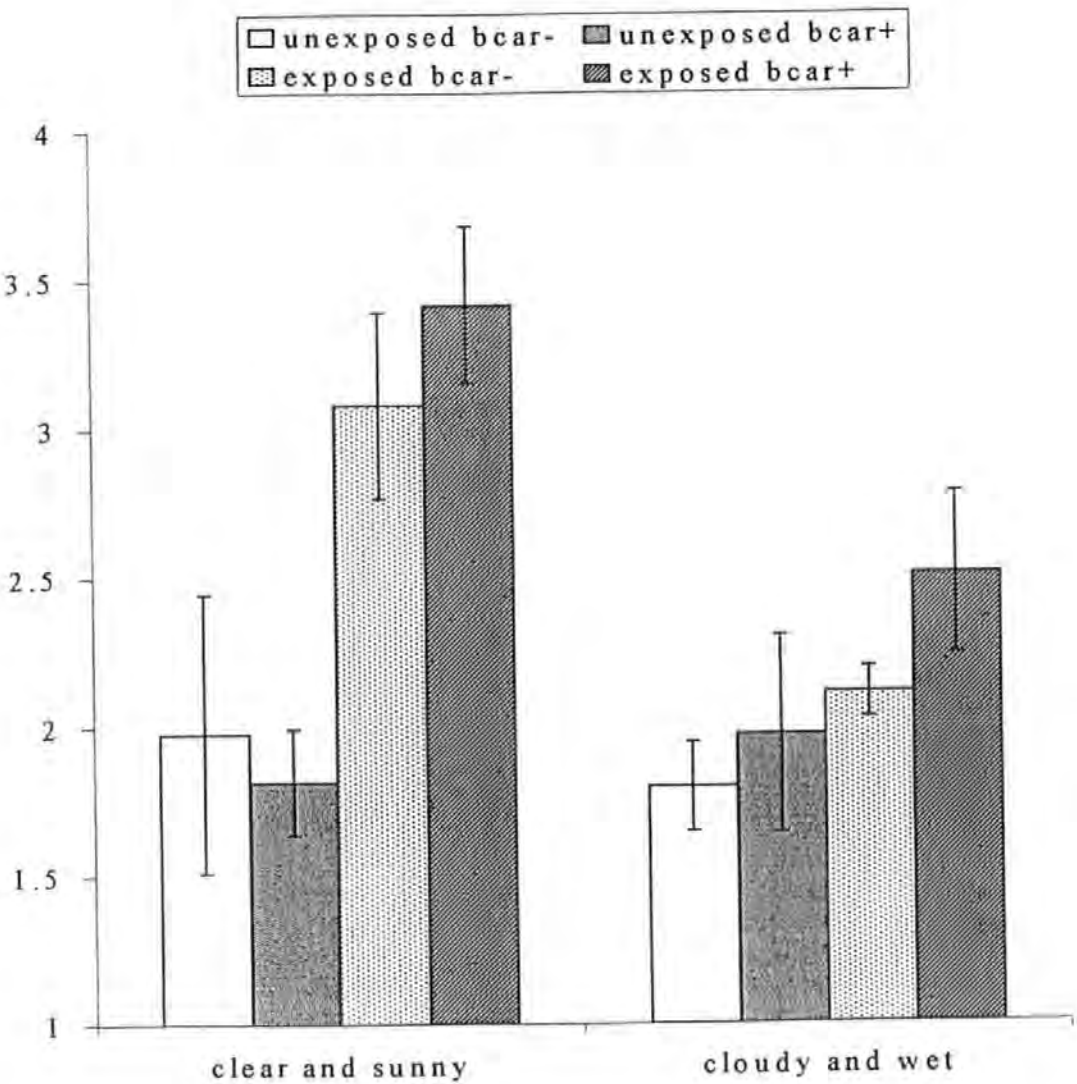
6.2.3 The modulating effects of the Vitamin ACE mixture

6.2.3.1 Introduction

The failure of the technique to reproducibly report significant modulations was thought to

be primarily due to the low concentrations of beta-carotene obtainable in aqueous solution.

Accordingly, a 10% cold water soluble form of beta-carotene was used as a modulant.

This was used from a stock solution. During initial experimentation, it was found that high

(> 1.4 mg / ml ACE matrix in DMEM equating to a beta-carotene concentration of

approximately 2.6 mM) concentrations of matrix suspension lysed the cells during

incubation. Hence, the final stock solution contained the following concentrations of

vitamins: beta-carotene 6.47 x 10^{-2} mg / ml (121 μM), vitamin C 2.5947 x 10^{-2} mg / ml

(147 μM), vitamin E 9.7147 x 10^{-3} mg / ml (23 μM). Two cell lines were used: a

melanocyte-enriched skin cell culture (i.e. post genetecin sulphate treatment), YBF15E

cultured from foreskin tissue; and a hybrid lymphocytic cell line, PUTKO. It was thought

that the radiant intensity of the Xe lamp after narrow band pass filtering was comfortably

within the cells normal redox capacity and so the tests were done with unfiltered radiation.

6.2.3.2 The effects of total Xe spectrum on the foreskin cell culture YBF15E after
incubation with the vitamin mixture ACE.

The cell line YBF15E was incubated for one hour in media which contained either 0%,

25%, 42% or 92% of the stock ACE solution. This equated to a beta-carotene

concentration series of 0 μM, 30 μM, 50μM and 110μM; a vitamin C concentration series

of 0 μM, 37 μM, 62 μM, and 135 μM and a vitamin E concentration series of 0 μM, 6 μM,

10μM and 21 μM. The cells were washed three times in PBS and resuspended in DMEM

without phenol red. The cells were irradiated embedded in agar with 60 seconds of total

Xe spectrum radiation (~ 120 mJ cm^{-2}). The assay was performed in duplicate and

readback by image analysis. The mean values of the parameters were plotted against

214

concentration of ACE (Figure 6.9). After irradiation the level of DNA damage was increased in the cells which had been incubated in the media without ACE supplementation, although only slightly. A concentration dependent photoprotection was seen as analysed by Comet Area. A slight photosensitisation was seen with 25% ACE but an overall phototoprotection was seen when analysed by the Tail Moment. The converse was true when the assay was analysed by Comet Moment: a slight photoprotection was followed by a photosensitisation, the overall trend was neutral. None of the modulations were significant by one tailed t-test at 95% confidence intervals.

6.2.3.3 The effects of total Xe spectrum radiation on PUTKO hybrid lymphocytes after incubation in ACE supplemented media

PUTKO hybrid lymphocytic cells were incubated in the stock ACE medium for one hour at 37 °C. They were washed three times in PBS and resuspended in DMEM without phenol red. The cells were embedded in agarose and irradiated for 0, 30, 60 or 120 seconds with total Xe spectrum radiation (approximately doses of 0 mJ cm^{-2}, 60 mJ cm^{-2}, 120 mJ cm^{-2} and 240 mJ cm^{-2}). The assay was performed in triplicate, SSB was measured immediately after irradiation and analysed by image analysis. The mean values of the replicates were plotted against dose (Figure 6.10, 6.11, 6.12) and the modulated dose responses were analysed by one tailed t-test as before. The strand breakage in the ACE supplemented medium was significantly higher than in the controls. The significance of the modulations was not, however, uniform with respect to the parameters analysed in that some modulations were significant by one parameter but not by a different parameter. The p values from the t-tests are given for the parameters of Tail Moment, Comet Moment and Comet Area in Table 6.2. The ACE mixture significantly increased SSB in the unirradiated cells as measured by the RRU and Tail Moments (p < 0.05). The ACE mixture significantly increased SSB in the 60 mJ cm^{-2}-irradiated cells as measured by all three parameters (p < 0.05 as measured by the Comet Moment and the area; p < 0.001 as

measured by the Tail Moment). The ACE mixture significantly increased SSB in the 120 mJ cm^{-2}-irradiated cells as measured by all three parameters (p < 0.001 as measured by the RRU and Tail Moments; p < 0.05 as measured by the Comet Area). The ACE mixture significantly increased SSB in the 240 mJ cm^{-2}-irradiated cells as measured by the Comet Moment (p < 0.05) only.

Table 6.2 PUTKO hybrid lymphocytes were incubated in the stock ACE medium and irradiated with total Xe spectrum radiation. SSB was measured immediately after irradiation and analysed by image analysis. The normal and modulated dose responses were compared by one tailed t-test, assuming equal variance. The p values are given in the table, underlined once for p values less than 0.05 and underlined twice for p values less than 0.001.

	0 mJ cm^{-2}	60 mJ cm^{-2}	120 mJ cm^{-2}	240 mJ cm^{-2}
Olive moment	0.007899	0.00092	0.000126	0.055814
RRU moment	0.048399	0.008266	0.000422	0.038892
Comet Area	0.111809	0.004286	0.002891	0.140001

6.2.4   Conclusions on the use of the ACE mixture as a photomodulant

The use of the cold water dispersible mixture of vitamins enabled the use of higher concentrations of beta-carotene than it had been possible to achieve with the synthetic powdered form. The photosensitisation of cells to UVR and visible radiation seen with the synthetic beta-carotene was also observed with the ACE mixture, despite the presence of antioxidant vitamins C and E, (at a higher molar concentration than the beta-carotene itself in the case of vitamin C) in the matrix. It was concluded that the use of 121 μM beta-carotene modulated the dose responses to the extent that statistical significance could be attained at some doses. The stock ACE mixture itself had significant clastogenicity as evidenced by the unirradiated PUTKO cells after incubation in the ACE suspension. The

216

possible mediators of this and the photosensitisation are discussed in Chapter 7. The effects of the ACE mixture on the melanocyte-enriched culture appeared as a weak concentration-dependent photoprotection and this is discussed in the light of the weak dose-related photoprotection seen in some experiments with the synthetic beta-carotene, also in Chapter 7.

Figure 6.9 The slight photoprotective effects of ACE on the melanocyte-enriched cell culture YBF15E. The cell line YBF15E was incubated for one hour in media which contained either 0%, 25%, 42% or 92% of the stock ACE solution. The cells were irradiated embedded in agar with 60 seconds of total Xe spectrum radiation (~ 120 mJ cm^{-2}). The assay was performed in duplicate and readback by image analysis. The mean values of the parameters were plotted against the amount of ACE supplementation. Error bars represent 1 s.d. of the mean.
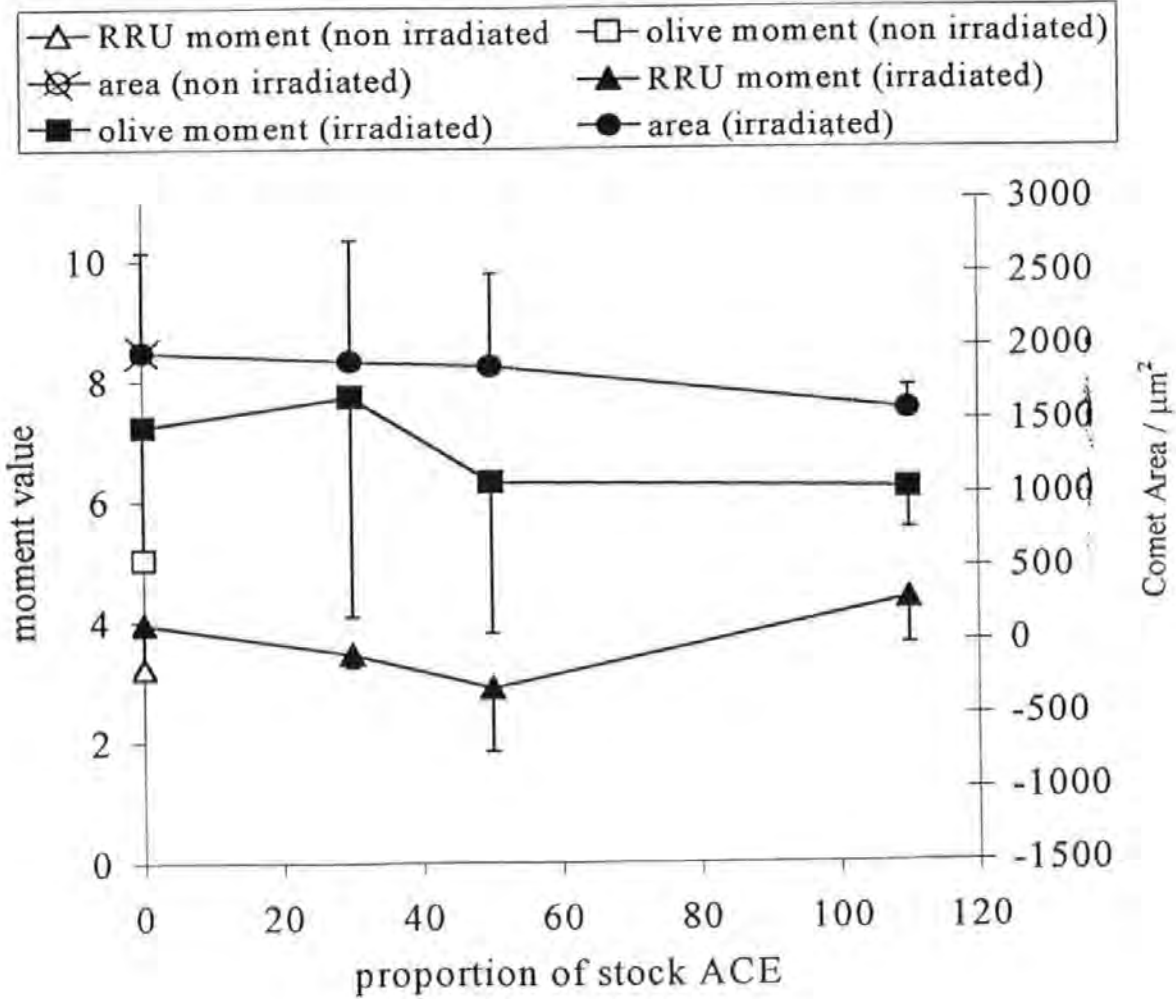
Figure 6.10 The photosensitising effects of ACE on PUTKO hybrid lymphocytic cells.
PUTKO hybrid lymphocytic cells were incubated in the stock ACE medium (solid
squares) or non supplemented medium (open squares) for one hour at 37 °C. The
cells were embedded in agarose and irradiated for 0, 30, 60 or 120 seconds with total
Xe spectrum radiation (approximately doses of 0 mJ cm^{-2}, 60 mJ cm^{-2}, 120 mJ cm^{-2}
and 240 mJ cm^{-2}). SSB was measured immediately after irradiation and analysed by
image analysis. The mean RRU moment values of the 3-fold replicated slides were
plotted against dose. Error bars represent 1 standard deviation.
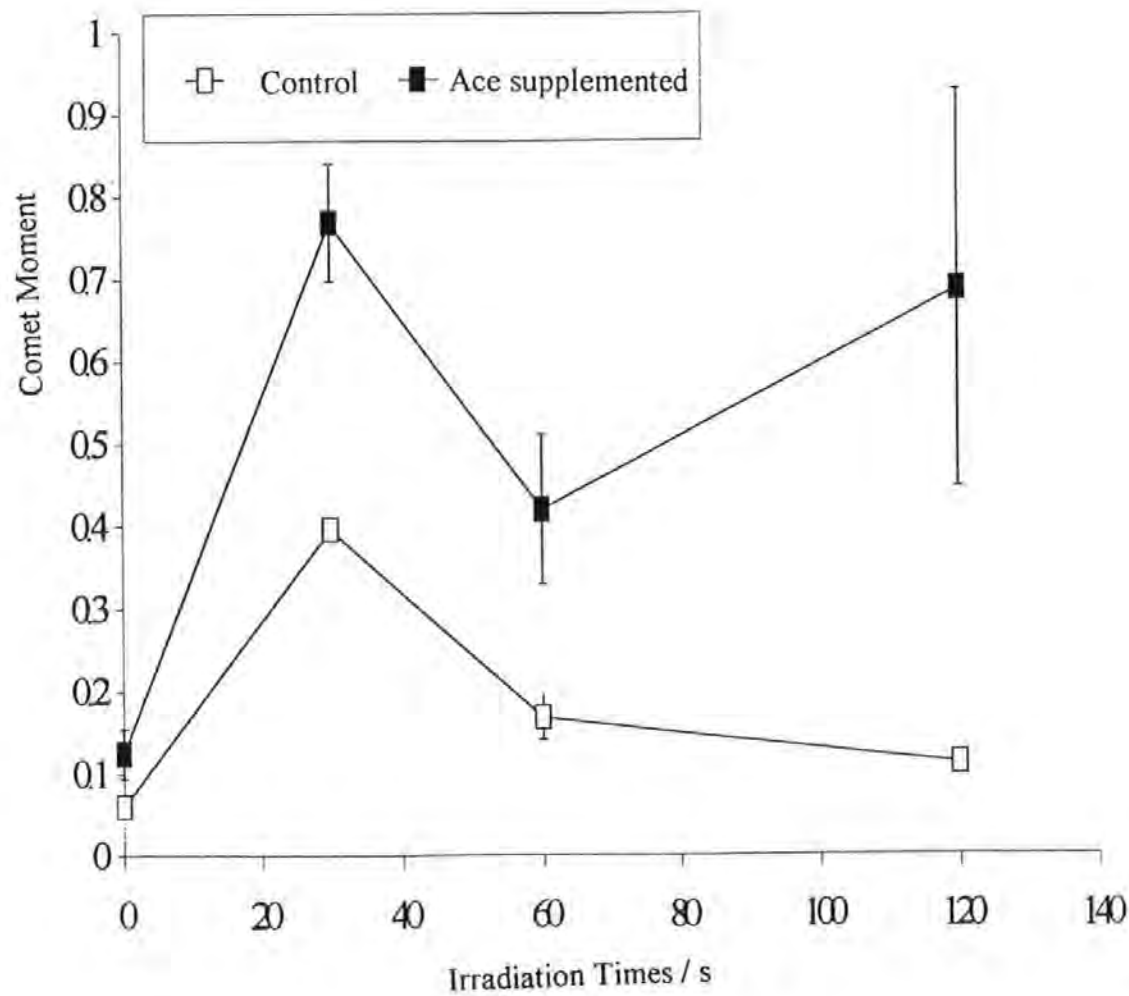
Figure 6.11 The photosensitising effects of ACE on PUTKO hybrid lymphocytic cells. PUTKO hybrid lymphocytic cells were incubated in the stock ACE medium (solid squares) or non supplemented medium (open squares)for one hour at 37 °C. The cells were embedded in agarose and irradiated for 0, 30, 60 or 120 seconds with total Xe spectrum radiation (approximately doses of 0 mJ cm^{-2}, 60 mJ cm^{-2}, 120 mJ cm^{-2} and 240 mJ cm^{-2}). SSB was measured immediately after irradiation and analysed by image analysis. The mean Olive moment values of the 3-fold replicated slides were plotted against dose. Error bars represent 1 standard deviation.
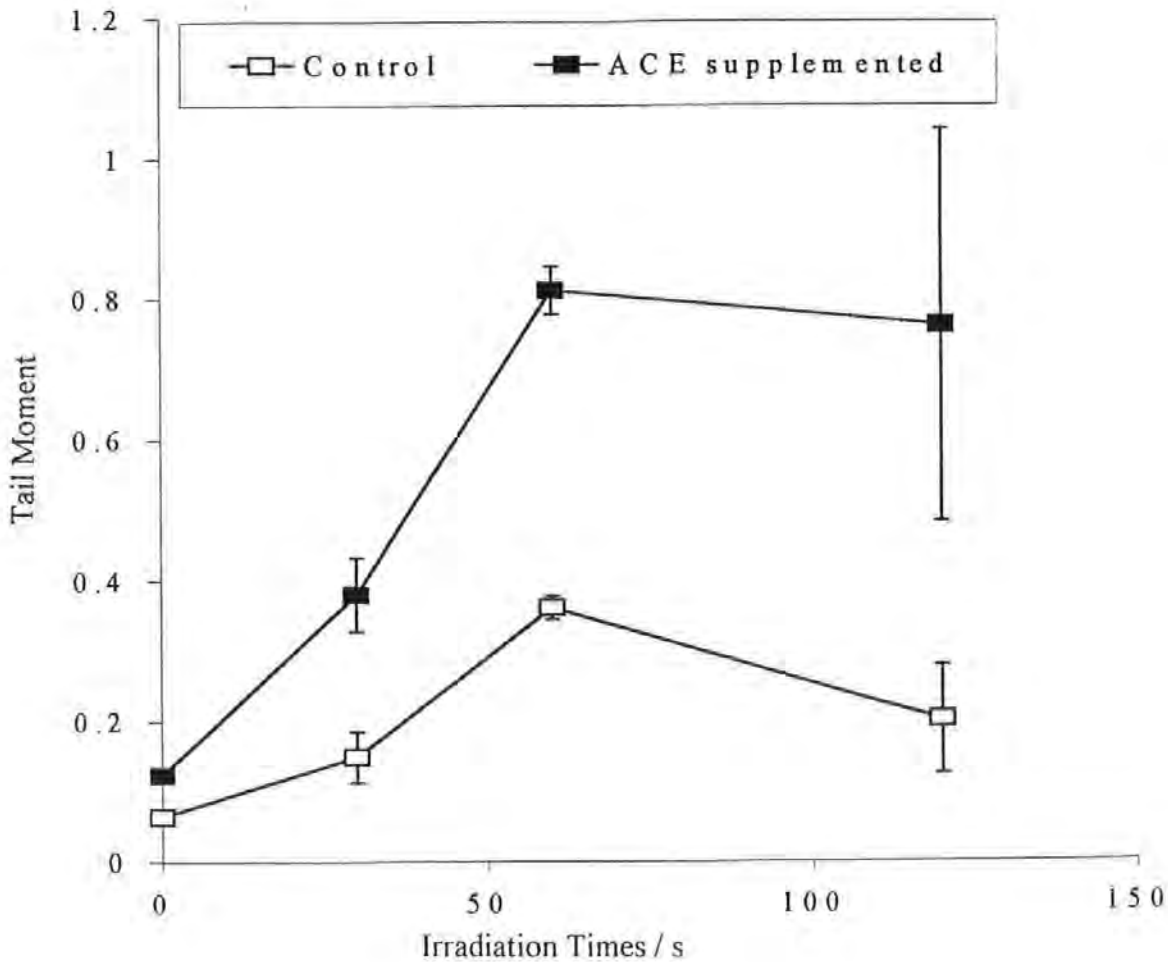
Figure 6.12 The photosensitising effects of ACE on PUTKO hybrid lymphocytic cells. PUTKO hybrid lymphocytic cells were incubated in the stock ACE medium (solid squares) or non supplemented medium (open squares)for one hour at 37 °C. The cells were embedded in agarose and irradiated for 0, 30, 60 or 120 seconds with total Xe spectrum radiation (approximately doses of 0 mJ cm^{-2}, 60 mJ cm^{-2}, 120 mJ cm^{-2} and 240 mJ cm^{-2}). SSB was measured immediately after irradiation and analysed by image analysis. The mean Comet Area of the 3-fold replicated slides were plotted against dose. Error bars represent 1 standard deviation.
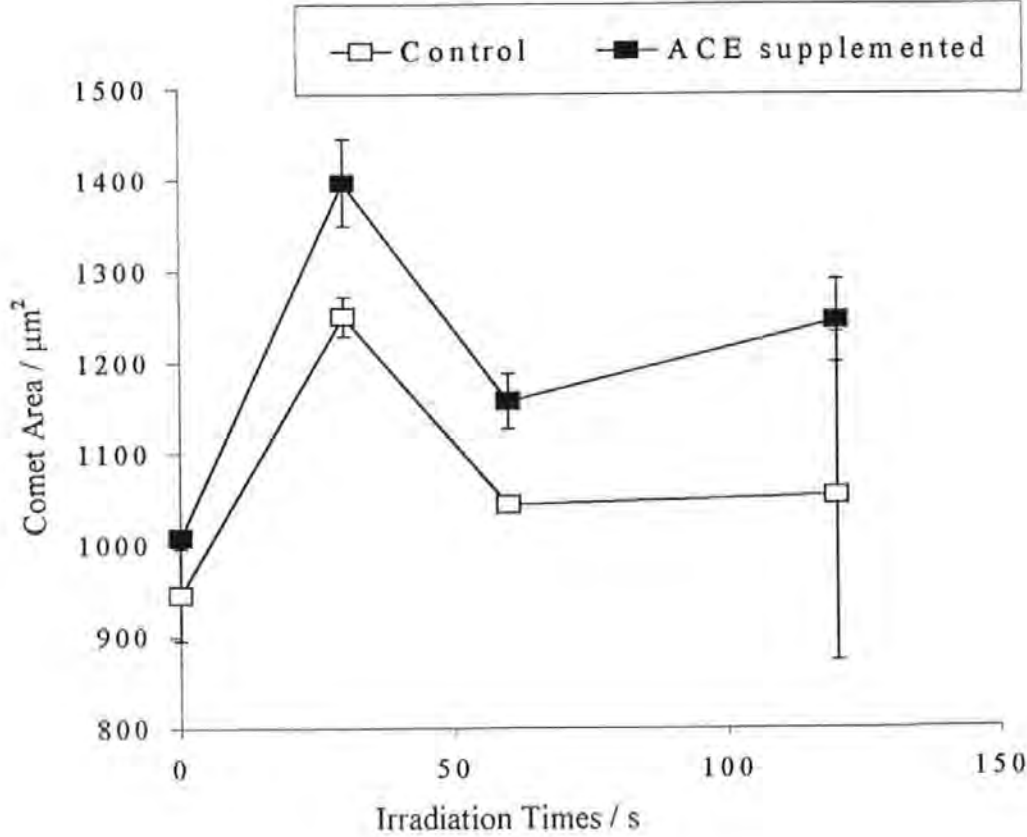
6.2.5 The modulating effects of o-phenanthroline

The modulating effects of o-phenanthroline were investigated initially in A2058 melanoma cells and formed part of the beta-carotene- and o-phenanthroline-induced modulation series of investigations of low dose responses to 405 nm radiation (Section 6.2.1.3.2.2). The effects of higher concentrations of o-phenanthroline-modulation at higher doses of total Xe lamp radiation were subsequently investigated using PUTKO hybrid lymphocytic cells.

6.2.5.1 The effects of low doses of 405 nm radiation on A2058 melanoma cells after incubation with o-phenanthroline

A2058 melanoma cells were incubated for one hour in either DMEM without phenol red or DMEM without phenol red that contained 50 μM o-phenanthroline. They were washed three times in PBS and resuspended in PBS, and 405 nm-irradiated at doses between zero and 17.1 mJ cm^{-2}. The investigation was performed in duplicate over three independent experiments as part of a beta-carotene/ o-phenanthroline investigation. The assay was read back by the visual inspection method. The mean comet values were analysed by one tailed t-test as before: there was no significant modulation of the dose responses by 50 μM o-phenanthroline. The mean comet value was normalised to the negative controls in each experiment, thus providing an internal standard. The normalised mean comet values were plotted against dose (Figure 6.13). The o-phenanthroline -treated cells displayed lower amounts of SSB at doses < 6 mJ cm^{-2}. The treatment was unable to prevent the '10 mJ cm^{-2} peak', but it did, however, attenuate it. When the comets were standardised to their own negative controls the dose response more closely resembled one that would be generated in one assay (although as noted above (Section 6.2.1.3.2.2), the early peak was shifted to the left by approximately one minute).

Figure 6.13 The photoprotective effects of o-phenanthroline. A2058 melanoma cells were incubated for one hour in DMEM without phenol red that did or did not contain 50 μM o-phenanthroline prior to 405 nm irradiation for doses in the range 0 mJ cm^{-2} to 17 mJ cm^{-2}. The figure is a composite of 3 experiments: to provide intra-assay comparison between the modulating effects of beta-carotene and o-phenanthroline, the experiments were conducted by dose, with two doses being performed per treatment. The three dose-pairs were these: 0 mJ cm^{-2} and 8.5 mJ cm^{-2}, 2.9 mJ cm^{-2} and 5.8 mJ cm^{-2}, 1.4 mJ cm^{-2} and 17.1 mJ cm^{-2}. Error bars have been omitted for clarity, the modulations were not significant.
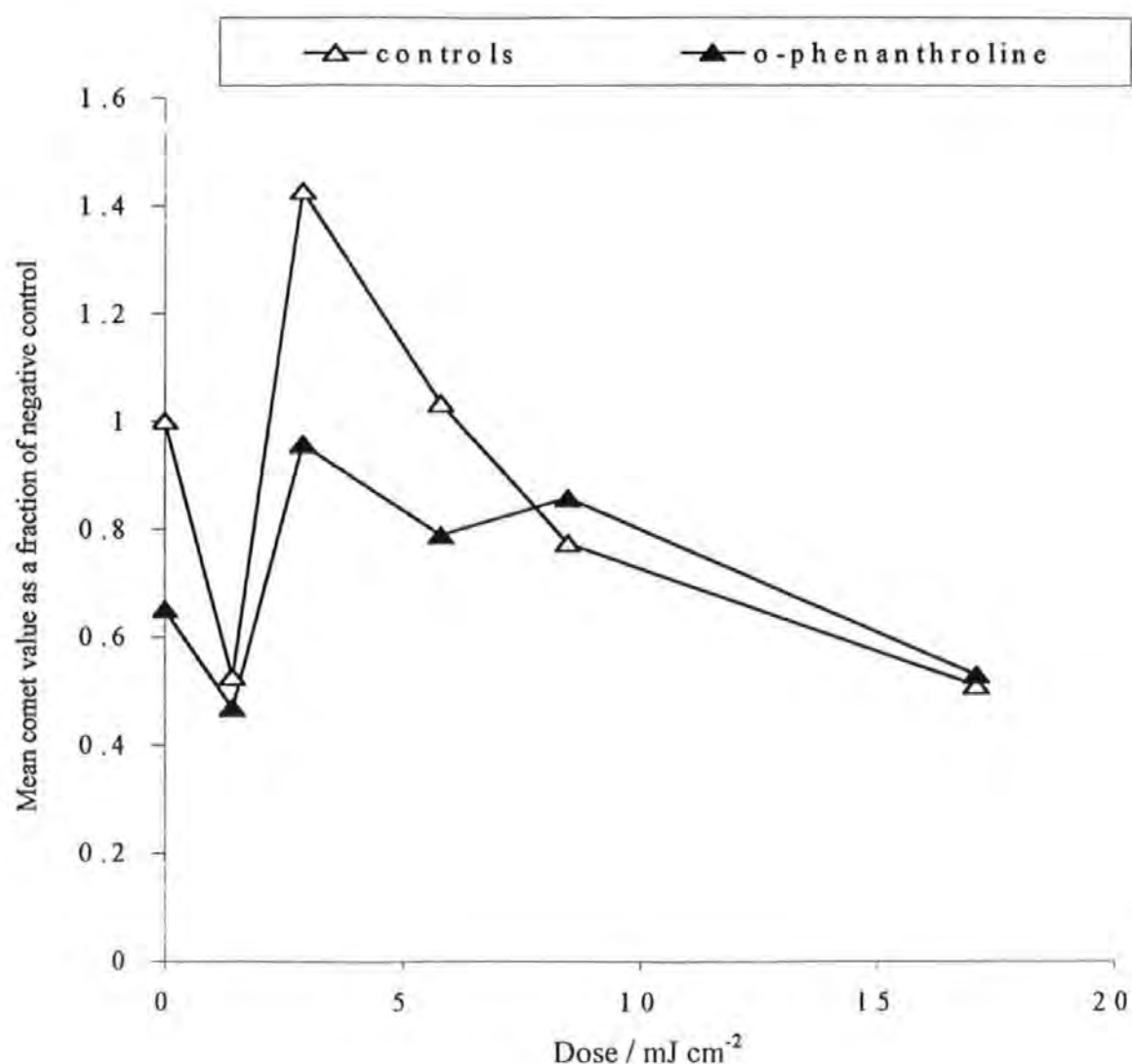
6.2.5.2 The effects of total Xe lamp radiation on PUTKO hybrid leukaemia cells after incubation with o-phenanthroline

PUTKO hybrid leukaemia cells were incubated for one hour in medium which contained either 0 mM , 2 mM, 5 mM, 10 mM or 15 mM o-phenanthroline. The cells were washed three times in PBS and resuspended in PBS. The cells were irradiated embedded in agarose for 60 seconds with total Xe spectrum radiation. SSB was read back by image analysis. Two independent experiments were performed and the means plotted against o-phenanthroline concentration. 2 mM and 5 mM were seen to be photoprotective, whereas 10 mM and 15 mM were seen to be photosensitising (Figure 6.14).

6.2.6 Conclusions on the use of o-phenanthroline as a photomodulant

50 μM o-phenanthroline reduced the number of strand breaks in A2058 melanoma cells, in the control cells and in the cells irradiated at low doses of 405 nm radiation. 2 mM and 5 mM o-phenanthroline reduced the number of strand breaks in PUTKO cells irradiated with unfiltered Xe lamp radiation. o-phenanthroline is therefore a DNA-protecting agent that itself does not appear to be affected by UVR.

10 mM and 15 mM o-phenanthroline increased the number of strand breaks after irradiation with total Xe spectrum radiation. Thus o-phenanthroline also has photosensitising properties. These data are discussed in Chapter 7.

Figure 6.14 The photoprotective and photosensitising effects of o-phenanthroline on PUTKO hybrid lymphocytic cells. PUTKO hybrid leukaemia cells were incubated for one hour in medium which contained either 0 mM , 2 mM, 5mM, 10mM or 15 mM o-phenanthroline. The cells were embedded in agarose and irradiated for 60 seconds with total Xe spectrum radiation. SSB was read back by image analysis. Two independent experiments were performed and the means plotted against o-phenanthroline concentration. Error bars represent the standard deviation of the two means.
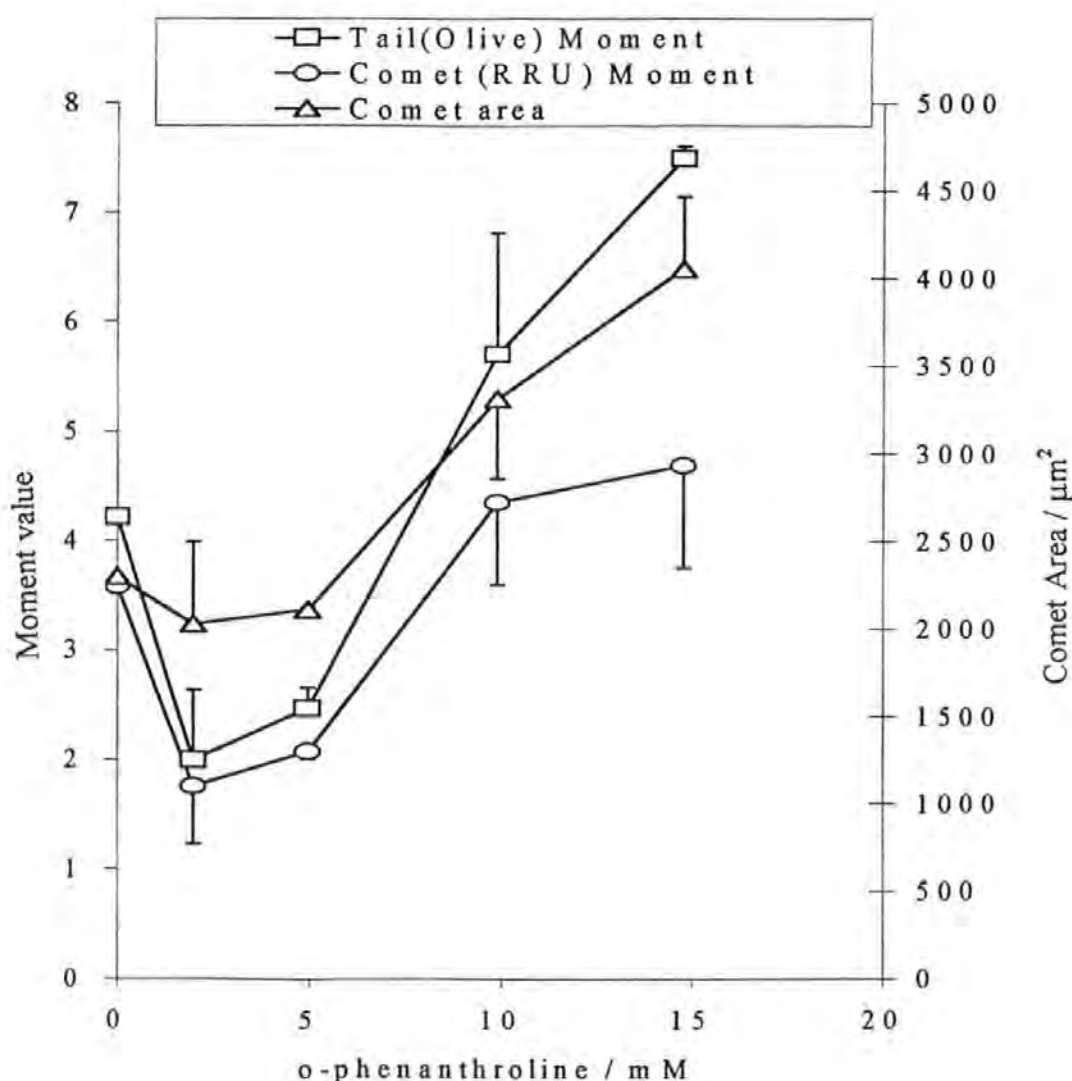
6.2.7 The modulating effects of 700 nM beta-carotene plus 50 μM o-phenanthroline

The effects of beta-carotene and o-phenanthroline on A2058 cells were investigated for synergy as part of the beta-carotene and o-phenanthroline series of experiments.

6.2.7.1 The effects of low doses of 405 nm radiation on A2058 melanoma cells after incubation with 700 nM beta-carotene plus 50 μM o-phenanthroline

A2058 melanoma cells were incubated for one hour in either DMEM without phenol red or DMEM without phenol red that contained 700 nM synthetic beta-carotene plus 50 μM o-phenanthroline. The cells were washed three times in PBS and resuspended in PBS. They were 405 nm-irradiated for doses between zero and 17.1 mJ cm^{-2}. The investigation was performed in duplicate.over three independent experiments as part of a beta-carotene/ o-phenanthroline investigation. The assay was read back by the visual inspection method. The mean comet values were analysed by t-test as before: there was a significant ($p<0.05$) modulation of the dose response to 8.5 mJ cm^{-2} by the combined modulants when compared to the unmodulated dose response. The beta-carotene plus o-phenanthroline modulated dose response was also significant when compared to the modulated dose responses by beta-carotene only or o-phenanthroline only. The mean comet value was normalised to the negative controls in each experiment, thus providing an internal standard. The normalised mean comet values were plotted against dose (Figure 6.15). The 700 nM beta-carotene plus 50 μM o-phenanthroline modulating treatment was repeated on the A2058 cell line at 405 nm radiation doses of 7 mJ cm^{-2}, 8.5 mJ cm^{-2}, 10 mJ cm^{-2} and 12 mJ cm^{-2}. A small peak was seen at 8.5 mJ cm^{-2} although this was not significantly different to the values of 7 mJ cm^{-2} and 10 mJ cm^{-2} ($p = 0.23$ and $p = 0.12$ respectively, one tailed t-test equal variance. Data not shown). It was observed that this modulation reinstated the 10 mJ cm^{-2} peak that had been left shifted (in time) due to the protocol employed. This

new peak thus corresponded to a peak at approximately 2 to 3 minutes from the start of the irradiation.

6.2.8 Conclusions on the use of both beta-carotene plus o-phenanthroline as a photomodulant

The use of the two modulants together significantly exacerbated the unmodulated response to $8.5\ mJ\ cm^{-2}$ 405 nm radiation (i.e. the peak was greatly enhanced) in A2058 cells. The peak in the modulated response corresponded to a time after starting irradiation of approximately 2 or 3 minutes representing delayed effects; the normal maximum appears at around 90 seconds. These data are discussed in Chapter 7.

Figure 6.16. The synergistic effects of beta-carotene and o-phenanthroline. A2058 melanoma cells were incubated for one hour in either DMEM without phenol red (open circles) or DMEM without phenol red that contained 700 nM synthetic beta-carotene and 50μM o-phenanthroline ((solid squares). They were washed three times in PBS and resuspended in PBS. They were 405 nm-irradiated for doses between zero and 17.1 mJ cm^{-2}. The investigation was performed in duplicate over three independent experiments as part of a beta-carotene/ o-phenanthroline investigation. The assay was read back by the visual inspection method. The mean comet values were plotted against dose. Error bars represent one standard deviation. The modulated response to 8.5 mJ cm^{-2} was significant (p<0.05) by one tailed t-test.
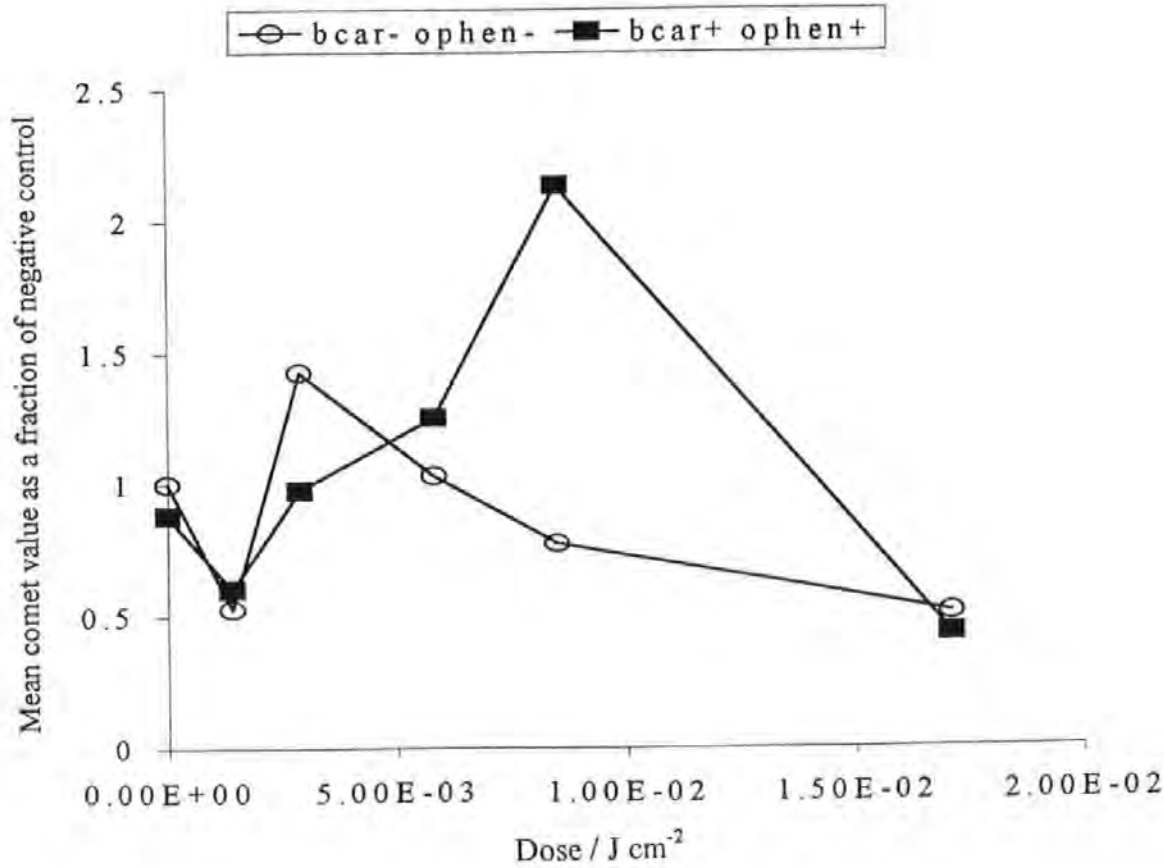
6.3 SUMMARY

6.3.1 *Antioxidant and prooxidant properties of the reagents studied*

The data were not consistent in that both beta-carotene and o-phenanthroline displayed photoprotective and photosensitising properties. This may have been due to the variation in experimental technique, the source and intensity of the UVR, and the development of the readback system. The normal dose responses of these cell types (Chapter 4) is that a peak of damage (as measured by the comet assay) is observed at around 10 mJ cm^{-2}; this is followed at higher doses by an increase in damage with dose. This makes a single interpretation of the photoprotective / photosensitisation effects of the modulating chemicals difficult. If these results are placed in the context of the (normal 405 nm response) model discussed in Chapter 5 (Section 5.3), a possible explanation follows. Beta-carotene acts as an antioxidant by scavenging UVR-induced reactive oxygen species (Krinski and Deneke, 1982) while o-phenanthroline acts as an antioxidant by preventing the formation of hydroxyl radical by Fenton reaction (de Mello-Filho and Meneghini, 1984). It is possible that the presence of these molecules were responsible for triggering an antioxidant response (perhaps an increase in SSB repair) through the induction of redox-sensitive genes (Sun *et al.*, 1997) that led to the fall in comet values. The use of 50 μM o-phenanthroline reduced the (hydroxyl-mediated) DNA damage, although not significantly. Beta-carotene appeared to cause the generation of clastogenic species in its own right; i.e. beta-carotene acted as a prooxidant and increased SSB (perhaps through an increase in lipid peroxidation (Palozza and Krinski, 1992); see following discussion). Alternatively, it could be that the partial scavenging of other (unidentified) reactive molecules by low concentrations of beta-carotene prevented a full induction of an antioxidant response. Either way, beta-carotene acted as a photosensitiser, and at a high concentration significantly so. The use of both o-phenanthroline and beta-carotene together greatly perturbed the normal response, resulting in extensive comet formation. It would appear

from the above results that ~10 mJ cm^{-2} of 405 nm radiation (or its time equivalent: approximately 1 1/2 minutes) is an especially sensitive point to synergistic effects of o-phenanthroline and beta-carotene, in the A2058 melanoma cell line at least. These data are discussed in the following chapter.

7 CHAPTER 7.

MODULATION OF NORMAL DOSE RESPONSES WITH

PROOXIDANT AND ANTIOXIDANT MOLECULES.

DISCUSSION

In the work described in the previous chapter, beta-carotene and o-phenanthroline were, paradoxically, observed to have both photoprotective and photosensitising properties. The two reagents appeared to synergise and photosensitise the melanoma cell line used for testing. These data will be discussed below.

7.1 BETA-CAROTENE

7.1.1 Background

The vitamin A precursor, beta-carotene, has been widely used as a photoprotectant (Roelandts 1995; Mathews-Roth 1997) and as an antioxidant *in vivo* and *in vitro* (Miller 1996; reviewed in Ames 1983; Palozza and Krinsky 1992; Dalton 1995). Beta-carotene is a major carotenoid in green plants. It has the highest potential vitamin A activity amongst the carotenoids, approximately 1/6 that of retinol (Miller *et al.* 1996). It has been used in many animal and clinical studies which seek to examine its properties as a protectant for cancer producing insults to the cell; the results of these studies have yet to show clear evidence for beta-carotene as an effective skin cancer therapeutic in humans. A protective role for beta-carotene in UVR-photocarcinogenesis (Epstein 1977), UVB-photocarcinogenesis (Black and Mathews-Roth 1991), Benzo(a)pyrene + UVA-photocarcinogenesis (Santamaria *et al.* 1981) oral (Tanaka *et al.* 1994), colon (Alabaster *et al.* 1995) and lymphocytic (Aidoo *et al.* 1995) chemical carcinogenesis has, however, been clearly demonstrated. A protective role for beta-carotene against oxidative stress has been

demonstrated in mammals (Umegaki *et al.* 1998), including humans (Pool-Zbel *et al.* 1998).

The anti-carcinogenic effect of carotenoids is not only related to their antioxidant activity or their vitamin A activity. Carotenoids have the capability to induce gap junctional communication in adjacent cells (Stahl *et al.* 1997) and thus facilitate the inter-cellular flux of low molecular weight compounds (e.g. nutrients, signalling molecules). Beta-carotene can activate the expression of genes for connexin 43, an integral component of gap junctions; the maintenance of cell-cell communication exerts a critical tumour-suppressing function (Yamasaki and Naus 1996).

It is an effective scavenger of singlet oxygen (Palozza and Krinsky 1992) and because of its conjugated nature, a potentially effective radical scavenger (Miller *et al.* 1996). There is evidence that the singlet oxygen quenching properties of beta-carotene account for its photoprotective properties, however (Stratton and Liebler 1997).

For singlet oxygen interactions the addition of exogenous antioxidant molecules to quench active oxygen species by direct energy transfer is a double-edged sword: it has been shown that beta-carotene can act in a prooxidant capacity (Pflaum *et al.* 1998; Cozzi *et al.* 1997). The antioxidant/prooxidant properties of beta-carotene are O_2-tension-dependent: at low oxygen tensions (15 torr) beta-carotene is an antioxidant but at normal atmospheric oxygen pressures the initial antioxidant activity is followed by a prooxidant action (Burton and Ingold 1984). The oxygen tension in mammalian tissues is generally low except, for example, in the lung; beta-carotene failed to protect against lung cancer incidence in Finnish smokers (The Alpha-Tocopherol, Beta-Carotene Cancer Prevention Study Group 1994). Of direct relevance to this study, the oxygen tension in epidermal tissues is high- it can be up to 90% of that in the lungs (D. Gould, personal communication)

Beta-carotene is a very hydrophobic molecule and would be expected to locate with the lipid components of cells (i.e. membranes) and is an extremely efficient quencher of lipid peroxidation (Felton 1995, Krinsky and Deneke 1982; Palozza and Krinsky 1992). It is

232

demonstrated in mammals (Umegaki *et al.* 1998), including humans (Pool-Zbel *et al.* 1998).

The anti-carcinogenic effect of carotenoids is not only related to their antioxidant activity or their vitamin A activity. Carotenoids have the capability to induce gap junctional communication in adjacent cells (Stahl *et al.* 1997) and thus facilitate the inter-cellular flux of low molecular weight compounds (e.g. nutrients, signalling molecules). Beta-carotene can activate the expression of genes for connexin 43, an integral component of gap junctions; the maintenance of cell-cell communication exerts a critical tumour-suppressing function (Yamasaki and Naus 1996).

It is an effective scavenger of singlet oxygen (Palozza and Krinsky 1992) and because of its conjugated nature, a potentially effective radical scavenger (Miller *et al.* 1996). There is evidence that the singlet oxygen quenching properties of beta-carotene almost entirely account for its photoprotective properties (Stratton and Liebler 1997).

For singlet oxygen interactions the addition of exogenous antioxidant molecules to quench active oxygen species by direct energy transfer is a double-edged sword: it has been shown that beta-carotene can act in a prooxidant capacity (Pflaum *et al.* 1998; Cozzi *et al.* 1997). The antioxidant/prooxidant properties of beta-carotene are O_2-tension-dependent: at low oxygen tensions (15 torr) beta-carotene is an antioxidant but at normal atmospheric oxygen pressures the initial antioxidant activity is followed by a prooxidant action (Burton and Ingold 1984). The oxygen tension in mammalian tissues is generally low except, for example, in the lung; beta-carotene failed to protect against lung cancer incidence in Finnish smokers (The Alpha-Tocopherol, Beta-Carotene Cancer Prevention Study Group 1994). Of direct relevance to this study, the oxygen tension in epidermal tissues is high- it can be up to 90% of that in the lungs (D. Gould, personal communication)

Beta-carotene is a very hydrophobic molecule and would be expected to locate with the lipid components of cells (i.e. membranes) and is an extremely efficient quencher of lipid peroxidation (Felton 1995, Krinsky and Deneke 1982; Palozza and Krinsky 1992). It is

hypothesised that beta-carotene acts as a radical trap, rather than a chain breaking antioxidant (like for example, vitamins C or E). Peroxyl radicals have been shown to add rapidly to the long chain of conjugated double bonds present in beta-carotene: beta-carotene interacts with peroxyl radicals arising from lipid peroxidation (Krinsky and Deneke 1982; Palozza and Krinsky 1992) thus:

beta-carotene + ROO• $\Rightarrow$ ROO-beta-carotene•

This breaks the chain reaction of lipid peroxidation and at normal physiological range of O_2 tensions, the peroxyl radical scavenging properties of beta-carotene are highly effective (Felton 1995). There is evidence, in a model system, that the beta-carotene is regenerated from the radical cation by vitamin E, but not vice versa (Mortensen *et al.* 1998). There is, however, no question that the formation of peroxyl radicals can have a major impact on carotenoid bleaching (Krinsky and Deneke 1982) resulting in destruction of the pigment. In the presence of high oxygen tensions, however, molecular oxygen (one of the decomposition products of hydrogen peroxide) may add to the peroxyl-carotenoid complex to produce a peroxyl radical with chain carrying ability (Larson 1995; Palozza and Krinsky 1992).The combination of the carotenoid radical with oxygen leads to the formation of a carotenoid-peroxyl radical.

beta-carotene• + O_2 $\Leftrightarrow$ beta-carotene-OO•
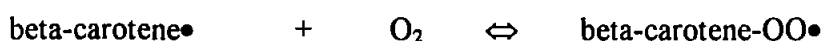
The fate of this reactive beta-carotene species is dependent on the oxygen tension: at low oxygen tensions the equilibrium of the reaction will be to the left, reducing the amount of chain-carrying peroxyl radical. At high oxygen tensions, however, the equilibrium of the reaction shifts to the right and (through autooxidation) the beta-carotene peroxyl radical can act as a prooxidant (Palozza and Krinsky 1992). Beta-carotene also forms an addition complex with superoxide anion radical (Conn *et al.* 1992) to which the above considerations also apply. In a nutshell, beta-carotene acts as a prooxidant at oxygen tensions above one tenth of normal atmospheric tension (Burton and Ingold 1984).

233

7.1.2 Discussion

Beta-carotene has been shown in this report to photosensitise cells *in* vitro. The oxygen tension under the assay conditions is normal atmospheric tension and thus beta-carotene will behave as a prooxidant. In the studies by Cozzi *et al.* (1997) and Plaum *et al.* (1998) 50 μM beta-carotene significantly increased hydrogen peroxide-induced chromosomal aberrations (Cozzi *et al.* 1997), while 10 μM beta-carotene increased oxidative damage in L1210 mouse lymphocytic cells after irradiation with visible light, although at low doses this increase was not significant (Pflaum *et al.* 1998).

It is proposed that the beta-carotene-mediated photosensitisation observed in these studies is most probably due to a peroxyl chain reaction which is propagated by a photoaddition reaction between beta-carotene and lipid peroxides. The chain terminates at the DNA backbone where the reaction of the diffusable chain carrier (i.e. a hydrophilic and not highly reactive molecule) with DNA (the chain terminator) results in SSB. The lipid-beta-carotene complex would not freely diffuse across the cell and so a small soluble molecule that can freely cross membranes would be a necessary intermediate. Hydrogen peroxide is an obvious candidate in this respect, although this is speculative.

The ACE mixture contained 2 additional vitamins (C and E) to beta-carotene. Vitamin C was shown in the study by Cozzi *et al.* (1997) to exert prooxidant effects also. This may have increased the prooxidant properties of the ACE mixture and may account for the highly significant modulation observed in the PUTKO cells after total Xe spectrum radiation, either by an additive or synergistic mechanism.

The photoprotective effects of the ACE mixture on YBF15E cells could be explained by two considerations. Firstly, the cells were cultured from a young donor (under 4 years) and they were assayed in their fourth passage. They would be likely to have a complement of antioxidant capacity comparable to *in vivo* conditions. When normal and transformed melanocytes from the same donors were compared, two populations of cells were found

with respect to antioxidant capacity. The transformed melanocytes and some, apparently normal, melanocytes contained an imbalance in the cellular antioxidant pool, whereas melanocytes from unaffected individuals and melanocytes from some affected donors formed a distinct population with a balanced pool. The normal melanocytes were better able to cope with exogenous peroxidative attacks (Picardo *et al.* 1996). Thus the YBF15E cells may have been better able to cope with the peroxidative stress from beta-carotene and the relatively high intensity radiation.

An alternative explanation could be advanced by considering the data from the YBF15E and the A2058 cell line together. Both the YBF15E and the A2058 cell lines produce melanin (personal observation, ECACC data sheet), the photoprotective pigment produced by melanocytes in response to UVR (Kollias *et al.* 1991; Eller *et al.* 1996; Tobin and Thody 1994). The absorption by melanin of the low intensity 405 nm radiation may account for the lower comet values observed in the A2058 cell line when compared to the MRC5 SV2 (Figure 4.3, Section 4.2.2.3.1) and may account for the non-significance of beta-carotene-modulation effects in this cell line. Absorption by melanin coupled with a physiological antioxidant capacity may account for the non-sensitisation of YBF15E by the ACE mixture. The concentration related reduction in strand breakage may have come from a photoprotection by the vitamin E content of the ACE supplementation. In this respect it may be relevant that the photosensitisations by beta-carotene or by ACE were exclusively in non-pigmented cells.

The photoprotection by beta-carotene observed in the early experiments is not easily explained. The photoprotection was observed with both Xenon lamp bulbs and thus is not explained by altered fluence. It is not explained by the physical presence of extracellular beta-carotene or by heat-treatment of beta-carotene. The explanation that is favoured is the following. The exclusion of phenol red from culture medium renders the medium photosensitive with the most likely consequence of antioxidant depletion (Guy *et al.*, 1996, T Kealey, personal communication). This was not known during the early experiments

235

and so the DMEM without phenol red may have had a reduced antioxidant nutrient content. This may have been enough to render the cells sensitive to oxidative stress prior to any modulation by beta-carotene. The addition of beta-carotene to these cells may have been genuinely antioxidant supplementation and photoprotection. Alternatively, the most highly sensitised cells may have been overwhelmed by the prooxidant properties of beta-carotene with the result that the comets were unreadable, and only comets from the less sensitive cells were read back. In other words the mean comet values attributed to the beta-carotene supplemented cells pertain to a resistant sub-population, whereas the comet values for the control cells include sensitive cells. The net result of this is that a lower level of damage will be observed in the beta-carotene-treated cells, i.e. a photoprotection.

7.2 O-PHENANTHROLINE

7.2.1 Background

As outlined above (Section 1.3.3.4), hydroxyl radical ($\bullet$OH) can be generated by the transition metal-catalysed Haber-Weiss reaction from H_2O_2 and $\bullet O_2^-$ thus

$$Fe^{2+} + H_2O_2 \longrightarrow Fe^{3+} + OH^- + \bullet OH \quad (1)$$

$$Fe^{3+} + \bullet O_2^- \longrightarrow Fe^{2+} + O_2 \quad (2)$$

$$\overline{\bullet O2^- + H_2O_2 \longrightarrow OH^- + O_2 + \bullet OH \quad (3)}$$
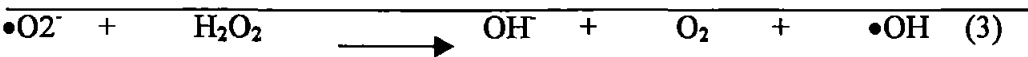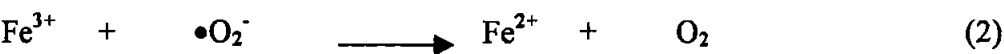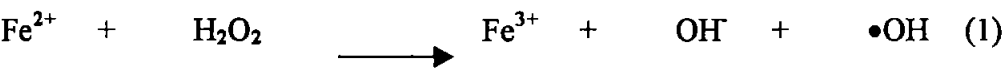
The sum of reaction (1) and (2) is reaction (3) and is the Haber-Weiss reaction. Protein-iron and DNA-iron complexes can participate in Fenton-type reactions and DNA strand breakage by hydroxyl radical occurs on the chromatin (Mello Filho and Meneghini 1984, Mello Filho and Meneghini 1985).

O-phenanthroline is a divalent metal chelating agent (Dawson *et al.* 1988) that can diffuse across the plasma and nuclear membrane and form complexes with some metals in the nucleus, including iron (Mello Filho and Meneghini 1985) and copper (Dizdaroglu *et al.* 1990, Birnboim 1992). O-phenanthroline:iron complexes do not participate in Fenton-

236

type reactions (Mello Filho and Meneghini 1985; Birnboim 1992) and so protect DNA from strand breakage by hydroxyl radical generation. O-phenanthroline protects cells from hydrogen peroxide-induced SSB (Byrnes 1996; Birnboim 1992; Kaneko *et al.* 1994) and gene mutation (Nassi-Calo *et al.* 1989;). It does not directly scavenge superoxide anion radical, hydrogen peroxide, or hydroxyl radical. It does not protect against hydroxyl radical-induced strand breakage by water radiolysis (Mello Filho and Meneghini 1985). O-phenanthroline: copper complexes on the other hand cause DNA strand breakage (Dizdaroglu *et al.* 1990; Milne *et al.* 1993; Birnboim 1992; Glass and Stark 1997; Pecci *et al.* 1997; Ueda *et al.* 1998). This is thought to be due to a reactivity of the chelated copper itself rather than through a Fenton-type reaction (Glass and Stark 1997) although this is still open to debate (Dizdaroglu *et al.* 1990). Copper-o-phenanthroline complexes can react with a number of biological reductants, these include ascorbic acid and glutathione: copper-o-phenanthroline-ascorbic acid and copper-o-phenanthroline-glutathione complexes increase hydrogen peroxide-induced strand breakage (Milne *et al.* 1993; Ueda *et al.* 1998). The addition of hydrogen peroxide with copper (II) produces the equilibrium (Pecci *et al.* 1997):

$$Cu(II)O_2H \quad \Leftrightarrow \quad Cu(I) \ O_2H$$

It is thought that the normal protective function of glutathione is to stabilise the Copper (I) complex and prevent copper (II)-mediated free radical generating reactions by shifting the equilibrium to the right (Milne *et al.* 1993).

Different iron species have been identified which, when complexed with o-phenanthroline have different protective qualities (Byrnes 1996). This may explain why, for example, strain differences between skin fibroblasts have been observed within the same laboratory: the 1BR/3 cell line was not protected from UVA by iron chelators whereas a foreskin-derived fibroblast cell line was protected by either of desferrioxamine or o-phenanthroline (Tyrrell and Pidoux 1989; Vile and Tyrrell 1995). Two modes of hydrogen peroxide-mediated cytotoxicity have been observed in CHO cells, the first at hydrogen peroxide

concentrations of less than 300 μM were inhibitable by o-phenanthroline; whereas a second mode, at hydrogen peroxide concentrations of over 2mM was not inhibitable by - phenanthroline (Kaneko *et al.* 1994). O-phenanthroline had little protective effect against SSB or Fpg-sensitive sites (oxidative base modifications) induced by visible light in L1210 mouse leukaemia cells (Pflaum *et al.* 1998).

DNA repair or replication is not immediately affected by 10 mM o-phenanthroline (Mello Filho and Meneghini 1985). It has become clear, however, that o-phenanthroline modulates enzyme activities linked to cellular metabolism (Gerber *et al.* 1996; Sun 1997) and DNA damage repair enzymes, including poly (ADP-ribose) polymerase (Jacobson *et al.* 1983; Satoh and Lindahl 1992) and p53 (Sun *et al.* 1997). A short explanation of the functions of these genes can be found in the General Introduction (Chapter 1, section 1.2.3) and Section 9.2.2.

7.2.2 Discussion

In this study, A2058 melanoma cells were sensitive to the effects of 50 μM o-phenanthroline. Blocking hydroxyl radical formation by chelating free iron reduced background SSB and very low dose (< 6 mJ cm^{-2}) 405 nm radiation-induced SSB (Section 6.2.5.1). This reduction appeared to be uniform (i.e. the modified response is almost parallel to the normal response) but did not prevent the formation of a small 10 mJ cm^{-2} peak (the peak appeared in the control cells at 3 mJ cm^{-2}). The partial reduction of SSB by o-phenanthroline implies either that some (but not all) SSB is due to hydroxyl radicals or that the concentration (50 μM) of o-phenanthroline was insufficient to chelate all the available iron. The effects of 50 μM o-phenanthroline and 1.43 mJ cm^{-2} 405 nm radiation are almost indistinguishable from the UVR alone (Figure 6.10). Hydroxyl radicals are extremely reactive, and DNA damage mediated by this radical would be expected very soon after its production. It is possible that one of the effects of very low doses of 405 nm irradiation is to increase the concentration of •OH within the solvent cage surrounding the

238

DNA. The effect of such a localised increase in •OH concentration could be limited by self-quenching and this would explain why 1.43 mJ cm^{-2} 405 nm radiation appeared independent of the chelating effects of o-phenanthroline. 405 nm irradiation generates other active species and so the relative protection by o-phenanthroline lessens with dose (time); by the time of the 10 mJ cm^{-2} peak, the effects of these other species are dominant and o-phenanthroline is non-protective, indeed it slightly photosensitises the cells.

The use of high concentrations of o-phenanthroline caused a photosensitisation in PUTKO cells, whereas lower concentrations acted photoprotectively. One explanation could be that at low concentrations the protective iron:o-phenanthroline complex is formed and o-phenanthroline is acting photoprotectively. At the higher concentrations, however, the clastogenic copper complex is also formed. The photosensitisation effects at the higher concentrations may be due to predominant effects of the clastogenic species. Examination of the dissociation constants, k_d, (log_{10} [metal-ligand complex] / [free metal] . [free ligand]) indicate that this is unlikely: copper ($k_d 8.0$) has almost a thousand fold higher binding affinity for o-phenanthroline than iron ($k_d 5.1$) (Dawson *et al.* 1988).

It is possible that at high concentrations o-phenanthroline acts as a photosensitiser. The stoichiometry of the iron: o-phenanthroline complex is 3:1 (Mello Filho and Meneghini 1985). The Fe (II)-o-phenanthroline (I) and Fe(II)-o-phenanthroline (II) complexes are formed quickly, whereas the final and more stable Fe(II)-o-phenanthroline (III) complex is formed more slowly. The first two complexes are reactive towards hydrogen peroxide whereas the final complex is stable (Asad *et al.* 1994). The photosensitisation observed in the PUTKO cells could therefore be the result of higher concentrations of the mono- and bis- complexes concomitant with higher concentrations of o-phenanthroline.

The chelating of Fe^{2+} and subsequent blocking of the Haber-Weiss reaction does protect cells from •OH-mediated damage. (But as an aside, and from an evolutionary perspective, the formation of hydroxyl radicals (and the constant generation of mutations) may have proved an evolutionary favourable way of disposing of hydrogen peroxide). If the Haber-

Weiss reaction is blocked by chelating the metal catalysts, the intra-cellular concentration of both superoxide anion radical and hydrogen peroxide may have increased more in treated cells than in untreated cells upon exposure to UVR. The chelating agent may also have disrupted antioxidant enzymes, either directly or through an altered redox balance, in which case any direct effects would be exaggerated. The increased concentrations of these reactive species could have caused damage at a later time point; for example, through hydrogen peroxide-mediated lipid peroxidation. The use of both o-phenanthroline and beta-carotene together illustrate this: the 10 mJ cm^{-2} peak was exacerbated by the use of these two chemicals. This could be interpreted thus. The formation of hydroxyl radical was blocked by o-phenanthroline, but at the cost of an intra-cellular increase in superoxide radicals and hydrogen peroxide. Beta-carotene, either by interacting directly with superoxide radicals, with peroxyl radicals, or both, facilitated a free-radical type chain reaction. This amplified the normal 10 mJ cm^{-2} peak. Extrapolating from this proposal, it is possible that this is an exaggeration of the normal dose response and that the 10 mJ cm^{-2} peak seen in the normal dose responses of the cell lines tested (Chapter 4, Section 4.2.2) is due to the same active species. The peak is, in either case, within the cells' repair capability: the rapid return to low comet values post-peak testifies to this.

CHAPTER 8.

MODULATION OF THE NORMAL REPAIR RESPONSES OF

HUMAN CELLS BY INORGANIC ARSENIC

RESULTS

8.1 INTRODUCTION

Arsenic is co-clastogenic with UVR (Wiencke *et al.*, 1997). A brief review of the many

effects of arsenicals in living cells is presented in Chapter 9 of this thesis; but in the

interests of clarity only those effects which have a direct bearing on the experiments

performed in this study will be outlined here. In essence , arsenic reacts with thiol groups

of proteins and interacts both directly and indirectly with DNA. These effects, either alone

or in combination, have been shown to inhibit DNA repair (Lynn *et al.*, 1997; Li and

Rossman, 1989; Hartwig *et al.*, 1997; Yager and Wiencke, 1997) and induce DNA-DNA

and DNA-protein cross links (Dong and Luo, 1993; Tice *et al.*, 1997). Arsenic causes the

generation of reactive oxygen species (Yamanaka *et al.*, 1991; Nordenson and Beckman,

1991) and induces a distinctive cellular stress response (Welch and Suhan, 1986).

The comet assay, as employed in this thesis, was used to detect immediate or short term

(less than 3 hours) effects of arsenic. The relationship between the assay and the arsenic-

mediated effect it is measuring is a dual one: for example, any arsenic mediated increase or

decrease in strand breakage is (artefactually) attenuated or exaggerated by the induction of

crosslinks, the time taken to excise and religate them and the relative inhibition of these

two processes. The confounding factors are summarised in Table 8.1. The experiments

are presented in Section 8.2. The multiple effects of arsenic necessitated extensive

redesigning of protocols. The results are presented in smaller sections that contain a

variety of methodologies and aims, these are outlined in the experimental description. The

results are discussed as a whole in Chapter 9.

Table 8.1. The effects of arsenic on the assay of SSB by comet assay

Cellular target	Consequences	Influence on comet assay results	Ref
DNA Ligase II	Inhibit DNA repair	Increased SSB if excision of lesions occurs.	Li and Rossman, 1989
DNA Ligase III	Inhibit DNA repair	Increased SSB if excision of lesions occurs. Main DNA repair associated ligase	Lynn *et al.*, 1997
Poly(ADP-ribose) Polymerase	Inhibit DNA repair	Increase in SSB if SSB repair is permitted	Yager and Wienke, 1997
Nucleotide Excision Repair Base Excision Repair	Inhibit DNA repair	Decreased SSB if time for excision to occur is permitted and ligation is not inhibited. Sensitivity of excision repair process to arsenic inhibition of excision and ligation stages is lesion dependent.	Hartwig *et al.*, 1997 Li and Rossman, 1989
DNA	Generation of oxygen radicals- leading to strand scission	Increased SSB due to radical attack on DNA or decreased SSB due to induction of stress response. Exposure (to arsenic) time sensitive	Yamanaka *et al.*, 1991 Nordenson and Beckman, 1991
Stress response	Induction of stress proteins	Decreased SSB with induction of response (induction time sensitive)	Welch and Suhan, 1986
DNA / proteins	DNA-protein crosslinks	Decreased SSB unless and until excision repair can remove lesions then increased SSB if ligation is also inhibited.	Dong and Luo, 1993 Tice *et al.*, 1997

The experiments described in this chapter were aimed at measuring the relative

contribution of some of these effects and are summarised in Table 8.2. In summary, the

combinations of UVR and arsenic employed were non-cytotoxic, but were clastogenic in

some cases. It was observed that arsenic inhibited DNA repair of both excisable lesions and direct SSB repair. The arsenic exposure levels were varied by time and concentration: this resulted in an increase in UVR-induced SSB after some arsenic treatments, but a decrease after others. The time courses of the phenomena were measured: it was found that the induction of either crosslinking or a protective response was induced within 1 hour of arsenic exposure with maximal strand breakage observed at 30 minutes exposure. This appeared to be an exaggeration of the untreated cellular response. It was not possible to distinguish between crosslinking or an actual reduction in SSB numbers, although it appeared that removal of crosslinks was detectable after incubation with lower concentrations of arsenic.

Table 8.2. Summary of experiments described in this chapter

Cell line	Treatment	Results
	CYTOTOXICITY	
MRC5	0-10 mM As(III) x 48 h	Dose dependent cytotoxicity
	0-400 μM As(V) x 48 h	Dose dependent cytotoxicity Maximal cytotoxicity ~75% (>100 μM)
	50 μM As(V) x 1 h plus 135 mJcm^{-2} 405 nm radiation	No cytotoxicity
	SSB – As only	
MRC5	50 μM As(V) x 1 h	No increase in SSB
MRC5 SV2	50 μM As(V) x 1 h	Slight increase in SSB
A2058	50 μM As(III) x 1 h	Decrease in SSB
	SSB – As + UVR	
MRC5	50 μM As(V) x 1 h plus 0 - 135 mJcm^{-2}	UVR dose dependent increase in SSB (non-significant
	0-200 μM As(V) x 1h plus 135 mJcm^{-2}	As concentration dependent decrease in SSB (<200 μM) Significant inhibition of DNA repair at 200 μM
	100 μM As(V) x 30 mins plus 60 s, 90 s or 120 s radiation	Inhibition of SSB repair
A2058	50 μM As(III) x 1 h plus 0-17 mJcm^{-2}	Non-significant modulation of SSB yield
	CROSSLINKING / INDUCTION OF PROTECTIVE RESPONSE	
PUTKO	100 μM As(V) x 0 – 130 mins plus 60 s unfiltered Xe lamp radiation	Increase in SSB in arsenic treated cells at 30 mins. Incubation time dependent reduction in SSB after 60 mins
	0-200 μM As(V) x 135 mins plus 60 s unfiltered Xe lamp radiation	Concentration dependent inhibition of SSB

8.2 RESULTS

8.2.1 Cytotoxicity

MRC5 are normal diploid fibroblasts and were selected for estimation of arsenic-mediated effects for this reason. The cytotoxic effects were tested (by Trypan Blue exclusion) in late passage MRC5 fibroblasts at exposure levels of 0-10 mM As(III) x 48 hrs, 0-400 μM As(V) x 48 hrs and 50 μM As(V) x 1 hr plus 135 mJ cm^{-2} 405 nm radiation. A sharp increase in cytotoxicity was seen from 0.1 mM As(III) with 100% cytotoxicity at 5 mM (Figure 8.1) although due to the extreme cytotoxicity of As(III) leading to highly fragmented cells and debris, estimates of cytotoxicity were made to the nearest 25%. A concentration dependent cytotoxicity was observed from 0-100 μM As(V) with maximal cytotoxicity of 85% above this (Figure 8.2). 100% cytotoxicity was obtained at 200 μM As(V) x 100 hrs (data not shown). No significant differences in viable cell numbers by Trypan blue exclusion test after 48 hrs were seen between arsenic-treated and phosphate-treated control cells (50 μM (AsO$_4$ or PO$_4$) x 1 hr followed by 135 mJ cm^{-2} 405 nm radiation, Figure 8.3).

Figure 8.1 The cytotoxic effects were tested in late passage MRC5 fibroblasts by exposure to 0-10 mM As(III) for 48 hrs; viable cell numbers were counted by Trypan blue exclusion.
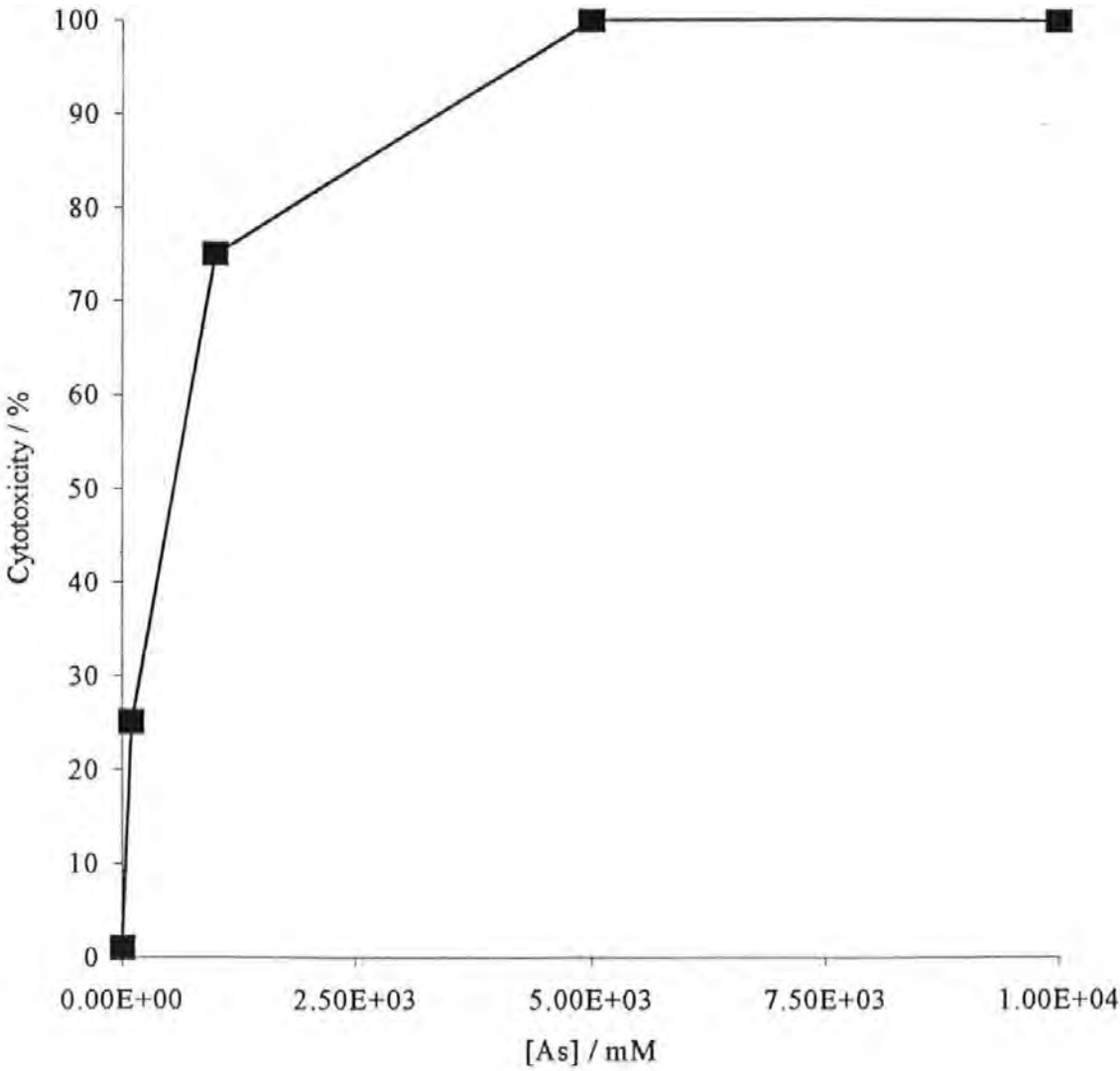
Figure 8.2 The cytotoxic effects were tested in late passage MRC5 fibroblasts by exposure to 0-400 μM As(V) for 48 hrs ; viable cell numbers were counted by Trypan blue exclusion
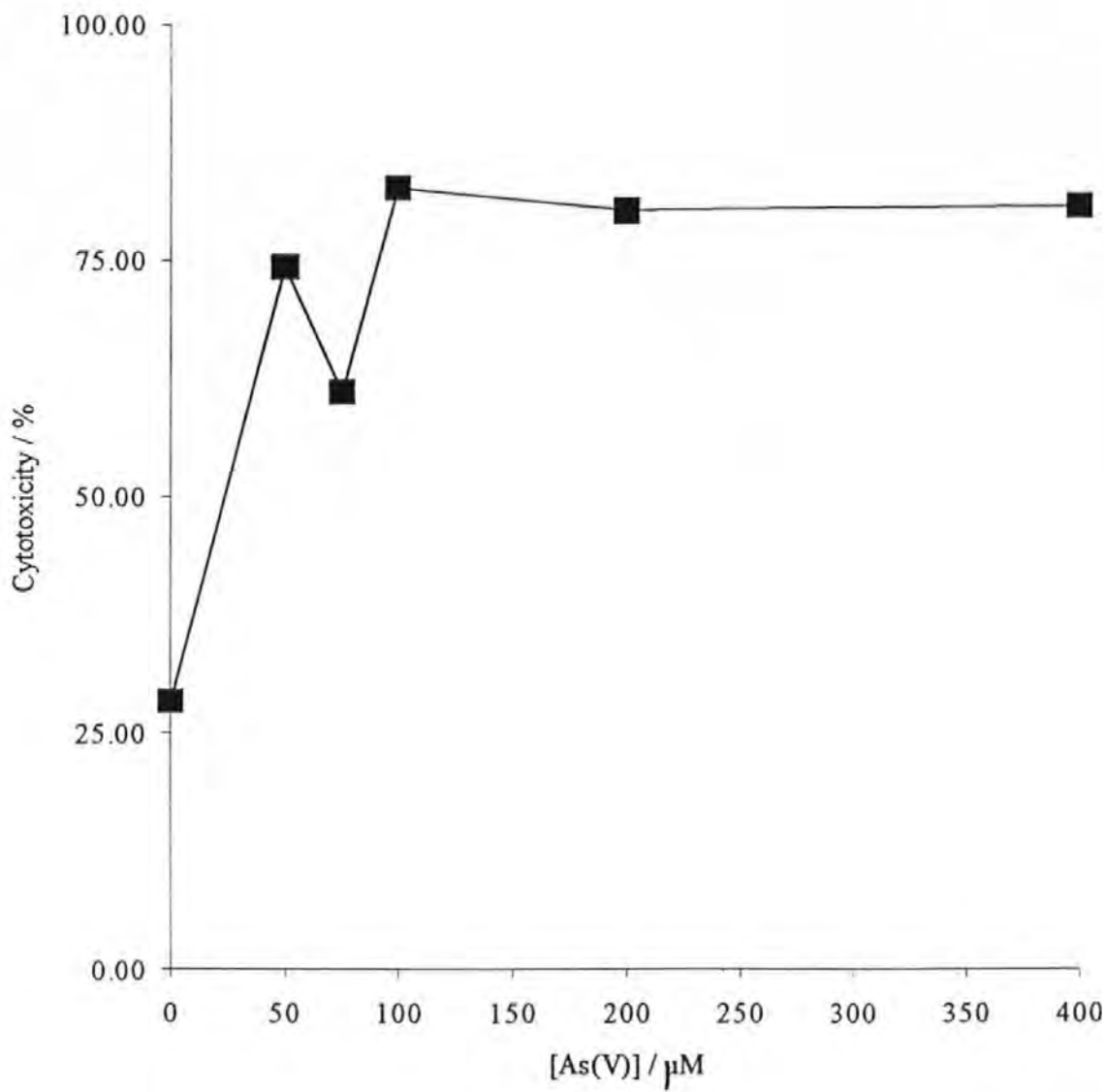
Figure 8.3 **The cytotoxic effects were tested in late passage MRC5 fibroblasts by exposure to 50 µM As(V) for 1 hr plus 135 mJ cm^{-2} 405 nm radiation; viable cell numbers were counted by Trypan blue exclusion after 48 hrs**
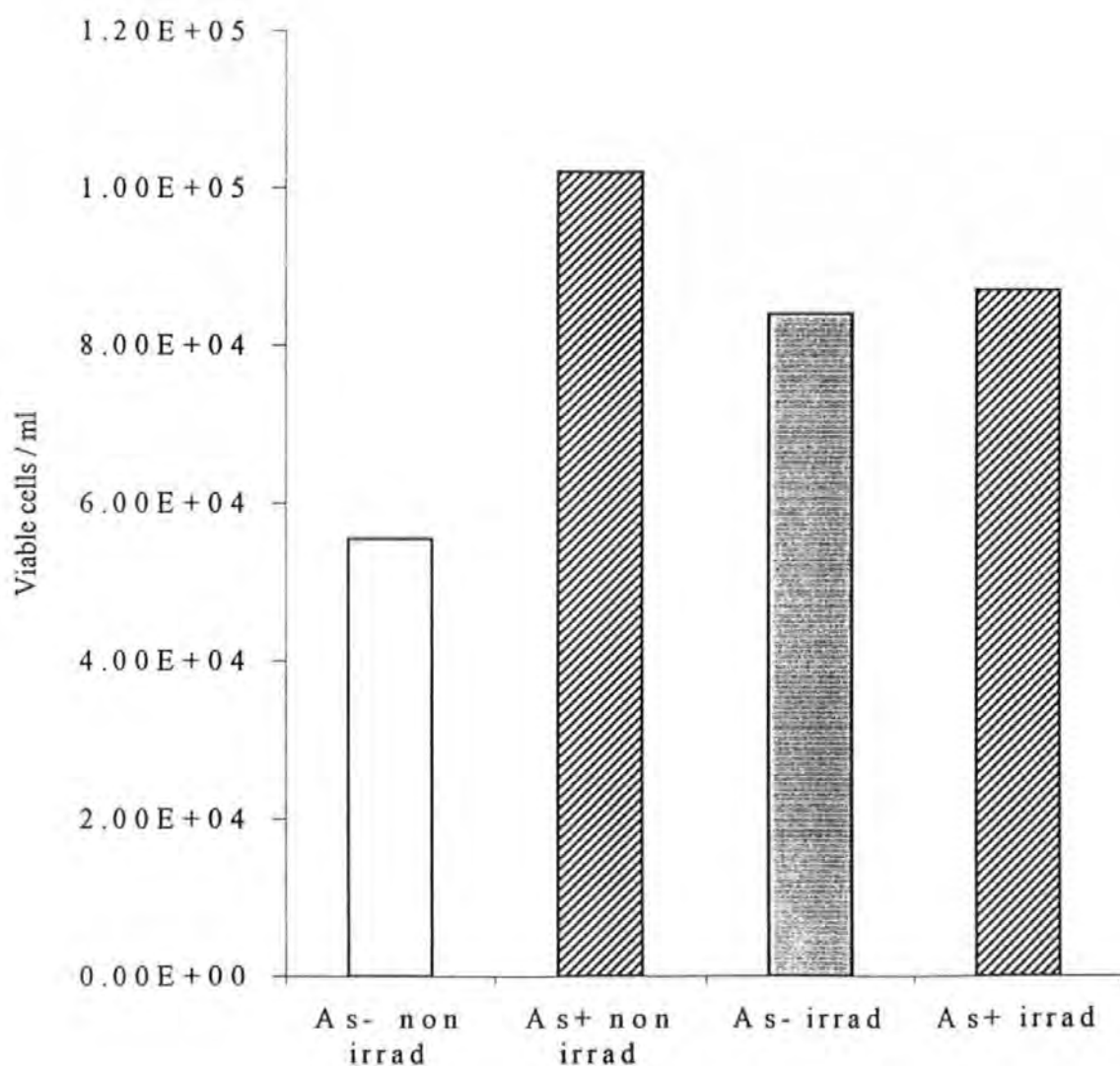
8.2.2 SSB induced by inorganic arsenic

Arsenic is weakly mutagenic but actively clastogenic *in vitro* and *in vivo* (Tice *et al.*, 1997; Yamanaka *et al.* , 1991; Nordenson and Beckeman, 1991). SSB induced by arsenic were assessed from the arsenic-treated but non-irradiated cells from the data obtained in the experimental series described in the following section (Section 8.2.3). Data were obtained (Table 8.1) for strand breakage induced by 50 µM As(V) for 1 hours exposure (9 determinations by visual inspection) and by 100 µM As(V) for 1 hours exposure (2 determinations by image analysis) in MRC5 fibroblasts, by 50 µM As(V) for 1 hours exposure (1 determination by visual inspection) in MRC5 SV2 fibroblasts, by 50 µM As(III) for 1 hours exposure in A2058 melanoma cells (2 determinations) and by 200 µM As(V) for 1 hours exposure in PUTKO lymphocytic cells (2 determinations by image analysis).

Table 8.1 SSB induced by arsenic in human cells

Cell line	[As(V)} / µM	N	Controls (mean comet value or Comet Area)	As-treated (mean comet value or Comet Area)
MRC5	50	9	2.45	2.47
	200	2	2.23	2.53
	200	2	726	752
MRC5 SV2	50	1	1.49	1.55
PUTKO	100	2	1044	1093
A2058	50µM As(III)	2	1.70	1.49

It was observed that arsenic did not induce SSB (or only weakly) in the cells and at the concentrations tested, and none of the increases were significant by student t-test where applicable. The hypothesis that arsenic does not cause direct SSB is supported by these data. As noted, however, arsenic induces DNA-DNA and DNA-protein crosslinks, these

are the only (currently known) mechanisms that reduce DNA migration in the comet assay (Tice *et al.*, 1997). SSB induced by arsenic may therefore be masked by the reduced mobility of crosslinked DNA in the assay.

8.2.3 SSB induced by arsenic and UVR

Arsenic is co-clastogenic with UVR (Wiencke *et al.*, 1997) and with other compounds (Yamamoto *et al.* 1995). Arsenic inhibits DNA nucleotide excision repair (NER) (Hartman *et al.*, 1997) and DNA base excision repair (Lynn *et al.*, 1997). It was therefore considered whether arsenic would increase SSB by the inhibition of SSB repair. This question was investigated in a number of ways using the comet assay.

(i)   A2058 melanoma cells were incubated in 50 μM As(III) for 1 hour and 405 nm irradiated for 5.8 or 17.1 mJ cm^{-2} and read back by visual inspection (Figure 8.4). The results were equivocal, with a decrease in SSB in the unirradiated cells, an increase in SSB after 5.8 mJ cm^{-2} The untreated and treated cells displayed similar levels of assayed SSB after 17.1 mJ cm^{-2} .

(ii)   MRC5 fibroblasts were incubated in media containing 50 μM As(V) for 1 hour, then 405 nm-irradiated for up to half an hour (135 mJ cm^{-2}) and compared to the identically treated phosphate controls using the visual readback method. A UVR dose dependent increase in SSB was observed (Figure 8.5).

(iii)   MRC5 fibroblasts were incubated in 0-200 μM As(V) for 1 hour prior to 135 mJ cm^{-2} 405 nm irradiation and read back by image analysis (Figure 8.6). A concentration dependent reduction in DNA migration was observed in arsenic treated cells in the concentration range 50-100 μM, but at 200μM arsenate the inhibition of repair processes raised the assayed number of strand breaks to one above the level of any SSB reducing effects.

Figure 8.4 A2058 melanoma cells were incubated in 50 μM As(III) for 1 hour and 405 nm irradiated for 5.8 or 17.1 mJ cm^{-2} and read back by visual inspection.
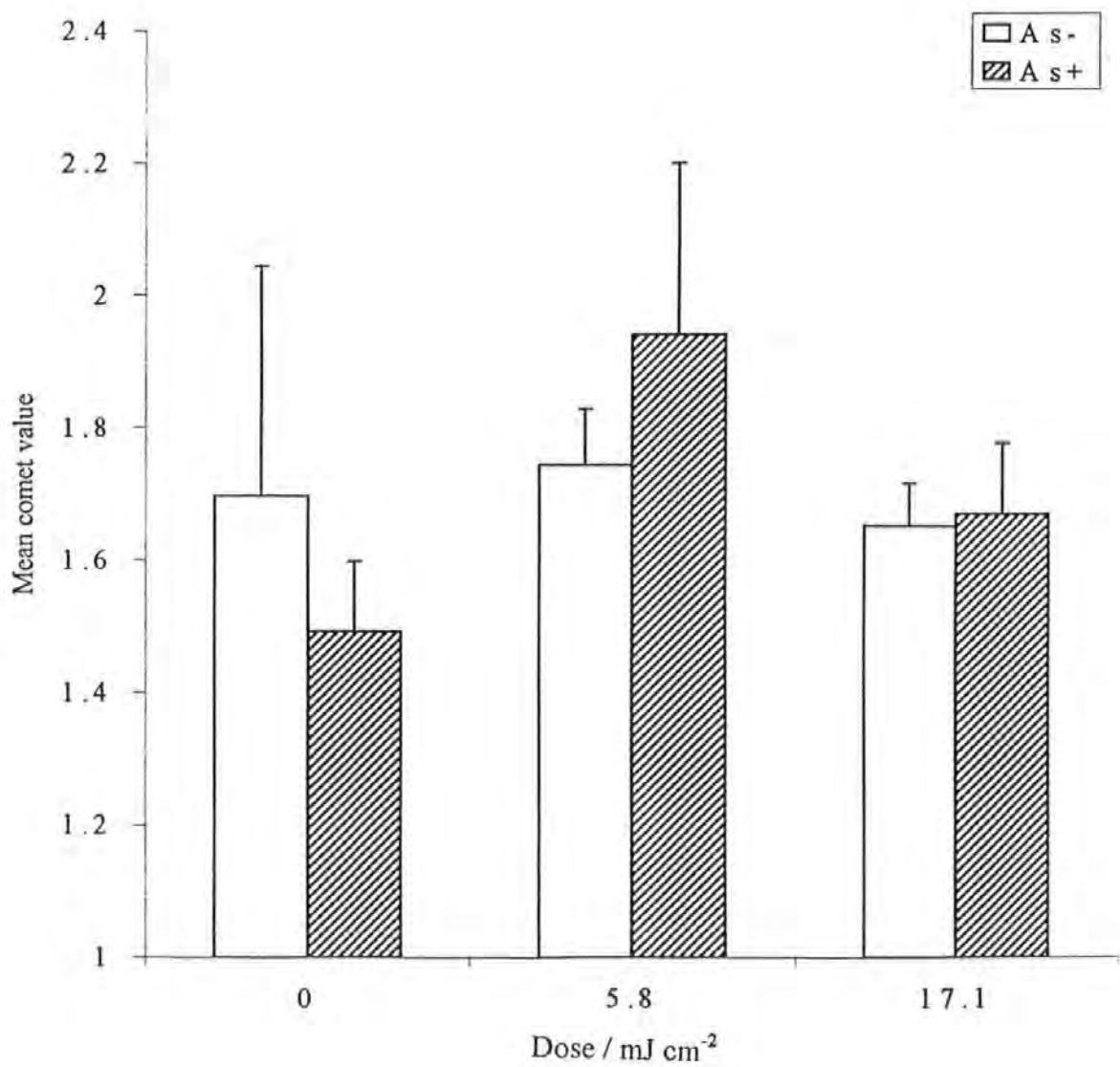
Figure 8.5 MRC5 fibroblasts were incubated in media containing 50 µM As(V) for 1 hour, then 405 nm-irradiated for up to half an hour (135 mJ cm^{-2}) and compared to the identically treated phosphate controls using the visual readback system

8.2.4 Induction of cross linking or protective responses

It was considered that in the previous experiments the arsenic-induced crosslinking could be masking SSB. This would be expected to be to be concentration dependent and so the results from the previous experiment (see Figure 8.6) appeared to indicate that the reduction in assayed SSB could be either crosslinking or a protective response. The time course of arsenic-mediated induction of the concentration dependent reduction in assayed SSB was therefore measured. High fluence radiation (total Xe lamp radiation) was chosen to optimise the irradiation time/repair time ratio and PUTKO cells were chosen for the study for two reasons (i) they were noted to be sensitive to the effects of unfiltered radiation and (ii) they are a suspension cell and not subject to trypsin induced damage and an associated stress response. The arsenic-induced crosslinks were investigated with respect to (i) [As] and (ii) time of exposure to arsenic (i.e. the time course of the induction).

8.2.4.1 Concentration dependent cross linking

PUTKO hybrid lymphocytes were incubated in 0, 100, 150, and 200 µM As(V) for 135 minutes (to ensure an effective induction of the response) prior to irradiation by 60 s unfiltered Xe lamp radiation. These cells were permitted to repair for 60 s, 120 s and 180 s before being assayed by image analysis (Figures 8.7: Comet Area, 8.8: Tail Moment and 8.9: Comet Moment). SSB repair was observed to take place in the control cells. The arsenic treated cells displayed very low levels of SSB immediately after irradiation. When analysed by Comet Area the arsenic treated cells displayed slight increases with repair time. The 50 µM arsenic-treated cells displayed a maximum after 120 seconds repair time. The 100 µM treated cells and 150 µM treated cells displayed an increase in Comet Area with repair time, the lower concentration produced the steeper increase. The 200 µM treated cells displayed a level of strand breakage that was higher than the other arsenic (V)-

treated cells immediately after irradiation and after 180 seconds repair time (the only 2 points successfully assayed). This was interpreted thus: a concentration dependent crosslinking was induced by the arsenic (V) treatment and was more or less successfully removed (dependent on the arsenic concentration) from the DNA by the excision repair processes. The incubation of cells in 200 μM arsenate appeared to induce in cells a level of strand breakage that was high enough to be detected above any crosslinking or protective response involved

8.2.4.2 Time course of induction

PUTKO hybrid lymphocytes were incubated in 100 μM As(V) for 0-160 minutes prior to irradiation by 60 s unfiltered Xe lamp radiation and readback by image analysis (Figures 8.10: Comet Area, 8.11:Tail Moment and 8.12: Comet Moment). An increase in SSB induction was observed after 30 minutes of arsenic treatment and a time dependent reduction in SSB was observed after 60 minutes . The phosphate-treated and irradiated cells almost followed this pattern in parallel, but at a lower level. The mock-irradiated cells of both treatments displayed much lower levels of SSB with the control cells showing excision activity at 120 minutes which was not evident in the arsenic-treated cells. The dose responses appeared to indicate that cross linking, as well as inhibition of excision repair and ligation were induced by arsenic treatment. The induction of a stress response appeared to be taking place in both cells.

Figure 8.7 PUTKO hybrid lymphocytes were incubated in 0-200 μM As(V) for 135 minutes prior to irradiation by 60 s unfiltered Xe lamp radiation. These cells were permitted to repair for 60 s, 120 s and 180 s before being assayed by image analysis (Comet Area). Possible crosslinking was observed in the arsenic treated cells, effects were concentration dependent.
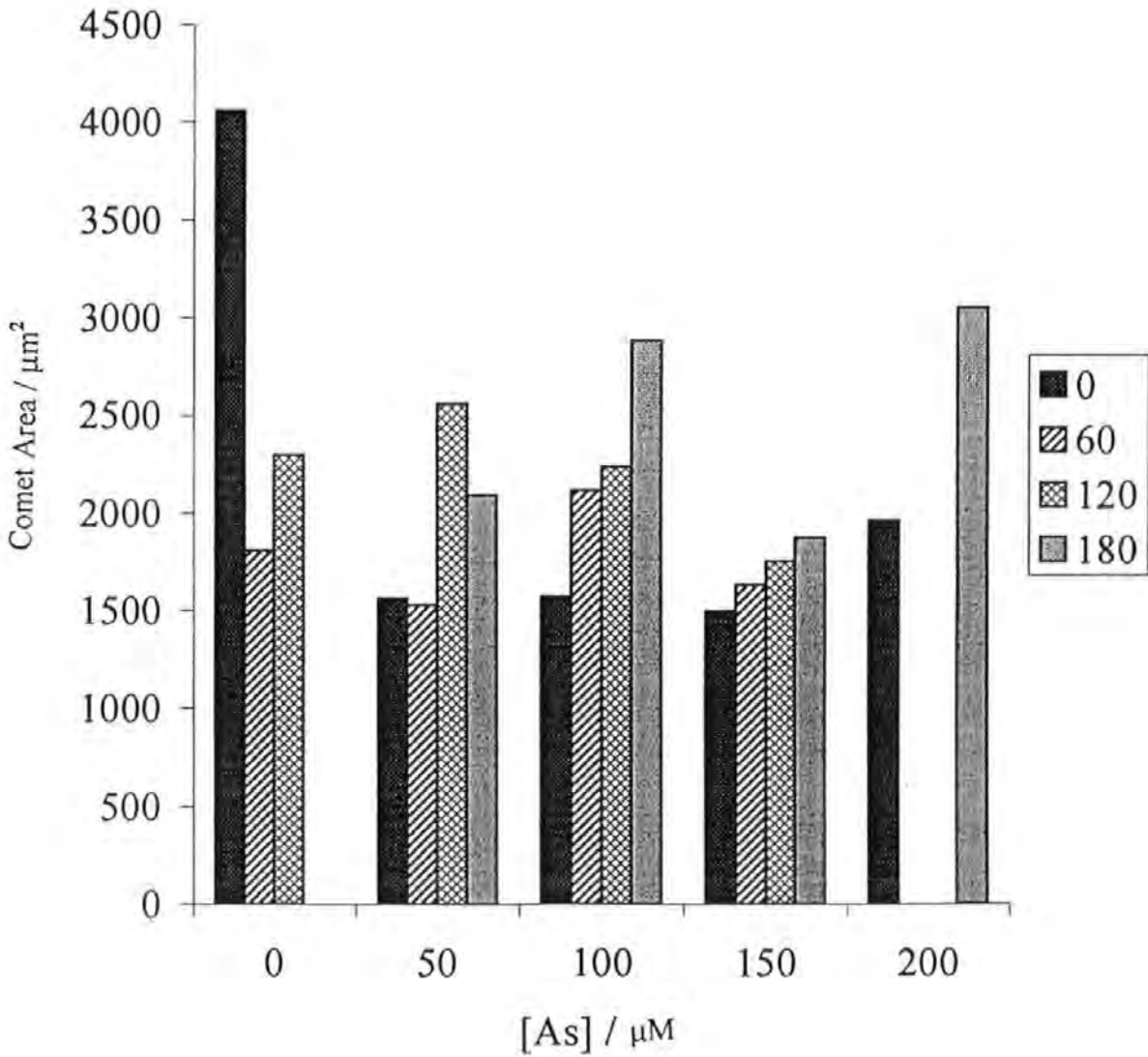
Figure 8.8 PUTKO hybrid lymphocytes were incubated in 0-200 μM As(V) for 135 minutes prior to irradiation by 60 s unfiltered Xe lamp radiation. These cells were permitted to repair for 60 s, 120 s and 180 s before being assayed by image analysis (Tail Moment). Possible crosslinking was observed in the arsenic treated cells, effects were concentration dependent.
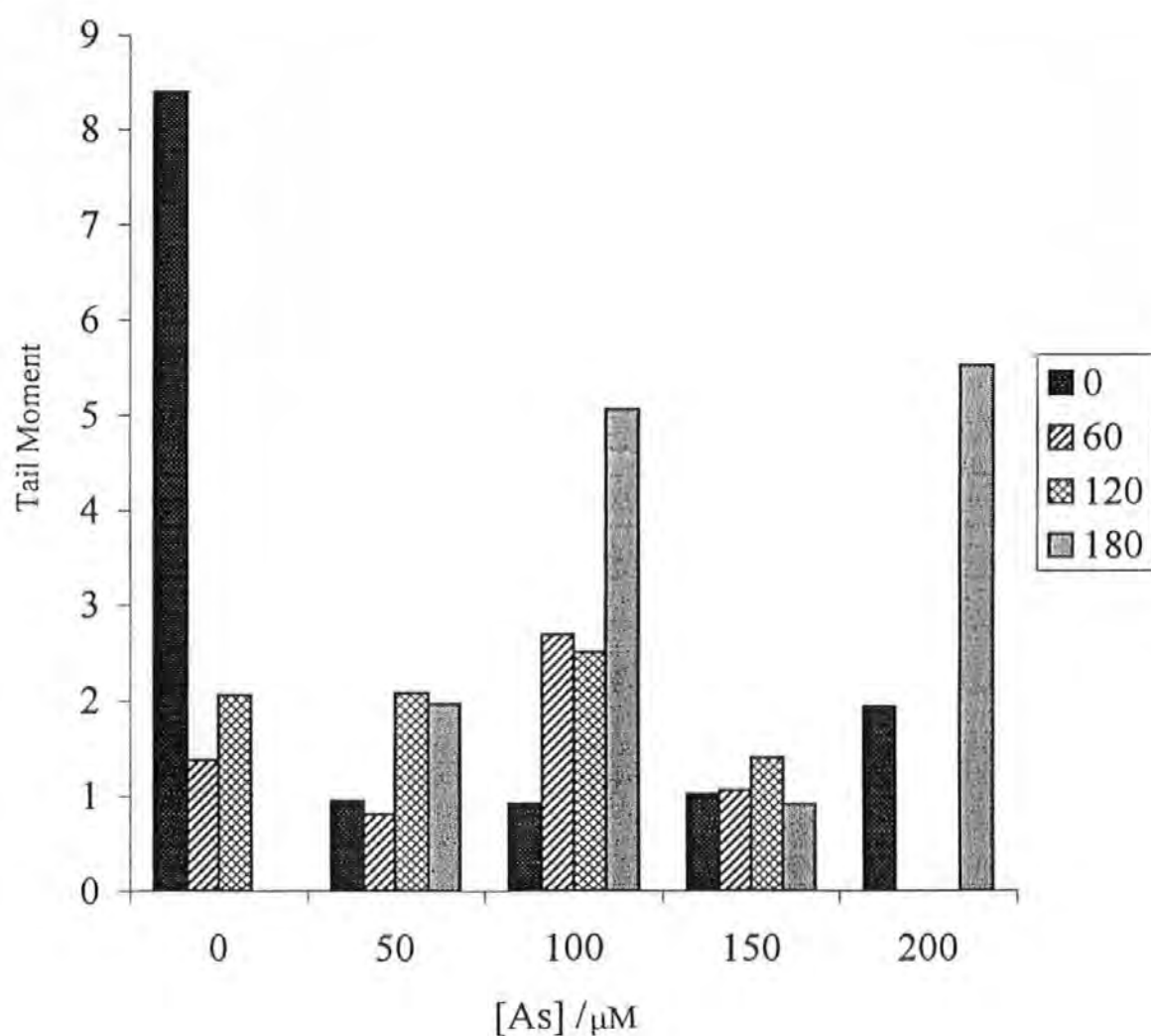
Figure 8.9 PUTKO hybrid lymphocytes were incubated in 0-200 μM As(V) for 135 minutes prior to irradiation by 60 s unfiltered Xe lamp radiation. These cells were permitted to repair for 60 s, 120 s and 180 s before being assayed by image analysis (Comet Moment). Possible crosslinking was observed in the arsenic treated cells, effects were concentration dependent.
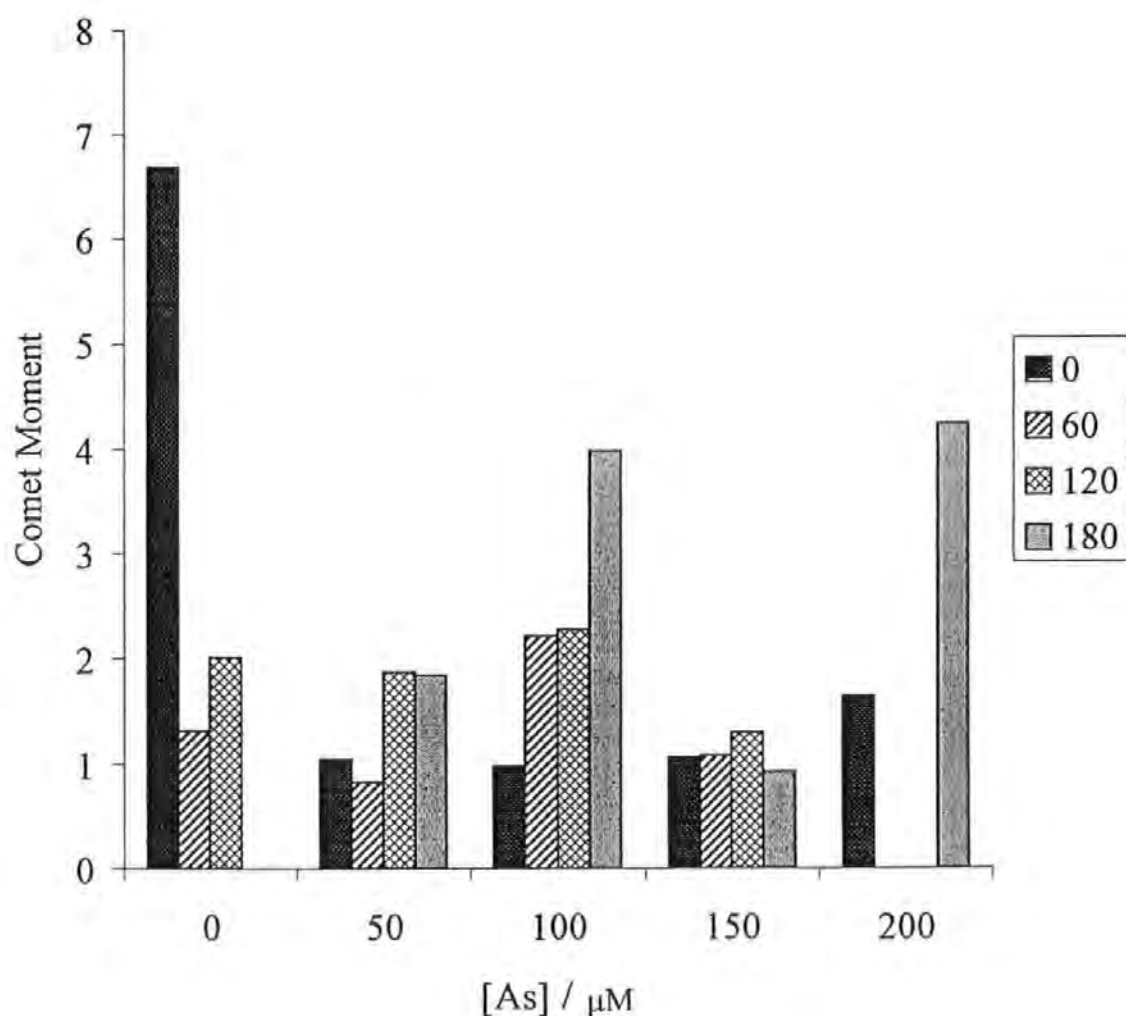
Figure 8.10 PUTKO hybrid lymphocytes were incubated in 100 μM As(V) for 0-160 minutes prior to irradiation by 60 s unfiltered Xe lamp radiation and readback by image analysis (Comet Area). Maximal SSB induction was observed after 30 minutes of arsenic treatment. Possible crosslinking was observed after 60 minutes.
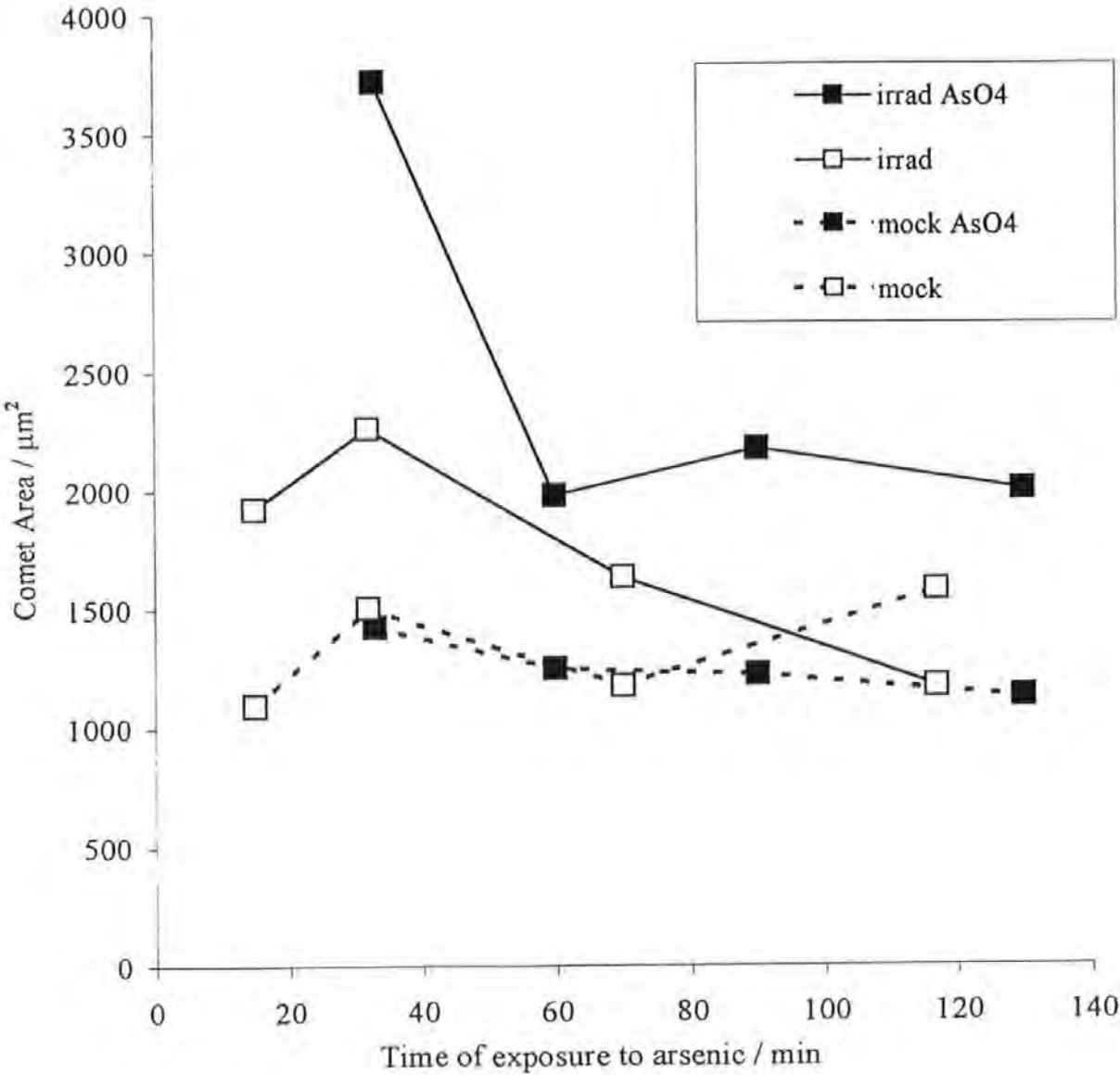
Figure 8.11 PUTKO hybrid lymphocytes were incubated in 100 µM As(V) for 0-160 minutes prior to irradiation by 60 s unfiltered Xe lamp radiation and readback by image analysis (Tail Moment). Maximal SSB induction was observed after 30 minutes of arsenic treatment. Possible crosslinking was observed after 60 minutes
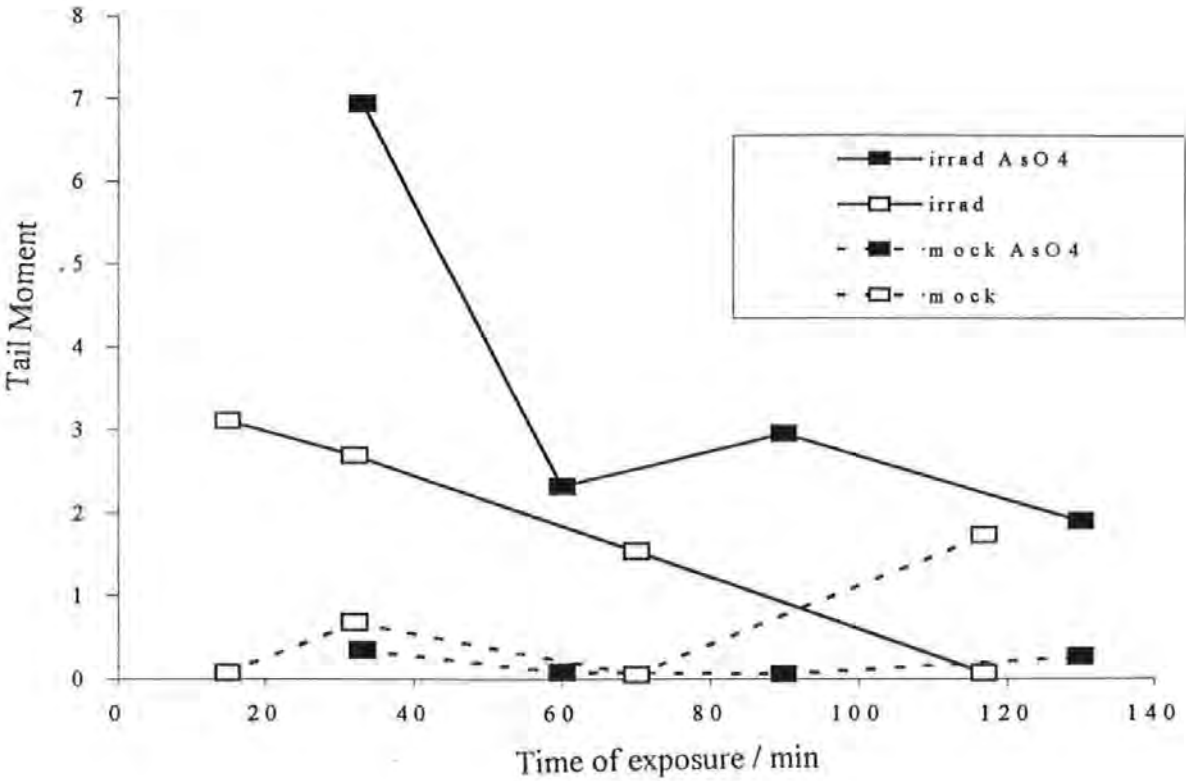
Figure 8.12 PUTKO hybrid lymphocytes were incubated in 100 μM As(V) for 0-160 minutes prior to irradiation by 60 s unfiltered Xe lamp radiation and readback by image analysis (Comet Moment) . Maximal SSB induction was observed after 30 minutes of arsenic treatment. Possible crosslinking was observed after 60 minutes
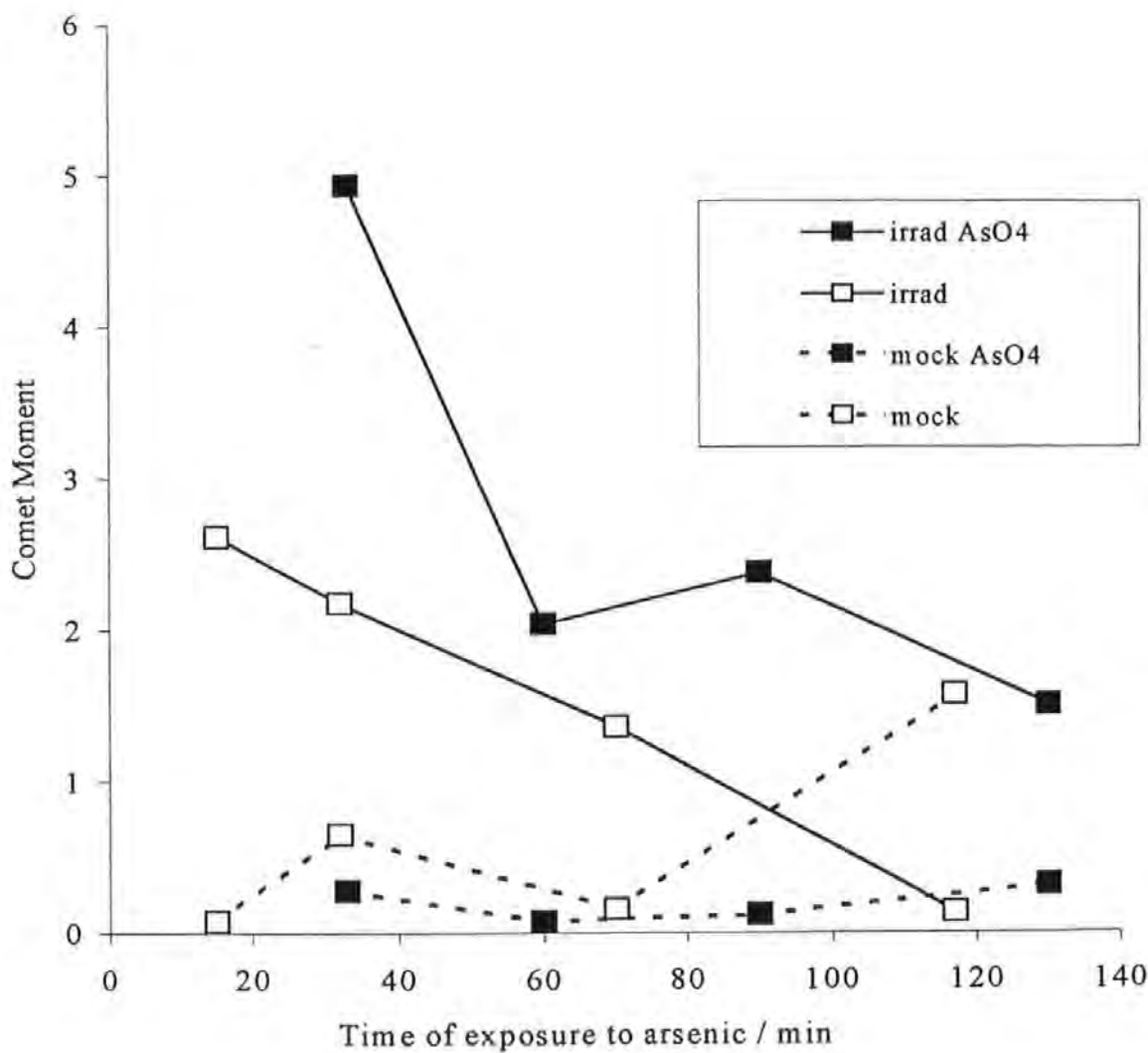
8.2.5 Arsenic mediated inhibition of excision repair

MRC5 were incubated for one hour in DMEM containing various concentrations of sodium arsenate or phosphate for one hour prior to 30 minutes 405 nm radiation (135 mJ cm^{-2}). The cells were placed directly into lysis buffer or allowed to repair for a period of time. The concentration and repair times were increased until significant ($p <$ 0.05, two-tailed student t-test) differences were observed between phosphate and arsenate treated cells. The experiments outlined below (Table 8.3) were performed. It was observed that 200 µM arsenate for one hour exposure was sufficient to significantly inhibit repair. This was in agreement with the findings from two other experiments in which cells that had been incubated with 200 µM arsenate for one hour appeared to induce effects that raised SSB yields above any threshold caused by possible crosslinking or protective responses.

Table 8.3 The inhibition of excision repair by arsenate.

		[As] / µM	Repair time / mins	Comments
MRC5	135 mJ cm^{-2} 405 nm	50	30	No significant differences between arsenic or control treatments
		75	40	
		100	40	
		200	60	Significant differences between arsenic and control treatments in both irradiated and irradiated plus repaired treatments (Figure 8.13)

Figure 8.13 MRC5 were incubated for one hour in DMEM containing 200 μM

sodium arsenate or phosphate for one hour prior to 30 minutes 405 nm radiation

(135 mJ cm^{-2}). The cells were placed directly into lysis buffer or allowed to repair for

one hour. Significant differences between arsenic (V) and control treatments in both

irradiated and irradiated plus repaired treatments were observed.
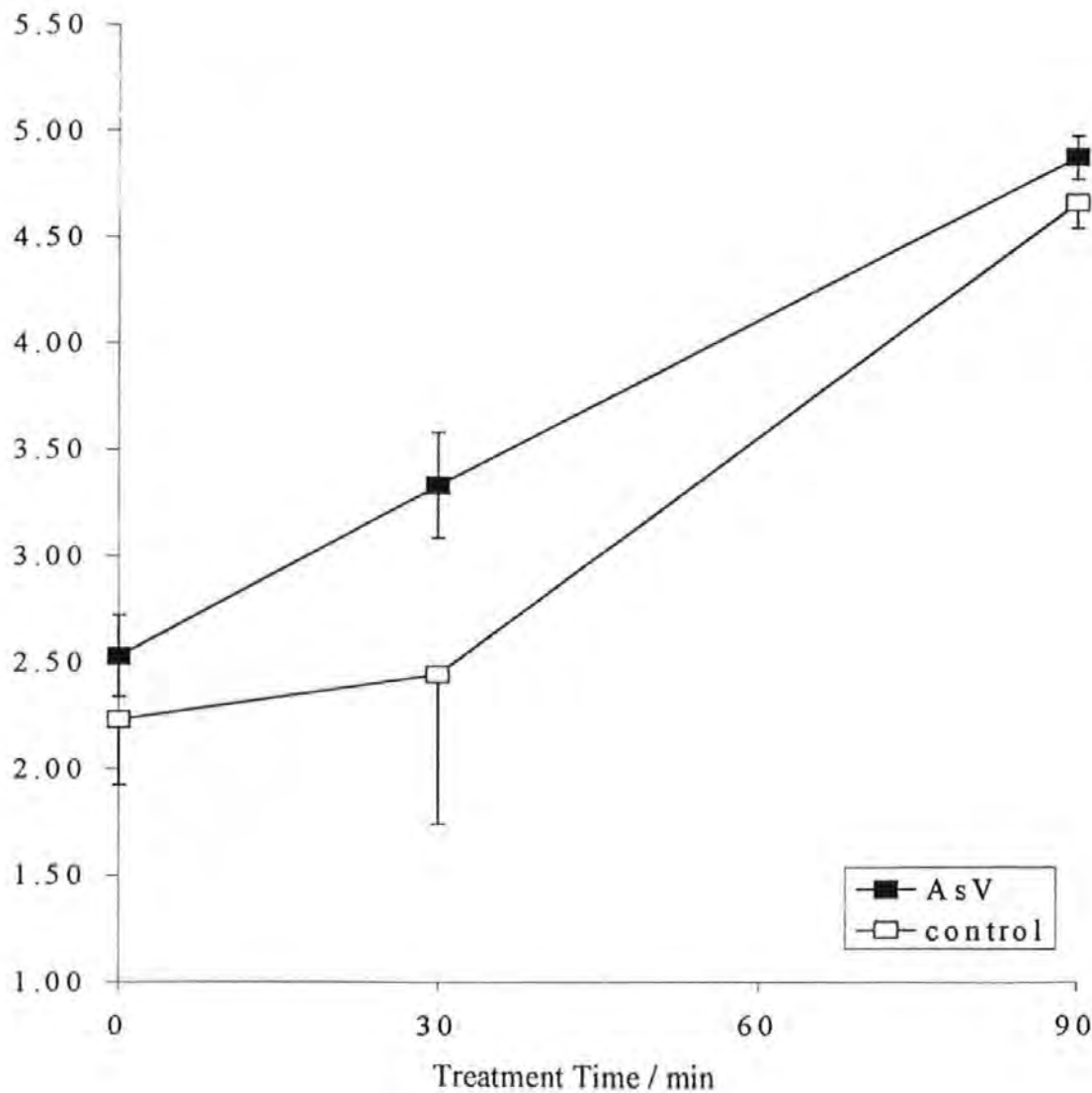
8.2.6 Inhibition of SSB repair by inorganic arsenic

It was considered that the higher levels of UVR SSB seen in arsenic treated cells could be due to an arsenic mediated inhibition of SSB repair.

MRC5 fibroblasts were incubated in 100 μM As(V) for 30 minutes (at which time the yield of SSB would be high, Section 8.2.4.2) and 405 nm irradiated for a) 60 s (Figures 8.14: Comet Area, 8.15: Tail Moment and 8.16:Comet Moment), b) 90 s (Figures 8.17: Comet Area, 8.18: Tail Moment and 8.19:Comet Moment), c) 120 s (Figures 8.20: Comet Area, 8.21: Tail Moment and 8.22:Comet Moment) and allowed to repair for 10 s (a, b, c), 120 s (b and c), and 240 s (a, b, c) before being assayed and read back by image analysis. Inhibited repair of SSB induced by UVR was clearly observed in arsenic-treated cells when compared to the phosphate treated controls.

Figure 8.14 MRC5 fibroblasts were incubated in 100 µM As(V) for 30 minutes and
405 nm irradiated for 60 s and allowed to repair for 10 s or 240 s before being assayed
and read back by image analysis using the parameter of Comet Area
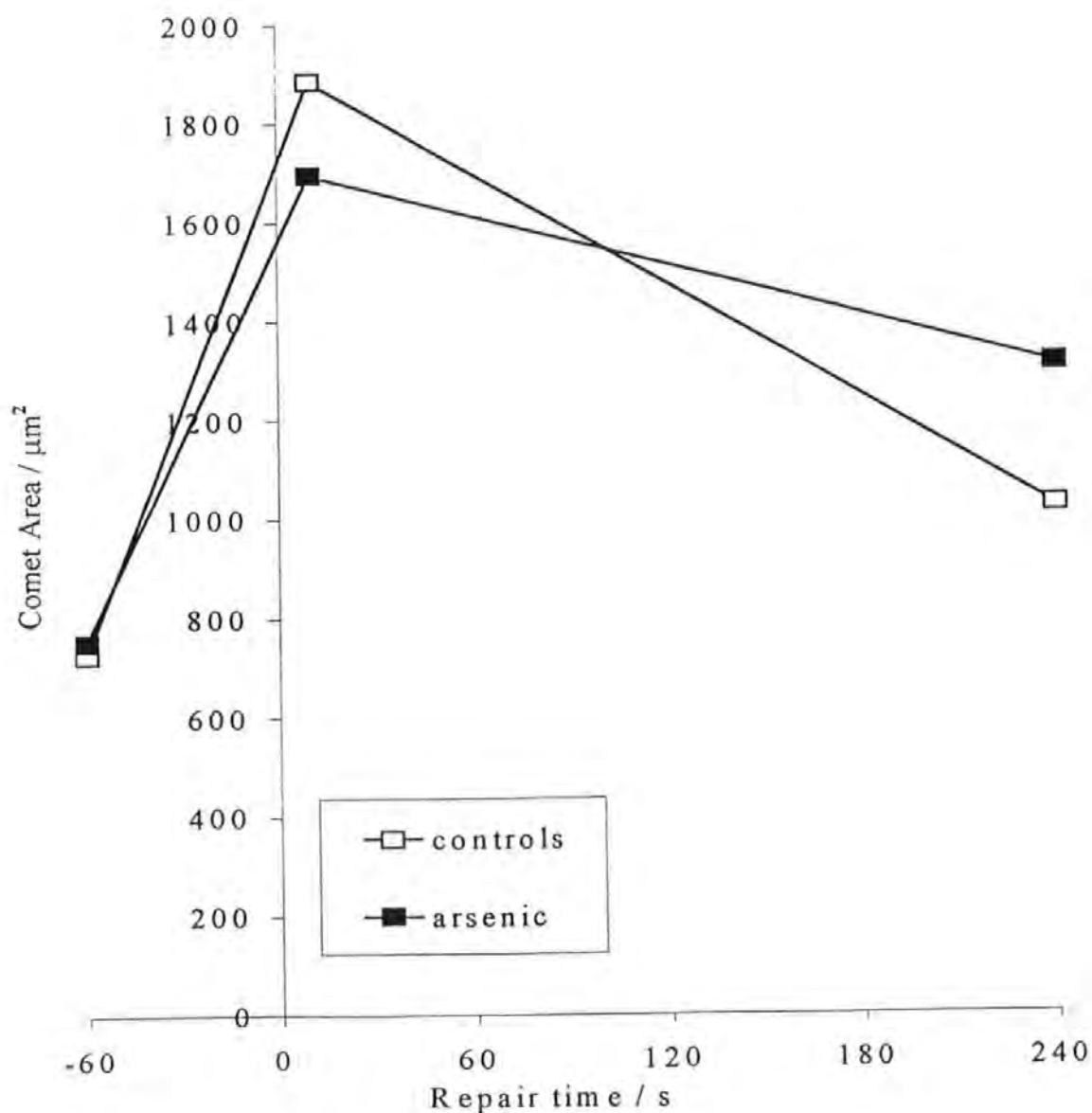
Figure 8.15 MRC5 fibroblasts were incubated in 100 µM As(V) for 30 minutes and 405 nm irradiated for 60 s and allowed to repair for 10 s or 240 s before being assayed and read back by image analysis using the parameter of Tail Moment
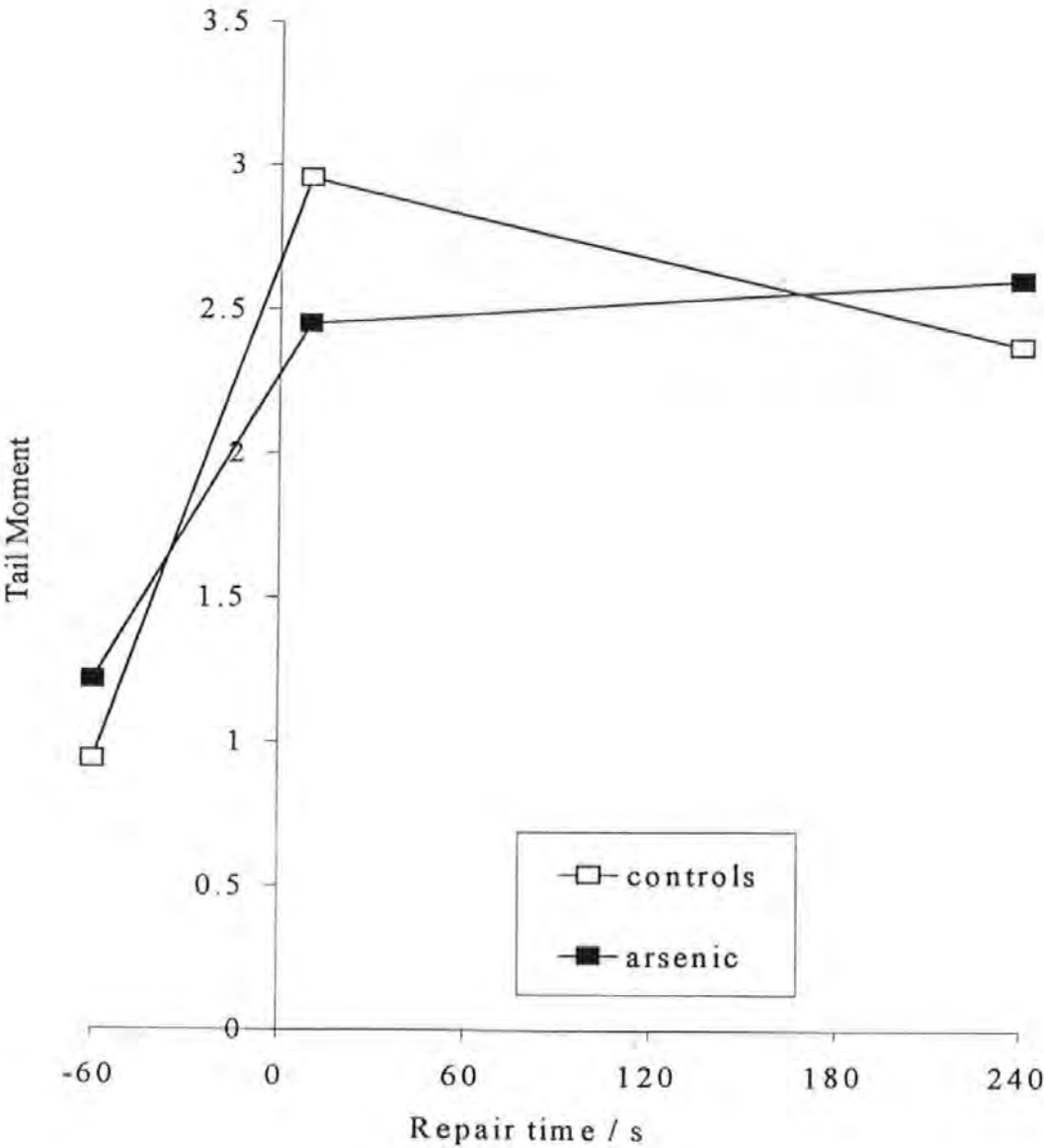
Figure 8.16 MRC5 fibroblasts were incubated in 100 μM As(V) for 30 minutes and 405 nm irradiated for 60 s and allowed to repair for 10 s or 240 s before being assayed and read back by image analysis using the parameter of Comet Moment
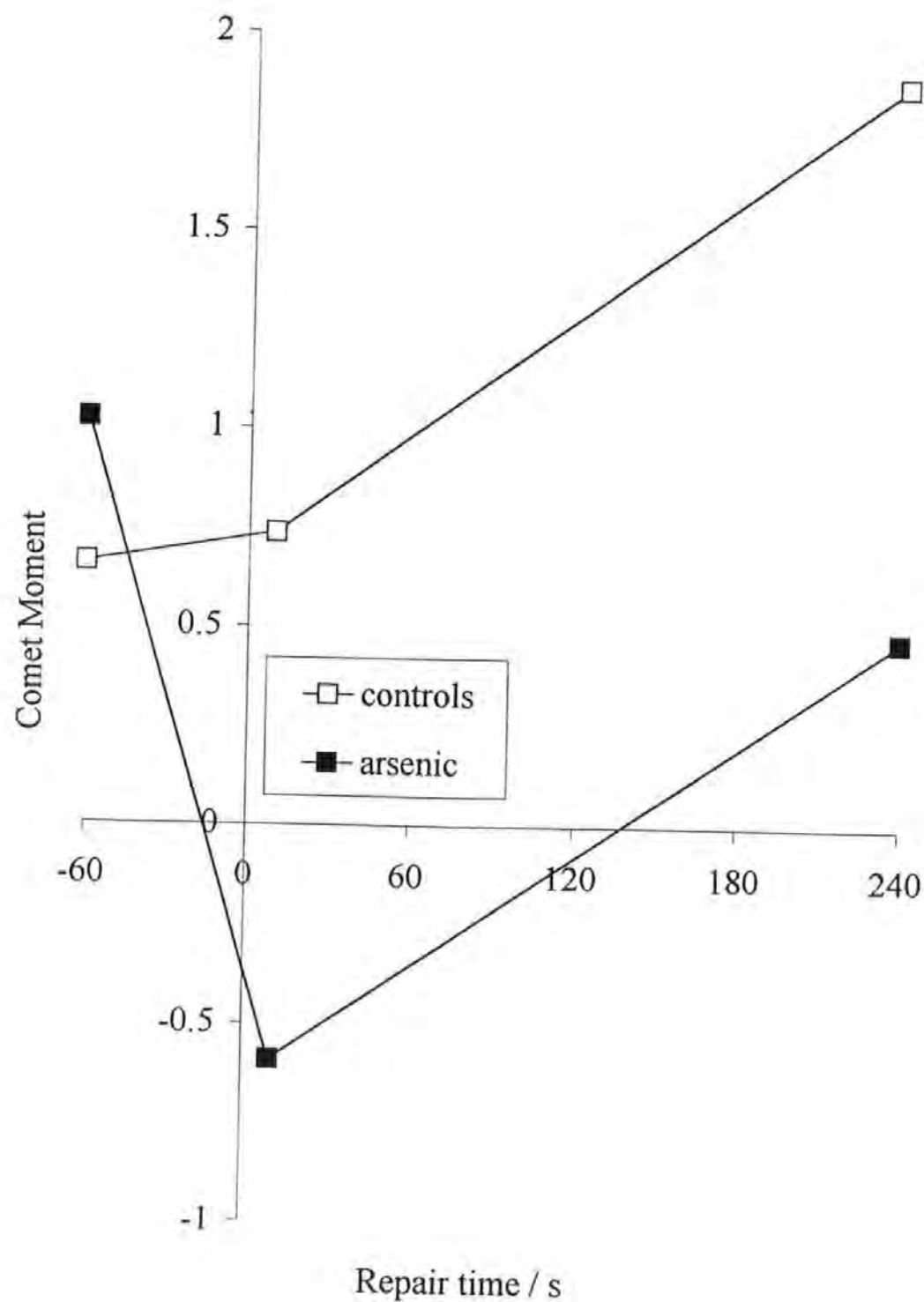
Figure 8.17 MRC5 fibroblasts were incubated in 100 μM As(V) for 30 minutes and 405 nm irradiated for 90 s and allowed to repair for 10 s, 120s and 240 s before being assayed and read back by image analysis using the parameter of Comet Area.
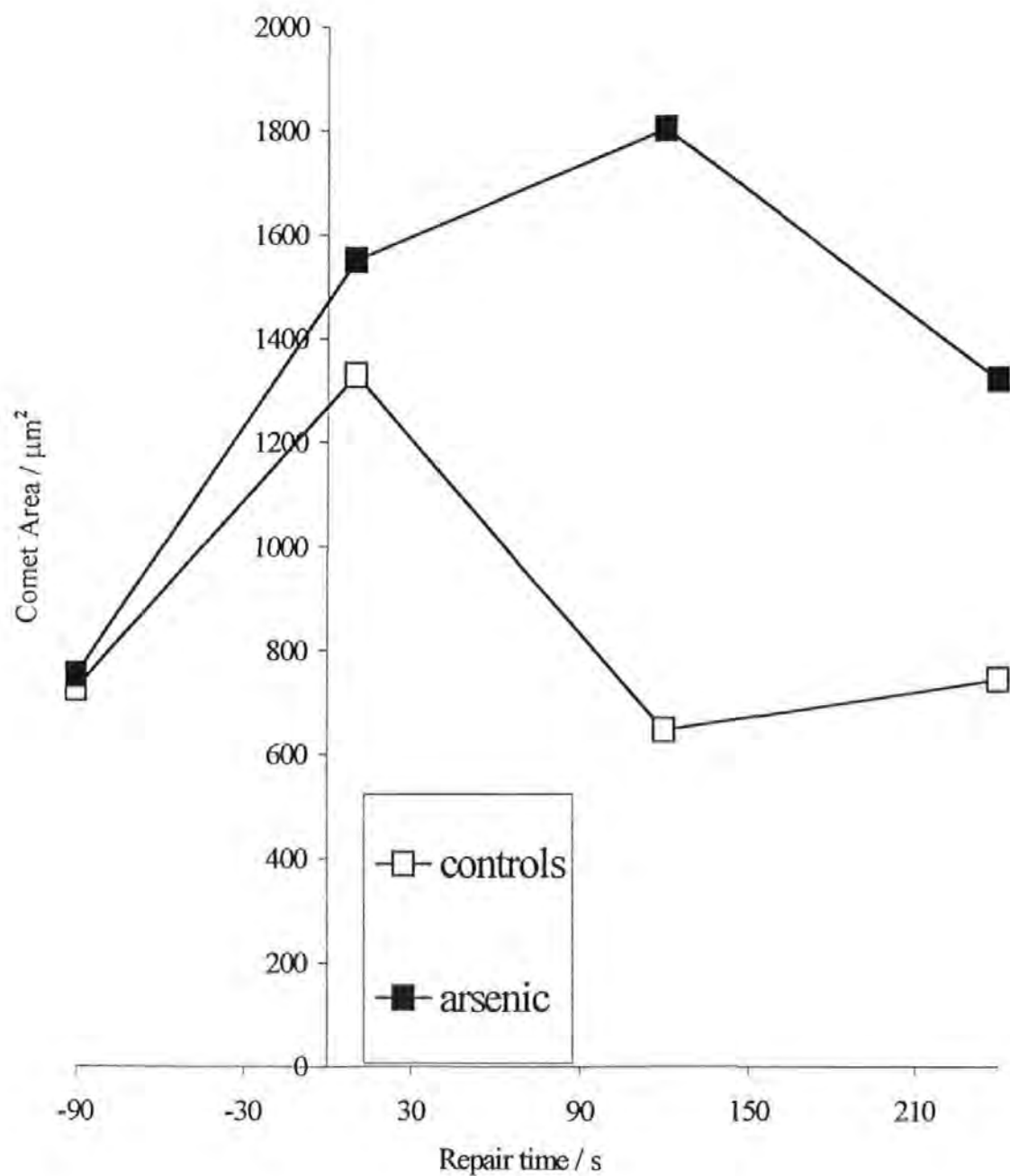
Figure 8.18 MRC5 fibroblasts were incubated in 100 μM As(V) for 30 minutes and 405 nm irradiated for 90 s and allowed to repair for 10 s, 120s and 240 s before being assayed and read back by image analysis using the parameter of Tail Moment.
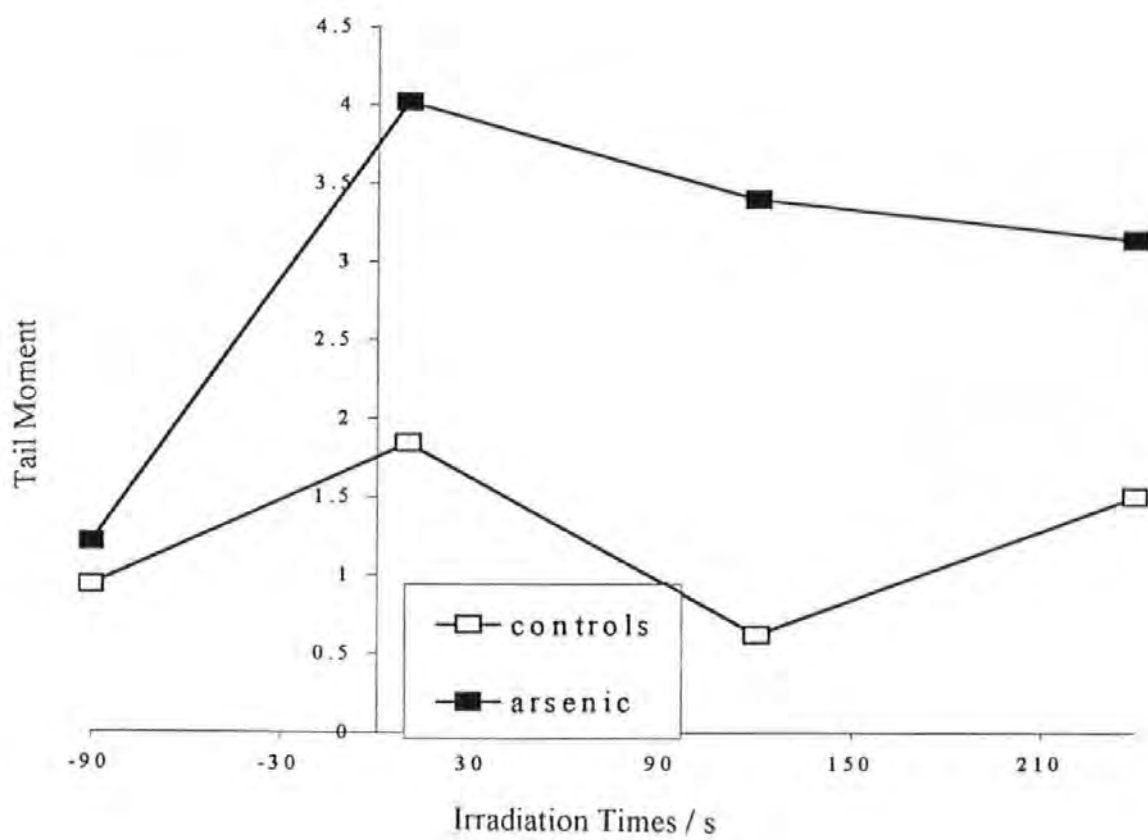
Figure 8.19 MRC5 fibroblasts were incubated in 100 μM As(V) for 30 minutes and 405 nm irradiated for 90 s and allowed to repair for 10 s, 120s and 240 s before being assayed and read back by image analysis using the parameter of Comet Moment
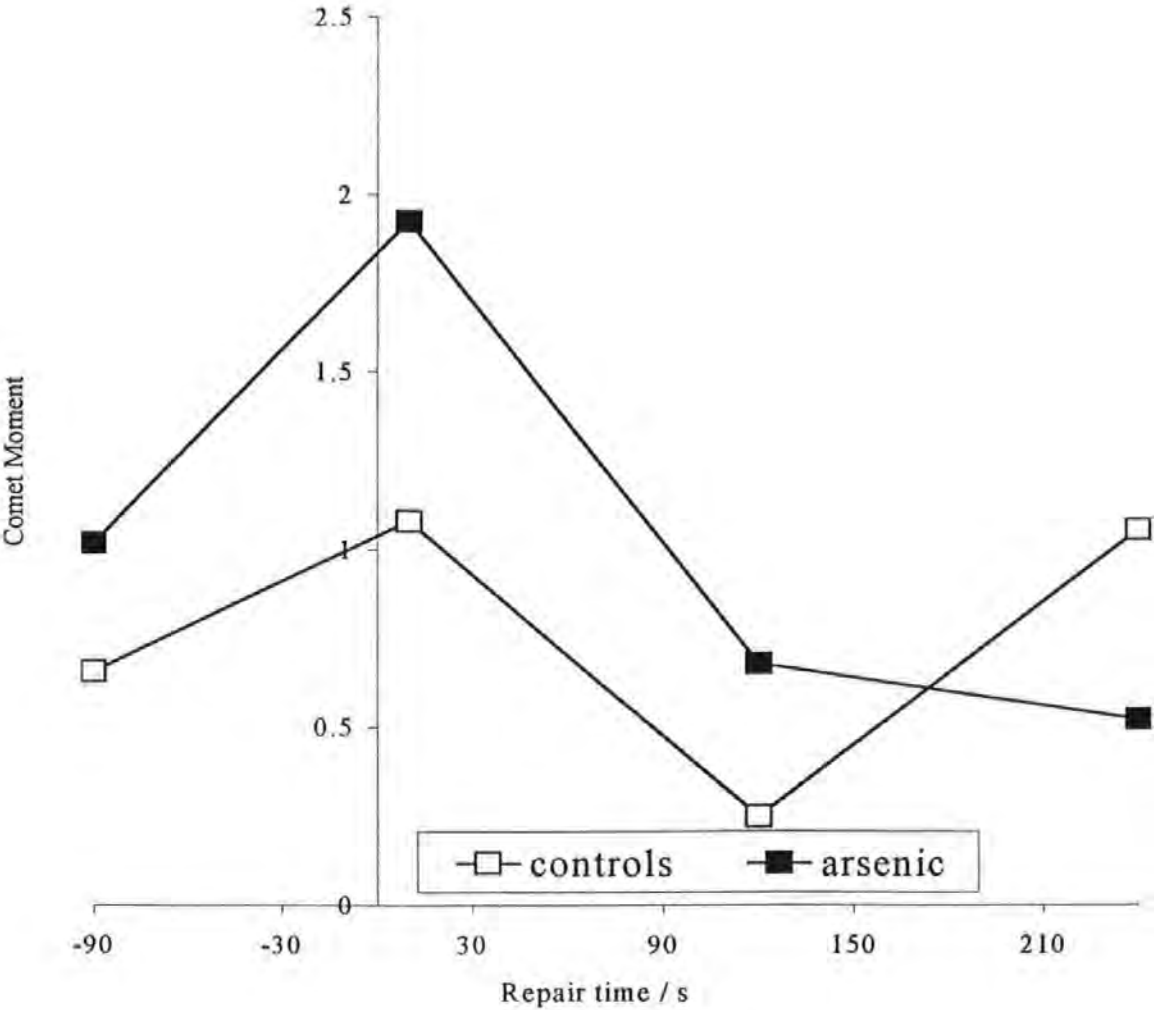
Figure 8.20 MRC5 fibroblasts were incubated in 100 μM As(V) for 30 minutes and 405 nm irradiated for 120 s and allowed to repair for 10 s, 120 s and 240 s before being assayed and read back by image analysis using the parameter of Comet Area.
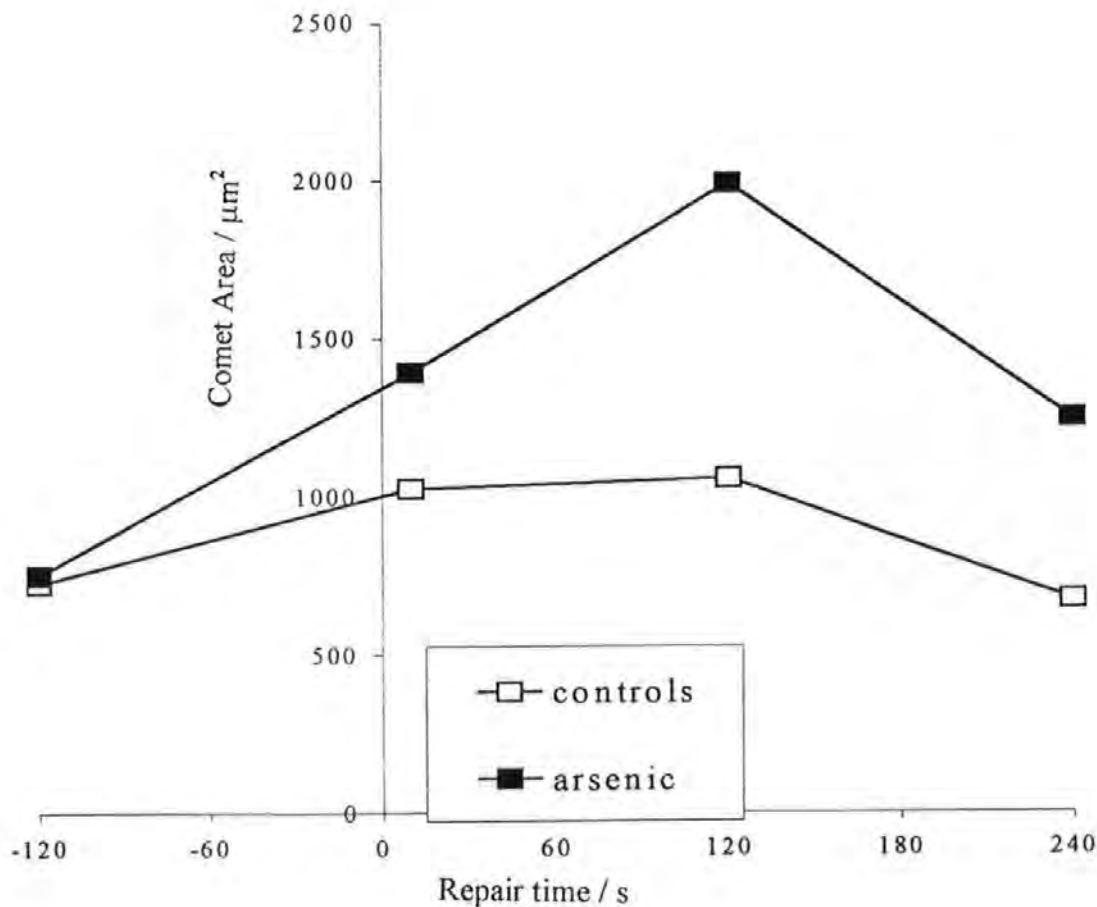
Figure 8.21 MRC5 fibroblasts were incubated in 100 μM As(V) for 30 minutes and 405 nm irradiated for 120 s and allowed to repair for 10 s, 120 s and 240 s before being assayed and read back by image analysis using the parameter of Tail Moment
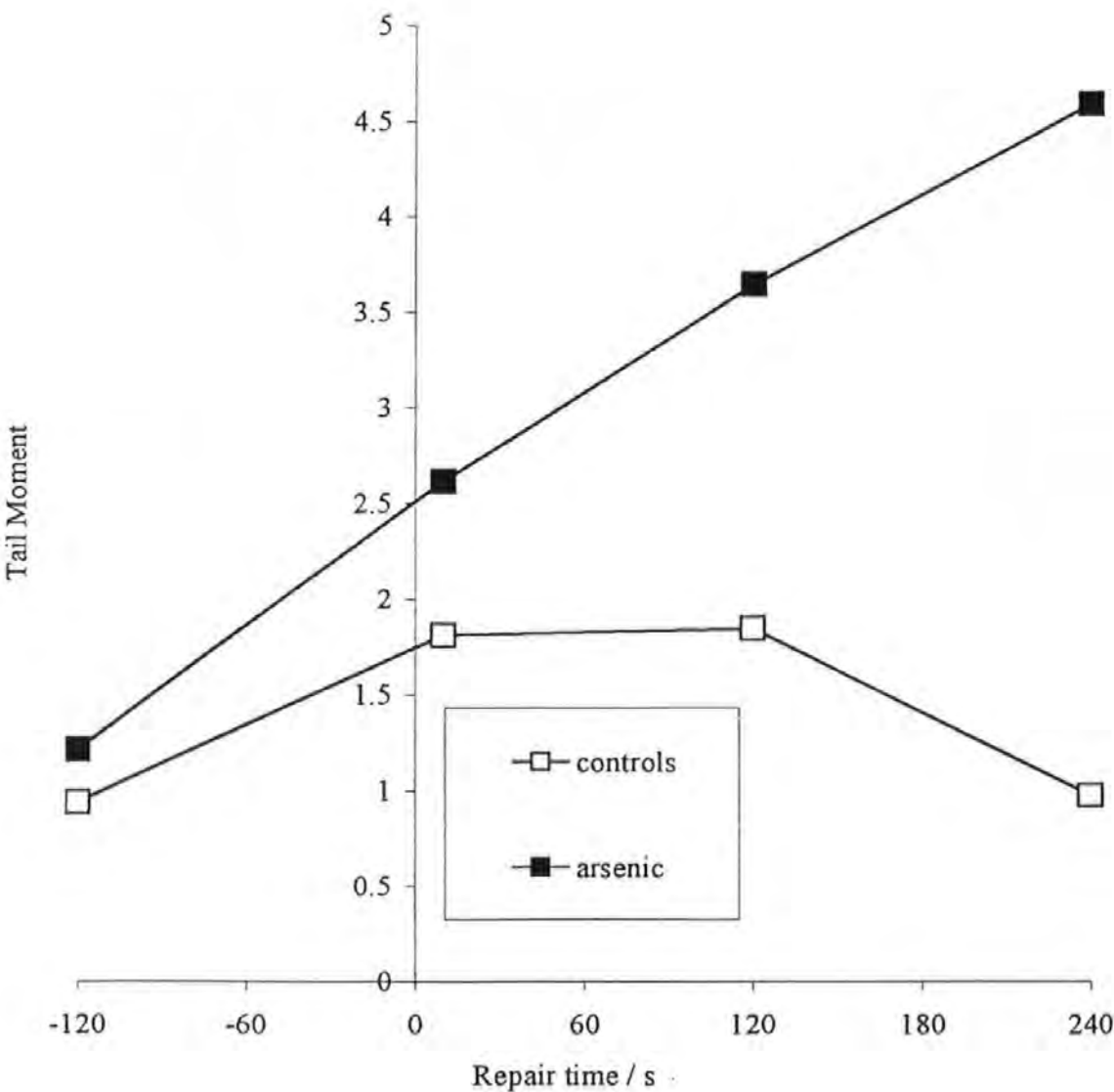
Figure 8.22 MRC5 fibroblasts were incubated in 100 μM As(V) for 30 minutes and 405 nm irradiated for 120 s and allowed to repair for 10 s, 120 s and 240 s before being assayed and read back by image analysis using the parameter of Comet Moment
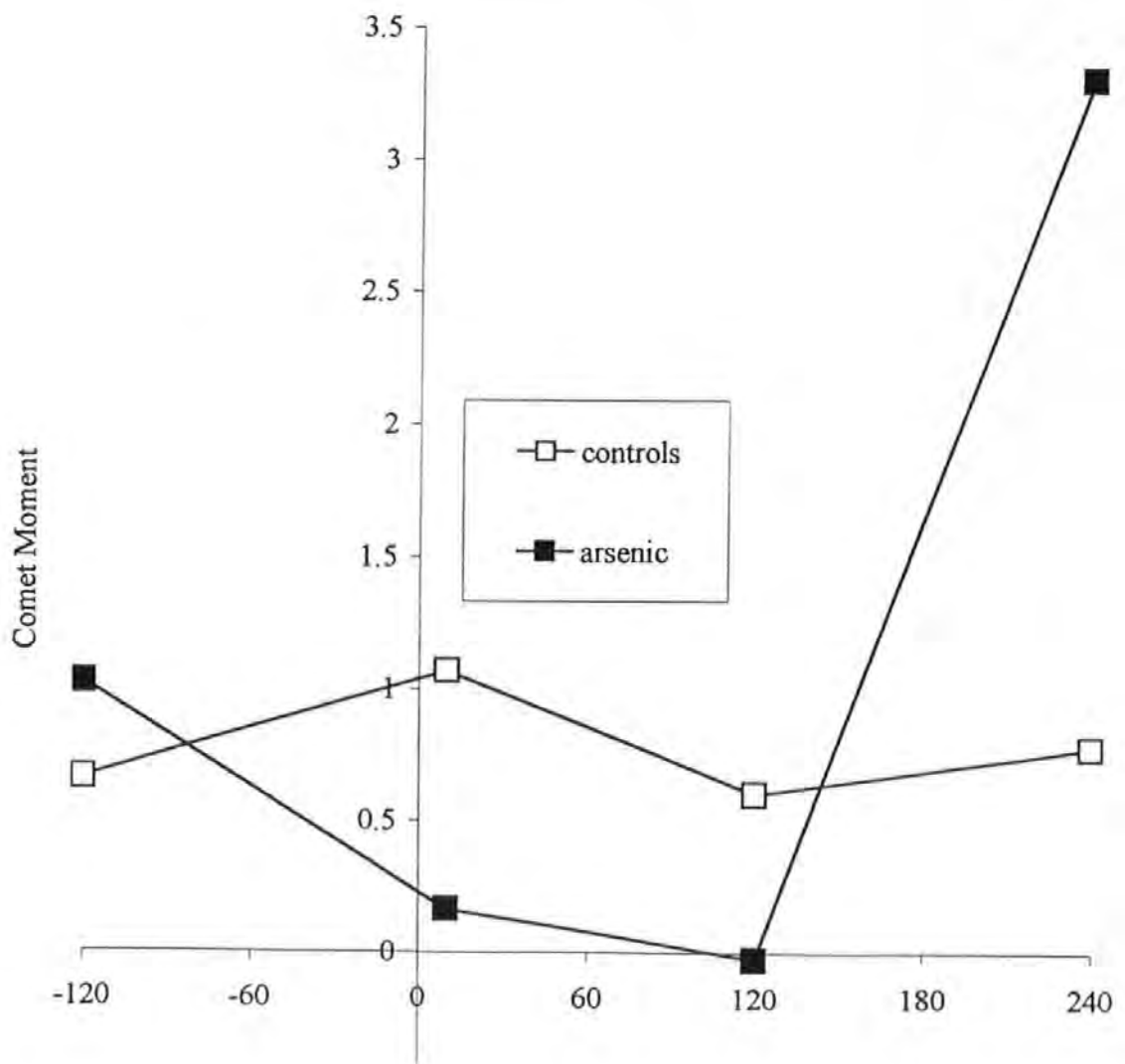
8.3 SUMMARY

A wide range of normal cellular processes in human cells are subject to modulation by arsenic and this has been demonstrated in this chapter. Specifically it was shown that:

(i)   Arsenic alone does not cause SSB in the cells under test

(ii)   SSB can be increased in cells after some treatments with arsenic prior to 405 nm irradiation

(iii)   One possible cause of an increase in SSB was demonstrated: arsenic was shown to inhibit the SSB repair process

(iv)   The ligation stage of Base Excision Repair was also inhibited by arsenic

(v)   The excision of some lesions (at least) was not inhibited by arsenic

(vi)   Arsenic was shown to induce a cellular response that appeared to eliminate SSB. This was attributed to DNA crosslinking as (suspected crosslink) excision activity had the effect of increasing the number of strand breaks assayed

(vii)   The excision of DNA crosslinks was not inhibited by arsenic

(viii) Enhanced UVR-induced SSB was observed after 30 minutes exposure to arsenic

(ix)   Reduced UVR-induced SSB was observed after 60 minutes exposure to arsenic; longer exposure reduced SSB even further

(x)   The cellular response that reduced UVR-induced SSB was also observed in the non-arsenic treated controls. This cellular response was not therefore entirely due to arsenic treatment

These data are discussed in the following chapter.

9 CHAPTER 9.

MODULATION OF THE NORMAL REPAIR RESPONSES OF

HUMAN CELLS BY INORGANIC ARSENIC

DISCUSSION

9.1 INTRODUCTION

In the work described in the previous chapter it was found that arsenic did not induce SSB by itself, although arsenic-treated cells displayed arsenic-related perturbations of normal cellular processes. Inhibition of DNA repair was observed in a number of experiments. Importantly, it was shown that 30 minutes exposure to 100 µM inorganic arsenic (V) inhibited SSB ligation after low doses of 405 nm radiation in normal human fibroblasts (Section 8.2.6). The excision repair of lesions induced by higher doses of inorganic arsenic (V) (200 µM x 1 hr) was also inhibited at the ligation stage (Section 8.2.5). The exposure of cells to arsenic was seen to induce either crosslinking or a protective response in a concentration-related manner (Section 8.2.4.1). It appeared that crosslinking was the more likely as phenomena that could be interpreted as excision and repair of crosslinks could be detected after some treatments. This supposed repair activity was more effective at the lower arsenic concentrations and would indicate that the excision stage of crosslink repair is not inhibited by arsenic. The time course of the arsenic-induced effects was measured: it was observed that ligation was inhibited after 30 minutes exposure, while the induction of cross links was apparent after 60 minutes (Section 8.2.4.2). For this reason, to discuss arsenic exposure in terms of µM h^{-1} would be misleading.

The comet assay is subject to an equilibrium thus (As↑ = enhanced by arsenic;

As↓ = inhibited by arsenic)

"Increased" comets ◄─────────────────► "Decreased" comets

Strand breaks	(As↑)	Strand break repair	(As↓)
Excision processes	(As↓)	Ligation processes	(As↓)
		Cross links	(As↑)
		Stress response	(As↑)
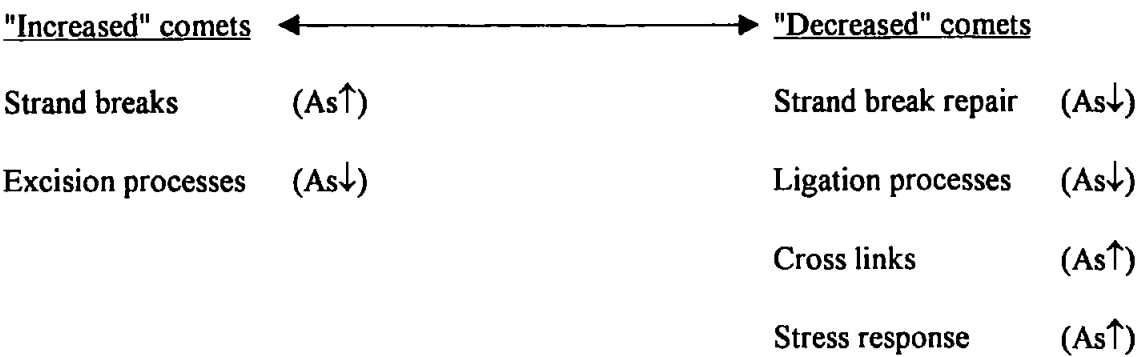
It appeared that 200 μM x 1 hr exposure represented a threshold above which the arsenic-induced perturbations resulted in an overall shift of the equilibrium to the left. However, incubation at lower concentrations of arsenic or for shorter times resulted in the equilibrium being shifted left or right to varying extents.

The purpose of this chapter is to examine the results from the previous chapter in the light of the above equilibrium. While a comprehensive review of the effects of arsenic is beyond the scope of this discussion, the main points of arsenic carcinogenesis are outlined. It is stressed at the outset that single cell gel electrophoresis, while an appropriate tool for the measurement of SSB, can not distinguish between some types of DNA damage. This is especially true when trying to distinguish between crosslinking and a protective response: both would be expected to reduce SSB. This limit on the interpretation of the results has limited the development of appropriate hypotheses.

9.2   THE EFFECTS OF INORGANIC ARSENIC ON CELLULAR SYSTEMS

9.2.1   Arsenic acts in the later stages of carcinogenesis

Inorganic arsenic is a skin carcinogen (Urbach, 1993) causing mainly squamous cell carcinoma. There is evidence for an association between male (but not female) cases of malignant melanoma and arsenic levels in stream sediments in the South-West of England

(Phillip *et al.*, 1983). Paradoxically, although no data exist for humans, arsenic is probably an essential nutrient in mammals (Levine *et al.*. 1988).

Arsenic is non-mutagenic (or at most, weakly so) (Tice *et al.*, 1997) and there is no satisfactory animal model for arsenic carcinogenesis (Jager and Ostrosky-Wegman, 1997). It appears that arsenic alone is non-carcinogenic (Jager and Ostrosky-Wegman, 1997) although it is undoubtedly co-carcinogenic: arsenic is co-clastogenic with UVR (Wiencke *et al.*, 1997) and with other compounds (Yamamoto *et al.* 1995). The co-carcinogenic effects of arsenic are mediated through a number of overlapping mechanisms and this makes the elucidation of the various processes very complex.

Arsenic is thought to act specifically as a tumour promotor by destabilising chromosomes (Barrett *et al.*, 1989; Gonsebatt *et al.*, 1997). It has been variously shown to cause sister chromatid exchanges, chromatid aberrations, aneuploidy and polyploidy, DNA amplification and morphological transformation (reviewed in Rudel *et al.*, 1996). Arsenic alters the methylation patterns in the promotor region of the p53 tumour suppressor gene (Mass and Wang, 1997) possibly disrupting the critical function of this gene. In the colorectal model of multistage carcinogenesis at least, the inactivation of the p53 protein results in aneuploidy and marks the transition to malignancy (Fearon and Vogelstein, 1990).

9.2.2 Arsenic inhibits DNA repair

Arsenic has been shown to inhibit DNA repair at several points. The detrimental effects of arsenic on the molecules responsible for the maintenance of DNA integrity are probably mediated through arsenic binding to thiol groups of the proteins involved - arsenic is known to be highly selective in reacting with closely spaced (vicinal) dithiol groups (Yager and Wiencke, 1997). Zinc finger type proteins, involved in DNA recognition and binding, contain dithiol groups as part of the recognition structure. Disruption of this structure is almost certain to affect the normal functioning of the protein.

The re-ligation of excised MMS-induced lesions (Lynn *et al.*, 1997) and MNU-induced lesions (Li and Rossman, 1989) and the interaction of the SSB binding protein poly(ADP-ribose) polymerase (PARP) (Yager and Wienke, 1997) were all inhibited by inorganic arsenic. In the previous chapter it was shown that inorganic arsenic inhibited excision repair (Section 8.2.5) at the ligation stage and arsenic also inhibited SSB repair (Section 8.2.6). SSB repair was only partially inhibited by arsenic, indicating that there may be more than one set of enzymes responsible for SSB repair. DNA Ligase III was shown to be more sensitive to arsenite inhibition than DNA Ligase II during Base Excision Repair (BER) (Lynn *et al.*, 1997). It is suggested that the partial inhibition of ligation seen in the experiments in the previous Chapter (Section 8.2.6) is primarily due to arsenic-mediated inhibition of DNA Ligase III; the lesions are repaired by other enzymes including possibly DNA Ligase II. The fidelity which these other enzymes repair SSB is unknown, if they were shown to be less accurate or effective, one of the factors contributing to chromosomal instability could be considered.

The inhibition of SSB repair by arsenic has not been demonstrated in the literature and in this respect this is a significant finding. Biologically, SSB are not considered to be an important lesion at short UVR wavelengths as the other lesions induced at these wavelengths represent considerably (up to 100 fold) more threat to cell survival whereas SSB at longer wavelengths are, however, biologically very important (Friedberg *et al.*, 1995; Cridland and Saunders, 1994). The rapidity with which SSB are repaired (2 or 3 minutes, Section 4.2.3) may reflect the evolutionary pressure applied to the rapid repair of strand breakage. The retardation of this process could be considerably important: the probability of two SSB occurring in close enough proximity to constitute a DSB is inversely proportional to the rate of SSB repair. Any inhibition of the SSB repair process will therefore increase the likelihood of DSB and chromosomal instability. This consideration applies particularly to the repair of the 'peaks' reported in Chapter 4 (and especially so if the peak is enhanced by a photosensitising compound e.g. beta-carotene).

The repair of the transitory high levels of SSB induced by 60, 90 or 120 s of 405 nm radiation was inhibited by arsenic. Arsenic therefore inhibits SSB repair after the most minimal of exposure - approximately the equivalent of exposing unprotected skin for two minutes to rainy May morning in Cornwall - and is therefore clinically relevant. Given the possibility that the 405 nm radiation induced peak is higher in male cells than female cells, a possible mechanism for the incidence of arsenic-related melanoma in males but not females is evident.

The incision of UVC-induced lesions was inhibited by arsenic (Hartwig *et al.*, 1997). (Although this conclusion was based on the reduction of assayed SSB and could also have been due to cross linking.) The lesions induced by short wavelength UVR are removed by Nucleotide Excision Repair (NER). NER utilises over 18 proteins to effect the incision stage (Hartwig *et al.*, 1998) whereas the BER pathway utilises two proteins to effect excision (Collins *et al.*, 1995) and thus is a smaller target for arsenic inactivation of dithiol containing proteins. Excision of 405 nm induced lesions are removed by BER and were not incision -inhibited by arsenic, although ligation was inhibited (Section 8.2.5).

9.2.3 Arsenic induces DNA crosslinks

Arsenic induces DNA-DNA crosslinks and DNA-protein crosslinks (Dong and Luo, 1993; Tice *et al.*, 1997). These crosslinks are associated with DNA strand breaks (Dong and Luo, 1993); however, in the comet assay the increased strand breakage is confounded with the fact that DNA-protein and DNA-DNA crosslinks reduce DNA migration in the comet assay (Tice *et al.*, 1997). In this thesis, concentration dependent reduction of DNA migration after 1 hour exposure time to arsenic was associated with the occurrence of crosslinking (Section 8.2.4.1)

If cross links occur, then their excision also appeared to be operating effectively (Section 8.2.4.1), thus it appears that from these data that arsenic does not inhibit the excision of crosslinks, although there is no way of judging what fraction of As-induced crosslinks

could have been removed. In the absence of quantitative data this conclusion must therefore be treated with caution, and in this respect the nature and number of adducts formed need to be identified.

The studies by Lynn *et al.* (1997), Hartman *et al.* (1997) and Li and Rossman (1989) employed arsenic incubation times of 2 or 4 hours, 18 hours and 3 hours respectively. These times would be sufficient to allow the induction of the protective stress response seen in Section 8.2.4.2 . The paper by Hartwig *et al.* (1997) demonstrated different effects of UVC + 20 μM As(III) to UVC + 10 μM As(III). Although the former induced a higher level of SSB compared to the controls, the excision and re-ligation kinetics paralleled the controls closely. The use of 10 μM As(III) initially reduced the UVC-induced SSB (which the authors attributed to impairment of excision), but an increase in SSB was observed with time. This was followed by a retarded (compared to the controls) ligation process. In the light of the experiments described in the previous chapter, the following alternative interpretation is offered. The reduction in initial SSB is due to DNA crosslinking and the excision activity measured is due to the excision of crosslinks and not the excision of UV-induced lesions. The retarded ligation is due to arsenic inhibition of DNA Ligases as reported in the studies by Li and Rossman (1989), Lynn *et al.* (1997) and as reported in this thesis. Arsenic (III) is 10 times more potent in its effects than arsenic(V) (Barrett *et al.*, 1989). The 20 μM and 10 μM As(III) concentrations employed by Hartman *et al.* (1997) are therefore comparable to the 200 μM (at which concentration an overall inhibition of DNA repair was observed) and 100 μM (at which concentration crosslinking was observed after 60 minutes exposure) concentrations of As(V) employed in this thesis.

9.2.4 Arsenic induces a specific stress response

Arsenic causes the generation of reactive oxygen species (Yamanaka *et al.*, 1991; Nordenson and Beckman, 1991) that may be responsible for the arsenic-mediated

280

induction of cellular shock proteins that has been observed (Welch and Suhan, 1986), although arsenic and some other metals also induce a unique 32 kDa stress protein. Arsenate is similar in structure and chemistry to phosphate and can compete for and replace the phosphate moiety in a variety of metabolic processes (Aposhian, 1989). This can lead to arsenate incorporation into DNA, the uncoupling of oxidative phosphorylation and the subsequent inhibition of glycolysis (Aposhian, 1989). This may also induce the stress response, not least as the response is sensitive to glucose concentration (Welch and Suhan, 1989).

It was observed that the protocol used to examine the time course of induction of the arsenic-induced stress response or crosslinking appeared to induce a stress response in non-arsenate treated cells, this stress response had the effect of reducing SSB after high intensity radiation and appeared to parallel the reduction in strand breakage seen in the arsenate treated cells. This single observation modifies the conclusion that the reduction in SSB after arsenate treatment is solely due to DNA crosslinking and must incorporate a factor common to both treatments. In this respect, it is possible that the lifting of the cells by Trypsin is sufficient to induce a stress response that can be detected against the low dose phenomena studied.

The repair of the transitory high levels of SSB induced by 60, 90 or 120 s of 405 nm radiation was inhibited by arsenic. Arsenic therefore inhibits SSB repair after the most minimal of exposure - approximately the equivalent of exposing unprotected skin for two minutes to rainy May morning in Cornwall - and may therefore be clinically relevant. Given the possibility that the 405 nm radiation induced peak is higher in male cells than female cells, a possible mechanism for the incidence of arsenic-related melanoma in males but not females is evident.

The incision of UVC-induced lesions was inhibited by arsenic (Hartwig *et al.*, 1997) (although this conclusion was based on the reduction of assayed SSB and could also have been due to cross linking). The lesions induced by short wavelength UVR are removed by Nucleotide Excision Repair (NER). NER utilises over 18 proteins to effect the incision stage (Hartwig *et al.*, 1998) whereas the BER pathway utilises two proteins to effect excision (Collins *et al.*, 1995) and thus is a smaller target for arsenic inactivation of dithiol containing proteins. Excision of 405 nm induced lesions are removed by BER and were not incision -inhibited by arsenic, although ligation was inhibited (Section 8.2.5).

9.2.3 Arsenic induces DNA crosslinks

Arsenic induces DNA-DNA crosslinks and DNA-protein crosslinks (Dong and Luo, 1993; Tice *et al.*, 1997). These crosslinks are associated with DNA strand breaks (Dong and Luo, 1993); however, in the comet assay the increased strand breakage is confounded by the fact that DNA-protein and DNA-DNA crosslinks reduce DNA migration in the comet assay (Tice *et al.*, 1997). In this thesis, concentration dependent reduction of DNA migration after 1 hour exposure time to arsenic was associated with the occurrence of crosslinking (Section 8.2.4.1)

If crosslinks occur, then their excision also appeared to be operating effectively (Section 8.2.4.1), thus it appears from these data that arsenic does not inhibit the excision of crosslinks, although there is no way of judging what fraction of As-induced crosslinks

could have been removed. In the absence of quantitative data this conclusion must therefore be treated with caution, and in this respect the nature and number of adducts formed need to be identified.

The studies by Lynn *et al.* (1997), Hartman *et al.* (1997) and Li and Rossman (1989) employed arsenic incubation times of 2 or 4 hours, 18 hours and 3 hours respectively. These times would be sufficient to allow the induction of the protective stress response seen in Section 8.2.4.2 . The paper by Hartwig *et al.* (1997) demonstrated different effects of UVC + 20 μM As(III) to UVC + 10 μM As(III). Although the former induced a higher level of SSB compared to the controls, the excision and re-ligation kinetics paralleled the controls closely. The use of 10 μM As(III) initially reduced the UVC-induced SSB (which the authors attributed to impairment of excision), but an increase in SSB was observed with time. This was followed by a retarded (compared to the controls) ligation process. In the light of the experiments described in the previous chapter, the following alternative interpretation is offerred. The reduction in initial SSB is due to DNA crosslinking and the excision activity measured is due to the excision of crosslinks and not necessarily the excision of UV-induced lesions. The retarded ligation is due to arsenic inhibition of DNA Ligases as reported in the studies by Li and Rossman (1989), Lynn *et al.* (1997) and as reported in this thesis. Arsenic (III) is 10 times more potent in its effects than arsenic(V) (Barrett *et al.*, 1989). The 20 μM and 10 μM As(III) concentrations employed by Hartman *et al.* (1997) are therefore comparable to the 200 μM (at which concentration an overall inhibition of DNA repair was observed) and 100 μM (at which concentration crosslinking was observed after 60 minutes exposure) concentrations of As(V) employed in this thesis.

9.2.4 Arsenic induces a specific stress response

Arsenic causes the generation of reactive oxygen species (Yamanaka *et al.*, 1991; Nordenson and Beckman, 1991) that may be responsible for the arsenic-mediated

induction of cellular shock proteins that has been observed (Welch and Suhan, 1986), although arsenic and some other metals also induce a unique 32 kDa stress protein. Arsenate is similar in structure and chemistry to phosphate and can compete for and replace the phosphate moiety in a variety of metabolic processes (Aposhian, 1989). This can lead to arsenate incorporation into DNA, the uncoupling of oxidative phosphorylation and the subsequent inhibition of glycolysis (Aposhian, 1989). This may also induce the stress response, not least as the response is sensitive to glucose concentration (Welch and Suhan, 1989).

It was observed that the protocol used to examine the time course of induction of the arsenic-induced stress response or crosslinking appeared to induce a stress response in non-arsenate treated cells. This stress response had the effect of reducing SSB after high intensity radiation and appeared to parallel the reduction in strand breakage seen in the arsenate treated cells. This single observation modifies the conclusion that the reduction in SSB after arsenate treatment is solely due to DNA crosslinking and must incorporate a factor common to both treatments. In this respect, it is possible that the lifting of the cells (whether by Trypsin or not) is sufficient to induce a stress response that can be detected against the low dose phenomena studied.

10 CHAPTER 10

SINGLE CELL GEL ELECTROPHORESIS:

A TECHNICAL DISCUSSION

10.1 THE COMET ASSAY

10.1.1 Introduction

The comet assay is a relatively new technique for the measurement of DNA damage. It

can be adapted for the detection of a variety of lesions. This thesis describes pilot studies

of the application of the assay to investigate UVR-induced lesions and their repair. A

number of variants were employed to study enzymatic (i.e. excision repair related) and

non-enzymatic (i.e. direct or photosensitised) SSB and the kinetics of rejoining these

breaks. The modulation of SSB induction by UVR was achieved with the use of redox-

active reagents, and the repair of SSB was shown to be arsenic inhibitable. In addition,

arsenic was observed to reduce the number of SSB assayed in a time and concentration

dependent manner. This was attributed to DNA crosslinking although no direct evidence

for this was obtained.

The comet assay is a rapid process when automated (see below) and has the potential for

useful clinical applications as well as a basic science research tool. It was one of the

research aims of this project that the assay be developed to screen agents for

photoprotective or photosensitising properties, either by the increase or decrease in the

actual number of lesions induced or by interfering with their repair. Hence the

investigation of redox active reagents and a repair inhibitor to modulate the normal

responses of test cells.

Examination of the comet parameters by image analysis indicated that information about

the loci of SSB could be inferred. Such information would potentially be very useful. This

Chapter summarises the main attributes of the assay as employed in this laboratory.

Section 10.2 contains an evaluation of the two readback systems; a short discussion of the image analysis parameters and their suitability for investigating high and low dose phenomena. Section 10.4 concludes the chapter with the formulation and discussion of a new assay parameter: the 'Area Moment', calculated in the same manner as the Tail Moment but using the Comet Area in place of the Tail length.

10.1.2 The comet assay readback systems

How do the two readback systems compare? The visual comet scoring system has several advantages over image analysis.

1. The comets are analysed by eye and therefore not subject to the limitations of camera integration; this ensures that the whole comet is assessed.

2. Analysis by eye disregards background fluorescence: small crystals of ethidium bromide immediately adjacent to a comet tail are included in the comet by the image analysis system and falsify the comet parameters if the comet is not rejected. This is a significant consideration where cells are scarce. Similarly, small areas of fluorescence from the distal parts of the tail are sometimes treated as separate comets by the software and affect the calculations.

3. Analysis-by-eye was inexpensive: the only additional equipment used in this laboratory was a hand-held Dictaphone to record comet scores.

4. Most importantly, the visual analysis method produced an almost identical result to the independent and blinded readback of the same experiment by image analysis. The comet assay readback system was therefore reliable with regard to objectivity.

The shortcomings of the visual scoring system are these.

1. The system is subjective and thus not immediately comparable to other laboratories' data. Within this laboratory the natural day-to-day fluctuations in assigning borderline comets resulted in high inter-assay variance.

2. The analysis-by-eye method is slow. It takes approximately 4 hours to score a 20-slide assay (the maximum number of slides that can be fitted into the same electrophoresis run). This is then read back into the computer in real time and takes approximately 3 hours. Data analysis takes 2 hours. The comet assay, when read back by eye is a 2½ day procedure.

3. There is no permanent record of results: they exist only as computer files and printouts. It is not possible to re-examine the comets or to re-analyse them.

The use of image analysis has advantages over the visual system.

1. Once the camera and software parameters are fixed, the inter-assay variance will reflect experimental conditions only. Furthermore, the data can be directly compared with data from other laboratories.

2. The image analysis system is fast. Fewer comets need to be analysed due to the objectivity; a previous assay can be read back piecemeal during any convenient times without loss of intra-assay integrity (it is thus possible to score one assay while performing another); the comet data are entered directly into a file. The comet assay procedure, when read back by image analysis is a one-day procedure.

3. More detailed information is returned. The physical parameters associated with comet formation comprise tail size and fluorescence intensity. Tail length is governed by the extent of DNA migration (i.e. the extent of DNA strand breakage). Fluorescence intensity is governed by two factors: total DNA (cell cycle dependent) and the amounts of DNA in the head and tail of the comet. Image analysis returns all of these parameters.

4. The actual comet images can be recorded on CD ROM, providing a permanent record. These images can therefore be re-analysed should the need arise.

The disadvantages of the image analysis system are these.

1. The integrating capacity of the CCD camera is orders of magnitude less than the human eye. The decision has to be taken, before analysis, as to whether the comet head or the tail is the more important region of the comet. To capture the whole tail (or as much as

284

possible of it) an upper threshold of fluorescence has to be assigned ('saturation'). This affects the analysis of DNA content: fluorescence values that fall above the threshold will be returned at the threshold value. Conversely, the saturation option if not utilised will result in partial tail capture and this will result in a loss of sensitivity to low dose phenomena.

2. The software can not accurately analyse high dose phenomena. The higher categories of comet have no peak of fluorescence at the head locus so the software assigns the comet head to the most likely peak in the image irrespective of its actual position. This returns extreme values for the comet parameters.

3. Image analysis hardware and software is expensive (~£15,000) and so represents a considerable investment in the assay itself.

The intra-assay variance was comparable (between 5% and 15% of the mean) for the same experiment when read back by both systems, but the pattern of variance differed. At low doses, the image analysis system had the lower variance whereas at the higher doses, the visual analysis system had the lower variance. A major flaw in the image analysis software is that the software pools all data by 'dose'. The distribution of comets does not follow a Gaussian distribution, making the parameter of standard deviation meaningless in this context. The means of the comets are Normally distributed and the parameter of standard deviation is a true measure of assay variance. (In all of the experiments reported, references to the standard deviation refer to the standard deviation of the means.) Grouping the data by dose would therefore result in pooling of Data Sets. If the data for replicates is used to calculate an overall mean and the spread of the replicates about that mean, the means of each determination should be calculated by the use of a code, with each slide in an assay being assigned a different 'dose'.

The use of both visual and image analysis readback systems has found acceptance in the literature. Both systems have advantages over the other, and taken together, the two systems overlap and provide a robust readback system.

285

10.1.3 Image analysis parameters

The image analysis system provides several readback parameters, some of which are more suited for the measurement of low or high dose phenomena. These are discussed below. SSB introduced into supercoiled DNA cause, first, relaxation of the DNA supercoils into large DNA loops; and second, at higher levels of strand breakage, DNA fragments that migrate more freely in the gel than loops (Ostling and Johanson, 1984). The assay as employed in this thesis has been optimised for the detection of low dose phenomena. It was proposed that the low levels of SSB-induction by the low fluence narrow band radiation cause DNA unwinding, whereas the higher fluence total Xe lamp radiation-induced SSB cause both unwinding and subsequent fragmentation of DNA. The differences between the image analysis parameters observed for the same comets can be reconciled on this basis.

(i) The Comet Area is especially sensitive to the relaxation and expansion of the DNA supercoiled molecules after unwinding induced by low levels of SSB.

(ii) The Tail Moment and the Comet Moment are especially sensitive to the migration of fragmented DNA from the nuclear space into the comet tail caused by higher levels of SSB.

Support for this idea can be seen in Figure 2a of the paper by McKelvey-Martin *et al.* (1997) where a maximum comet head diameter was seen after 5 μM H_2O_2 treatment (in a series of 0-15 μM H_2O_2). The authors concluded that head diameter was not a useful parameter of comet analysis, but in the light of the above it may prove useful for low dose phenomena.

The Tail Moment is calculated on the basis of the migration of the bulk of the DNA; i.e. it is calculated from the distance between the centres of mass in the comet head and comet tail (Olive *et al.*, 1990) and the fraction of total DNA in the comet tail. It is thus largely independent of Comet Area. Examination of the dose responses measured by Tail Moment

and by Tail length shows this very close relationship. The Tail Moment should be largely unaffected by DNA unwinding.

The Comet Moment is calculated by a different method (Kent *et al.*, 1995) incorporating the whole comet image. The migration of DNA is measured from the centre of mass of the comet head. Distances towards the anode have positive values and distances towards the cathode have negative values. An undamaged cell will thus have a Comet Moment close to zero, and the Comet Moment will increase with dose as more fragmented DNA migrates into the comet tail. The DNA mass will consist of both supercoiled DNA and relaxed loops of DNA and expansion of the loops will be restricted by the sides of the perinuclear cavity in the agarose. If the expansion of the DNA loops is biased towards the direction of the cathode, for example by immobilised DNA at replication centres (Jackson and Cook, 1986; Klaude *et al.*, 1996) or by arsenic induced crosslinking to fixed cellular structures, then the Comet Moment will be a negative one and will decrease with dose (unwinding) until the fragmentation threshold is reached- above which the Comet Moment increases with dose. This was clearly observed in the YLB7L cells (see Figure 4.8).

10.2 THE AREA MOMENT: A NEW ASSAY PARAMETER FOR THE MEASUREMENT OF LOW DOSE PHENOMENA.

10.2.1 Description

It was proposed above that the Comet Area is sensitive to the relaxation of DNA supercoiling induced by low numbers of SSB. The Tail Moment was developed to linearise high dose phenomena and thus contains an inherently reduced sensitivity to low dose phenomena. The Comet Moment appears sensitive to unwinding although it was not possible to consistantly predict whether the Comet Moment would increase or decrease with DNA unwinding.

One of the difficulties encountered in this work was the failure to achieve statistical significance at low doses. This was due to a number of factors, one of which was a high

287

assay variance. It was necessary to employ high concentrations of modulants and /or high levels of unfiltered radiation to increase the signal to noise ratio sufficiently to achieve statistically significant results. While this approach is useful, in that the unfiltered Xe lamp radiation is a useful model of sunlight (Henderson, 1970), it was one of the primary aims of the project to investigate the effects of narrow band radiation.

It was considered that the use of a new parameter, calculated as the product of the Comet Area and the DNA content of the tail (and therefore closely related to Olive's Tail Moment) might provide a more robust parameter for the detection of small changes. The image analysis-derived data were copied and 'backed up' to a second computer and the comet assay analysis software was rewritten to calculate an 'Area Moment' as follows. For each comet image, the Comet Area was multiplied by the fraction of DNA in the tail and then analysed by the software macros. This generated a mean Area Moment in addition to (and directly comparable with) the means of the other parameters described throughout this thesis. The mean Area Moment for every image analysed experiment described in the preceding chapters was calculated in this way. In all 12,968 comets from 223 treatments (223 'batches' of comets) were reanalysed.

10.2.2 Dose responses measured by the Area Moment

It was hypothesised that the Area Moment would have qualities of both the Comet Area and the Tail Moment i.e. it would be sensitive to DNA unwinding at low doses but still retain linearity at high doses. Figures 10.1 to 10.4 are representative examples of previously described experiments and show the qualities of the Area Moment 'in action'. It can be seen from these Figures that the Tail and Area Moments measure an identical dose response in YLB7L cells (Figure 10.1) and essentially the same repair process in MRC5 fibroblasts (Figure 10.2). The dose responses of MMB4L cells to 310 nm or 405 nm or unfiltered radiation show a close relation ship to each other when analysed by the Area Moment (compare, for example, Figure 10.3 with Figures 4.19 to 4.23) The two peaks

observed in PUTKO cells after total Xe radiation are more pronounced than when analysed by other parameters (compare Figure 10.4 with Figures 4.24 to 4.28). The Area Moment is therefore a fully functional parameter of analysis directly comparable to the Tail Moment.

Figure 10.1 The dose response of YLB7L cells to 405 nm radiation measured by the Tail Moment and the Area Moment. This is the same experiment that is described in Section 4.2.2.3
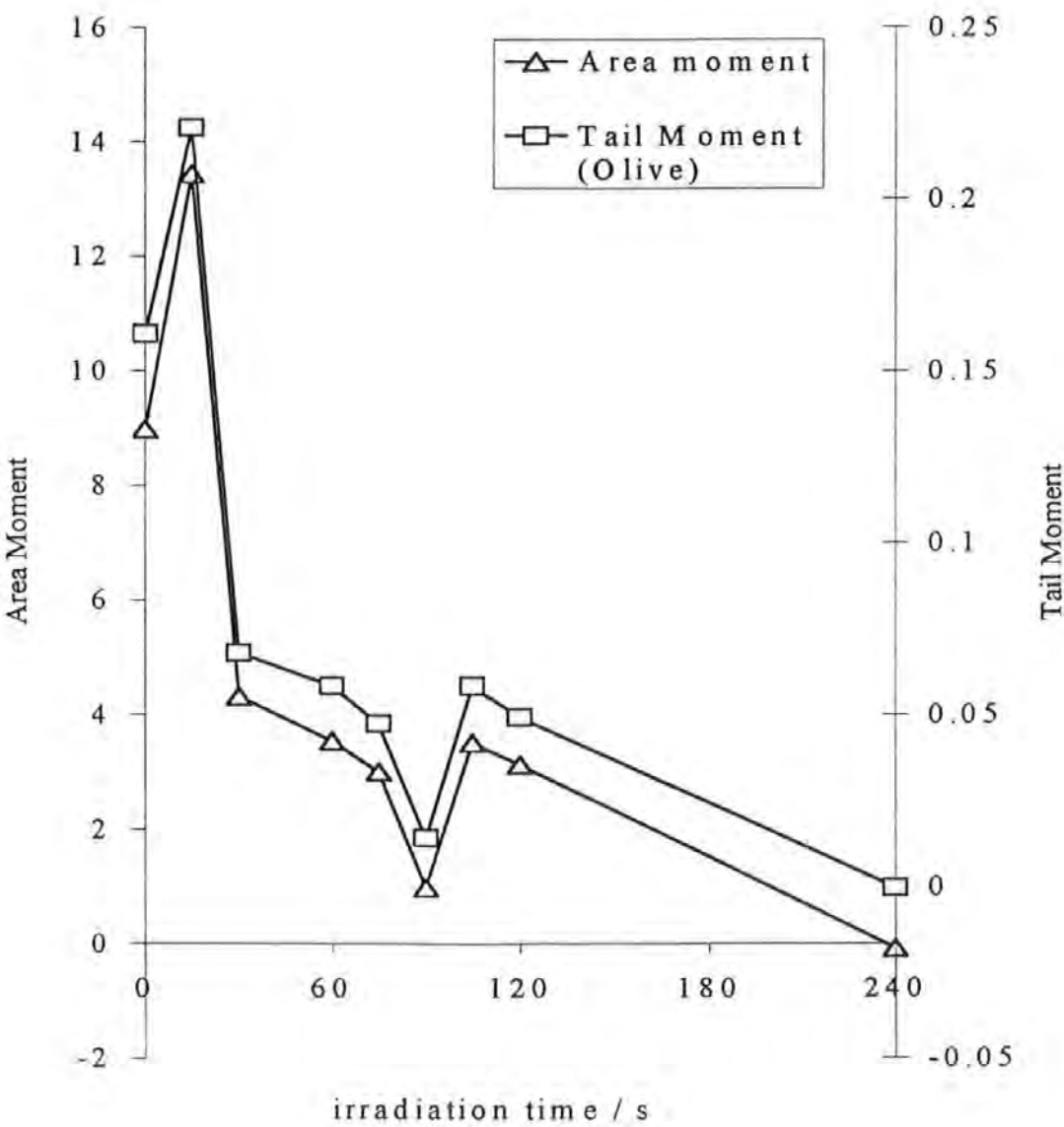
Figure 10.2 The repair of SSB in MRC5 fibroblasts measured by the Tail Moment, Comet Moment and Area Moment. This is the same experiment that is described in Section 4.2.3
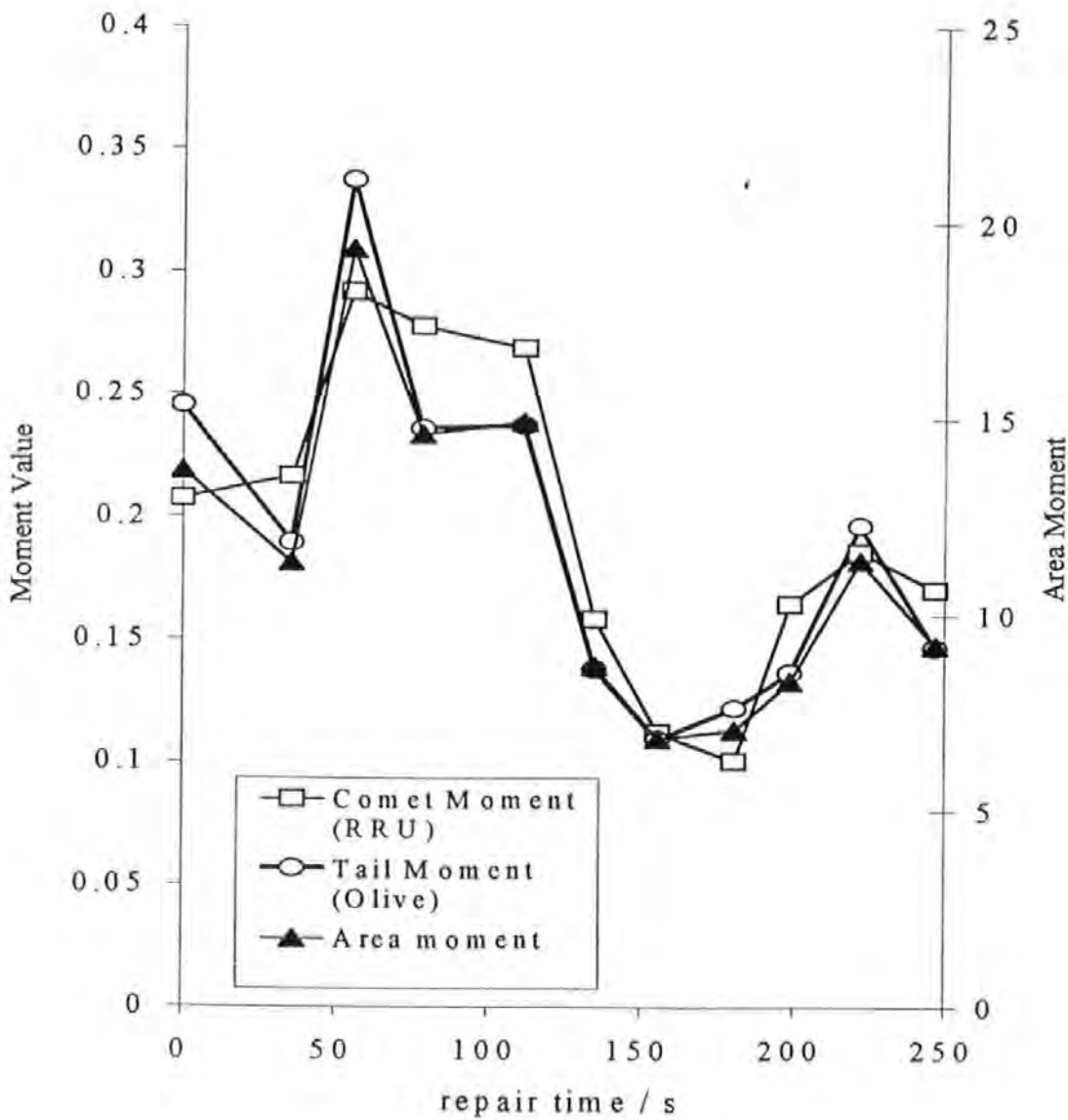
Figure 10.3 The dose responses of MMB4L cells to 405, 310 and unfiltered Xe radiation measured by the Area Moment. This experiment is described in Section 4.2.2.6
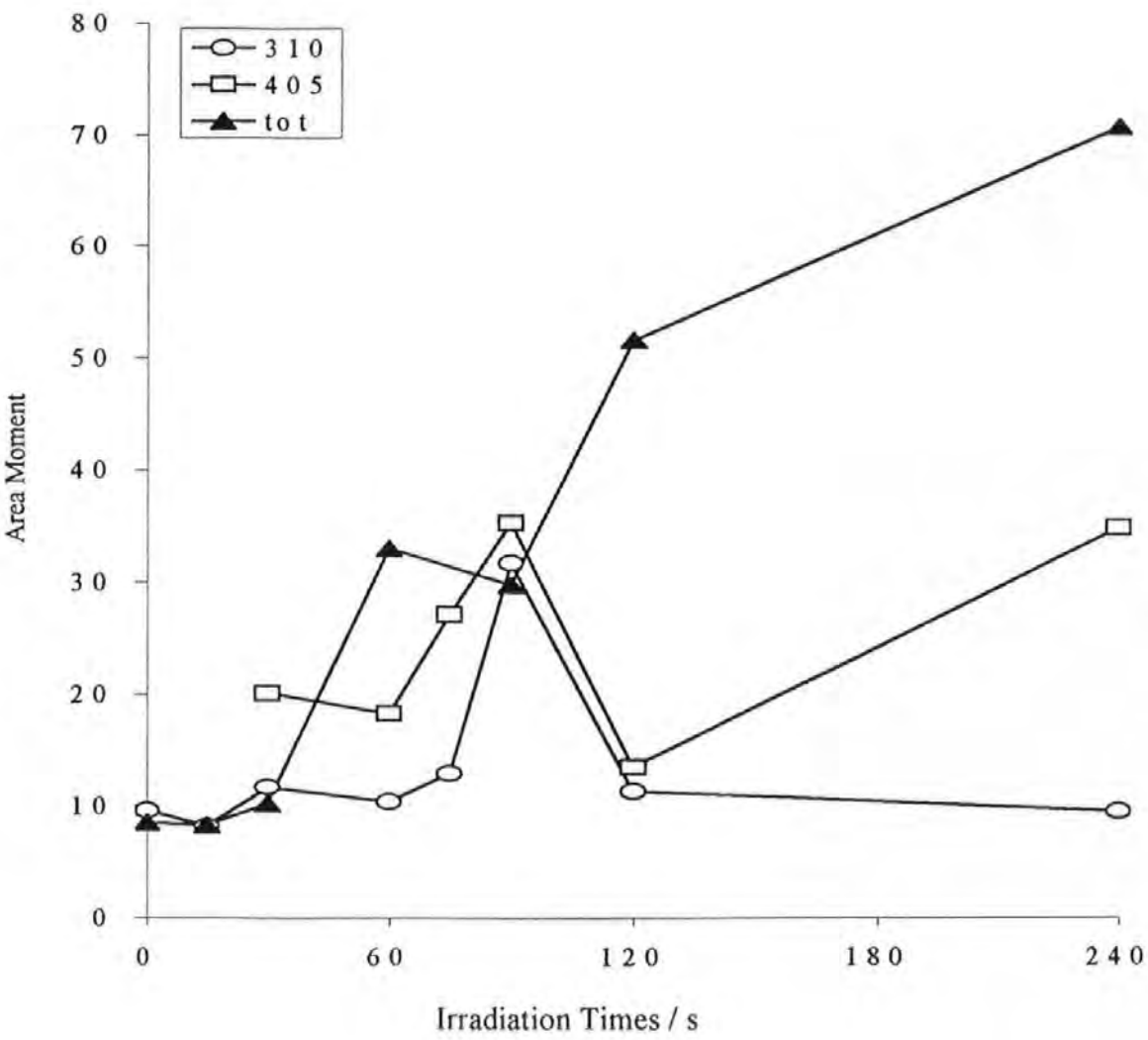
Figure 10.4 The dose responses of PUTKO cells to 405, 310 and unfiltered Xe radiation measured by the Area Moment. This experiment is described in Section 4.2.2.6.6
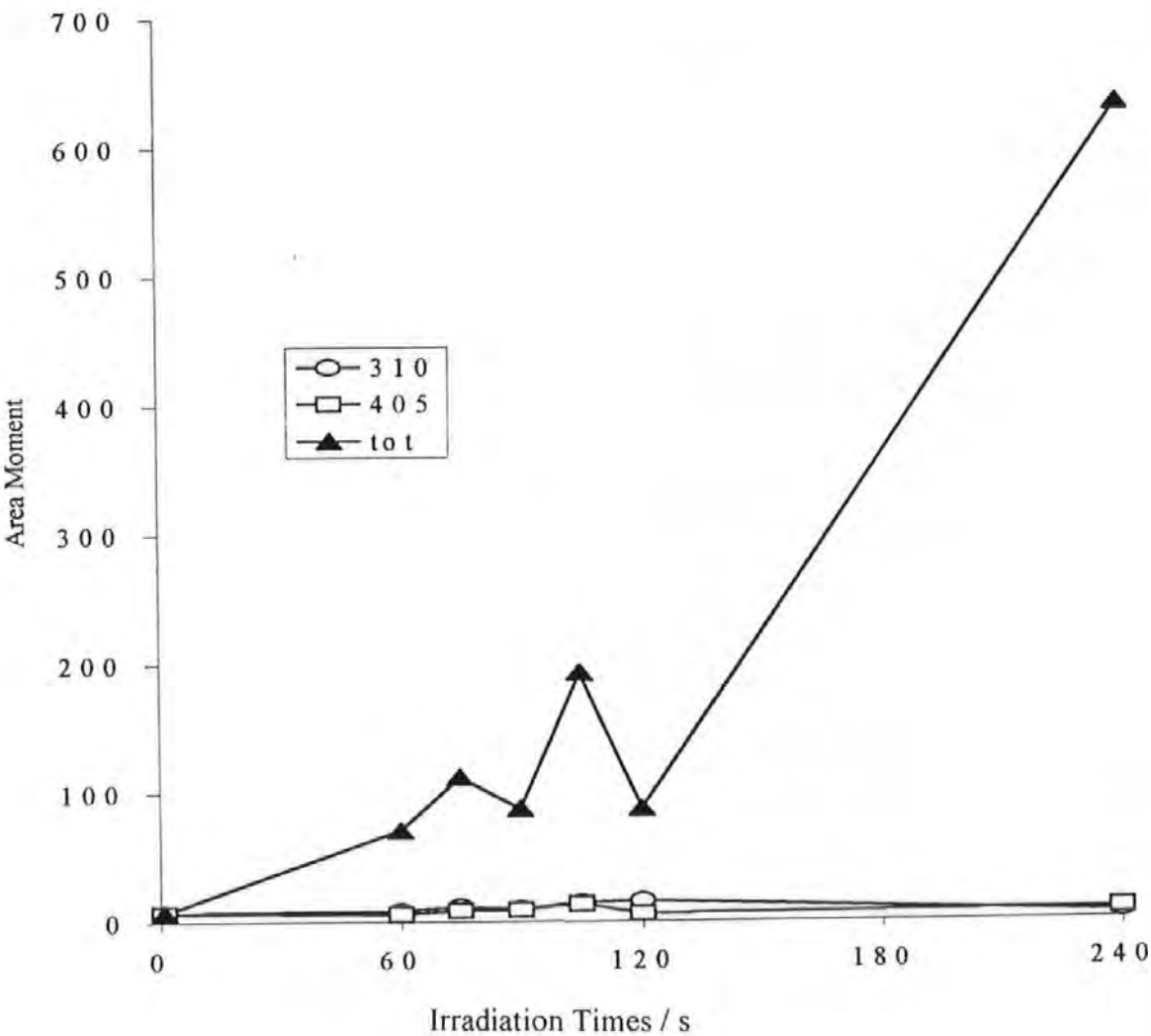
10.2.3 *Coefficients of Variation of Image analysis parameters*

Coefficients of variation (CV) were calculated for the four parameters of Comet Area, Area Moment, Tail Moment and Comet Moment as follows. The mean parameter value for each batch of comets was divided by its standard deviation and expressed as a percentage by multiplying by 100. Batches containing less than 50 comets were rejected

CV values were calculated for each assay parameter for 204 batches (12, 326 comets). From these the mean CV and standard devition, the minimum and maximum CV values were calculated (Table 10.1); the distribution of CV for the Comet Area, Area Moment and Tail Moment are displayed as histograms in Figure 10.5 . The distribution of the Comet Moment is markedly different to that of the other parameters (Figure 10.6) due to the negative Comet Moment values in the source data; in addition the range of values is very large by comparison.

It can be seen from Table 10.1 that the Comet Area has the lowest mean CV, the three Moments have a mean CV which are similar, approximately 3 times that of the Comet Area. The range of CV was smallest for the Comet Area and highest for the Comet Moment (approximately 24 times that of the Comet Area). The Tail and Area Moments had similar mean CV values, approximately 4-5 times that of the Comet Area. The Area Moment is therefore as reliable a parameter as the Tail Moment based on the (n=204) data set. The population variances were estimated for the four parameters. Predictably, the Comet Area had the lowest estimated variance, the Comet Moment the highest (~20 times that of the Comet Area) and the Area and Tail Moments similar values (~twice that of the Comet Area). Of the Tail and Area moments, the estimated variance of the Area Moment was marginally lower

Figure 10.5 The distribution of the Coefficients of Variation in various treatments assayed by Comet Area, Area Moment and Tail Moment

Each division = 5% of the range of CV for each parameter
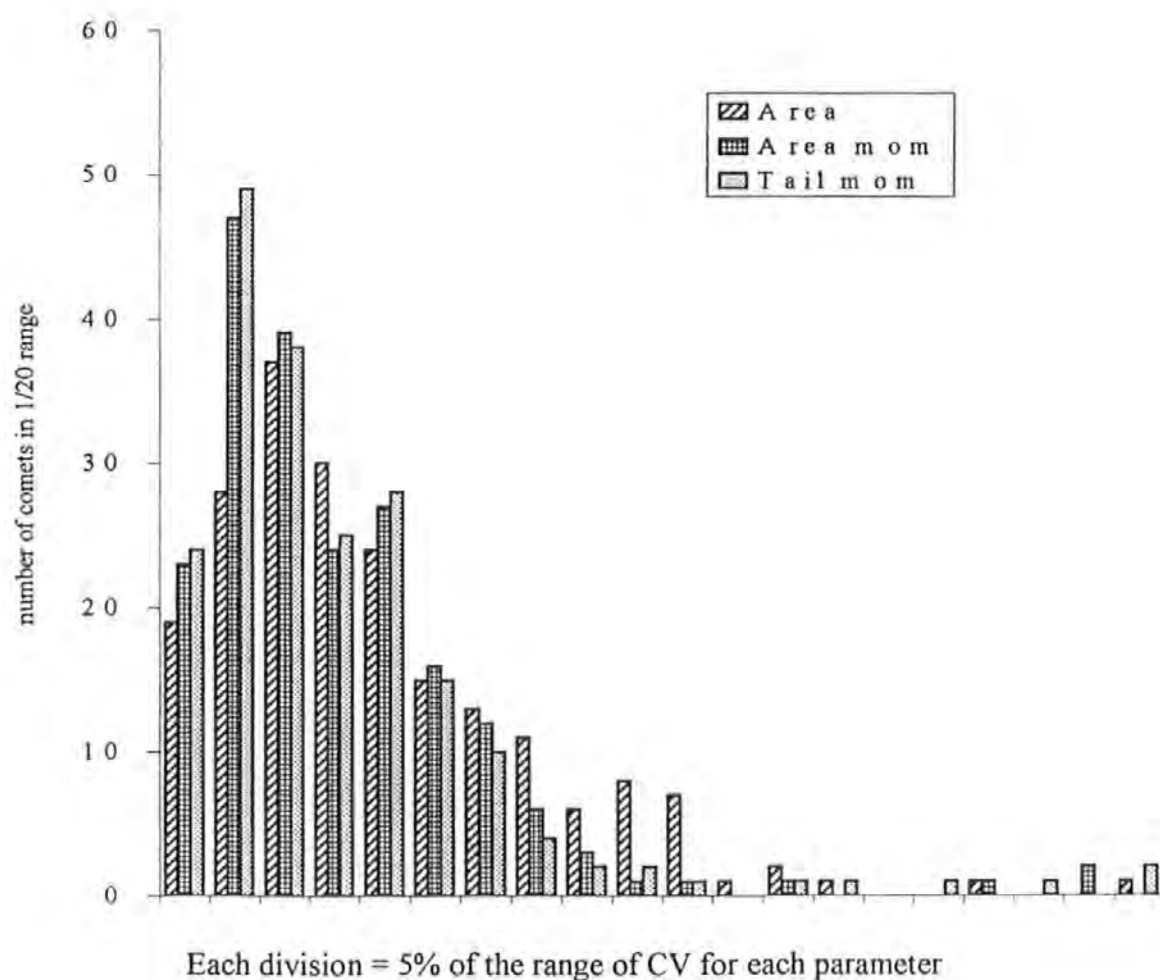
Figure 10.6 The distribution of the Coefficients of Variation for a variety of treatments assayed by Comet Moment

Each division = 5% of the range of CV for the Comet Moment
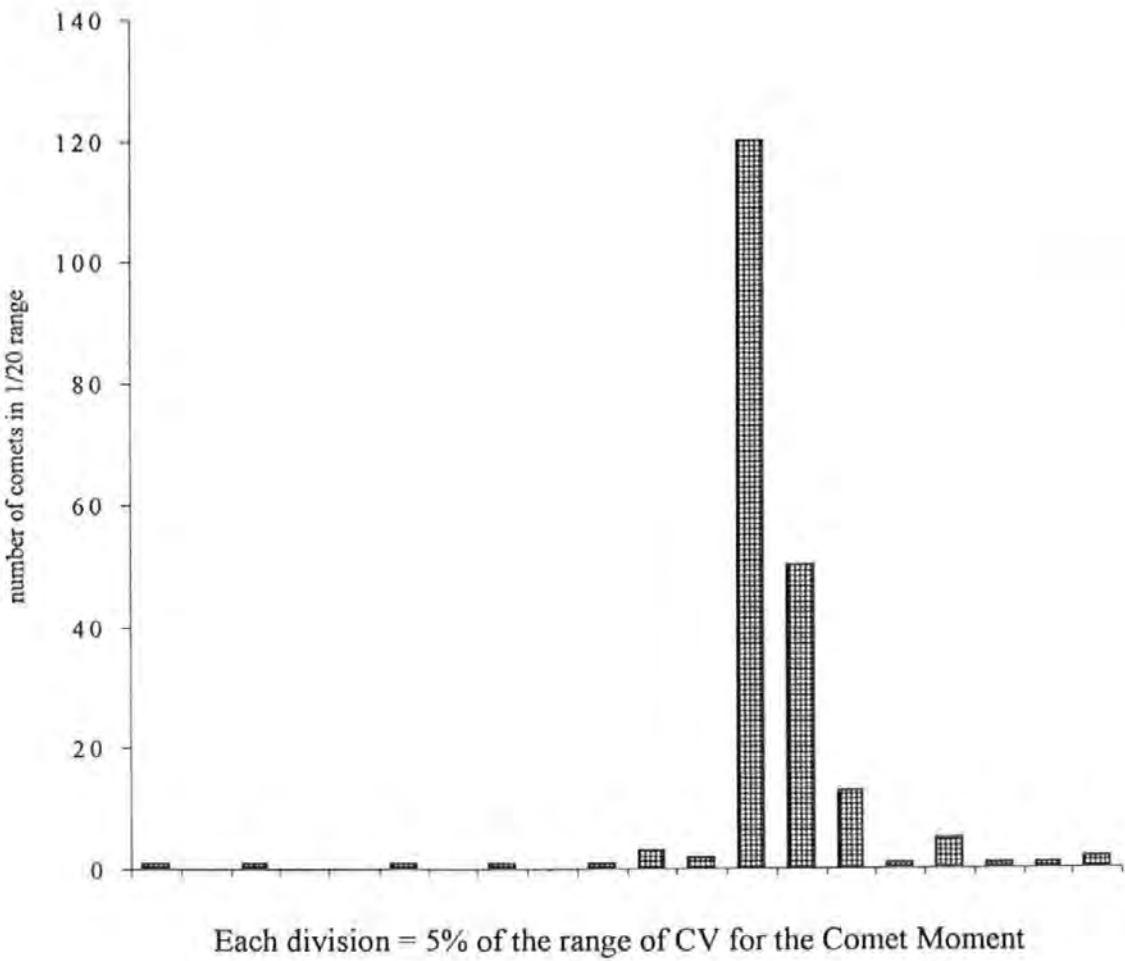
Table 10.1 The Coefficients of Variation for the image analysis parameters of Comet Area, Area Moment, Tail Moment and Comet Moment calculated from the whole (n=204) data set that fitted the inclusion criteria

	Area	Area Moment	Tail Moment	Comet Moment
Mean CV	42.3	163.5	159.1	161.4
Standard Deviation	22.6	97.9	98.3	316.8
Minimum CV	11.3	50.2	48.0	-2039.4
Maximum CV	152.8	695.9	687.1	1364.4
Estimated Variance	5.1	95.9	96.6	1003.6

The Area Moment, however, was formulated to be sensitive to low dose phenomena with a particular application of measuring small differences between the effects of various treatments. The data for the image analysed experiments for which (a) at least duplicate batches containing (b) at least 50 comets from (c) each of the control and modulated cells described in Sections 6.2.1.3.2.1, 6.2.3.2, 6.2.3.3, 6.2.5.2 and 8.2.4.1 were extracted from the reanalysed data. The CV values are given in Table 10.2 . The Comet Area had the lowest CV (approximately 2-3 times lower than the Moments; of the 3 Moments, the CV was lowest for the Area Moment and highest for the Comet Moment.

10.2.4 Levels of Significance obtained with the image analysis parameters

The data for each of the four parameters were tested by t test. (The variance was first tested by f test and the appropriate form of t test subsequently employed.) The p values from the t tests are presented in Table 10.3. It can be seen that the same levels of significance were returned by analysis by Area Moment as when analysed by the Tail Moment in all but one case. In this instance, the p value calculated from the Tail Moment was of borderline significance ($p=0.056$) whereas that calculated from the Area Moment was significant ($p=0.045$). Examination of Figure 6.11 (the 'non-significant' response

measured by Tail Moment) indicates that the use of the Area Moment avoided a Type II error. This confirms that the Area Moment is potentially a useful new parameter and can better detect low dose phenomena than the three other parameters tested. This conclusion is also supported by the observation that of the four 'mean p values' calculated from the four parameters, the mean p value from the Area Moment analyses is the lowest, indicating an overall higher sensitivity to the differences between treatments.

Table 10.2 The Coefficients of Variation for the 'modulation' experiments (n=4)

Experiment	Treatment	Comet Area	Area Moment	Tail Moment	Comet Moment
PUTKO / o-phenanthroline treated + 60s unfiltered Xe lamp radiation	2.5 mM	23.2	32.5	32.2	30.0
	6.25 mM	0.6	8.6	7.7	141.2
	12.5 mM	13.8	24.4	19.4	17.2
	18.75 mM	10.1	2.7	1.5	19.9
	Mean CV	**11.9**	**17.1**	**15.2**	**52.1**
YBF15M / ACE treated + 60 s unfiltered Xe lamp radiation	Neg. Controls	22.7	49.1	52.3	56.0
	Xe only	34.6	31.3	28.4	17.9
	Xe + 30 mM	43.1	57.3	47.1	6.2
	Xe + 50 mM	33.8	45.2	39.7	36.0
	Mean CV	**33.5**	**45.7**	**41.9**	**29.0**
PUTKO 110 mM ACE treated / unfiltered Xe radiation	Neg. Controls	5.3	2.6	5.0	1.5
	ACE only	0.4	9.7	8.3	24.6
	60s Xe only	1.7	13.8	10.1	0.8
	ACE +60s Xe	3.4	9.4	6.4	9.3
	30s Xe only	0.3	12.0	11.3	16.0
	ACE +30s Xe	2.6	8.5	9.0	21.6
	120 s Xe only	17.0	26.7	38.3	4.8
	ACE +120s Xe	3.6	34.0	36.6	35.1
	Mean CV	**4.3**	**14.6**	**15.6**	**14.2**
A2058/ 700nM b-car + 90s 405 nm radiation	No b-car	8.9	30.0	32.8	74.6
	b-car treated	15.9	74.7	69.8	60.7
	Mean CV	**12.4**	**52.4**	**51.3**	**67.6**
PUTKO/ 60s unfiltered Xe lamp only	Controls	22.5	89.0	126.1	96.8
	Irradiated	7.8	18.7	19.5	24.3
	Mean CV	**15.1**	**53.8**	**72.8**	**60.6**
Overall	**Mean CV**	**13.6**	**29.0**	**30.1**	**34.7**

Table 10.3. The p values from the ttests from the experiments described in Section and Table 10.2. p values in bold are significant at 5%, p values in underlined bold are significant at 0.1%.

Experiment	Treatment	Comet Area	Area Moment	Tail Moment	Comet Moment
PUTKO / o-phenanthroline treated + 60s unfiltered Xe lamp radiation	2.5 mM vs 6.25 mM	0.8467	0.4357	0.4235	0.4999
	2.5 mM vs 12.5 mM	0.1085	0.0587	0.0547	0.0568
	6.25 mM vs 12.5 mM	0.1660	0.0628	0.0552	0.5007
	2.5 mM vs 18.75 mM	**0.0442**	**0.0034**	**0.0070**	0.0607
	6.25 mM vs 18.75 mM	0.0942	**0.0010**	**0.0010**	0.5008
	12.5 mM vs 18.75 mM	0.2298	0.1133	0.1509	0.7277
YBF15M / ACE treated + 60 s unfiltered Xe lamp radiation	Neg. Controls vs Xe only	0.3114	0.2374	0.2354	0.3438
	Xe only vs Xe + 30 mM ACE	0.4667	0.4022	0.4252	0.2174
	Xe only vs Xe + 50 mM ACE	0.4422	0.4515	0.3407	0.1306
PUTKO 110 mM ACE treated / unfiltered Xe radiation	Neg. Controls vs ACE only	0.1118	**0.0192**	**0.0158**	0.0470
	60s Xe only vs 60s Xe + ACE	**0.0043**	**0.0005**	**0.0001**	0.0060
	30s Xe only vs 30s Xe + ACE	0.0578	**0.0008**	**0.0009**	**0.0083**
	120s Xe only vs 120s Xe + ACE	0.1400	**0.0448**	0.0558	0.0916
A2058/ 700nM b-car + 90s 405 nm radiation	No b-car vs b-car treated	0.6093	0.8243	0.8047	0.4262
PUTKO/ 60s unfiltered Xe lamp only	Controls vs Irradiated	**0.0128**	0.0665	0.8672	0.0887
Overall	n p<0.05	3	3	2	3
	n p<0.001	0	3	3	0
	Mean p value	0.2430	0.1815	0.2292	0.2471

11 APPENDIX A.

THE CONSTRUCTION AND DEVELOPMENT OF THE

IRRADIATION ARRAY

11.1 METHODS

11.1.1 Dosimetry

11.1.1.1 Actinometry

The Hatchard and Parker potassium ferrioxalate actinometer was developed in the late

1950s (Calvert and Pitts 1966). It is a robust and sensitive system for measuring light

intensity over a wide range of wavelengths, from the far ultra-violet to the upper end of the

visible spectrum (up to wavelengths of approximately 570 nm). The actinometer is based

on the photochemical reduction of the iron (III) ion (Fe^{3+}) to the iron (II) ion (Fe^{2+}) with

simultaneous oxidation of the oxalate ion. The iron (II) ion produced is complexed with

the organic molecule 1-10 phenanthroline, producing an intense red colour. Iron (II) and

iron (III) ions both form a complex with 1-10 phenanthroline. The Fe^{2+} complex

$[(C_{12}H_8N_2)_3Fe]^{2+}$ absorbs light strongly at 510 nm, whereas the Fe^{3+} complex does not.

The orange-red Fe^{2+} complex is independent of acidity in the pH range 2-9 and is stable for

long periods (hours), and provides a spectrophotometric method of calculating the yield of

iron (II) ion. This value can then be converted to the number of photons absorbed by the

actinometer by reference to a table of quantum yields (which increase as wavelength

decreases) given in the literature (Calvert and Pitts 1966).

The method for actinometric determination of light intensity as described in Calvert and

Pitts (1966) uses 20 or 25 ml volumetric flasks in their procedure. This requires

appropriate volumes of photolyte and subsequent high doses of UVR (in the region of 10

to 10^3 Joules cm^{-2}) to obtain measurable conversion of Fe^{3+} to Fe^{2+} due to the long

irradiation times required for delivery of narrow band wavelengths which proved difficult to apply in this work. This was due to the low power output of the xenon arc lamp which would require irradiation times extending into several hours. The 24 well plates used for the *in vitro* culture of animal cells and modified for use as an irradiation vessel in this work (Section 11.1.1.1.5) hold approximately 3 ml each (this can be delivered with high accuracy using calibrated micropipettes). It was decided, therefore, to develop a system of actinometry using the standard 24 well plates used in tissue culture, for if such protocols could be developed then they would translate directly to the experimental systems being studied (Section 2.3).

11.1.1.1.1 Standardisation of the iron (II) solution against potassium dichromate

The standard method of potassium ferrioxalate actinometry described in Calvert and Pitts (1966) uses spectrophotometry to determine Fe^{2+} concentration. It is necessary to standardise an Iron (II) sulphate solution against potassium dichromate because the Fe^{2+} ion is liable to oxidation in solution, and thus the actual concentration of Fe^{2+} may differ from the theoretical concentration. It was also necessary to calibrate the spectrophotometer used in this work as individual instruments vary slightly in their measurement of absorption coefficients. Known dilutions of a standardised Fe^{2+} solution were complexed with 1-10 phenanthroline and the absorbance at 510 nm taken on the instrument to be calibrated. The results were plotted as absorbance versus concentration of Fe^{2+}, the gradient of the line gave the molar absorbance coefficient (ε_{510}) for the Fe^{2+} : 1-10 phenanthroline complex for that spectrophotometer.

The standard iron (II) sulphate solution was prepared as follows: 27.802 g iron (II) sulphate heptahydrate in 100 ml 1.0 M sulphuric acid was made up to 1000 ml in a 1 litre volumetric flask. The Fe^{2+} concentration in this solution was determined by the potassium dichromate method described in Vogel (1978). This method titrated the Fe^{2+} against a standard 0.0167 M potassium dichromate solution (4.903 g potassium dichromate

accurately weighed and made up to 1000 ml with distilled water in a 1 litre volumetric flask) using phenylanthranilic acid (0.1 g n-phenylanthranilic acid in 5 mM sodium hydroxide, dissolved by vigorous stirring) as an indicator (sharp green to violet red colour change at the endpoint).

After preparation, 25.0 ml of iron (II) sulphate stock solution was delivered by 50 ml A-grade burette to a 25 ml conical flask containing a rotating magnetic stirrer and 100 ml 1.0 M sulphuric acid. 0.5 ml phenylanthranilic acid was added followed by the potassium dichromate solution. Approximately 25 ml potassium dichromate was required to fully oxidise the iron (II). The stoichiometry of the reaction was used to calculate the exact iron (II) content of the stock solution: 1 mole of potassium dichromate oxidises 6 moles of iron (II). The mean of 6 determinations was used to calculate the concentration of iron (II) in the stock solution.

11.1.1.1.2 Calibration of the SP1800 UV/VIS spectrophotometer

The molar absorption coefficient, ε, is an experimentally derived constant for a particular complex or molecule. The working value of ε for each piece of equipment has to be determined by individual laboratories although a consensus value of ε_{510} for Fe^{2+} : 1-10 phenanthroline has been established at $1.11 \times 10^4 \, M^{-1} \, cm^{-1}$ in the literature (Calvert and Pitts 1966). The absorbance of the Fe^{2+} : 1,10 phenanthroline complex plotted against wavelength displayed a single maximum at 510 nm in the range 400 -700 nm.

The experimental determination of ε_{510} for the Fe^{2+}:1-10 phenanthroline complex on the SP1800 was undertaken as follows. An aliquot of 4.00 ml of the standardised iron (II) sulphate solution was diluted to 1000 ml with 50 mM sulphuric acid to yield a calibration solution of approximately 400 μM Fe^{2+} (the exact concentration of this calibration solution being calculated from the concentration of the standardised solution).

The method of calibration of the spectrophotometer described in Calvert and Pitts (1966) was adapted for use with a 24 well plate as follows: 750 µl of acetate buffer (49.22 g sodium acetate in 600 ml water and 180 ml 1.0 M sulphuric acid, made up to 1000 ml in a 1 litre volumetric flask); 500 µl 1-10 phenanthroline (0.1 g in 100 ml warm water and dissolved by vigorous stirring) and 1750 µl 50 mM sulphuric acid were added to two wells (A1 and A2) of a 24 well plate. These two wells provided the negative controls (i.e. the baseline A_{510} of the iron-free solution) to the calibration series. The positive control (A3) (i.e. the use of a highly concentrated iron (II) solution to verify that the 1,10 phenanthroline : iron (II) complex was present) was provided by the replacement of 100 µl sulphuric acid by 100 µl 0.1 M iron (II) sulphate in 50 mM sulphuric acid. The calibration series was constructed (in triplicate) by replacing between 100 µl and 575 µl (inclusive in 25µl increments) of sulphuric acid from wells A4 to D6 (the plates have 4 rows labelled A to D and 6 columns labelled 1 to 6) with the same volume of the calibration iron (II) solution. The plates were then placed in the dark. The absorbance at 510 nm was taken in the SP1800 spectrophotometer after 2 hours. The mean values of the three readings was plotted against iron (II) concentration and the data regressed to fit the function $y = mx + c$. The regression coefficient gave the experimental value for ε_{510} and was returned as 1.155 x 10^4 M^{-1} cm^{-1}. This value was subsequently used as ε_{510} in all subsequent usage of the potassium ferrioxalate dosimeter.

11.1.1.1.3 Synthesis of potassium ferrioxalate crystals

The potassium ferrioxalate crystals used to make up the actinometer are not available commercially. Hence it was necessary to synthesise these crystals. Problematically, the light sensitivity of the ferrioxalate ion requires that all manipulations are performed under red safelight conditions. These conditions were not available in the laboratory until the refurbishment was completed. Hence protocols were developed which permitted the performance of chemical actinometry in the open laboratory. Wrapping of all equipment

in multiple layers of aluminium foil to exclude light proved effective at excluding all ambient light for periods of at least 6 weeks. (This was verified by complexing aliquots of the stored ferrioxalate solutions with 1-10 phenanthroline and determining that the iron (II) content remained constant throughout this period.)

Synthesis was performed (Calvert and Pitts 1966) by adding 150 ml of 1.5 M potassium oxalate solution (41.4 g $C_2O_4K_2.H_2O$ dissolved in 100 ml H_2O and made up to 150 ml) to the foil covered reaction vessel. (This was a 250 ml conical flask fitted with a glass funnel and an angled glass tube connected to a vacuum aspirator via a Buchner flask). The solution was warmed to approximately 30 - 40 ^{0}C by an electrical hotplate. The stirrer was turned to full speed. The system was sealed and placed under reduced pressure until the soft rubber tubing connecting the apparatus to the vacuum pump just collapsed. 50 ml of 1.5 M iron (III) chloride solution (20.3 g $FeCl_3.6H_2O$ dissolved in 30 ml H_2O and made up to 50 ml) was poured into the funnel. It was added slowly to the reaction vessel until the solution was drawn down into the vessel. The temperature was maintained in the range 30 - 40 ^{0} C. The vacuum was finely adjusted to a point where the rubber tubing was partially collapsed while the clamp was in a slightly open position. This provided a steady flow of air through the warmed vessel. The vessel was left for approximately 4 hours under these conditions. (The time had been previously determined by a trial and error procedure.)

After 4 hours the volume of liquid in the reaction vessel had been reduced to an estimated 75 ml. The vacuum aspirator was closed off, and the pressure in the vessel allowed to equilibrate with the atmosphere, the clamp was then closed. The vacuum aspirator was disconnected at the Buchner flask and the crystallisation allowed to occur for three to five days.

After the first crystallisation period, the supernatant was decanted into a foil-covered 100 ml conical flask, via the funnel. It was then labelled SN(1) (for Supernatant 1). The clamp was closed and the system set up under reduced pressure as before.

50 ml distilled water was added to the reaction vessel and the system gently warmed to no more than 30 ^{0} C, when the magnetic stirrer was free from the crystallised mass within the flask. This confirmed that the crystallisation had been successful. Another 50 ml distilled water was added to the reaction vessel under reduced pressure as before, and the system was warmed to no more than 40 ^{0} C. At this point it was judged that the crystals had been dissolved as they could no longer be heard or felt to be a 'sludge' when the reaction vessel was swirled. The vessel was allowed to equilibrate as before, the tubing disconnected and the system was left in the dark for 1 week to recrystallise. The supernatant was decanted as before, labelled SN(2) and stored in a locked cupboard. The crystalline mass was warmed to 40 - 50 ^{0} C and the air flow through adjusted as before. The system was left under these conditions for approximately 6 hours, after which time the vacuum aspirator was closed and the system allowed to equilibrate with the atmosphere. The tubing was disconnected at the Buchner flask and the system left undisturbed for 2 weeks while the crystals dried. During the whole period of crystal synthesis the crystals or their solution were not exposed to ambient light for more than an estimated 5 seconds.

Two concentrations of acidified potassium ferrioxalate solution are generally employed in actinometric determinations of light intensity (Calvert and Pitts 1966), 6 mM for wavelengths shorter than 450 nm and a 0.15 M solution for wavelengths longer than this. To obtain a solution of 6mM from the supernatant SN(2) (of unknown concentration) the following procedure was used. In outline, the procedure determined the iron (II) concentration of the supernatant SN(2) and then diluted an aliquot of supernatant SN(2) in sulphuric acid to obtain the actinometer solution.

Different volumes of SN(2) were added to wells of a 24 well plate in triplicate, 750 µl of acetate buffer, 500 µl of 1-10 phenanthroline, and a volume of 50 mM sulphuric acid to make a final volume of 3.00 ml in each well. The plates were exposed to ambient light for 2 hours and the absorbance was taken at 510 nm. The volume of the SN(2) aliquot was adjusted empirically and the procedure repeated until the resulting absorbance fell within

the determination limits 0 < A (for absorbance, no units) < 2, as absorbance values above 2 are not reliable (Calvert and Pitts 1966). The procedure was then repeated in six-fold replicate with this empirically determined volume and the iron (II) concentration of the photoreduced supernatant was calculated. An assumption was made that the unexposed supernatant (SN2) contained the same concentration of iron (III). The actual equilibrium between iron (III) and iron (II) in the supernatant was not investigated.

The actinometric vessel required 50 ml of actinometer solution (6mM potassium ferrioxalate in 6.25 mM sulphuric acid). The volume needed to yield this was calculated at 2200 μl of SN(2). A solution was made up and exposed to the xenon arc lamp for different times, prior to complexing with 1-10 phenanthroline; a higher absorbance was observed in the irradiated solution than in non irradiated solution. confirmed that the actinometer was sensitive to light in a dose dependant manner. The remaining actinometer solution was exposed to ambient light for 2 hours (to ensure full conversion to the iron (II) state). The final iron (II) concentration was determined as 5.4 mM, and the volume of SN(2) used to make the actinometer solutions was subsequently adjusted to 2450 μl to make up the 6 mM solution required.

11.1.1.1.4 Actinometric measurements: an irradiation cell for use in the open laboratory

After some initial trials, a radiation cell was constructed from a 50 ml Pyrex beaker that was covered in three layers of aluminium foil in order to measure the radiant intensity of the xenon arc lamp radiation source. An accurately measured window of 1cm x 1cm was cut in a heavy duty sticky label. A window of 1.2 cm x 1.2 cm was cut in the foil covering the beaker and the sticky label placed over this hole so that the smaller window fell within the larger. The edges of the window were then stuck down to the beaker surface and coloured with black lab marker pen to prevent transmission of light through the label. A lid was made from 3 layers of foil to fully cover the open beaker and overlap the sides by 1 cm. A hole was made in this lid to allow the entry of a 200 μl pipette tip as far as the

pipette tip's shoulder. A collar was made to surround the beaker (and thus cover the window) held in place by a rubber band. A cover was made for the hole in the lid and moulded to fit irregular contours. The light proof radiation cell was clamped at a distance of 75 mm from the exit slit of the arc lamp and a rotating magnetic stirrer placed immediately below. The orientation and height of the radiation cell was adjusted so that the light path was perpendicular to and centred on the 1 cm square window.

The radiation cell was filled as follows; 50 ml 6.25 mM sulphuric acid was delivered by pipette into the cell. 2450 μl was removed by micropipette. 2450 μl of SN(2) was added to the radiation cell by micropipette (the tip having been wrapped in aluminium foil). The cover was immediately replaced over the hole and the solutions allowed to equilibrate for two minutes. Three 100 μl aliquots were removed from the radiation cell and delivered to the three wells of a previously prepared (750 μl acetate buffer, 500 μl 1-10 phenanthroline, 1650 μl 50mM sulphuric acid) 24 well plate labelled t = 0 (A4 - 6). The mean absorbance of the actinometric solution prior to irradiation was used to calculate initial iron (II) concentration.

11.1.1.1.5 Actinometric measurements: the 24 well plate method for use in the open laboratory

A 24 well plate method for actinometry was subsequently developed. The plate was prepared by the addition of 750 μl acetate buffer, 500 μl 1-10 phenanthroline, 1650 μl 50 mM sulphuric acid to each well of a 24 well plate which was then wrapped in a quadruple layer of catering grade aluminium foil leaving the upper surface uncovered. A further double layer of foil was wrapped from the top surface around to the bottom and a further single layer was used to completely enclose the whole plate. The top surface of the plate was pressed gently with the palm of the hand to reveal the positions of the wells beneath. The wells were labelled with a fine tipped lab marker. Finally the foil was pierced at the edge of each well with a 200 μl pipette tip, and the plate pressed firmly down onto the

bench until it was both level and stable. A double thickness foil sheet was folded into a cover to completely protect the plate from all ambient light.

The 24 well plates set up as above were then modified by the removal of 100 µl sulphuric acid. The same volumes of sulphuric acid (negative controls) or stock iron (II) solution (positive control) or non-irradiated 6 mM potassium ferrioxalate in 6.25 mM sulphuric acid solution (blanks) or irradiated 6 mM potassium ferrioxalate in 6.25 mM sulphuric acid solution (actinometer) were then added. Thus each well contained 750µl acetate buffer, 500µl 1-10 phenanthroline, 1650 µl 50 mM sulphuric acid and 100µl of one of the above reagents to make a total volume of 3.00 ml.

100 µl of actinometer solution was added through the holes made in the foil into the appropriate wells (i.e. unexposed solution into the wells labelled '0' other wells being labelled with the time for which the actinometer solution had been exposed). The cover was removed from the plate for as short a time as possible (judged to be a total of less than 30 seconds per plate). The actinometer was left to develop, the iron (II):1-10 phenanthroline complex containing solution withdrawn by pipette through the holes in the foil, and absorbances taken after two hours.

11.1.1.1.6 Calculation of incident radiant intensities

The amount of radiation that effected the photochemical change was calculated from iron (II) concentrations in several stages. Because the incident radiation was from a poly-chromatic source, and because Pyrex transmits only wavelengths above 300 nm (and the ferrioxalate actinometer absorbs between 250 and 577 nm) only radiation falling between the limits of 300 and 577 nm can be measured by this technique. The amount of energy of a photon is wavelength dependent and hence the amount of Fe^{2+} produced per photon absorbed (quantum yield) varies with wavelength. Hence it was necessary to weight the calculation by a factor that would compensate for the polychromacity of the radiation. This was done by assuming the total irradiance under the curve (300-577 nm) of the xenon

arc spectrum (Henderson 1970) as unity and apportioning fractions of that to defined areas under the curve (called sections 1, 2....s in the calculations below).

The weighted quantum yield was calculated as the sum of the products of the fractions under the curve and the quantum yields for the corresponding area, as given by Calvert and Pitts (1966). The weighted photon energy was calculated as the sum of the products of the fractions under the curve and the energy of one photon of the wavelength at the mid-points (rounding down) of the section.

The calculation therefore followed the sequence: conversion of absorbance to $[Fe^{2+}]$ in the radiation cell, conversion of $[Fe^{2+}]$ to number of Fe^{2+} ions in the irradiation cell, calculation of number of Fe^{2+} ions formed per unit time, calculation of weighted quantum yield, calculation of number of photons absorbed per unit time, calculation of weighted photon energy, calculation of energy delivered to system per unit time, conversion of energy to mW cm^{-2}.

Figure 11.1 The output spectrum of 3 high pressure xenon arc lamps (Henderson 1970).
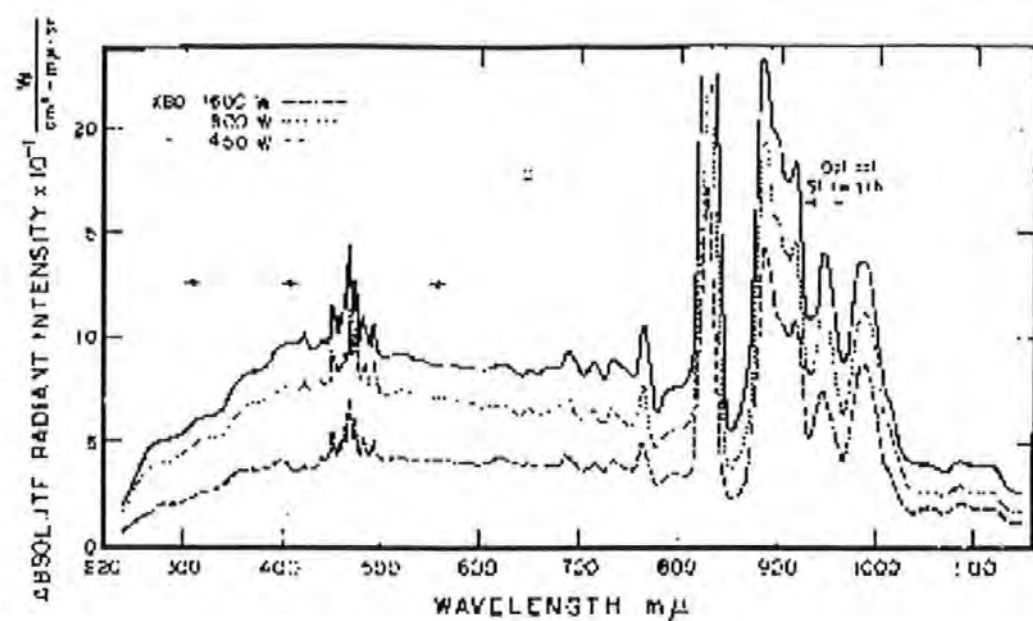
11.1.1.1.6.1 Conversion of Absorbance of the iron (II) : 1-10 phenanthroline complex at 510 nm to an iron (II) ion concentration ($[Fe^{2+}]$).

$[Fe^{2+}]$ is derived from the relationship $A = \varepsilon cl$ and the concentration of photolyte in the radiation cell is found from the formula (Calvert and Pitts 1966)

$[Fe^{2+}] = (A/\varepsilon.l) \cdot (V2/V3)$ {units: moles/litre}

where A = Absorbance

ε = molar extinction coefficient for the 1-10 Phenanthroline : Fe^{2+} complex

c = $[Fe^{2+}]$ in mol dm^{-3}

l = pathlength of spectrophotometer cuvette in centimetres

V2 = volume of diluted photolyte used in spectrophotometric determination

V3 = volume of aliquot taken from radiation cell for spectrophotometric determination

11.1.1.1.6.2 Conversion of $[Fe^{2+}]$ to number of iron (II) ions (nFe^{2+}).

nFe^{2+} is given by the formula (Calvert and Pitts 1966)

$nFe^{2+} = ([Fe^{2+}]) \cdot (N_A) \cdot (V1/1000)$

where N_A = Avagadro Constant

V1 = volume of photolyte in radiation cell

$[Fe^{2+}]$ = concentration of iron II ions in mol dm^{-3}

11.1.1.1.6.3 Calculation of number of Fe^{2+} ions (n Fe^{2+}) formed per unit time.

nFe^{2+} formed per unit time was found by subtracting $[nFe^{2+}]$ at t=T-1 from $[nFe^{2+}]$ at t=T.

where t = T-1 and t = T are consecutive points in the time series and represent 1 unit of time (seconds).

11.1.1.1.6.4 Calculation of the weighted quantum yield for Fe^{2+} formation by the XBO lamp

The weighted quantum yield was determined from the formula

$$est = (s1.X1) + (s2.X2) + \ldots\ldots(ss.Xs)$$

where est = weighted quantum yield

    ss = fraction of spectrum for section s from figure 11.1

    Xs = quantum yield for section s (Calvert and Pitts 1966)

11.1.1.1.6.5 Calculation of number of photons absorbed per unit time

The number of photons absorbed per unit time (Q) was calculated from the formula

$$Quanta = (nFe^{2+})/est$$

based on the formula for calculating the number of photons absorbed per unit time (Q) from nFe^{2+} given in Calvert and Pitts (1966) as Quanta = (nFe^{2+})/ quantum yield

11.1.1.1.6.6 Calculation of weighted photon energy

The weighted photon energy was calculated from the formula

$$E_{est} = (s1.hc/\lambda x) + (s2.hc/\lambda x) + \ldots\ldots(sx.hc/\lambda x) \quad \{units: \ Joules\}$$

where E_{est} = weighted photon energy

    h = Planck Constant (value: 6.6262×10^{-34} J s)

    c = speed of light (value: 2.9979×10^{8} m s^{-1})

    λx = wavelength at mid point of section s as above (Section 11.1.1.1.6.4)

11.1.1.1.6.7 Calculation of energy delivered to the system per unit time

The energy delivered to the system per unit time was determined by the formula (Calvert and Pitts 1966)

$$E = (Q) . (E_{est}) \qquad \{units: \ Joules/unit \ time\}$$

11.1.1.1.6.8   Conversion of energy from Joules to mW cm^{-2}.

The conversion of energy delivered to mW cm^{-2} was calculated from the formula

$$mW\ cm^{-2} = (E) . (1000)/(t) . (a)$$

where mW cm^{-2} = incident radiant intensity at irradiation cell surface

t = number of seconds per unit time

a = radiation area in cm^2 of the window in irradiation cell permissive to the passage

of radiation.

11.2   CHARACTERISATION OF THE XBO XENON ARC LAMP

11.2.1   Quantitative and qualitative determination of the radiation by actinometry

11.2.1.1 Output of the lamp

11.2.1.1.1 The output of the xenon arc lamp: variation with distance from the exit slit

It was important to examine the variation of light intensity with distance from the source.

Hence, the 24 well plates were prepared for actinometry (Section 11.1.1.1.5). The plates

were labelled to accommodate 2 negative controls (A1, A2) and a positive control (A3).

The remaining wells were labelled thus: one well for the determination of initial iron (II)

concentration for each of the distances from the source, and three wells for the

determination of iron (II) concentration after irradiation at the varied distance. The

incident fluence was determined at 9 distances measured from the outer edge of the exit

slit. In each case the radiation cell was positioned in the light path before adding the

actinometric solution. Three 100 µl aliquots of actinometric solution were collected from

the exposed wells at the completion of the irradiation; experiments were carried out in two

series, the results of the first series determined the irradiation times and distances for the

second series. Series 1 distances were 7.5, 15.0 and 30.0 cm with irradiation times of 15

minutes. Series 2 distances were 5.9, 8.0, 9.0, 10.0, 12.0 and 20.0 cm. Irradiation times

were adjusted empirically for the second series in an attempt to ensure that the absorbance values did not go out of range ($0 < A < 2$). The times for the second series were 8, 12, 15, 15, 15 and 20 minutes respectively. Finally the ambient radiation levels were measured by mock irradiating (i.e. leaving the shutter closed with the lamp on) an actinometric solution for 20 minutes. This value was then subtracted from the measured output; the result was termed the 'weighted output'. The radiant intensities were calculated as before and plotted as a function of the inverse square of distance (Calvert and Pitts 1966).

11.2.1.1.2 The output of the xenon arc lamp: warm up time

The warm up time (i.e. time from igniting the lamp to stable emission intensity) of the lamp was estimated by measuring the fluctuation in radiant intensity with time by actinometry. This was performed in the open laboratory (Section 11.1.1.1.4). The 24 well plates were prepared as described (Section 11.1.1.1.5). The lamp was switched on , the collar was removed and the beaker irradiated for 18 minutes. 100 µl aliquots were removed from the beaker at 1 minute intervals by micropipette and delivered to the appropriate wells labelled t = 1 to 18. The plates were then left to develop for 2 hours. The plate was at all times protected by the removable foil cover except for the short periods when delivering the aliquot to the well (estimated at 1 second each time) Absorbance at 510 nm for each of the wells was taken and plotted against time.

11.2.1.1.3 The output of the xenon arc lamp: divergence of the light beams

The non-linearity of the light beam causes attenuation over distance in incident radiant intensity. In the simplest of terms this can be viewed as a fall in the number of photons per unit area with distance. The standard formula (Dr. P.M.Wood, University of Bristol, undergraduate communication), $C1 \cdot V1 = C2 \cdot V2$ (where V1 is an aliquot of a solution concentration C1 and C2 is the concentration of the solution after dilution of the aliquot to volume V2), was adapted to estimate the fall in concentration of photons per unit area with distance.

The non-linearity was thus estimated by a series of calculations based on the formula

$$A1 \cdot F1 = A2 \cdot F2$$

where A1 = the area of the light beam at distance 1 (cm^2)

A2 = the area of the light beam at distance 2 (cm^2)

F1 = the measured fluence at distance 1 ($mW\ cm^{-2}$)

F2 = the measured fluence at distance 2 ($mW\ cm^{-2}$)

The area A1 at distance 5.9 cm was considered to be the unit measurement of area: when

the 1 cm^2 square window of the radiation cell was placed within the light beam, the square

A1 had the dimensions: 2f x 2f (i.e.1 x 1 cm). The square A1 was assumed to be

positioned symmetrically in the centre of the light beam. For these experiments, the top

edge of A1 was therefore at f cm above this centre and the lower edge of A1 at f cm below

the centre. The non-linearity of the light beam (i.e. the extent to which it spreads with

distance) was given the theoretical value of theta. The area of A1 at distance d increased to

A2 at distance d' with the dimensions 2f' x 2f'. The f and d values are related thus:

$$\tan theta = f' / d'$$

where f' = the height of the top edge of A2 above the top edge of A1 (cm) and

d ' = the distance between A1 and A2 (cm)

Rearranging and substituting these values, the value of theta is given by the formula:

$$\theta = \tan^{-1} (((F2 / F1)^{1/2}) / d)$$

where   d = the distance between the two points

F = the measured fluence at each point

The calculation was repeated in sequence starting with the values obtained from the first

two points of the series (i.e. A1 at 5.9 cm and A2 at 7.5 cm) and working down the

combinations of the distances to finish with the values of A1 at 20 cm and A2 at 30 cm.

The values obtained for θ were plotted against the 'A1' distances. The maximum values for

θ at each distance, the minimum values for θ at each distance, and the mean value for θ at

each distance were regressed against distance. The regression coefficient returned the value of tan θ, the regression constant returned the value of f at the exit slit. The calculated values for f and the regressed values of theta were used to estimate the extent of non-linearity of the light source.

11.2.2 The construction of the irradiation array

<u>11.2.2.1 Introduction</u>

The Xenon arc lamp emission spectrum closely approximates to that of the solar spectrum (Henderson 1970). Hence it can be used as a source of artificial daylight, or with the use of filter technology, as a source of defined wavelengths. The use of a narrow band-pass filter of a wavelength which corresponds to a peak (for a medium pressure arc lamp) or a spectral line (for a low pressure arc lamp) in the lamp's emission spectrum will result in the transmission of nearly monochromatic radiation; this needs to be of sufficient intensity to effect the desired changes in the system being studied. The power output of the lamp at individual wavelengths is therefore of central importance to the irradiation protocols described in this work.

The extent to which the radiation has been focused into a parallel beam (collimation) is also of importance. The greater the divergence, the greater the surface area that the lamp's output has to cover. Light intensity is therefore inversely proportionate to the square of the distance between the light source and the incident surface (Calvert and Pitts 1966).

The aim of the following experiments was to characterise a 150W XBO Xenon arc lamp (Applied Photophysics Ltd. England). The following characteristics were measured: radiant intensity output at varying distances from the lamp, the extent of non-linearity of the beam and the output of the lamp after filtering through 405 ± 5 nm or 310 ± 5 nm narrow band pass filters (Coherent-Ealing Ltd, England). To achieve measurement of these characteristics it was necessary to develop protocols for chemical actinometry and to

317

calibrate the UV spectrophotometer (Unicam SP1800) for these protocols. The characterisation of the xenon arc lamp in these ways was necessary to construct an irradiation array specifically tailored to the aims of this project, namely to deliver UVR (to various types of cell cultures) with the following properties:

(i)   to deliver a known quantity of radiation (i.e. a known number of photons)

(ii)   the radiation to be of a narrowly defined wavelength

(iii)   in a reproducible manner

(iv)   the incident radiation to fall upon the cell cultures from the perpendicular or the oblique

(v)   the cell cultures to be irradiated in sterile conditions

(vi)   the facility for agarose-embedded cells to be irradiated

11.2.2.2 Construction of the irradiation array

To meet these requirements the following apparatus was constructed (Figure 2.3). The array was comprised of the lamp power pack upon which rested the lamp housing itself. An X-Y plotter was placed immediately in front of the power pack and directly below the light beam. A concave mirror (from an old spectrophotometer) was clamped in the centre of the light beam focussing the beam onto a plywood lid that had been made to fit the X-Y plotter. The lid had a 20 mm hole bored approximately 1/3 of the length and 1/2 of the width, making it reversible. In the first position the light beam travelled 30 cm from the exit slit, in the second position, 40 cm. The lid was made to be removable to facilitate the placing of a cell culture plate onto the bed of the X-Y plotter. The position of the irradiation beam was marked onto the black card. The sample to be irradiated was placed centrally on this mark. (It was proposed that the X-Y plotter arms themselves would be moved by 2 sets of switches that deliver integrals units of voltage to the plotter. One set of switches would move the plotting point parallel to the X axis, the other would move the plotting point parallel to the Y axis. One unit of voltage would move the plotting point a

318

distance equivalent to the distance between the centre of one well of a 24 well plate to the centre of the adjacent well.) The lid was also made to be reversible, thus two positions were available for irradiating cells and hence two levels of radiant intensity, the estimated ratio of intensity between the two positions is 1.3 ± 0.2 to 1. The concave mirror could be moved so that the reflected light could be positioned to strike the cells from the perpendicular or from the oblique. The whole apparatus could be reassembled reproducibly by the use of etched marks on the clamps, stands and bodies of the main components. The bed of the X-Y plotter and the plywood lid were both painted matt black. The 20 mm hole was positioned on the horizontal and therefore no specialist filter holders were required to hold the narrow band pass filters in situ; the array lends itself to the possibility of using chemical filters without adaptation.

Figure 11.2 The construction of the irradiation array
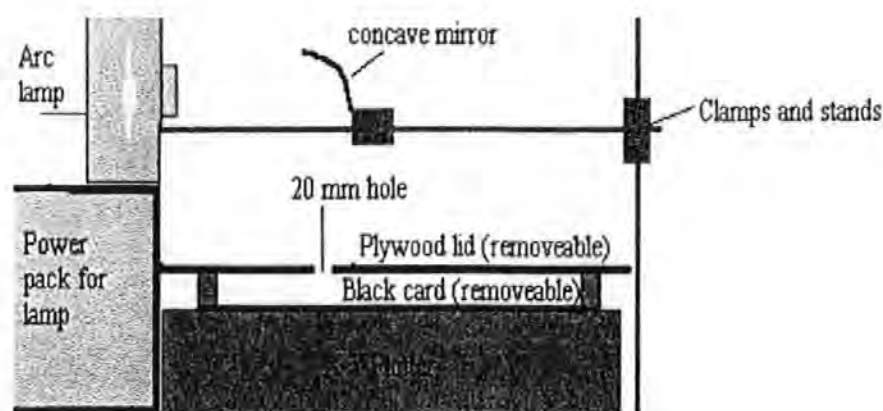
11.2.2.2.1 Delivery of unfiltered radiation

The delivery of unfiltered radiation was effected in two ways.

Either by placing the sample to be irradiated

(1) below the 20 mm hole in the lid in which case a small circle of approximately 25 mm in diameter could be irradiated

or, (2) above the hole in which case an area of up to 25 cm² could be irradiated.

11.2.2.2.2 Delivery of narrow band pass filtered radiation

Narrow band pass filters (Coherent-Ealing Ltd. UK) were used to transmit only 405 ± 5 nm or 310 ± 5 nm radiation. The delivery of narrow band pass filtered radiation was effected by the placing of an appropriate filter immediately above the hole with the sample to be irradiated directly below. The non-linear nature of the radiation source would be expected to result in a non-uniform radiant intensity over the irradiating area. This was measured by radiometry after 405 nm narrow band pass filtering in 8 areas of the irradiation bed. The use of narrow band pass interference filters permit the transmission of a narrow bandwidth of radiation. The nature of the filters means that transmitted radiation is usually attenuated to between 10 and 15 % of the incident radiation of the desired wavelength. The

wavelengths chosen for the initial investigations were 405 nm (UVA / violet) and 310 nm (UVB). The transmitted radiant intensities were measured by radiometry and by chemical actinometry. The radiometric determination of radiant intensity was calibrated by actinometric determination of the radiant intensity. The 24 well plate method was modified slightly in that although all 24 wells were filled with the actinometric solution, only wells A6, A2, B4, C2, C6 and D4 were irradiated. This was because light scattering caused a dose dependent rise in wells adjacent to the target well. The intervening cells acted, therefore, as a light absorbing screen between determination wells. The total power values obtained by ferrioxalate actinometry were regressed against time and the radiant intensity calculated from this regression.

11.2.2.2.3 The output of the xenon arc lamp: stability of output at 310 nm and at 405 nm

The stability of the lamp output at each of the two wavelengths was measured by radiometric recording of the radiant intensity at 1 second intervals for approximately 15 minutes. These data were plotted against time and means were taken to provide a working figure for the calculation of incident radiant intensity for the irradiation protocols.

11.2.3 Results

11.2.3.1 The characteristics of the XBO xenon arc lamp

11.2.3.1.1 Calibration of SP 1800

The extinction coefficient (ε_{510}) for the Fe^{2+} : 1,10 phenanthroline complex, the Hatchard and Packer ferrixolate actinometer (Section 11.1.1.1.1) was determined on the SP1800 spectrophotometer. Different concentrations of a standardised Fe^{2+} solution were complexed with 1,10 phenanthroline in triplicate. The absorbance of each solution was taken at 510 nm and the mean absorbance plotted against [Fe^{2+}]. The slope of the

calibration curve (ε_{510}) was measured at 1.155 x 10^4 $M^{-1}cm^{-1}$ (Figure 11.3) in agreement with the literature values of 1.15 x 10^4 $M^{-1}cm^{-1}$(Calvert and Pitts 1966).

11.2.3.1.2 Output of the Xe arc lamp: variation with distance

The output of the Xe lamp was measured at 9 distances from the exit slit by ferrioxalate actinometry (Table 11.2). The measured output was weighted to account for ambient radiation and plotted against the inverse square of distance (Figure 11.4). A strong linear correlation was observed, confirming that the relationship between measured fluence and distance was governed by the inverse square law.

11.2.3.1.3 The output of the Xe arc lamp: warm up time

The fluctuation in Xe lamp output during the first 20 minutes of operation was measured by ferrioxalate actinometry. The energy delivered to the actinometer correlated strongly with irradiation time, but with a marked fluctuation during the first 10 minutes (Figure 11.5). This was taken as an indication of the minimum warm up time and the lamp was used after a 30 minute warm up time thereafter. The stability of the output was also measured after 30 minutes warm up time and narrow band pass filtering by radiometry (Figure 11.6)

Figure 11.3 The calibration of the SP1800. Different concentrations of a standardised Fe^{2+} solution were complexed with 1,10 phenanthroline in triplicate. The absorbance of each solution was taken at 510 nm and the mean absorbance plotted against $[Fe^{2+}]$. The slope of the calibration curve (ε_{510}) was measured at 1.155 x 10^4 $M^{-1}cm^{-1}$.

$y = 1.1553E+04x - 2.0122E-02$
$R^2 = 9.9962E-01$
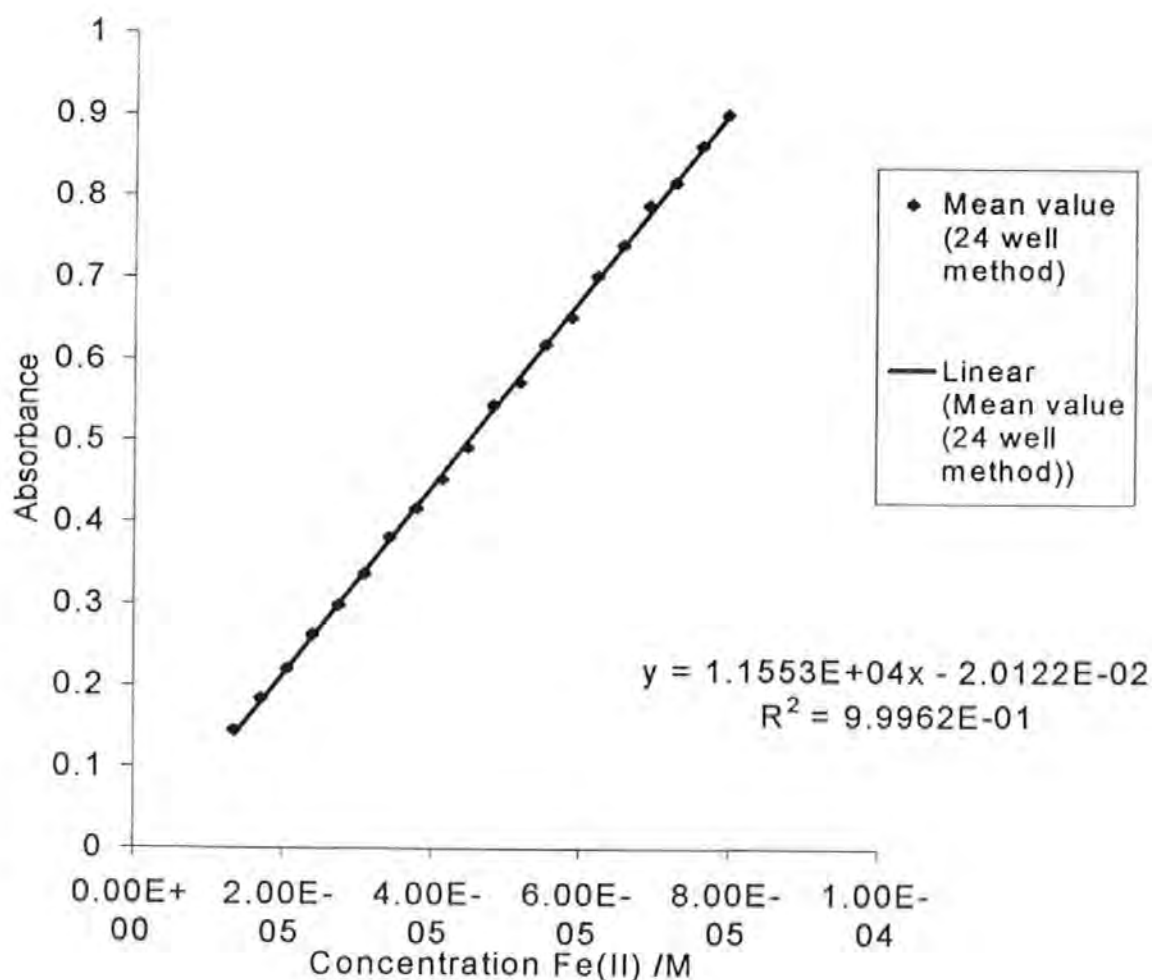
Table 11.2 The total output of the Xenon arc lamp was measured by chemical actinometry at 9 distances from the exit slit of the arc lamp. 3 aliquots of irradiated actinometric solution were taken and the mean of these recorded as mean output (see also Figure 11.4).

distance from exit slit (cm)	irradiation time (seconds)	Mean output (mW cm^{-2})	Standard deviation (mW cm^{-2})
Ambient	1200	0.00	0.44
5.9	480	126.02	9.03
7.5	900	86.94	1.12
8.0	720	67.23	5.57
9.0	900	57.23	1.85
10.0	900	45.25	0.46
12.0	900	20.47	0.39
15.0	900	12.98	1.69
20.0	1200	5.06	0.42
30.0	900	1.93	0.13

Figure 11.3 The output of the Xe lamp: variation with distance. The output of the Xe lamp was measured in triplicate at 9 distances from the exit slit by ferrioxalate actinometry (Table 11.2). The measured output was weighted to account for ambient radiation and plotted against the inverse square of distance. Error bars represent one standard deviation for each set of replicates.

The plot shows Output / mW (y-axis, 0.00 to 160.00) versus $1 / (distance\ (cm))^2$ (x-axis, 0.0000 to 0.0400).

$$y = 4.7461E+03x - 5.4445E+00$$
$$R^2 = 9.8713E-01$$
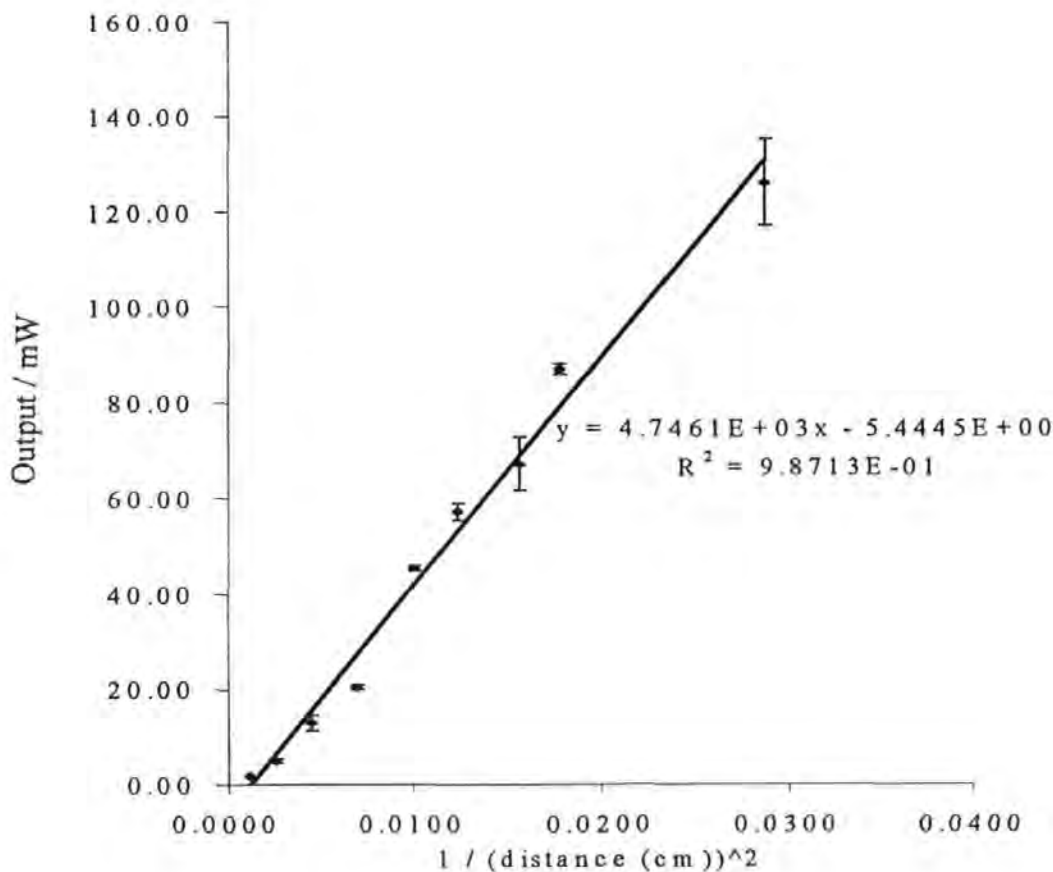
Figure 11.5 The warm up time of the lamp. The fluctuation in Xe lamp output during the first 20 minutes of operation was measured by ferrioxalate actinometry. The energy delivered to the actinometer correlated strongly with irradiation time, but with a marked fluctuation during the first 10 minutes.

The effect of High pressure Xenon Arc Lamp on Potassium Ferrioxalate solution

$y = 71.127x + 94$
$R^2 = 0.994$
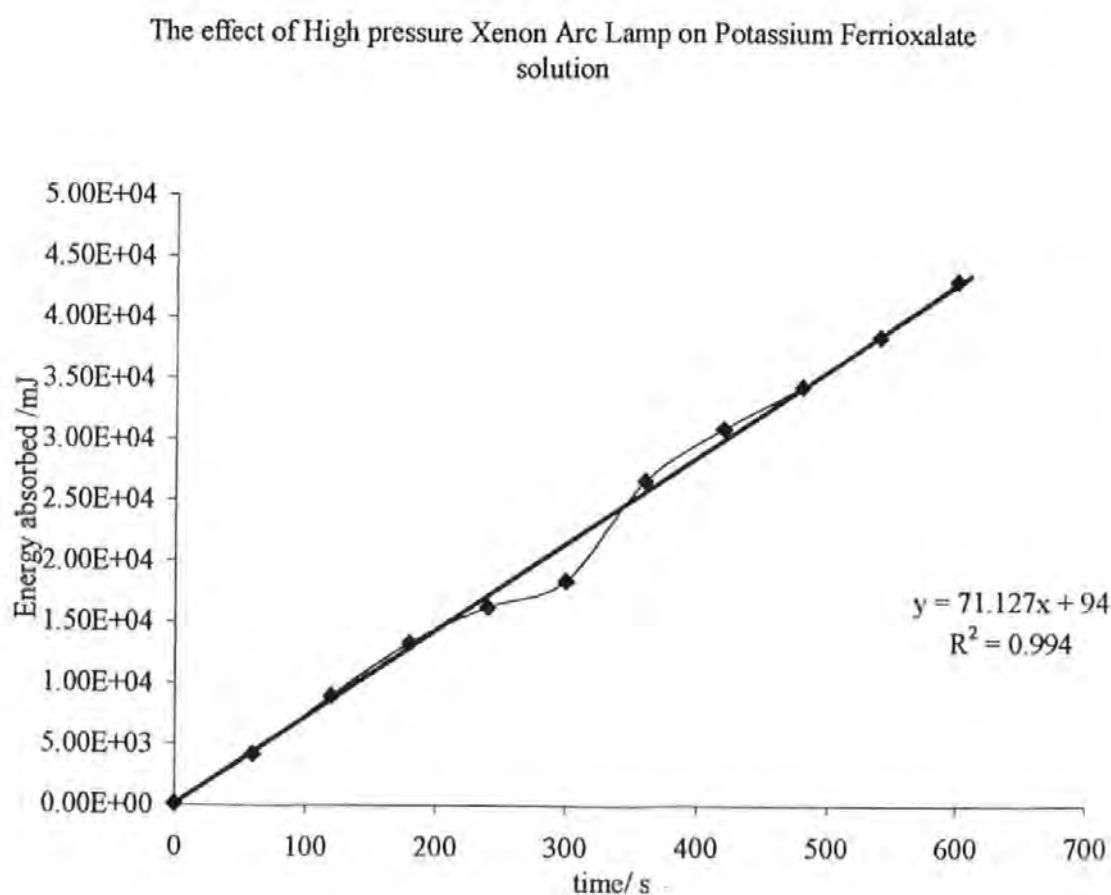
Figure 11.6 Stability of output after narrow band pass filtering. The fluctuation in Xe lamp output during the first 20 minutes of operation was measured by ferrioxalate actinometry. The energy delivered to the actinometer correlated strongly with irradiation time, but with a marked fluctuation during the first 10 minutes. The stability of the output was measured after 30 minutes warm up time and narrow band pass filtering by radiometry.
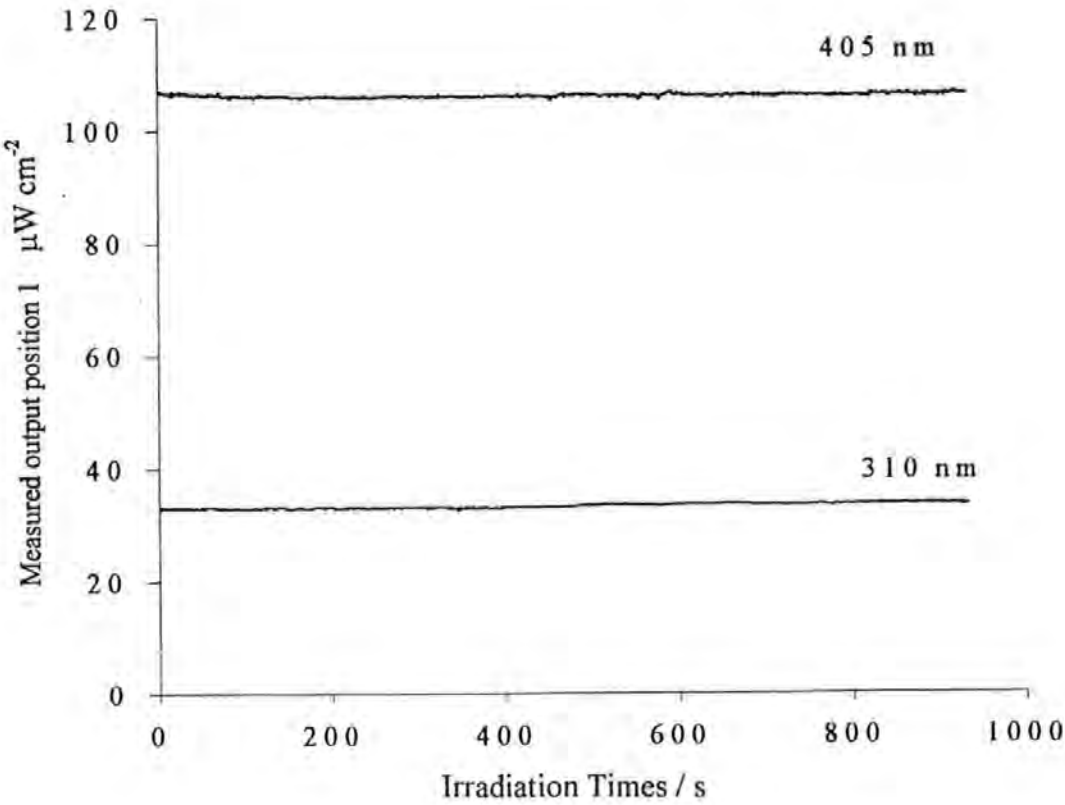
11.2.3.1.4 The output of the Xe lamp: non-linearity of the light beam

The non-linearity of the light beam was measured by calculating the fall in incident radiant intensity with distance. Three estimates of non-linearity were made corresponding to the outer and inner fractions of the light beam, and an overall estimate of non-linearity. The estimates of non-linearity were obtained by calculating the maximum and minimum angles of divergence (thus the outer and inner parts of the light beam) and the mean angle of divergence (see Figure 11.7, Table 11.3 and methods for details).

Table 11.3 The maximum, minimum, and mean values of the non-linearity coefficient, 'theta', were obtained by regression of the maximum, minimum and mean values of the length ('f') of the sides of an imagined square which increased with distance as a result of the non-linear beam. This gave three values for tan theta. A maximum, corresponding to the outermost parts of the beam; a minimum, corresponding to the innermost parts of the beam; and a mean value which corresponded to the overall extent of non-linearity (see Figure 11.7).

	tan theta	theta (degrees)
Maximum values of f	0.1514	8.6
Minimum values of f	0.0128	0.7
Mean values of f	0.0838	4.8

328

Figure 11.7 Estimates of non-linearity. The non-linearity of the light beam was
measured by calculating the fall in incident radiant intensity with distance. Three
estimates of non-linearity were made corresponding to the outer and inner fractions
of the light beam, and an overall estimate of non-linearity. The estimates of non-
linearity were obtained by calculating the maximum and minimum angles of
divergence (thus the outer and inner parts of the light beam) and the mean angle of
divergence (see methods for details of the calculations).
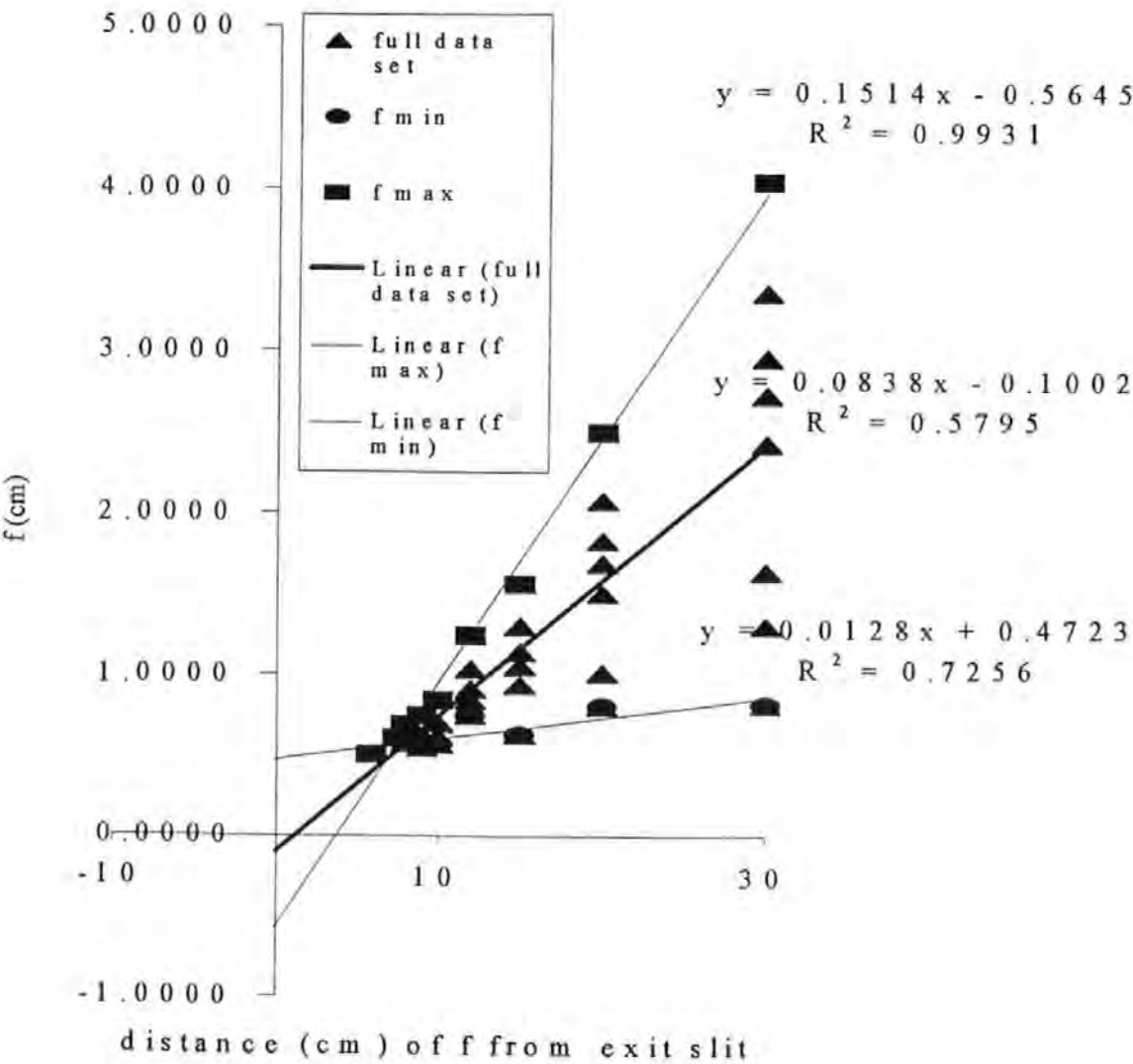
The three angles converged at a distance of approximately 7 cm from the exit slit and this was interpreted as the focal point of the collimating lens of the arc lamp. The regression equations were solved simultaneously for maximum theta and mean theta, maximum theta and minimum theta, mean theta and minimum theta. These calculations returned respective focal lengths of 6.8683 cm, 7.4805 cm and 8.0634 cm (mean value 7.4722). Substituting this value back into the equations returned respective f values (the height of the top edge of a 1 cm square placed centrally in the light beam) of 0.5668 cm, 0.5260 cm, 0.5679 cm with a mean f value of 0.5536 cm indicating that the centre of the 1 cm x 1 cm window of the radiation cell had been positioned within 0.6 mm of the beam centre. The working model of the Xe arc lamp used to construct the irradiation array is given in Figure 11.8.

The non-linearity of the light beam in 8 areas of the irradiation bed was measured after 405 nm narrow band pass filtering (Figure 11.9). The measured fluences ranged from 77 μW cm^{-2} to 90 μW cm^{-2} (mean 82.75 μW cm^{-2}, st dev 4.77 μW cm^{-2} approximately $\pm$ 8% of the mean).

11.2.3.1.5 The output of the Xe lamp: narrow band pass filtering

The output of the Xe lamp was measured by ferrioxalate actinometry after 405 nm and 310 nm narrow band pass filtering. Total power delivered to a 24 well actinometer was regressed against irradiation time (Figure 11.10). The regression coefficient indicated the incident fluence falling on the whole well at each wavelength. This incident fluence was converted to W cm^{-2} by division by 1.88 (the area of the actinometer well in cm^2) and to μW cm^{-2} by division by 10^6.

Figure 11.8 The working model of the Xe lamp.

LAMP HOUSING
incorporating

(Not to Scale)

Focal point of condenser

Dissipation of light beam due to non-linearity
(Approximately to Scale)

Highly non-linear Outer zone   Less non-linear inner zone   Linear region

?

Measured outputs at varying distances from exit slit
Narrow line indicates increased size of square
Bold line indicates 1 cm square window

Xenon arc lamp
? Condensing lens
? Collimating lens
Reflecting mirror(s)
Exit slit

	Regressed f/d	theta
	0.1514	8.6109
	0.0838	4.7922
	0.0128	0.7348

◆ full
   data
   set

■ f min

■ f max

distance (cm) d/Y from exit slit

Figure 11.9 The non-linearity of the light beam in 8 areas of the irradiation bed was measured after 405 nm narrow band pass filtering. The measured fluences ranged from 77 µW cm^{-2} to 90 µW cm^{-2} (mean 82.75 µW cm^{-2}, st dev 4.77 µW cm^{-2} approximately ± 8% of the mean). Grey squares represent wells A1 to B2 of 96 well plate, white squares indicate interim measurement, circle represents approximate area of irradiation bed.
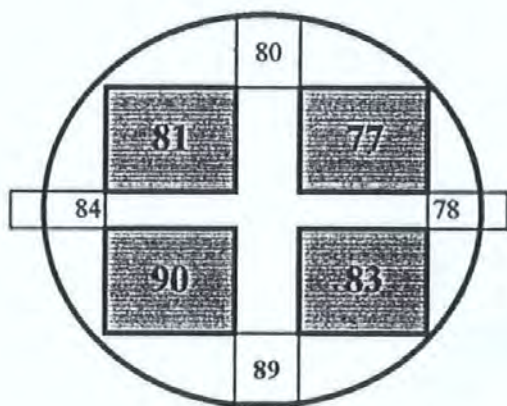
The fluences after 405 nm narrow band pass filtering were calculated at 110 μW cm^{-2} and 18.5 μW cm^{-2} respectively. The figure for 405 nm fluence obtained by ferrioxalate actinometry agreed strongly with that obtained by radiometry (106 μW cm^{-2}). The radiometer-measured fluence at 310 nm was not in agreement (35 μW cm^{-2}). This was thought to be due to a high degree of light scattering at 310 nm. Accordingly, a 24 well actinometer was irradiated by 405 nm or 310 nm radiation in alternate wells, the intervening wells acting as actinometers to measure light scattering. The pattern of irradiation could be seen clearly at 405 nm (Figure 11.11) indicating that light scattering, although detectable, was at baseline levels at this wavelength. At 310 nm, however, the pattern of irradiation was not discernible due to a high degree of light scattering (Figure 11.12).

11.2.3.1.6 Output of the Xe arc lamp: Variation in output

The output of the lamp varied noticeably during the period of study. The fitting of a replacement bulb resulted in a substantial fall in output at both wavelengths. Output at 405 nm fell from 106 μW cm^{-2} to 84 μW cm^{-2} and output at 310 nm fell from 35 μW cm^{-2} to 21 μW cm^{-2} (the values are the last measurements of 405 nm and 310 nm fluence taken for the old bulb and the first measurements from the new bulb taken after the bulb had been 'burned in' by running for 24 hours). Inter-experimental variation in lamp output was calculated from radiometry readings taken during experiments. The mean output after 405 nm filtering using the second bulb was calculated at 75.27 μW cm^{-2} (σ = 4.36 μW cm^{-2}, n=25). Mean stability at 405 nm was measured at over 900 points in each of 4 independent experiments. During operation the mean of these 4 experiments was 74.34 μW cm^{-2} and the mean standard deviation was 0.023 μW cm^{-2} (0.03% of the mean).

Figure 11.10 The output of the Xe lamp was measured by ferrioxalate actinometry after 405 nm and 310 nm narrow band pass filtering. Total power delivered to a 24 well actinometer was regressed against irradiation time.
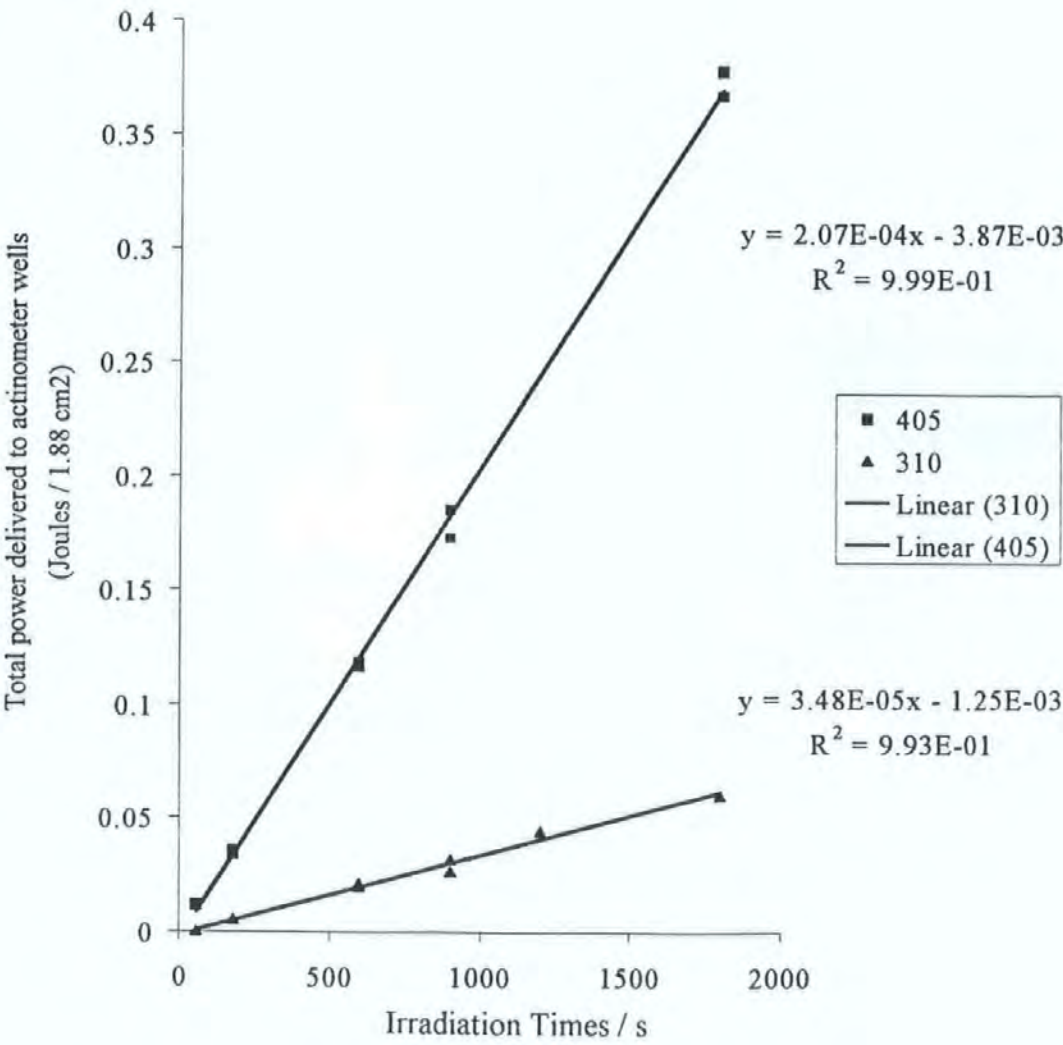
Figure 11.11 The extent of light scattering at 405 nm. A 24 well actinometer was irradiated by various doses of 405 nm radiation in alternate wells, the intervening wells acting as actinometers to measure light scattering. The pattern of irradiation (grey columns) could be seen clearly at 405 nm indicating that light scattering, although detectable, was at baseline levels at this wavelength.
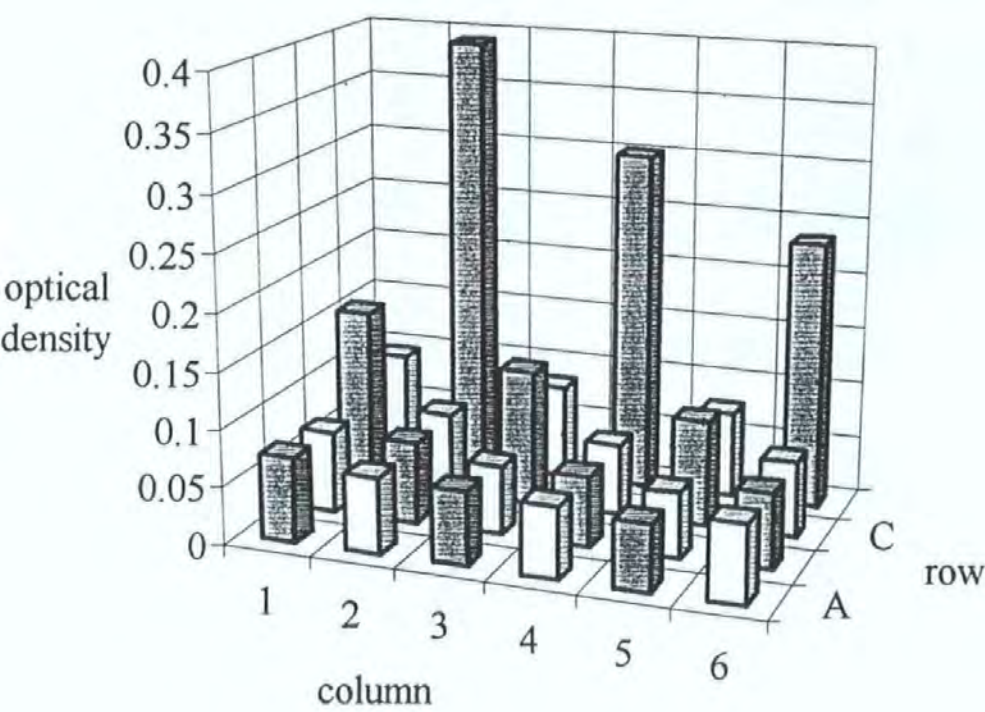
Figure 11.12

The extent of light scattering at 310 nm. A 24 well actinometer was irradiated by 310 nm radiation in alternate wells, the intervening wells acting as actinometers to measure light scattering. The pattern of irradiation (grey columns) was not discernible due to a high degree of light scattering
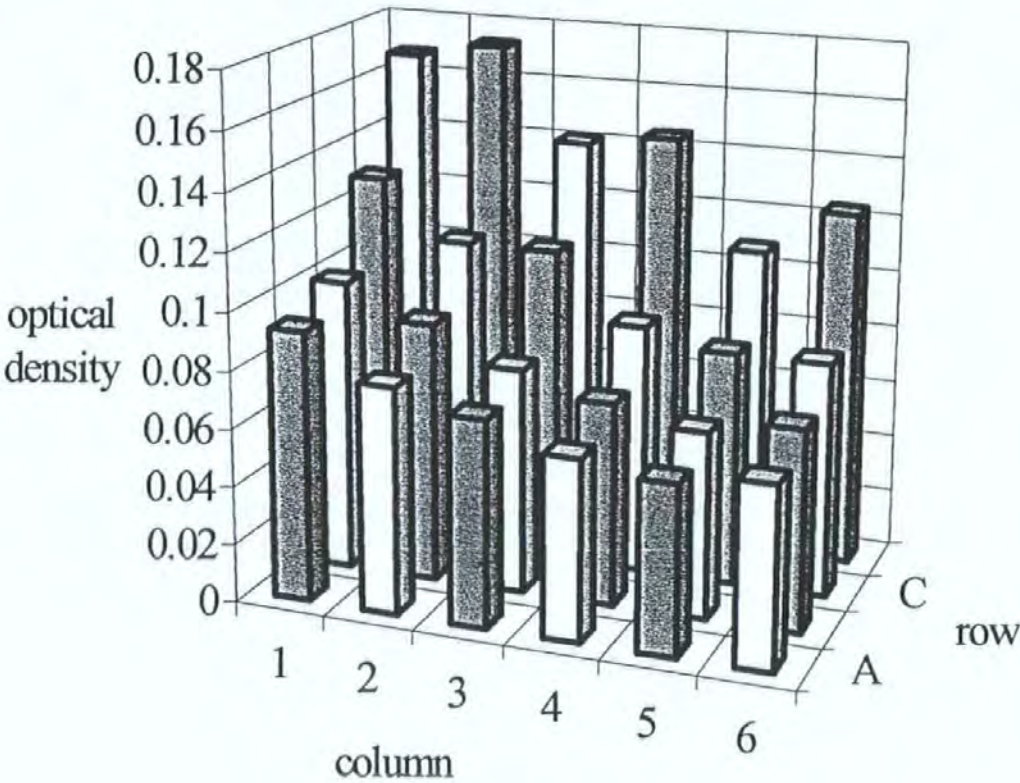
REFERENCES

Adam D, Dimitrijevic N and Schartl M

Tumour suppression in Xiphophorus by an accidentally acquired promoter.

Science. **259**: 816-819. (1993)

Aidoo A, Lyn-Cook LE, Lensing S, Bishop ME and Wamer W.

In vivo antimutagenic activity of beta-carotene in rat spleen lymphocytes.

Carcinogenesis. **16**: 2237-2241. (1995)

Alabaster A, Tang Z, Frost A and Shivapurkar N

Effect of beta-carotene and wheat bran fiber on colonic aberrant crypt and tumour

formation in rats exposed to azoxymethane and high ditary fat.

Carcinogenesis. **16**: 127-132. (1995)

Alapetite.C, Wachter.T, Sage.E and Moustacchi.E

Use of the alkaline comet assay to detect DNA repair deficiencies in human fibroblasts

exposed to UVC, UVB, UVA and gamma-rays.

International Journal of Radiation Biology. **69**: 359-369. (1996)

Alberts B, Bray D, Lewis J, Raff M, Roberts K and Watson JD

Molecular biology of the cell.

2nd Ed. Garland Publishing, New York. ISBN: 0 8240 3696 4 (Pbk) (1989)

Ames BN

Dietary carcinogens and anticarcinogens.

Science. **221**: 1256-1264. (1983)

Amstad.PA and Cerutti.PA

Ultraviolet-B-light-induced mutagenesis of C-H-ras codons 11 and 12 in human skin

fibroblasts

International Journal of Cancer. **63**: 136-139. (1995)

Anderson D, Yu T-W and McGregor DB

Comet Assay responses as indicators of carcinogen exposure

Mutagenesis. **13**: 539-555. (1998)

Andreassi.L, Rubegni.P, Stanghellini.E, Cevenini.G and Flori.ML

Constitutional skin color in Caucasians [letter]

Journal of Investigative Dermatology. **106**: 1154-1155. (1996)

Aposhian HV

Biochemical toxicology of arsenic

Reviews in Biochemcal Toxicology. **1**: 265-299. (1989)

Appel KE, Furstenberger G, Hapke HJ, Hecker E, Hildebrandt AG, Koransky W, Marks F, Neumann HG, Ohnesorge FK and Schulte-Hermann R

Chemical cancerogenesis: definitions of frequently used terms

Journal of Cancer Research and Clinical Oncology. **116**: 232-236. (1990)

Applegate.LA, Lautier.D, Frenk.E and Tyrrell.RM

Endogenous glutathione levels modulate the frequency of both spontaneous and long wavelength ultraviolet induced mutations in human cells

Carcinogenesis. **13**: 1557-1560. (1992)

Applegate.LA, Scaletta.C, Labidi.F, Vile.GF and Frenk.E

Susceptibility of human melanoma cells to oxidative stress including UVA radiation

International Joiurnal of Cancer. **67**: 430-434. (1996)

Asad NR, Asad LM, Almeida CE and Leitao AC

Lethal interaction between hydrogen peroxide and o-phenanthroline in Escherichia coli

Braz. J. Med. Biol. Res. **27**: 2551-2555. (1994)

Ashby.J, Tinwell.H, Lefevre.PA and Browne.MA

The single cell gel electrophoresis assay for induced DNA damage (comet assay): measurement of tail length and moment.

Mutagenesis. **10**: 85-90. (1995)

Aubin.FJ, Agache.PG and Humbert.P

Age should be considered as a risk factor for basal cell carcinoma and DNA repair capacity [letter, comment]

Journal of Investigative Dermatology. **106**: 798-799. (1996)

Autier.P, Dore.JF, Schifflers.E, Cesarini.JP, Bollaerts.A, Koelmel.KF, Gefeller.O,
Liabeuf.A, Lejeune.F and Lienard.D

Melanoma and use of sunscreens: an Eortc case-control study in Germany, Belgium and
France The EORTC Melanoma Cooperative Group.

International Joiurnal of Cancer.. **61**: 749-755. (1995)

Barrett JC, Lamb PW, Wang TC and Lee TC

Mechanisms of arsenic-induced cell transformation

Biological Trace Element Research. **21**: 421-429. (1989)

Basu-Modak.S and Tyrrell.RM

Singlet oxygen: a primary effector in the ultraviolet A/near-visible light induction of the
human heme oxygenase gene

Cancer.Research. **53**: 4505-4510. (1993)

Bates S and Vousden KH

p53 in signalling checkpoint arrest or apoptosis

Current Opinion in Genetics and Development **6**: 12-19. (1996)

Bates.S, Rowan.S and Vousden.KH

Characterisation of human cyclin G1 and G2: DNA damage inducible genes

Oncogene. **13**: 1103-1109. (1996)

Bessou.S, Surleve.Bazeille.JE, Sorbier.E and Taieb.A

Ex vivo reconstruction of the epidermis with melanocytes and the influence of UVB

Pigment Cell Research. **8**: 241-249 (1995)

Birchmeier W and Behrens J

Cadherin expression in carcinomas: role in the formation of cell junctions and the
prevention of invasiveness

Biochimica et Biophysica Acta. **1198**: 11-26. (1994)

Birnboim HC

Effect of lipophilic chelators on oxyradical-induced DNA strand breaks in human
granulocytes: paradoxical effect of beta-carotene.

Arch. Biochem. Biophys. **294**: 17-21. (1992)

Black HS

Potential involvement of free-radical reactions in ultraviolet light-mediated cutaneous damage

Photochemistry and Photobiology **46**: 213-221. (1987)

Black.HS and Mathews-Roth.MM

Protective role of butylated hydroxytoluene and certain carotenoids in photocarcinogenesis

Photochemistry and Photobiology. **53**: 707-716. (1991)

Bock C, Dittmar H, Gemeinhardt H, Bauer E and Greulich K-O

Comet assay detects cold repair of UV-A damages in a human B-lymphblast cell line

Mutation Research **408**: 111-120. (1998)

Bohr VA

Gene specific damage and repair of DNA adducts and cross-links

in *'DNA adducts, identification and biological significance'*Eds Hemminki K, Dipple A, Shuker DEG, Kadlubar FF, Segerback D,and Bartsch H.IARC Scientific Publications No 125, Lyon. ISBN: 92 832 2125 7 (1994)

Bohr VA, Smith CA, Okumoto DS and Hanawalt PC

DNA repair in an active gene: removal of pyrimidine dimers from the DHFR gene of CHO cells is much more efficient than in the genome overall

Cell. **40**: 359-369. (1985)

Brash D E, Rudolph J A, Simon J A, Lin A, McKenna G J, Baden H P, Halperin A J, and Ponten J

A role for sunlight in skin cancer: UV-induced p53 mutations in squamous cell carcinoma

Proc.Nat.Acad.Sci,USA. **88**, 10124-10128 (1991)

Burcham PC

Genotoxic lipid peroxidation products: their DNA damaging properties and role in formation of endogenous DNA adducts

Mutagenesis. **13**: 287-305. (1998)

Burton GW and Ingold KU

Beta-carotene: an unusual type of lipid antioxidant

Science **224**: 569-573. (1984)

Byrnes RW

Evidence for involvement of multiple iron species in DNA single-strand scission by H2O2 in HL-60 cells

Free Radic. Biol. Med. **20**: 399-406. (1996)

Cadenas E.

Mechanisms of oxygen activation and reactive oxygen species detoxification

in '*Oxidative stress and antioxidant defences in biology*' "Ed. Ahmad.S. Chapman and Hall, New York..ISBN:0.412.03971.0 (1995)

Cadet J.

DNA Damage caused by oxidation, deamination, ultraviolet radiation and photoexcited psoralens

in '*DNA adducts, identification and biological significance*'Eds Hemminki K, Dipple A, Shuker DEG, Kadlubar FF, Segerback D,and Bartsch H.IARC Scientific Publications No 125, Lyon. ISBN: 92 832 2125 7 (1994)

Cadi.R, Beani.JC, Jacrot.M, Pinel.N and Amblard.P

UV-induced squamous cell carcinomas in the hairless mouse- Morphological characteristics and transplantation in the syngenic and nude mouse

Acta.Derm.Venereol. **71**: 32.6 (1991)

Calvert J.G. and Pitts J.N.

Photochemistry

John Wiley and Sons, (USA) (1966)

Castellano M, Pollock PM, Walters MK, Sparrow LE, Down LM, Gabrielli BG, Parsons PG and Hayward NK

CDKN2A/p16 is inactivated in most melanoma cell lines

Cancer Research. **57**: 4868-4875. (1997)

Cerutti PA

Prooxidant states and tumour promotion

Science. **227**: 375.381 (1985)

Chen Y, Miles AM and Grisham MB

Pathophysiology and reactive oxygen metabolites

in *'Oxidative stress and antioxidant defences in biology'* "Ed. Ahmad.S. Chapman and

Hall, New York.. ISBN:0.412.03971.0 (1995)

Churchill.ME, Peak.JG and Peak.MJ

Correlation between cell survival and DNA single-strand break repair proficiency in the

Chinese hamster ovary cell lines AA8 and EM9 irradiated with 365-nm ultraviolet-A

radiation

Photochemistry and Photobiology. **53**: 229-236. (1991)

Clingen.PH, Arlett.CF, Roza.L, Mori.T, Nikaido.O and Green.MH

Induction of cyclobutane pyrimidine dimers, pyrimidine(6-4)pyrimidone photoproducts,

and Dewar valence isomers by natural sunlight in normal human mononuclear cells

Cancer Research. **55**: 2245-2248. (1995)

Collins.AR, Ma.AG and Duthie.SJ

The kinetics of repair of oxidative DNA damage (strand breaks and oxidised pyrimidines)

in human cells

Mutation Research. **336**: 69-77. (1995)

Conn Pf, Lambert C, Land EJ, Schalch W and Truscott TG

Carotene-Oxygen radical interactions

Free Rad. Res. Comms. **16**:401-408. (1992)

Coohill TP, Peak MJ and Peak JG

The effects of the ultraviolet wavelengths of radiation present in sunlight on human cells in

vitro

Photochemistry and Photobiology. **46**: 1043-1050. (1987)

Coulomb B, Saiag P, Bell E, Breitburd F, Lebreton C, Heslan M and Dubertret L

A new method for studying epidermalisation in vitro

British Journal of Dermatology. **114**: 91-101 (1986)

Cozzi R, Ricordy R, Aglitti T, Gatta V, Perticone P and De Salvia R

Ascorbic acid and beta-carotene as modulators of oxidative damage

Carcinogenesis. **18**:223-228. (1997)

Cridland NA and Saunders R D

Cellular and Molecular effects of UVA and UVB

HMSO. ISBN No: 0 85951 374 2 (1994)

Dalton DA

Antioxidant defences of plants and fungi

in *'Oxidative stress and antioxidant defences in biology'* "Ed. Ahmad.S. Chapman and

Hall, New York..ISBN:0.412.03971.0 (1995)

Dawson RMC, Elliot DC, Elliot WH and Jones KM

Data for biochemical research

3rd Ed. Clarendon Press, Oxford UK.. ISBN 0 19 855299 8 (1988)

de Gruijl.FR

Action spectrum for photocarcinogenesis

Recent Results in Cancer Research. **139**: 21-30 (1995)

de Gruis NA, van der Velden PA, Sandkuijl LA, Prins DE, Weaver-Feldhaus J, Kamb A,

Bergman W and Frants RR

Homozygotes for CDKN2 (p16) germline mutation in Dutch familial melanoma kindreds

Nature Genetics. **10**: 351-353. (1995)

de Mello Filho AC and Meneghini R

In vivo formation of single strand breaks in DNA by hydrogen peroxide is mediated by the

Haber-Weiss reaction

Biochimica et Biophysica Acta. **781**: 56-63. (1984)

343

de Mello Filho A C and Meneghini R

Protection of mammalian cells by o-phenanthroline from lethal and DNA damaging effects produced by active oxygen species

Biochimica et Biophysica Acta. **847**: 82-89. (1985)

Demple B and Harrison L

Repair of oxidative damage to DNA

Annual Reviews in Biochemistry. **63**: 915-948. (1994)

Dizdaroglu M, Aruoma OI and Halliwell B

Modification of bases in DNA by copper ion-1,10-phenanthroline complexes

Biochemistry. **29**: 8447-8451. (1990)

Donawho C and Kripke ML

Photoimmunology of cutaneous melanoma

in *'Photoimmunology'* Eds. Krutmann J and Elmets CA.Blackwell Science, Oxford UK..ISBN: 0 86542 826 3 (1995)

Donawho C and Wolf P

Sunburn, sunscreen, and melanoma

Current Opinion in Oncology. **8**: 159-166. (1996)

Dong.JT and Luo.XM

Arsenic-induced DNA-strand breaks associated with DNA-protein crosslinks in human fetal lung fibroblasts

Mutation Research. **302**: 97-102. (1993)

Draetta.GF

Mammalian G1 cyclins

Current Opinion in Cell Biology. **6**: 842-846 (1994)

Eisinger M, Marko O and Weinstein IB

Stimulation of growth of human melanocytes by tumour promotors.

Carcinogenesis. **4**: 779-781. (1983)

Eller M.S, Ostrom K.and Gilchrest B.A.

DNA damage enhances melanogenesis

Proc. Nat. Acad. Sci, USA. **93**: 1087-1092 (1996)

Epstein JH

Effects of beta-carotene on ultraviolet induced cancer formation in the hairless mouse skin

Photochemistry and Photobiology. **25**: 211-213. (1977).

Fairbairn.DW, Olive.PL and O'Neill.KL

The comet assay: a comprehensive review

Mutation Research. **339**: 37-59. (1995)

Fairbairn.DW, Rowe.KC and O'Neill.KL

Video enhanced laser scanning microscopic analysis of DNA comet formation.

Cell.Biol.Int. **18**: 195-200 (1994)

Fearon ER and Vogelstein B

A genetic model for colorectal tumorigenesis

Cell. **61**: 759-767. (1990)

Felton GW

Oxidative stress of vertebrates and invertebrates

in *'Oxidative stress and antioxidant defences in biology'* Ed. Ahmad.S. Chapman and Hall, New York..ISBN:0.412.03971.0 (1995)

Finkel E

Sorting the hype from the facts in melanoma

Lancet. **351**: 1866. (1998)

Flindt-Hansen.H, McFadden.N, Eeg.Larsen.T and Thune.P

Effect of a new narrow-band UVB lamp on photocarcinogenesis in mice

Acta.Derm.Venereol. **71**: 245-248 (1991)

Foote CS

Definition of Type I and Type II photosensitized oxidation

Photochemistry and Photobiology. **54**: 659 (1991)

Fountain JW, Bale SJ, Housman DE and Dracopoli NC

Genetics of melanoma

Cancer Surveys. 9: 645-671. (1990)

Franks LM

What is cancer?

in *'Introduction to the cellular and molecular biology of cancer'.* 2nd Ed.Eds. Franks LM
and Teich NM.Oxford University Press, Oxford UK..ISBN:0 19 854732 3 (1991)

Friedberg EC, Walker GC and Siede W.

DNA repair and mutagenesis

American Society for Microbiology, Washington DC..ISBN:1 55581 088 8 (1995)

Gensler.HL and Welch.K

Prevalence of tumor prevention rather than tumor enhancement when repetitive UV
radiation treatments precede initiation and promotion

Carcinogenesis. 13: 9-13. (1992)

Gerber E, Bredy A and Kahl R

Ortho-phenanthroline modulates enzymes of cellular energy metabolism

Toxicology. 110: 85-93. (1996)

Gilchrest BA, Eller MS, Geller AC and Yaar M

The pathogenesis of melanoma induced by ultraviolet radiation

New England Journal of Medicine. 340: 1341-1348. (1999)

Giles GG, Armstrong BK, Burton RC, Staples MP and Thursfield VJ

Has mortality from melanoma stopped rising in Austrailia? Analysis of trends between
1931 and 1994

British Medical Journal. 312: 1121-5. (1996)

Glass GA and Stark AA

Promotion of glutathione-gamma-glutamyl transpeptidase dependent lipid peroxidation by
copper and ceruplasmin: the requirement for iron and the effects of antioxidants and
antioxidant enzymes.

Environ. Mol. Mutagen. 29: 73-80. (1997)

Gonsebatt ME, Vega L, Salazar AM, Montero R, Guzman P, Blas J, Del Razo LM, GarciaVargas G, Albores A, Cebrian ME, Kelsh M and Ostrosky-Wegman P
Cytogenetic effects in human exposure to arsenic
Mutation Research. **386**: 219-228. (1997)

Gonzalez-Zulueta M, Bender CM, Yang AS, Nguyen T, Beart RW, Van Tornout JM, and Jones PA
Methylation of the 5' CpG island of the p16/CDKN2 tumor suppressor gene in normal and transformed human tissues correlates with gene silencing
Cancer Research. **55**: 4531-4535. (1995)

Gorospe M, Cirielli C, Wang X, Seth P, Capogrossi and Holbrook NJ
p21wafl/cip1 protects against p53 mediated apoptosis of human melanoma cells
Oncogene. **14**: 929-935. (1997)

Green MHL, Lowe JE, Waugh APW, Harcourt, Roza L and Arlett CF
Consequences of depletion of the ozone layer for human health: studies using the "comet" assay
Symposium Proceedings *"Biolgical indicators of global change"* pp 53-67. Eds Symoens JJ, Devos P, Rammeloo J, Verstraeten Ch. Royal Academy of Overseas Sciences (Brussels). (1993)

Green MHL,Lowe JE, Delaney CA and Green IC
Comet assay to detect nitric oxide -dependent DNA damage in mammalian cells
Methods in Enzymology **269**: 243-266. (1996)

Grether-Beck.S, Olaizola.Horn.S, Schmitt.H, Grewe.M, Jahnke.A, Johnson.JP, Briviba.K, Sies.H and Krutmann.J
Activation of transcription factor AP-2 mediates UVA radiation- and singlet oxygen-induced expression of the human intercellular adhesion molecule 1 gene
Proc.Natl.Acad.Sci.U.S.A. **93**: 14586-14591. (1996)

Guy.R, Green.MR and Kealey.T
Modeling acne in vitro
Journal of Investigative Dermatology. **106**: 176-182 (1996)

347

Guyton KZ and Kensler TW

Oxidative mechanisms in Carcinogenesis

British Medical Bulletin. **49**: 523-544. (1993)

Halaban R and Alfano FD.

Selective elimination of fibroblasts from cultures of normal human melanocytes. .

In Vitro **20**: 447-450. (1984)

Hall J, English D.R, Artuso M, .Armstrong B.K and Winter M

DNA repair capacity as a risk factor for non melanocytic skin cancer-a molecular epidemiological study

International Journal of Cancer. **58**: 179-184. (1994)

Hall PA, McKee PH, Menage H du P, Dover and Lane DP

High levels of p53 in UV irradiated normal human skin

Oncogene. **8**: 203-207. (1993)

Halliwell B and Aruoma O I

DNA Damage by oxygen-derived species

Febs Letters **289**: 9-19 (1991)

Hanawalt PC

Overview

in '*DNA damage and repair. Vol II: DNA repair in higher eukaryotes'.* Eds Nickoloff JA and Hoekstra MF. Humana Press, New Jersey. ISBN: 89603 500 X. (1998)

Hartwig A, Groblinghoff UD, Beyersmann D, Natarajan AT, Filon R and Mullenders LH.

Interaction of arsenic (III) with nucleotide excision repair in UV-irradiated human fibroblasts

Carcinogenesis. **18**: 399-405 (1997)

Healy.E, Sikkink.S and Rees.JL

Infrequent mutation of p16INK4 in sporadic melanoma

Journal of Investigative Dermatology, **107**: 318-21 (1996)

Hedley SJ, Wagner M, Bielby S, Smith.Thomas L, Gawkrodger DJ and MacNeil S

The influence of extracellular matrix proteins on cutaneous and uveal melanocytes

Pigment Cell Research. **10**: 54-59 . (1997)

Henderson.ST

Daylight and its spectrum

Adam Hilger, Bristol. Library of Congress number 73-106185. (1970)

Henshaw DL, Eatough JP and Richardson RB

Radon as a causative factor in induction of myeloid leukaemia and other cancers.

Lancet. **335** :1008-1012 (1990)

Herbold.KW, Zhou.J, Haggerty.JG and Milstone.LM

CD44 expression on epidermal melanocytes

Journal of Investigative Dermatology, **106**: 1230-1235. (1996)

Hiraku Y, Inoue S, Oikawa S, Yamamoto K, Tada S, Nishino K and Kawanishi S

Metal-mediated oxidative damage to cellular and isolated DNA by certain tryptophan metabolites

Carcinogenesis **16**: 349-56 (1995)

Holubar.K

What is a caucasian? [letter]

Journal of Investigative Dermatology. **106**: 800 (1996)

Hooghe RJ, Verschaeve L and Vankerkom J

DNA comets for monitoring pollution

Microscopy and Analysis (Trade), November 1995

Huang P, Olive PL and Durand RE

Use of the comet assay for assessment of drug resistance and its modulation in vivo

British Journal of Cancer. **77**: 412-416. (1998)

IARC monographs on the evaluation of carcinogenic risks to humans. Volume 55: Solar and Ultraviolet radiation

International Agency for Research on Cancer.. ISBN: 92 832 1255 X (1992)

Iizawa.O, Kato.T, Tagami.H, Akamatsu.H and Niwa.Y

Long-term follow-up study of changes in lipid peroxide levels and the activity of superoxide dismutase, catalase and glutathione peroxidase in mouse skin after acute and chronic UV irradiation.

Arch.Dermatol.Res. **286**: 47-52 (1994)

Ingram AJ

Review of chemical and UV light-induced melanomas in experimental animals in relation to human melanoma incidence

Journal of Applied Toxicology. **12**: 39-43. (1992)

Jacobson EL, Antol KM, Juarrez-Salinas H and Jacobson MK

Poly(ADP-ribose) metabolism in ultraviolet irradiated human fibroblasts

Journal of Biological Chemistry **258**: 103-107. (1983)

Jaer JW and Ostrosky-Wegman P

Arsenic-a paradoxical human carcinogen

Mutation Research. **386**: 181-184. (1997)

Janeway CA Jr and Travers P

Using the immune response to attack tumours

in *'Immunobiology: the immune system in health and disease'* Garland Publishing, New York.. ISBN: 0 8153 1691 7 (1994)

Jornot L, Petersen H and Junod AF

Differential protective effects of o-phenanthroline and catalase on H2O2-induced DNA damage and inhibition of protein synthesis in endothelial cells

J. Cell. Physiol. **149**: 408-413. (1991)

Kamb A

Human melanoma genetics

Journal of Investigative Dermatology Symposium proceedings. **1**: 177-182. (1996)

Kamb A.

Cell cycle regulators and cancer

Trends in Genetics **11**: 136-140 (1995)

Kaneko M, Kodama M and Inoue F

Bimodal pattern of killing of Chinese hamster V79 variant cells by hydrogen peroxide

Free Radic. Res. **20**: 229-39. (1994)

Kelfkens.G, de.Gruijl.FR and van.der.Leun.JC

Tumorigenesis by short-wave ultraviolet A: papillomas versus squamous cell carcinomas

Carcinogenesis. **12**: 1377-1382. (1991)

Kendall JF, Gould D and Salter LF.

Preliminary investigations of interactions between low fluence levels of 310 nm and 405 nm radiation and exogenous dietary chemicals

British Journal of Dermatology. **139** (S51):63. (1998)

Kent.CR, Eady.JJ, Ross.GM and Steel.GG

The comet moment as a measure of DNA damage in the comet assay

International Journal of Radiation Biology. **67**: 655-660 (1995)

Kielbassa C, Roza L and Epe B

Wavelength dependence of oxidative DNA damage induced by UV and visible light

Carcinogenesis. **18**: 811-816. (1997)

Klaude.M, Eriksson.S, Nygren.J and Ahnstrom.G

The comet assay: mechanisms and technical considerations

Mutation Research. **363**: 89-96 (1996)

Klein.Szanto.AJ, Silvers.WK and Mintz.B

Ultraviolet radiation-induced malignant skin melanoma in melanoma-susceptible transgenic mice

Cancer Research. **54**: 4569-4572 (1994)

Koivukangas.V, Kallioinen.M, Autio.Harmainen.H and Oikarinen.A

UV irradiation induces the expression of gelatinases in human skin in vivo

Acta.Derm.Venereol. **74**: 279-282 (1994)

Kollias. N,Sayre.RM, Zeise L and Chedekel M.R.

Photoprotection by melanin

Journal of Photochemistry and Photobiology. 9: 135-160. (1991)

Kraemer.KH, Lee.MM, Andrews.AD and Lambert.WC

The role of sunlight and DNA repair in melanoma and nonmelanoma skin cancer- The

xeroderma pigmentosum paradigm

Arch.Dermatol. 130: 1018-10121. (1994)

Krinsky NI and Deneke SM

Interaction of oxygen and oxy-radicals with carotenoids

Journal of the National Cancer Institute. 69: 205-210 (1982)

Larsen.CJ

p16INK4a: a gene with a dual capacity to encode unrelated proteins that inhibit cell cycle

progression

Oncogene. 12: 2041-2044. (1996)

Larson RA

Antioxidant mechanisms of secondary natural products

in '*Oxidative stress and antioxidant defences in biology*' "Ed. Ahmad.S. Chapman and

Hall, New York. ISBN:0.412.03971.0 (1995)

Larue.L, Dougherty.N and Mintz.B.

Genetic predisposition of transgenic mouse melanocytes to melanoma results in malignant

melanoma after exposure to a low ultraviolet B intensity nontumorigenic for normal

melanocytes

Proc.Natl.Acad.Sci.U.S.A. 89: 9534-9538. (1992)

Larue.L, Dougherty.N, Bradl.M and Mintz.B

Melanocyte culture lines from Tyr-SV40E transgenic mice: models for the molecular

genetic evolution of malignant melanoma

Oncogene. 8: 523-531. (1993)

Lavker.R and Kaidbey.K

The spectral dependence for UVA-induced cumulative damage in human skin

Journal of Investigative Dermatology, **108**: 17-21 (1997)

Lee JAH

The relationship between malignant melanoma of skin and exposure to sunlight

Photochemistry and Photobiology. **50**: 493-496. (1989)

Lee.JE, Reveille.JD, Ross.MI and Platsoucas.CD

HLA-DQB1*0301 association with increased cutaneous melanoma risk

International Journal of Cancer. **59**: 510-513. (1994)

Le-Poole I C,Van Den Wijngaard R M J G J, Westerhof W, Dormans J A M A, Van Den Berg F M and Verkruisen R P.

Organotypic culture of human skin to study melanocyte migration.

Pigment Cell Research. **7**: 33-43 (1994)

Levine AJ

The tumor suppressor genes

Annual Reviews in Biochemistry. **62**: 623-51. (1993)

Levine T, Rispin A, Scott CS, Marcus W, Chen C and Gibb H

Special report on ingested inorganic arsenic-Skin cancer,nutritional essentiality

United States Environmental Protection Agency EPA/625/3.87/013 (1988)

Ley RD

Ultraviolet radiation A-induced precursors of cutaneous melanoma in Mondelphis domestica

Cancer Research. **57**: 3682-3684. (1997)

Ley RD, Applegate LA, Padilla RS and Stuart TD

Ultraviolet radiation-induced malignant melanoma in Mondelphis domestica

Photochemistry and Photobiology. **50**: 1-5. (1989)

Li J-H and Rossman TG

Inhibition of DNA ligase activity by arsenite: a possible mechanism of its comutagenesis

Molecular Toxicology. 2: 1-9. (1989)

Li.G, Ho.VC, Berean.K and Tron.VA

Ultraviolet radiation induction of squamous cell carcinomas in p53 transgenic mice

Cancer Research. 55: 2070-2074 (1995)

Lindahl T, Karran P and Wood RD

DNA excision repair pathways

Current Opinion in Genetics and Development. 7: 158-169. (1997)

Liu B, Parsons R, Papadopoulos N, Nicolaides NC, Lynch HT, Watson P, Jass JR, Dunlop M, Wyllie A, Peltomaki P, De La Chappelle A, Hamilton SR, Vogelstein B and Kinzler KW

Analysis of mismatch repair genes in hereditary non-polyposis colorectal cancer patients

Nature Medicine 2: 169-174. (1995)

Liu.L, Lassam.NJ, Slingerland.JM, Bailey.D, Cole.D, Jenkins.R and Hogg.D

Germline p16INK4A mutation and protein dysfunction in a family with inherited melanoma

Oncogene. 11: 405-412. (1995)

Loganzo F Jr, Nabeya Y, Maslak P and Albino AP

Stabilisation of p53 protein is a critical response to UV radiation in human melanocytes: implications for melanoma development

Molecular and Cellular Differentiation. 2:23-43. (1994)

Lu.X, Burbidge.SA, Griffin.S and Smith.HM

Discordance between accumulated p53 protein level and its transcriptional activity in response to u-v- radiation

Oncogene. 13: 413-418 (1996)

Lynn S, Lai H.L, Gurr J.R and Jan KY

Arsenite retards DNA break rejoining by inhibiting DNA ligation

Mutagenesis. 12: 353-358. (1997)

354

MacKie RM, Hole D, Hunter JAA, Rankin R, Evans A, McLaren K, Fallowfield M,
Hutcheon A and Morris A
Cutaneous malignant melanoma in Scotland: incidence, survival, and mortality, 1979-94
British Medical Journal. **315**: 1117-21. 1997

Marks,R.
An overview of skin cancers
Cancer. **75**: 607-612. (1995)

Marshall CJ
Tumor suppressor genes
Cell. **64**: 313-326. (1991)

Mass MJ and Wang L
Arsenic alters cytosine methylation patterns of the promoter region of the tumour
suppressor gene p53 in human lung cells: a model for a mechanism of carcinogenesis
Mutation Research. **386**: 263-277. (1997)

Mathews-Roth M M
Carotenoids and Photoprotection
Photochemistry and Photobiology. **65S**: 148S-151S (1997)

Mathews-Roth M M
Techniques for studying Photoprotective function of carotenoid pigments
Methods in Enzymology. **213**: 479-484. (1992)

McCarthy PJ, Sweetman SF, McKenna PG and McKelvey-Martin VJ
Evaluation of visual and image analysis quantification of DNA damage in the alkaline
comet assay
Mutagenesis. **12**: 209.214 (1997)

McKelvey-Martin VJ, Ho ETS, McKeown SR, Johnston SR, McCrthy PJ, Rajab NF and Downes CS

Emerging applications of the single cell gel electrophoresis (Comet) assay. I. Management of invasive transitional cell human bladder carcinoma. II. Fluorescent in situ hybridisation Comets for the identification of damaged and repaired DNA sequences in individual cells
Mutagenesis. **13**: 1-8. (1998)

McKelvey-Martin.VJ, Green.MH, Schmezer.P, Pool.Zobel.BL, De.Meo.MP and Collins.A
The single cell gel electrophoresis assay (comet assay): a European review
Mutation Research. **288**: 47-63. (1993)

Melia J
Changing incidence and mortality from cutaneous malignant melanoma
British Medical Journal. **315**: 1106-7. (1997)

Miller NJ, Sampson J, Candeias LP, Bramley PM and Rice-Evans CA
Antioxidant activities of carotenes and xanthophylls
FEBS Letters. **384**: 240-242. (1996)

Milne L, Nicotera P, Orrenius S and Burkitt MJ
Effects of glutathione and chelating agents on copper-mediated DNA oxidation: prooxidant and antioxidant properties of glutathione.
Arch. Biochem. Biophys. **304**: 102-109. (1993)

Mintz.B and Silvers.WK
Transgenic mouse model of malignant skin melanoma
Proc.Natl.Acad.Sci.U.S.A.. **90**: 8817-8821 (1993)

Mintz.B, Silvers.WK and Klein.Szanto.AJ
Histopathogenesis of malignant skin melanoma induced in genetically susceptible transgenic mice
Proc.Natl.Acad.Sci.U.S.A.. **90**: 8822-8826. (1993)

Mitchell MS
Active specific immunotherapy of melanoma
British Medical Bulletin. **51**: 631-646. (1995)

Morin B, Davies MJ and Dean RT

The protein oxidation product 3,4-dihydroxyphenylalanine (DOPA) mediates oxidative DNA damage

Biochemical Journal. **330**: 1059-1067. (1998)

Moriwaki.S, Stefanini.M, Lehmann.AR, Hoeijmakers.JH, Robbins.JH, Rapin.I, Botta.E, Tanganelli.B, Vermeulen.W, Broughton.BC and Kraemer.KH

DNA repair and ultraviolet mutagenesis in cells from a new patient with xeroderma pigmentosum group G and cockayne syndrome resemble xeroderma pigmentosum cells

Journal of Investigative Dermatology. **107**: 647-653. (1996)

Mortenson A, Skibsted LH, Willnow A and Everett SA

Re-appraisal of the tocopherol radical reaction with beta-carotene: evidence for oxidation of vitamin E by the beta-carotene radical cation.

Free Radic. Res. **28**: 69-80. (1998)

Muller R

Transcriptional regulation during the mammalian cell cycle

Trends in Genetics. **11**: 173-178. (1995)

Murrell GAC, Francis MJO and Bromley L

Modulation of fibroblast proliferation by oxygen free radicals

Biochemical Journal. **265**:659-665 (1990)

Nassi-Calo L, Mello Filho C and Meneghini R

o-phenanthroline protects cells from hydrogen peroxide-induced gene mutation and morphological transformation

Carcinogenesis **10**: 1055-1057. (1989)

Newton JA

Genetics of melanoma

British Medical Bulletin. **50**: 677-687. (1994)

Newton JN and Redburn J

Incidence of melanoma in four counties, 1989-92

British Medical Journal.. **310**: 502-503. (1995)

Nordenson I and Beckman L

Is the genotoxic effect of arsenic mediated by oxygen free radicals?

Hum. Hered. **41**: 71-73. (1991)

Noz.KC, Bauwens.M, van.Buul.PP, Vrolijk.H, Schothorst.AA, Pavel.S, Tanke.HJ, and Vermeer.BJ

Comet assay demonstrates a higher ultraviolet B sensitivity to DNA damage in dysplastic nevus cells than in common melanocytic nevus cells and foreskin melanocytes

Journal of Investigative Dermatology **106**: 1198-1202 (1996)

Olive PL

Molecular approaches for detecting DNA damage.

in *'DNA damage and repair. Vol II: DNA repair in higher eukaryotes'*. Eds Nickoloff JA and Hoekstra MF. Humana Press, New Jersey. ISBN: 89603 500 X. (1998)

Olive PL, Banath JP and Durand RE

Heterogeneity in radiation-induced DNA damage and repair in tumor and normal cells measured using the "comet" assay

Radiat. Res. **122**: 86-94. 1990

Olive.PL and Banath.JP

Detection of DNA double-strand breaks through the cell cycle after exposure to X-rays, bleomycin, etoposide and 125IdUrd-

International Journal of Radiation Biology. **64**: 349-358. (1993)

Olive.PL and Banath.JP

Induction and rejoining of radiation-induced DNA single-strand breaks: "tail moment" as a function of position in the cell cycle

Mutation Research. **294**: 275-283. (1993)

Ostling O and Johanson KJ

Microelectrophoretic study of radiation-induced DNA damages in individual mammalian cells

Biochem. Biophys. Res. Commun. **123**: 291-298. .(1984)

Palozza P and Krinsky NI

Antioxidant effects of carotenoids in vivo and in vitro: an overview

Methods in Enzymology. **213**: 403-420. (1992)

Peak JG and Peak MJ

Ultraviolet light induces double-strand breaks in DNA of cultured human P3 cells as measured by neutral filter elution

Photochemistry and Photobiology. **52**: 387-393. (1990)

Peak JG, Pilas B, Dudek EJ and Peak MJ

DNA breaks caused by monochromatic 365 nm ultraviolet-A radiation or hydrogen peroxide and their repair in human epithelioid and Xeroderma Pigmentosum cells

Photochemistry and Photobiology. **54**: 197-203. (1991)

Peak MJ and Peak JG

Convex curvatures of alkaline elution profiles of DNA from human cells irradiated with 405 nm UVA: evidence for induction of slowly developing alkali-labile sites

Photochemistry and Photobiology. **50**: 379-383. (1989)

Peak MJ and Peak JG

Hydroxyl radical quenching agents protect against DNA breakage caused by both 365-nm UVA and by gamma radiation

Photochemistry and Photobiology. **51**: 649-652. (1990)

Peak MJ, Peak JG and Carnes BA

Induction of direct and indirect single-strand breaks in human cell DNA by far- and near-ultraviolet radiations: action spectrum and mechanisms

Photochemistry and Photobiology. **45**: 381-387. (1987)

Peak.JG and Peak.MJ

Induction of slowly developing alkali-labile sites in human P3 cell DNA by UVA and blue- and green-light photons: action spectrum.

Photochemistry and Photobiology. **61**: 484-487. (1995)

Pecci L, Montefoschi G and Cavallini D

Some new details of the copper-hydrogen peroxide interaction

Biochem. Biophys. Res. Commun. **235**: 264-267. (1997)

Pedley.J, Ablett.EM, Pettit.A, Meyer.J, Dunn.IS, Sturm.RA and Parsons.PG

Inhibition of retinoblastoma protein translation by UVB in human melanocytic cells and reduced cell cycle arrest following repeated irradiation

Oncogene. **13**: 1335-1342. (1996)

Petrocelli.T, Poon.R, Drucker.DJ, Slingerland.JM and Rosen.CF

UVB radiation induces p21Cip1/WAF1 and mediates G1 and S phase checkpoints

Oncogene. **12**: 1387-1396 (1996)

Pflaum M, Boiteux S and Epe B

Visible light generates oxidative DNA base modifications in high excess of strand breaks in mammalian cells

Carcinogenesis. **15**: 297-300. (1994)

Pflaum M, Kielbassa C, Garmyn M and Epe B

Oxidative DNA damage induced by visible light in mammalian cells: extent, inhibition by antioxidants and genotoxic effects

Mutation Research. **408**: 137-146. (1998)

Phillip R, Hughes AO, Robertson MC and Mitchell TF.

Malignant melanoma incidence and association with arsenic

Br. Med. Chir. J. **98**: 165-169. (1983)

Picardo.M, Grammatico.P, Roccella.F, Roccella.M, Grandinetti.M, Del.Porto.G and Passi.S

Imbalance in the antioxidant pool in melanoma cells and normal melanocytes from patients with melanoma

Journal of Investigative Dermatology **107**: 322-326 (1996)

Picksley SM and Lane DP

p53 and Rb: their cellular roles

Current Opinion in Cell Biology. **6**: 853-858. (1994)

Pitcher H and Longstreth JD

Melanoma mortality and exposure to ultraviolet radiation: and empirical relationship

Environment International. **17**: 7-21. (1991)

Pitot HC and Dragan YP

Facts and theories concerning the mechanisms of carcinogenesis

Faseb. J. **5**: 2280-2286 (1991)

Pool-Zabel BL, Bub A, Muller H, Wollowski I and Rechkemmer G

Consumption of vegetables reduces genetic damage in humans: first results of a human intervention trial with carotenoid-rich foods

Carcinogenesis :1847-1850. (1998)

Prolla T, Baker S and Liskay RM

Genetics of mismatch repair, microsatellite instability, and cancer

in '*DNA damage and repair. Vol II: DNA repair in higher eukaryotes*'. Eds Nickoloff JA and Hoekstra MF. Humana Press, New Jersey. ISBN: 89603 500 X. (1998)

Przedborski S and Schon EA

Loss of ROS - a radical response

Nature Genetics. **18**: 99-100. (1998)

Ranade K, Hussussian CJ, Sikorrski RS, Varmus HE, Goldstein AM, Tucker MA, Serrano M, Hannon GJ, Beach D and Dracopoli NC

Mutations associated with familial melanoma impair p16ink4 function

Nature Genetics. **10**:114-116. (1995)

Rees JL

The melanoma epidemic: reality and artefact

British Medical Journal. **312**: 137-138. (1996)

Rees JL and Healy E

Melanocortin receptors, red hair, and skin cancer

Journal of Investigative Dermatology Symposium proceedings. **2**: 94-98. (1997)

361

Robinson.ES, VandeBerg.JL, Hubbard.GB and Dooley.TP

Malignant melanoma in ultraviolet irradiated laboratory opossums: initiation in suckling young, metastasis in adults, and xenograft behavior in nude mice

Cancer Research. **54**: 5986-5991. (1994)

Rodriguez H, Holmquist GP, D'Agostino (Jr) R, Keller J and Akman SA

Metal ion-dependent hydrogen peroxide-induced damage is more sequence specific than metal specific

Cancer Research. **57**:2394-2403. (1997)

Roelandts.R

Photo(chemo)therapy and general management of erythropoietic protoporphyria

Dermatology. **190**: 330-331. (1995)

Ross.GM, McMillan.TJ, Wilcox.P and Collins.AR

The single cell microgel electrophoresis assay (comet assay): technical aspects and applications Report on the 5th LH Gray Trust Workshop, Institute of Cancer Research, (1994)

Mutation Research. **337**: 57-60. (1995)

Rowley R

Mammalian cell-cycle responses to DNA-damaging agents

in '*DNA damage and repair. Vol II: DNA repair in higher eukaryotes*'. Eds Nickoloff JA and Hoekstra MF. Humana Press, New Jersey. ISBN: 89603 500 X. (1998)

Rudel.R, Slayton.TM and Beck.BD

Implications of arsenic genotoxicity for dose response of carcinogenic effects

Regul. Toxicol.Pharmacol. **23**: 87-105. (1996)

Runger.TM, Epe.B and Moller.K

Repair of ultraviolet B and singlet oxygen-induced DNA damage in xeroderma pigmentosum cells

Journal of Investigative Dermatology. **104**: 68-73. (1995)

Sachsenmaier.C, Radler.Pohl.A, Zinck.R, Nordheim.A, Herrlich.P and Rahmsdorf.HJ
Involvement of growth factor receptors in the mammalian UVC response
Cell. **78**: 963-972. (1994)

Santamaria L, Bianchi A, Arnaboldi A and Andreoni L
Prevention of the Benzo(a) Pyrene photocarcinogenic effect by beta-carotene and
canthaxanthine
Medicine Biologie Environmen. **9**: 113-120. (1981)

Satoh MS and Lindahl T
Role of poly(ADP-ribose) formation in DNA repair
Nature **356**: 356-368. (1992)

Schartl.A, Malitschek.B, Kazianis.S, Borowsky.R and Schartl.M
Spontaneous melanoma formation in nonhybrid Xiphophorus
Cancer Research. **55**: 159-165. (1995)

Schwartz D, Almog N, Peled A, Goldfinger N and Rotter V
Role of wild type p53 in the G2 phase: regulation of the gamma-irradiation induced delay
and DNA repair
Oncogene. **15**: 2597-2607. (1997)

Serrano M.,.Hannon G.J and Beach D.
A new regulatory motif in cell cycle control causing specific inhibition of cyclin D/CDK4
Nature **366**, 704-707. (1993)

Setlow RB, Grist E, Thompson K and Woodhead AD
Wavelengths effective in induction of malignant melanoma
Proc. Natl. Acad, Sci. USA. **90**: 6666-6670. (1993)

Setlow R.B., Woodhead A.D. and Grist E.
Animal model for ultraviolet radiation-induced melanoma: Platyfish-swordtail hybrid
Proc.Nat.Acad.Sci,USA. **86**: 8922-8926 (1989)

Singh NP, McCoy MT, Tice R and Schneider EL

A simple techniqe for the quantitation of low levels of DNA damage in individual cells

Exp. Cell. Res. 175: 184-191 (1988)

Smith.ML, Kontny.HU, Zhan.Q, Sreenath.A, O'Connor.PM and Fornace.AJ Jr

Antisense GADD45 expression results in decreased DNA repair and sensitizes cells to u-v-
-irradiation or cisplatin

Oncogene. 13: 2255-2263. (1996)

Stahl.W, Nicolai.S, Brivaba.K, Hanasch.M, Broszeit.G, Peters.M, Martin.H.D and Sies.H

Biological activities of natural and synthetic carotenoids: induction of gap junctional
communication and singlet oxygen quenching

Carcinogenesis. 18: 89.92. (1997)

Stratton SP and Liebler DC

Determination of singlet oxygen-specific versus radical-mediated lipid peroxidation in
photosensitised oxidation of lipid bilayers: effect of beta-carotene and alpha-tocopherol.

Biochemistry. 36: 12911-12920. (1997)

Sun Y

Induction of glutathione synthetase by 1,10-phenanthroline

FEBS Letters. 408: 16-20. (1997)

Sun Y, Bian J, Wang Y and Jacobs C

Activation of p53 transcriptional activity by 1,10-phenanthroline, a metal chelator and
redox sensitive compound

Oncogene. 14: 385-393. (1997)

Tanaka T, Makita H, Ohnishi M, Hirose Y, Wang A, Mori H, Satoh K, Hara A and
Ogawa H

Chemoprevention of 4-Nitroquinoline 1-oxide -induced oral carcinogenesis by dietary
circumin and Hesperidin: comparison with the protective effect of beta-carotene

Cancer Research. 54: 4653-4659 (1994)

The Alpha-Tocopherol, Beta-Carotene Cancer Prevention Study Group

The effect of vitamin E and beta-carotene on the incidence of lung cancer and other cancers in male smokers

New.Engl.J.Med. **330**: 1029-1035 (1994).

Thompson LH

Nucleotide Excision Repair: its relation to human disease

in *'DNA damage and repair. Vol II: DNA repair in higher eukaryotes'*. Eds Nickoloff JA and Hoekstra MF. Humana Press, New Jersey. ISBN: 89603 500 X. (1998)

Thornton I and Farago M

The geochemistry of arsenic

in *'Arsenic: exposure and health effects'*. 1st edn. Eds Abernathy CO, Calderon RL and Chappell WR. Chapman and Hall. (1997)

Tice RR

The single cell gel / Comet assay: a microgel electrophoretic technique for the detection of DNA damage and repair in individual cells.

Environmental Mutagenesis. 315-339. (1995)

Tice RR, Yager JW, Andrews P and Crecelius E

Effect of hepatic methyl donor status on urinary excretion and DNA damage in B6C3F1 mice treated with sodium arsenite

Mutation Research. **386**: 315-334. (1997)

Tice.RR and Strauss.GH

The single cell gel electrophoresis/comet assay: a potential tool for detecting radiation-induced DNA damage in humans

Stem.Cells.Dayt. **13** Suppl 1: 207-214. (1995)

Tobin.D and Thody.AJ

The superoxide anion may mediate short- but not long.term effects of ultraviolet radiation on melanogenesis

Exp.Dermatol. **3**: 99-105 (1994)

Tompkinson AE, Chen J, Besterman J and Husain I

Cellular functions of mammalian DNA Ligases

in 'DNA damage and repair. Vol II: DNA repair in higher eukaryotes'. Eds Nickoloff JA
and Hoekstra MF. Humana Press, New Jersey. ISBN: 89603 500 X. (1998)

Tornaletti S, Rozek D, Pfeifer GP

The distribution of UV photoproducts along the human p53 gene and its relation to
mutations in skin cancer

Oncogene. 8: 2051-2057. (1993)

Tyrrell R M and Pidoux M

Singlet Oxygen involvement in the inactivation of cultured human fibroblasts by UVA
(334nm, 365nm) and near visible (405 nm) radiations

Photochemistry and Photobiology. 49: 407-412 (1989)

Tyrrell RM.

Ultraviolet radiation and free radical damage to skin

in 'Free radicals and oxidative stress: environment, drugs and food additives' Eds.
Rice.Evans C, Halliwell B, Lunt GG.(Biochemical Society Symposium No 61.)Portland
Press, London.. ISBN: 1 85578 069 0 (1995)

Tyrrell.RM

The molecular and cellular pathology of solar ultraviolet radiation

Mol.Aspects.Med. 15: 1-77. (1994)

Tyrrell.RM, Applegate.LA and Tromvoukis.Y

The proximal promoter region of the human heme oxygenase gene contains elements
involved in stimulation of transcriptional activity by a variety of agents including oxidants

Carcinogenesis. 14: 761-765. (1993)

Ueda J, Takai M, Shimazu Y and Ozawa T

Reactive oxygen species generated from the reaction of copper (II) complexes with
biological reductants cause DNA strand scission

Arch. Biochem.Biophys. 357:231-239. (1998)

Umegaki K, Uramoto H, Suzuki J and Esashi T

Feeding mice palm carotene prevents DNA damage in bone marrow and reduction of peripheral leukocyte counts, and enhances survival following X-ray irradiation

Carcinogenesis. :1943-1947. (1998)

Urbach.F

Environmental risk factors for skin cancer

Recent.Results.Cancer Research. **128**: 243-262. (1993)

Valle VD, Duro D, Bernard O and Larsen CJ

The human protein p19arf is not detected in hemopoietic human cell lines that abundantly express the alternative beta transcript of the p16ink4a/MTS1 gene

Oncogene. **15**: 2475-2481. (1997)

Vidal.MJ, Loganzo.F Jr, de.Oliveira.AR, Hayward.NK and Albino.AP

Mutations and defective expression of the WAF1 p21 tumour-suppressor gene in malignant melanomas

Melanoma.Research. **5**: 243-250 (1995)

Vile.GF and Tyrrell.RM

UVA radiation-induced oxidative damage to lipids and proteins in vitro and in human skin fibroblasts is dependent on iron and singlet oxygen

Free.Radic.Biol.Med. **18**: 721-730. (1995)

Vile.GF, Basu.Modak.S, Waltner.C and Tyrrell.RM

Heme oxygenase 1 mediates an adaptive response to oxidative stress in human skin fibroblasts

Proc.Natl.Acad.Sci.U.S.A. **91**: 2607-2610. (1994)

Vile.GF and Tyrrell.RM

Oxidative stress resulting from ultraviolet A irradiation of human skin fibroblasts leads to a heme oxygenase-dependent increase in ferritin

Journal of Biological Chemistry. **268**: 14678-14681 (1993)

Vogel's Textbook of Quantitative Inorganic Analysis

4th Ed. Longman, USA (1978)

Walker.GJ, Palmer.JM, Walters.MK and Hayward.NK
A genetic model of melanoma tumorigenesis based on allelic losses
Genes.Chromosomes.Cancer. 12: 134-141 (1995)

Weinberg RA
Oncogenes, antioncogenes, and the molecular bases of multistep carcinogenesis
Cancer Research. 49: 3713-3721. (1989)

Welch WJ and Suhan JP
Cellular and Biochemical events in mammalian cells during and after recovery from
physiological stress
J. Cell Bio. 103: 2035-2052. (1986)

Wenczl E, Pool S, Timmerman AJ, van der Schans GP, Roza L and Schothorst AA
Physiological doses of ultraviolet irradiation induce DNA strand breaks in cultured human
melanocytes, as detected by means of an immunochemical assay
Photochemistry and Photobiology 66: 826-830. (1997)

Wick.ST, Dubay.MM, Imanil.I and Brizuela.L
Biochemical and mutagenic analysis of the melanoma tumor suppressor gene product/p16
Oncogene. 11: 2013-2019. (1995)

Wiencke JK, Yager JW, Varkonyi A, Hultner M and Lutze LH
Study of arsenic mutagenesis using the plasmid shuttle vector pZ189 propagated in DNA
repair proficient human cells
Mutation Research. 386: 335-344. (1997)

Wigley C and Balmain A.
Chemical carcinogenesis and precancer
in *'Introduction to the cellular and molecular biology of cancer'*. 2nd Ed.Eds. Franks LM
and Teich NM.Oxford University Press, Oxford UK..ISBN:0 19 854732 3 (1991)

Wilson SH and Singhal RK
DNA Polymerase involvement in DNA repair
in *'DNA damage and repair. Vol II: DNA repair in higher eukaryotes'*. Eds Nickoloff JA
and Hoekstra MF. Humana Press, New Jersey. ISBN: 89603 500 X. (1998)

Wiseman H and Halliwell B
Damage to DNA by reactive oxygen and nitrogen species: role in inflammatory disease and progression to cancer
Biochemical Journal. **313:** 17-29. (1996)

Wittbrodt J, Adam D, .Malitscheek B, .Maueler W, .Raulf F, Telling A, Robertson S.M and Schartl M
Novel putative receptor tyrosine kinase encoded by the melanoma-inducing Tu locus in Xiphophorus
Nature **341:** 415-421 (1989)

Woolf N
Neoplasia: disorders of cell proliferation and differentiation
in *'Cell, tissue and disease: the basis of pathology'* 2nd Ed. Balliere Tindall, London..
ISBN: 0 7020 1125 8 (1988)

Xiong Y., Hannon G.J.,.Zhang H,. Casso D,. Kobayashi R and D.Beach
p21 is a universal inhibitor of cyclin kinases
Nature **366:** 701-704 (1993)

Yager JW and Wiencke JK
Inhibition of poly(ADP-ribose) polymerase by arsenite
Mutation Research. **386:**345-351 (1997)

Yamamoto.S, Konishi.Y, Matsuda.T, Murai.T, Shibata.MA, Matsui.Yuasa.I, Otani.S, Kuroda.K, Endo.G and Fukushima.S
Cancer induction by an organic arsenic compound, dimethylarsinic acid (cacodylic acid), in F344/DuCrj rats after pretreatment with five carcinogens
Cancer Research. **55:** 1271- 1276. (1995)

Yamanaka K, Hasegawa A, Sawamura R and Okada S
Cellular response to oxidative damage in ling induced by the administration of dimethylarsinic acid, a major metabolite of inorganic arsenics, in mice.
Toxocol. Appl. Pharmacol. **108:** 205-213. (1991)

Yamasaki H and Naus CCG

Role of connexin genes in growth control

Carcinogenesis. **17**: 1199-1213. (1996)

Yendle JE, Tinwell H, Elliott BM and Ashby J

The genetic toxicity of time: importance of DNA-unwinding time to the outcome of single-cell gel electrophoresis assays.

Mutation Research. **375**: 125-136. (1997)

Ziegler.A, Leffell.DJ, Kunala.S, Sharma.HW, Gailani.M, Simon.JA, Halperin.AJ, Baden.HP, Shapiro.PE and Bale.AE,

Mutation hotspots due to sunlight in the p53 gene of nonmelanoma skin cancers

Proc.Natl.Acad.Sci.U.S.A. **90**: 4216-4220. (1993)